Geophysical Monitoring for Climatic Change

No. 17

Summary Report 1988

Geophysical Monitoring for Climatic Change No. 17

Summary Report 1988

James W. Elkins, Editor
Rita M. Rosson, Assistant Editor

Air Resources Laboratory
Geophysical Monitoring for Climatic Change

Boulder, Colorado

December 1989

NOTICE

Mention of a commercial company or product does not constitute an endorsement by NOAA Environmental Research Laboratories. Use for publicity or advertising purposes of information from this publication concerning proprietary products or the tests of such products is not authorized.

ACKNOWLEDGMENTS

Contents

GMCC Station Information

Name:	**Barrow (BRW)**	**Mauna Loa (MLO)**
Latitude:	71.3233	19.533
Longitude:	156.6067	155.578
Elevation:	0 km	3.4 km
Time Zone:	GMT -9	GMT -10
Office Hours:	8:00 am-5:00 pm	8:00 am-5:00 pm
Telephone		
Office hours:	(907) 852-6500	(808) 961-3788
After hours:	(907) 852-6500	(808) 961-3788
Postal Address:	Officer in Charge NOAA/ERL/ARL/GMCC Pouch 8888 Barrow, AK 99723	U.S. Dept. of Commerce NOAA - Mauna Loa Observatory P.O. Box 275 Hilo, HI 96720
Freight Address:		U.S. Dept. of Commerce NOAA - Mauna Loa Observatory 154 Waianuenue Ave. Hilo, HI 96720

Name:	**Samoa (SMO)**	**South Pole (SPO)**
Latitude:	-14.2522	-90.000
Longitude:	170.5628	0.000
Elevation:	0.03 km	2.8 km
Time Zone:	GMT -11	GMT +12
Office Hours:	8:00 am-5:00 pm	8:00 am-5:00 pm
Telephone:		
Office hours:	011-(684) 622-7455	Relayed through GMCC Boulder
After hours:	011-(684) 699-9953	
Postal Address:	U.S. Dept. of Commerce NOAA - GMCC Samoa Observatory P.O. Box 2568 Pago Pago, American Samoa 96799	Officer in Charge, GMCC Program Box 400 USARP C/O NAVSUPPFORANTARCTICA FPO San Francisco, CA 96692 ATTN: South Pole #S-257

GMCC Staff, 1988

Director's Office

James Peterson, Director
Bernard Mendonca, Deputy Director
Ellen Hardman, Secretary
Antonio Diaz, Guest Scientist
Dale Gillette, Physical Scientist
Jon Kahl, NRC Post Doctorate
Tezz Marquardt, CIRES
Patrick Reitelbach, Electronic Technician
Rita Rosson, Clerk-Typist
Pedro Sancho, Guest Scientist
Russell Schnell, CIRES
Patrick Sheridan, NRC Post Doctorate
Paul Stockton, Physical Science
  Technician
Denise Theede, Program Clerk
Thomas Watson, Physical Science Aid
Chi Zhou, CIRES

Acquisition and Data Management Group

Gary Herbert, Chief
Dee Dee Giebelhaus, Secretary
Richard Clark, Computer Programmer
Michael Ellis, Physical Science Aid
Joyce Harris, Computer Specialist
James McCutcheon, CIRES
Steve Roughton, Computer Assistant
Kenneth Thaut, Electronic Technician

Aerosols and Radiation Monitoring Group

John DeLuisi, Chief
Marilyn Van Asche, Secretary
Christa Anderson, Physical Science Aid
Barry Bodhaine, Meteorologist
Michaela Cronin, Physical Science Aid
Ellsworth Dutton, Meteorologist
Rudy Haas, Mathematician
Bradley Halter, Meteorologist
David Kanzer, Physical Science Aid
Fred Kreiner, Physical Science Aid
David Longenecker, CIRES
David Massey, Physical Science Aid
Donald Nelson, Meteorologist
Timothy Quakenbush,
  Physical Science Aid
Patrick Reddy, CIRES
Kurt Shallenberger, CIRES
Michael Shanahan, Physical Science Aid
Lois Stearns, Meteorologist
Robert Stone, CIRES
Barbara Thomson, Physical Science Aid
James Wendell, Electronic Technician

Air Quality Group

Joe Boatman, Chief
Dee Dee Mitchell, Secretary
Cynthia Crouch, CIRES
Laureen Gunter, Meteorologist
Young Kim, CIRES
Menachem Luria, NRC Post Doctorate
John Ray, CIRES
Herman Sievering, CIRES
Charles Van Valin, Research Chemist
Dennis Wellman, Engineer
Stan Wilkison, Computer Programmer

Carbon Cycle Group

Pieter Tans, CIRES
Lee Prendergast, Secretary
Thomas Conway, Research Chemist
Ronald Garrett, Physical Science Aid
Darryl Kaurin, CO-OP
Duane Kitzis, CIRES
Patricia Lang, CIRES
Russell Martin, CIRES
Kenneth Masarie, CIRES
Paul Novelli, CIRES
Vernon Preston, CO-OP
L. Paul Steele, CIRES
John Taylor, CIRES
Kirk Thoning, CIRES
Lee Waterman, Research Chemist

Ozone Group

Walter Komhyr, Chief
Lee Prendergast, Secretary
Mark Anderson, Physical Science Aid
Maureen Ballard, CIRES
Brian Bowman, Physical Science Aid
Sean Coleman, Physical Science Aid
Robert Evans, CIRES
Leigh Fanning, Physical Science Aid
Paul Franchois, CIRES
Robert Grass, Physicist
Timothy Kauffman, Physical Science Aid
Gloria Koenig, Computer Programmer
Jeffrey Lathrop, CO-OP
Kent Leonard, CIRES
Michael O'Neill, CO-OP
Samuel Oltmans, Physicist
Frank Polacek, III, Meteorological
  Technician
Dorothy Quincy, CIRES
LaRae Williams, Physical Science Aid

Nitrous Oxide and Halocarbons Group

James Elkins, Chief
Marilyn Van Asche, Secretary
Christina Brunson, CIRES
James Butler, CIRES
Ellen DeMoney, CIRES
Keith Egan, CIRES
Kevin Gurney, CIRES
Brad Hall, CIRES
Thayne Thompson, Physicist

Barrow Observatory

Daniel Endres, Station Chief
James Wendell, Electronic Technician
Timothy Quakenbush, Electronic
  Technician

Mauna Loa Observatory

Elmer Robinson, Director
Judith Pereira, Program Support
  Technician
Ame Austring, Physical Scientist
Lynne Borman, Physical Science Aid
John Chin, Physicist
Thomas DeFoor, Electronic Engineer
Thomas Garcia, Meteorological
  Technician
Barbara Kerecman, Data Clerk
Darryl Kuniyuki, NOAA Jr. Fellow
Mamoru Shibata, Electronic Technician
Alan Yoshinaga, Chemist

Samoa Observatory

Steven Ryan, Station Chief
M. Emily Wilson-Godinet,
  Electronic Technician

South Pole Observatory

Robert Poston, Lt. j.g.,NOAA Corps
Ted Mullen, Electronic Technician
Elizabeth Crozer, Lt., NOAA Corps
Mark Winey, Elect. Engineer

GEOPHYSICAL MONITORING FOR CLIMATIC CHANGE
NO. 17
SUMMARY REPORT 1988

1. Summary

At MLO, a highlight of the year was hosting the GMCC Annual Meeting on the occasion of the 30th anniversary of CO_2 monitoring at the observatory. A commemorative ceremony recognized Prof. C. D. Keeling of SIO, who began the program. The program still continues with the same analyzer that was put into operation in 1958. Additions to the MLO program included sulfur analyzers, a new CNC counter, and a solar spectroradiometer. Special efforts were made to calibrate the World Standard Dobson instrument as part of accelerating international interest regarding apparent, long-term global decreases of stratospheric ozone. At BRW, we supported a major field program, the NASA-sponsored ABLE 3-A, designed to explore budgets of trace species in the boundary layer. Numerous improvements were made to observatory facilities and the large suite of cooperative programs continued with a few additions and subtractions.

Ongoing GMCC core measurement programs included CO_2 and CH_4 from the flask network and observatories; total column ozone; ozone vertical distribution by ECC sonde and Umkehr technique; surface ozone; stratospheric water vapor by balloon soundings at Boulder; CFC-11, CFC-12, and N_2O from flask samples and observatory analyzers; stratospheric aerosols at MLO using lidar; aerosol light scattering; CN concentration; direct and diffuse solar and infrared radiation; meteorological variables; and chemistry of precipitation.

The Aerosols and Radiation Monitoring Group monitoring of CN concentration and aerosol light-scattering coefficient shows no statistically significant long-term trends. Stratospheric aerosols, as indicated by atmospheric solar transmission and turbidity data, were near long-term background levels with no significant volcanic perturbation. We continued to modestly expand our surface radiation budget measurements, especially for comparison to similar satellite data. Special aerosol and radiation projects were undertaken at SPO to characterize conditions there. A new technique was developed to use ground-based Dobson-Umkehr UV measurements for comparison to, and direct calibration of, satellite UV sensors for total ozone and ozone profile retrievals.

The Carbon Cycle Group continued CO_2 sampling at the observatories and cooperative sites. The global annual mean for 1988 was about 2.6 ppm greater than that for 1987, a significantly larger year-to-year increase than in the previous 7 years (about 1.5 ppm yr^{-1}). Several analyses suggested that this was a temporary change related to the concurrent ENSO event. The globally averaged linear growth rate of CH_4, May 1983 to December 1988, was 12.24 ± 0.08 ppb yr^{-1}. The 1988 mean global concentration was about 1675 ppb. A program of CO monitoring was begun with extensive effort devoted to development of a precise analytical system, evaluation of flask stability, and preparation of standards.

The Ozone Group (formerly Monitoring Trace Gases) continued monitoring of total ozone, Dobson-Umkehr and ozonesonde profiles, surface ozone, and stratospheric water vapor along with international Dobson calibration work. Measurements of surface ozone continue to show intriguing, but not fully explained, long-term changes. Increases have occurred at BRW during summer and autumn and at MLO during winter. Decreases have occurred at SMO and SPO during austral summer months. Oxidation of increasing methane amounts has been suggested as a cause for the decreasing ozone. Photolysis of methane in the stratosphere has been suggested as a cause of the increasing water vapor there.

The Acquisition and Data Management Group continued regular meteorological measurements at the observatories. At BRW, SMO, and SPO, annual distribution and frequency of hourly average resultant wind direction and speed were quite similar to 11-year climatologies. The group cooperated with many groups to provide air mass trajectories that are so useful for interpretation of air chemistry measurements. A new technique, cluster analysis, was employed to summarize and/or explore the structure of large trajectory data sets.

The Air Quality Group participated in several field programs; most focused on the national acid precipitation program and all used the NOAA King Air research aircraft as the primary data collection platform. Wide-ranging operations from the western Atlantic Ocean to the central United States yielded several high-quality data sets and associated publications.

The Nitrous Oxide and Halocarbons Group continued flask sampling of N_2O, CFC-11, and CFC-12 as well as quasi-continuous in-situ sampling of N_2O, CFC-11, CFC-12, CFC-113, CH_3CCl_3, and CCl_4. Growth rates of CFC-11 and CFC-12, for example, were about 4% per year. Extensive laboratory tests were conducted prior to beginning monitoring of several very-low-concentration halocarbons--HCFC-22, CFC-113, H-1301, and H-1211. The group continued its emphasis on preparation and maintenance of the primary gas standards required for precise long-term monitoring.

Within the Director's Office research continued on the impact of open sources of alkaline substances on the neutralization of some acids and the concurrent effect on the pH of wet deposition in the western United States. The AGASP program focused on data analysis from AGASP-II (special issues of *Journal of Atmospheric Chemistry* and *Atmospheric Environment* are forthcoming) and planning for AGASP-III, to be operated out of Norway during March1989. A special effort was made this year to obtain contributions to this volume from our cooperating programs. Many scientists responded; their contributions constitute Section 10.

2. Observatory Reports

2.1. MAUNA LOA

E. ROBINSON

2.1.1. OPERATIONS

Two large special research projects were carried out at MLO during 1988. First, a major photochemistry experiment, MLOPEX, was conducted May 1-June 4 by NCAR researchers, with additional investigators from NOAA/AL and several universities. The purpose of MLOPEX was to examine photochemical relationships of major odd-nitrogen compounds along with some of the odd-hydrogen and odd-oxygen compounds, and to obtain data directly applicable to modeling remote tropospheric production and loss of O_3. Second, a major aerosol program, MABIE, was conducted by NASA/MSFC. This program was in operation from November 15 to December 15 and also included investigators from NOAA/WPL and several universities. The NOAA/WPL contribution involved the operation of a CO_2 pulsed Doppler lidar system and included several intercomparisons with the MLO ruby lidar. The MABIE program is part of NASA's global aerosol backscatter experiment to develop design data for a satellite-based laser wind sounding system.

Weekly ozonesonde flights and lidar observations continued with the support of NOAA/NESDIS. The results of these MLO observations are factored into ground-truth calibrations for satellite observational systems. Analyses of the MLO ozonesonde record, which now includes more than 4 years of data, show expected seasonal cycles but, to date, no obvious trends in ozone layer characteristics. The 1988 lidar data showed that the stratospheric aerosol continued to decrease, but very slowly. This was similar to conditions in 1987, and it doubtless reflects the fact that no major volcanic eruptions that could have injected aerosol materials into the stratosphere occurred during 1988.

Additions to the GMCC instrumentation at MLO in 1988 included a pulsed fluorescence SO_2 analyzer operating in parallel with the flame photometric total sulfur analyzer and a TSI alcohol-based CNC operating in parallel with the G.E. CNC. The original TSI installation was made in May, and it became fully operational several months later. It will be operated in parallel with the G.E. CNC for about a year, and if it proves satisfactory, the venerable G.E. unit will be retired, perhaps to the MLO museum. MLO has also assumed responsibility for operating the high-precision spectroradiometer formerly operated by the University of Arizona.

Kilauea volcano continued to erupt from a vent 38.4 km south of Hilo (64 km east-southeast of MLO) at 250 m. The sixth year of this eruption began in January 1988. Volcanic plume haze from this eruption was frequently noticed around the island and was the subject of health and other impact assessments. At MLO occasional haze events occurred as part of the typical midday upslope wind pattern and were identifiable by above-background total sulfur and SO_2 concentrations.

2.1.2. PROGRAMS

Table 2.1 lists the major GMCC and cooperative programs carried out at MLO in 1988. Comments on some of the programs follow:

Carbon Dioxide

The GMCC Siemens Ultramat-3 IR analyzer and the SIO Applied Physics IR analyzer were operated in parallel without problems throughout the year. Routine maintenance and calibrations were done on both instruments without difficulty. The Siemens analyzer has been in operation since August 5, 1987, and it has proved to be reliable and durable. In April 1988 the sample line to the Siemens analyzer was changed from aluminum tubing to a Dekabon line, and the inlet was moved from 21 m to 40 m, at the top of the tall tower. Preliminary CO_2 average concentration for 1988 at MLO was 350.8 ppm. The growth rate was approximately 1.9 ppm yr^{-1}.

The weekly CO_2, CH_4, and other-gas sampling programs using flasks at MLO and at Cape Kumukahi were carried out according to schedule through the year without any special problems.

Outgassing from the volcanic vents at the caldera and along the northeast rift zone of Mauna Loa continued to cause some observable periodic disturbance of portions of the CO_2 data record. These erratic record periods were easily identified and could be separated from the clean-air record and discarded without difficulty. These venting events occurred mostly between 0000 and 0800 LST during the nocturnal downslope wind regime, i.e., wind directions between south and southeast. The frequency of monthly occurrences of observable outgassing from volcanic vents on Mauna Loa are listed in Table 2.2. It should be noted that the tabulation in previous annual *Summary Reports* indicated only the number of days of occurrences and not the number or percentage of hours of data that are affected. Table 2.2 shows the total time of vent activity. The 1988 annual frequency is low, just 2.3% or 199.7 hours. The low percentage of observed disturbances in April and December are likely due to changes in volcanic vent.

Methane

The methane gas chromatograph was in normal operation during the year. When the pure-air generator malfunctioned on November 8, 1988, it was decided to remove this unit and to provide the necessary clean air with cylinder air sent from GMCC in Boulder. This change eliminates GC flame-out problems when power interruptions occur.

Nitrous Oxide and Halocarbons

Operation of the RITS halocarbon GC continued with only minor problems. Some modifications to the RITS GC were made in 1988. In November, the system was reconfigured to allow column backflushing after each run for the halocarbon. An additional 2 Mbytes of memory and a new software upgrade were added to the HP computer.

TABLE 2.1. Summary of Sampling Programs at MLO in 1988

Program	Instrument	Sampling Frequency	Remarks
Gases			
CO_2	Siemens Ultramat-3 IR analyzer*	Continuous	MLO
	3-L glass flasks	1 pair wk^{-1}	MLO and Kumukahi
	0.5-L glass flasks, through analyzer	1 pair wk^{-1}	MLO
CO_2, CH_4	0.5-L glass flasks, P^3	1 pair wk^{-1}	MLO and Kumukahi
CH_4, CO, CO_2	Carle automated GC	1 sample (24 min)$^{-1}$	MLO
Surface O_3	Dasibi ozone meter*	Continuous	MLO
Total O_3	Dobson spectrophotometer no. 76	3 day^{-1}	Weekdays
O_3 profile	Dobson spectrophotometer no. 76	2 day^{-1}	Automated Umkehr method
	Balloonborne ECC sonde	1 wk^{-1}	From Hilo Airport
CFC-11, CFC-12, N_2O,	300-mL stainless steel flasks	1 pair wk^{-1}	MLO
CFC-11, CFC-12, N_2O	HP5890 automated GC	1 sample (3 h)$^{-1}$	MLO
CCl_4, CH_3CCl_3			
N_2O	Shimadzu automated GC	1 sample (3 h)$^{-1}$	MLO
Total sufur gases	CSI flame photometric analyzer*	Continuous	MLO
SO_2	TECO pulsed fluorescence analyzer*	Continuous	MLO; Installed Nov.
Aerosols			
Condensation nuclei	Pollak CNC	5 wk^{-1}	
	G.E. CNC*	Continuous	
	TSI CNC*	Continuous	Installed May
Optical properties	Four-wavelength nephelometer*	Continuous	450, 550, 700, 850 nm
Stratospheric aerosols	Lidar	1 profile wk^{-1}	694.3 nm
Solar Radiation			
Global irradiance	Eppley pyranometers (3) with Q, OG1, and RG8 filters*	Continuous	
Direct irradiance	Eppley pyrheliometers (2) with Q filter*	Continuous	
	Eppley pyrheliometer with Q, OG1, RG2, and RG8 filters	3 day^{-1}	
	Eppley /Kendall active cavity radiometer	1 mo^{-1}	
Diffuse irradiance	Eppley pyranometer with shading disk and Q filter*	Continuous	
Turbidity	J-series sunphotometers, J-202 and J-314	3 day^{-1}	380, 500, 778, 862 nm; narrowband; replaced Mainz II in April
	Mainz II sunphotometer M120	3 day^{-1}	380, 412, 500, 675, 862 nm; Operational Jan.-April
	PMOD three-wavelength sunphotometer*	Continuous	380, 500, 778 nm; narrowband
Solar spectroradiometry	Solar spectroradiometer	Discrete	Transfer of U. of Arizona program April 1988
Meteorology			
Air temperature	Aspirated thermistor*	Continuous	2- and 40-m heights
	Max.-min. thermometers	1 day^{-1}	Standard shelter
	Hygrothermograph	Continuous	MLO and Kulani Mauka
Temperature gradient	Aspirated thermistors*	Continuous	2- and 40-m heights
Dewpoint temperature	Depoint hygrometer*	Continuous	2-m height
Relative humidity	Hygrothermograph	Continuous	MLO and Kulani Mauka
Pressure	Capacitance transducer*	Continuous	
	Microbarograph	Continuous	
	Mecurial barometer	5 wk^{-1}	NWS calib. 12/1/88
Wind (speed and direction)	Bendix Aerovane*	Continuous	8.5- and 40-m heights
Precipitation	Rain gauge, 8-in	5 wk^{-1}	
	Rain gauge, 8-in	1 wk^{-1}	Kulani Mauka
	Rain gauge, weighing bucket	Continuous	Weekly chart record
	Rain gauge, tipping bucket*	Continuous	
Total precipitable water	Foskett IR hygrometer*	Continuous	

TABLE 2.1. (continued)

Program	Instrument	Sampling Frequency	Remarks
Precipitation Chemistry			
pH	pH meter, Hilo lab.	Daily	Rainwater collections, 3 sites
Conductivity	Conductivity bridge, Hilo lab.	Daily	Rainwater collections, 3 sites
Chemical components	Ion chromatograph, Hilo lab.	Daily	Rainwater collections, 3 sites
Cooperative Programs			
CO_2 (SIO)	Applied Physics IR analyzer	Continuous	MLO
CO_2, ^{13}C, N_2O (SIO)	5-L evacuated glass flasks	1 pair wk^{-1}	MLO and Kumukahi
Surface SO_2 (EPA)	Chemical bubbler system	Every 12 days	24-h (0000-2400) sample
CO_2, CO, CH_4, $^{13}C/^{12}C$ (CSIRO)	Pressurized glass flask sample	1 mo^{-1}	MLO
CO_2, CH_4, and other trace gases (NCAR)	Evacuated stainless steel flasks	1 pair wk^{-1}	MLO and Kumukahi
Total suspended particles (DOE)	High-volume sampler	Continuous	1 filter wk^{-1}
Total O_3, SO_2 (AES Canada)	Brewer spectrophotometer, MK-II; Umkehr-automated	Continuous	Out of service April 1988
Turbidity (AES Canada)	Sonotek sunphotometer no. 5698	1-3 day^{-1}	MLO
CH_4 ($^{13}C/^{12}C$) (Univ. of Washington)	35-L evacuated flask	1 mo^{-1}	MLO
Total suspended particles (EPA)	High-volume sampler	Every 12 days	24-h (0000-2400) sample
Ultraviolet radiation (Temple Univ.)	UV radiometer (erythema)	Continuous	Integrated radiation responsible for sunburn
Ultraviolet radiation (Smithsonian)	8-wavelength UV radiometer	Continuous	290-325 nm, narrowband
Solar aureole intensity (CSU)	Multi-aperture tracking photometer	Continuous	2, 5, 10, 20, 30° fields of view
Precipitation collection (DOE)	Exposed collection pails	Continuous	MLO
Precipitation collection (ISWS)	Aerochemetric automatic collector	Continuous	Analysis for ^7Be and ^{10}Be
Precipitation collection (Univ. of Virginia)	Aerochemetric automatic collector	Continuous	Organic acid analysis
Wet-dry deposition (ISWS)	Aerochemetric automatic collector	Continuous	NADP
Aerosol chemistry (Univ. of Washington)	Nuclepore filters	Continuous	Upslope-downslope discrimination
Aerosol chemistry (Univ. of Calif.-Davis)	Programmed filter sampler	Integrated 3 day^{-1} sample	1 continuous and 1 downslope sample (3 days)$^{-1}$
Aerosol size distrib. and chem. (Univ. of Hawaii)	Particle counters	Continuous	Operated Jan.-April 1988
^{13}C (USGS, Denver)	10-L stainless steel flasks	Biweekly	MLO
Various trace gases (OGC)	Stainless steel flasks	1 set wk^{-1} (3 flasks)	MLO and Kumukahi
HNO_3, HCl vapor, and aerosols (URI)	Filter system	Daily 2000-0600 LST	MLO operational August 1988

*Data from this instrument recorded and processed by CAMS.

TABLE 2.2. Monthly Occurrences of Outgassing from Volcanic Vents on Mauna Loa

	Jan.	Feb.	March	April	May	June	July	Aug.	Sept.	Oct.	Nov.	Dec.	Year
Total time (hours)	29.0	18.8	24.6	6.5	10.9	12.2	11.1	27.5	12.2	20.1	10.8	6.0	199.7
Percent of time	3.9	2.8	3.3	0.9	2.7	1.7	1.5	3.7	1.7	2.7	1.5	0.8	2.3

Ozone

As in previous years the ozone program consisted of three major components; surface air monitoring using a Dasibi ozone monitor, total ozone and Umkehr ozone profiles using Dobson techniques, and ozone profiles using balloonborne ECC ozonesondes flown from the Hilo NWS station.

Surface air ozone monitoring was essentially continuous through the year. Normal routine calibrations and maintenance were carried out regularly.

Dobson spectrophotometer no. 76, one of the GMCC computerized instruments, was in operation throughout the year and provided both direct-sun total ozone measurements and computer-controlled Umkehr ozone profiles. No prolonged downtimes were experienced by the Dobson program. Direct-sun Dobson observations were made on observation days by the MLO staff whenever weather conditions were favorable. During 1988 this amounted to 194 Dobson observation days, or 80% of the total 243 possible days of observation. During the 1988 summer the WMO World Standard Dobson instrument no. 83 was again calibrated by the Langley plot method, using a series of measurements at MLO. Also at this time intercomparison calibrations were carried out between no. 83 and MLO Dobson no. 76 and SMO Dobson no. 42. These special observations continued the pattern of frequent standardizations and intercomparisons of the GMCC Dobson instruments as well as the WMO World Standard no. 83.

The 1988 ozonesonde operations consisted of 51 total instrument launches; of these, 44, or 86%, resulted in usable ozone profiles. Of the seven unproductive launches, instrument failure after launch and in mid-flight was the most common problem. The 44 successful flights consisted of 42 using the large 40-km plastic balloon and 2 using 2,000-g rubber balloons. The 42 plastic balloons rose to an average altitude of 41.2-km, and all but 2 exceeded the target altitude of 40 km. Both of the 2,000-g rubber balloon flights in 1988 exceeded 35 km altitude. The 1988 results are similar to those of 1987 [*Bodhaine and Rosson*, 1988], when all but 3 of 48 successful flights exceeded 40 km and the average altitude of rise was 41.4 km.

Sulfur Gases

A CSI flame-photometric total sulfur analyzer (i.e., SO_2 plus other sulfur gases) has been in operation since the latter part of 1987. The instrument is calibrated manually once per week. During November 1988 a TECO pulsed fluorescence SO_2 monitoring instrument was added to the system and set up to sample in parallel with the CSI flame photometric unit. These two instruments are on loan to MLO from the GMCC Air Quality Group. Both systems operated without problems. The pulsed fluorescence instrument is programmed to have an automatic, once-daily, calibration cycle. The TECO instrument is sensitive specifically to SO_2 with a detection limit of approximately 0.05 ppbv. The CSI flame-photometric unit has a higher detection limit of about 0.5 ppbv, and it is sensitive to the total atmospheric gaseous sulfur concentration, detecting various sulfur compounds, such as CS_2 and OCS, in addition to SO_2. The results from these two sulfur gas analysis systems operated at MLO are summarized in Section 7 of this *Summary Report*.

Aerosols

The MLO aerosol program was augmented in May with the addition of a TSI CNC. The TSI is a continuous expansion-type CNC in which the condensing vapor is isopropyl alcohol instead of the water used in the pulsation expansion G.E. CNC. The TSI system became fully operational in the fall and has operated reliably since then. After a period of about a year of consistent operation in parallel with the G.E. CNC, it is expected that the old G.E. CNC system can be retired. The Pollak CNC continued to provide daily standard CN concentrations that were used to calibrate both the old G.E. and the new TSI CNC instruments.

Monitoring of stratospheric aerosol layers was carried out through periodic lidar observations. Figure 2.1 shows the integrated non-Rayleigh backscatter values for the MLO lidar observations between 16 and 33 km for the period 1985-1988. During 1988 a total of 37 lidar observations of stratospheric aerosol profiles were obtained. Whenever possible these lidar observations were coordinated with an overpass of the SAGE-II satellite. It was possible to implement a number of the lidar improvements that are part of the ongoing lidar upgrade program. An interim chassis was assembled to operate the laser in the planned horizontal position, and to increase the separation of the telescope and the laser aperture; the required vertical beam was obtained through the use of a 90° beam-bender coupled with a collimator. A 15-cm by 1.6-cm ruby laser rod was also installed in place of the older 7.6-cm rod. Other planned modifications to the lidar cannot be implemented until major modifications to the lidar building can be done. No significant stratospheric aerosol injections were detected in 1988. As shown by Figure 2.1, the average non-Rayleigh backscatter continued to decrease in a more-or-less linear fashion, averaging about 25% yr[-1] during 1987 and 1988.

Solar Radiation

The major change in the solar radiation program in 1988 was the assumption by the MLO staff of the program of solar spectroradiometry, which previously had been under develop-
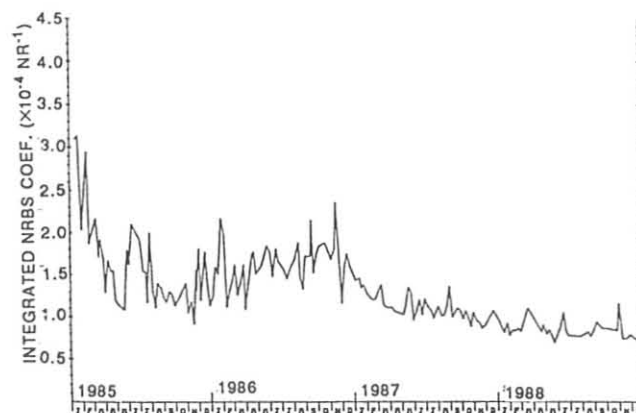

Fig. 2.1. Non-Rayleigh backscatter coefficient values, 1985-1988, for MLO lidar observations between 16 and 33 km.

ment by the University of Arizona through the support of a NOAA research grant. The objective of this program is to carry out a long-term program of solar spectroradiometry of sufficient precision and accuracy to track changes in the solar "constant." Considerable additional engineering of the system has been carried out. Turbidity measurements were again being made with the older J-series sunphotometers when in April the newer Mainz II unit no. M120 failed and had to be returned to the factory. The other components of the MLO solar radiation program were continued with little change from prior years. These are listed in Table 2.1.

Meteorology

The meteorological measurement program was accomplished without major problems during the year. In February the wind speed and direction systems were calibrated. The MLO mercury barometer was calibrated by NWS in December, and a new table of barometer correction factors was calculated. The mercury barometer is read daily and used to establish the calibration factor for the CAMS continuously recording pressure sensor.

Precipitation Chemistry

The precipitation chemistry program consisted of a combination of NOAA/ARL and cooperative programs. The NOAA/ARL program included collections 5 days per week from three sites: Hilo, 35 km on Saddle Road, and at MLO. The collected precipitation from these sites as well as rain and/or snow samples from SMO, BRW, and SPO were analyzed in the MLO Hilo chemistry laboratory.

Cooperative Programs

The SIO CO_2 monitoring program marked 30 years of continuous operation at MLO. This anniversary was the occasion for holding the 1988 GMCC Annual Meeting in Hilo. A commemorative ceremony was also held at MLO to mark this special event on March 28, 1988, exactly 30 years from the day on which the first meaningful data were generated by SIO's CO_2 analyzer. The commemoration was opened by a typical Hawaiian blessing suited to the occasion and then a presentation of certificates of recognition to Dr. C.D. Keeling of SIO and GMCC researchers. The SIO program of CO_2 monitoring at MLO is continuing with the same Applied Physics IR CO_2 analyzer that was put into operation in March 1958.

Three new cooperative programs were begun in 1988, all aerosol sampling studies. Two of the programs are continuing. One of these, which is being operated for the Crocker Nuclear Laboratory, University of California at Davis, collects a weekly set of two 3-day integrated filter samples; one is collected continuously and one is collected only during expected downslope wind conditions (i.e., 2000 to 0600 LST). This program is part of a nationwide background aerosol program related to the evaluation of visibility in remote, unpolluted locations. The second new and continuing aerosol sampling program begun in 1988 is an expansion of the periodic filter sampling done previously by URI, School of Oceanography, on a quarterly basis. The expansion involves weekly filter changes by MLO staff of a batch of daily filters. One filter is exposed daily during the period of expected downslope winds,

2000-0600 LST, at the 23-m level of the tall tower. URI analyzes these filters for HNO_3, HCl, and other related constituents. The third new aerosol study carried out by the University of Hawaii was relatively short lived, January through April. It combined particle size distribution measurements with a controlled heating cycle to infer both particle size and chemical composition.

In April 1988, the Brewer MKII ozone spectrophotometer of Atmospheric Environment Service, Canada, was damaged by power surges caused by nearby lightning strikes, and it had to be returned to Canada. The program had not been resumed by year's end.

Table 2.1 lists the 22 cooperative program experiments operated by 17 different institutions at MLO. In each program, MLO staff members may take specific samples (e.g., flasks or filters) or monitor the continuously operating sampling instruments; however, in all cases, the output of the experiment is returned to the P.I. for analysis and data interpretation. A number of these programs are described by the P. I.'s in short summary reports that are included in Section 10 of this *Summary Report*. In addition to the programs listed in Table 2.1, there were a number of cases during 1988 when individual investigators came to MLO to carry out discrete, short-period studies in which MLO staff members did not become directly involved; these short-period studies by visiting P.I.'s are not listed. Two of the more extensive programs, the NCAR MLOPEX and the NASA MABIE, were mentioned previously.

2.2. BARROW

D. ENDRES

2.2.1. OPERATIONS

The GMCC operation at BRW completed another successful year of data collection in 1988. The academic and scientific community's increased interest in Arctic science continued. BRW had a supporting role for a host of visitors. Among the visitors to the station were the NOAA Administrator and the Vice Chancellor for Research and Dean of the Graduate School at the University of Alaska, Fairbanks. In March BRW personnel had a key role in helping to establish contacts and logistic ground support between NASA and the North Slope Borough for the ABLE-3A flights over the Arctic in July. In July BRW hosted special projects for ABLE-3A, and its long-term data were incorporated as ground truth for the NASA ABLE-3A flights. During March there was a personnel change when the electronics technician took a position in Boulder. During the summer months a new program was started in which the BRW personnel assisted in the training of the new SPO crew. Training went well and it is expected that the program will continue into the future. An ongoing relationship in which the observatory and its personnel are called on by the North Slope Borough for technical information and expertise continued in 1988. As part of this exposure, GMCC personnel were featured in several media articles ranging from radio interviews to magazine articles to public television interviews.

Work was done on both vehicles by GMCC personnel. DEW Line personnel were often too busy with their own vehicles to offer assistance. Because of the endless difficulty involved with securing a local mechanic, it was decided it would be easier to have GMCC personnel do vehicle repairs when possible. This included doing the routine oil changes and tune-ups, replacing the engine and transmission in the GMC pickup truck, and doing a complete brake job.

To remedy poor telephone performance, several splices were cleaned and retaped in the phone line to the observatory in hopes that it would solve the noise problems. It was decided that this was not the answer and that new lines would be needed. Negotiations were undertaken by USGS in Fairbanks on GMCC's behalf. It is expected that the new lines will be installed within a year.

Air conditioning was installed because of severe overheating problems due in part to the number of instruments with heaters at the station. The temperature was found to be over 28°C on several occasions. The air conditioner also helped with the static problem due to lack of humidity in the station.

A major change in housing occurred when NWS decided that it would best serve its interests if GMCC were to give up the half of the duplex it occupied and be given complete control of the double-wide modular house. By October plans were drawn up by the BRW staff to remodel the double-wide house into a duplex. The BRW staff did the construction, and by the end of the year were well on the way to having half of the house done.

The clean room in the observatory was reorganized in an attempt to make more room for new projects. Power is the main concern for future expansion. Some circuits are pulling the maximum rated load, and any further expansion is impossible.

In the CAMS units, all A/D boards were adjusted. A new I/O card was installed when an old one failed. A new LED was installed because an old one burned out and caused several tape drive errors. Updated versions of the data collection programs were also installed over the course of the year.

2.2.2. PROGRAMS

Table 2.3 summarizes the measurement programs at BRW; operational highlights are as follows:

Carbon Dioxide
The bearings in the chopper motor of the URAS-2T analyzer seized, and the motor was replaced. New regulators were installed to replace the aging ones. The old regulators were becoming harder to adjust, and replacement-parts cost was prohibitive.

Flask sampling was routine for the entire year.

Methane
The CH_4 GC underwent a major upgrade in early July. A new data acquisition system and new hardware for sample selection was installed. New sample lines that run up to the top of the meteorology tower were also put in at that time. They replace the lines that ran to the rail along the top of the observatory building. The system continued to operate without incident all year.

Surface Ozone
A new Dasibi meter was installed when a power surge overloaded the power supply and caused erratic performance in the old unit.

Total Ozone
The Dobson spectrophotometer operated well most of the year. The only problem was a clock drive for the pen, which quit late in the year.

Ozone Profiles
Balloons were launched on a cut-back schedule this year. Instead of one launch per week, one was scheduled every 2 weeks.

Nitrous Oxide and Halocarbons
Several minor operational upgrades were made by station personnel. New versions of the data acquisition program were installed on two different occasions, and minor repairs were made on the exhaust plumbing to the HP GC. NOAH personnel visited the site twice for routine maintenance and upgrades.

Aerosols
An aethelometer was installed in March to measure black carbon. A high correlation has been seen between black carbon, CO_2, and CH_4 values. The aethalometer ran well all year and gave good data. Filters can also be analyzed at a later date for carbon content.

The nephelometer blower was dismantled, and all gears and bearing surfaces were cleaned and lubricated after channel 4 kept dropping out. The grease in the drive gears was dried up, causing the valve to drag and not turn to the correct position. After the cleaning, the nephelometer ran fine except for a blown fuse.

The G.E. CNC underwent the normal maintenance procedures and ran well all year.

Solar Radiation
There were no unusual occurrences, and all instruments ran fine. During the Arctic night, instruments were sent to Boulder for calibration.

Meteorology
Several record highs and several record lows were recorded this year. A new hygrothermometer that was installed in September to replace the old unit that quit earlier in the year ran fine the rest of 1988.

Precipitation
Samples were collected as available. They were sent to MLO for analysis of pH and conductivity.

Cooperative Programs
Fifteen cooperative programs were hosted at BRW during 1988. Operational highlights are listed here, and a complete listing of the cooperative programs is included in Table 2.3. This arrangement between GMCC and outside researchers is a continuing program that maximizes the talents, expertise, and

TABLE 2.3. Summary of Sampling Programs at BRW in 1988

Program	Instrument	Sampling Frequency
Gases		
CO_2	URAS-2T IR analyzer	Continuous
	3-L glass flasks	1 pair wk^{-1}
	0.5-L glass flasks, through analyzer	1 pair wk^{-1}
CO_2, CH_4, CO	0.5-L glass flasks, P^3	1 pair wk^{-1}
CH_4, CO, CO_2	Carle automated GC	1 sample (24 min)$^{-1}$
Surface O_3	Dasibi ozone meter	Continuous
Total O_3	Dobson spectrophotometer no. 91	3 day^{-1}
O_3 profile	Balloonborne ECC sonde	2 mo^{-1}
CFC-11, CFC-12, N_2O	300-mL stainless steel flasks	1 pair wk^{-1}
CFC-11, CFC-12, N_2O, CCl_4, CH_3CCl_3	HP5890 automated GC	1 sample (3 h)$^{-1}$
N_2O	Shimadzu automated GC	1 sample (3 h)$^{-1}$
Aerosols		
Condensation nuclei	Pollak CNC	1 day^{-1}
	G.E. CNC	Continuous
Optical properties	Four-wavelength nephelometer	Continuous
Black carbon	Aethelometer	Continuous
Solar and Terrrestrial Radiation		
Albedo	Eppley pyranometer and pyrgeometer	Continuous
Global irradiance	Eppley pyranometers with Q and RG8 filters	Continuous
Direct irradiance	Tracking NIP	Continuous
	Eppley pyrheliometer with Q, OG1, RG2, and RG8 filters	Discrete
Terrestrial (IR) radiation	Eppley pyrgeometer	Continuous
Turbidity	Sunphotometers with 380-, 500-, 778-, and 862-nm narrowband filters	Discrete
Meteorology		
Air temperature	Thermistor, 2 levels	Continuous
	Max.-min. thermometers	1 day^{-1}
Dewpoint temperature	Dewpoint hygrometer	Continuous
Pressure	Capacitance transducer	Continuous
	Mercurial barometer	Discrete
Wind (speed and direction)	Bendix Aerovane	Continuous
Precipitation	Rain gauge, tipping bucket	
Precipitation Chemistry		
pH	pH meter (samples analyzed at MLO)	Discrete
Conductivity	Conductivity bridge (samples analyzed at MLO)	2 mo^{-1}
Cooperative Programs		
Total surface particulates (DOE)	High-volume sampler (1 filter wk^{-1})	Continuous
Aerosol chemistry (URI)	High-volume sampler (2 filters wk^{-1})	Continuous
Aerosol chemistry (Univ. of Alaska)	High-volume filters (3 filters wk^{-1})	Continuous
Precipitation gauge (ASCS)	Wyoming shielded precipitation gauge	2 mo^{-1}
Magnetic fields (USGS)	Magnetometer	1 station check wk^{-1}
^{13}C (USGS)	10-L stainless steel flasks	1 pair mo^{-1}
Various trace gases (OGC)	Stainless steel flasks	1 set wk^{-1} (3 flasks set^{-1})
CO_2, CH_4 and other trace gases (NCAR)	3-L stainless steel flasks	1 pair wk^{-1}
^{13}C, ^{18}O, CO_2 (CSIRO)	5-L glass flasks	1 pair (2 wk)$^{-1}$
CO_2, ^{13}C, N_2O (SIO)	5-L evacuated glass flasks	1 pair wk^{-1}
Halocarbon monitoring (Univ. of Calif., Irvine)	Various stainless steel flasks	1 set (3 mo)$^{-1}$
Earthquake detection (Univ. of Alaska)	Seismograph	Continuous; check site 1 wk^{-1}, change tape 1 mo^{-1}
$^{13}CH_4$ ($^{13}C/^{12}C$) (Univ. of Washington)	35-L stainless steel flasks	1 (2 wk)$^{-1}$
NO_x, NO_y (Univ. of Alaska)	Chemiluminscence	Continuous during the summer
Ultralow frequency waves (Univ. of Tokyo)	Magnetometer	Continuous

instrumentation of both groups to engage in research efforts at a remote site. All projects are related and complementary to the general GMCC research mission.

A system to measure NO_x and NO_y was set up and run during the summer. It is expected that it will be used again during the next spring Arctic haze episode.

The sample hose for the URI filter sampler was cracked and was patched temporarily. URI was notified, and a new hose was ordered. The new hose was received and installed in November.

A filter sample project for the University of Alaska, Fairbanks, was terminated. It had been running for about 2 years.

A new rain gauge was set up this summer and the old one pulled down by USDA Soil Conservation Service/Snow Survey. The old gauge had deteriorated because of the weather.

The University of Tokyo had a recorder installed to measure ultralow-frequency waves. This is part of a USGS project to examine geomagnetics.

A new pump was required for the DOE filter sampler. A power outage caused the old pump to lock up, and it could not be restarted.

2.3. SAMOA

S. RYAN

2.3.1. OPERATIONS

SMO facilities operated well in 1988. Some upgrades were completed in the housing units; GMCC housing unit T-11 had a patio extension, a two-car carport, and an outdoor storage area constructed. A new refrigerator was installed, and some minor interior remodeling was performed.

At the observatory the main air conditioner was repaired in May, two new batteries were installed in the photovoltaic system, the EKTO UPS was repaired after a 4-mo down time, and the Dobson dome was repainted. Both vehicles performed well. The Toyota pickup truck had a rusted frame member replaced in September.

On February 28, Chief Va'a Iuli died in an automobile accident in California. He was buried alongside his brother and sister in the family plot on the lower observatory road on March 5. The monthly lease checks have been put into an escrow account pending the naming of the next Iuli title holder.

Utility power problems began anew with several severe power surges in May. Power outages increased at year's end. In December the observatory was without utility power for a total of 24 hours.

2.3.2. PROGRAMS

Table 2.4 summarizes the programs at SMO for 1988. Further discussion of some of the programs follows.

Carbon Dioxide
The system was converted from a single sampling line to dual sampling lines that are each sampled for 25 minutes each hour. The new configuration required installation of a new plumbing/switching apparatus, revised CAMS software, additional freezer traps, refrigerator cooling plumbing, and a second sampling line from Matatula Point. Conversion was completed by September.

A new Cincinnati subzero cooler was installed in February. It failed in May and had to be replaced by a Cryocool unit. In December, the chopper motor assembly in the URAS analyzer had to be replaced.

Surface Ozone
Observations continued in 1988 with Dasibi ozone meter no. 1323.

Total Ozone
In January, a desiccant drying system with a low-volume positive pressure pump was installed. After tests were performed, which showed this device to be ineffective, a higher volume recirculation system was installed in July, which has given good results. A four-observations-per-day schedule was continued throughout 1988.

Ozone Profiles
A cutback in supply shipments to Samoa reduced the number of ozonesonde flights this year. A total of 37 launches were made, and 31 (84%) provided good data. In January, two members of the Trace Gases Group visited to conduct a series of stratospheric water vapor balloon launches.

Nitrous Oxide and Halocarbons
Now into its third year, the RITS GC continued automated operations. Some modifications were made in 1988. In January, two bakeouts and an H_2 ECD conditioning were performed. Software was upgraded three times during the year, and the troublesome HP Thinkjet printer was replaced by an Epson in July. Several weeks of CFC-11 data were lost in October because of a low ambient airflow rate. In November, the system was reconfigured to allow column backflushing after each run for the halocarbons, 2 Mbytes of additional memory were added to the HP computer, and new batteries were ordered for the UPS.

Flask sampling continued on a weekly basis.

Aerosols
The four-wavelength nephelometer operated well throughout the year; occasional problems were solved by board swapping or spider removal. In March, the G.E. CNC counter calibration offset voltage was lowered to its minimum setting to reduce a high background problem. The instrument performed well in this mode throughout the rest of the year.

Solar Radiation
A new terminal box and cabling to the rooftop pyranometers was installed in May, and the tracking pyrheliometer was exchanged with a freshly calibrated unit from Boulder. A sunphotometer had to be replaced because of a faulty memory chip.

9

TABLE 2.4. Summary of Sampling Programs at SMO in 1988

Program	Instrument	Sampling Frequency
Gases		
CO_2	URAS-2T IR analyzer	Continuous
CO_2, CH_4	3-L glass flasks	1 pair wk^{-1}
	0.5-L glass flasks, through analyzer	1 pair wk^{-1}
	0.5-L glass flasks, P[3]	2 pair wk^{-1}
Surface O_3	Dasibi ozone meter	Continuous
Total O_3	Dobson spectrophotometer no. 42 or 65	4 day^{-1}
O_3 profile	Balloonborne ECC sonde	1 wk^{-1}
CFC-11, CFC-12, N_2O	300-mL stainless steel flasks	1 pair wk^{-1}
CFC-11, CFC-12, N_2O, CCl_4, CH_3CCl_3	HP5890 automated GC	1 sample (3 h)$^{-1}$
N_2O	Shimadzu automated GC	1 sample (3 h)$^{-1}$
Aerosols		
Condensation nuclei	Pollak CNC	1 day^{-1}
	G.E. CNC	Continuous
Optical properties	Four-wavelength nephelometer	Continuous
Solar Radiation		
Global irradiance	Eppley pyranometers with Q and RG8 filters	Continuous
	Eppley pyranometers with Q filters on tilted mounts	Continuous
Direct irradiance	Eppley pyrheliometer with Q filter	Continuous
	Eppley pyrheliometer with Q, OG1, RG2, and RG8 filters	Discrete
Turbidity	Sunphotometers with 380-, 500-, 778-, and 862-nm narrowband filters	Discrete
Meteorology		
Air temperature	Thermistors (2)	Continuous
	Max.-min. thermometers	1 day^{-1}
Pressure	Capacitance transducer	Continuous
	Microbarograph	Discrete
	Mercurial barometer	1 wk^{-1}
Wind (speed and direction)	Bendix Aerovane	Continuous
Precipitation	Rain gauge, weighing bucket	Continuous
	Rain guage, tipping bucket	Continuous
	Rain guage, plastic bulk	1 day^{-1}
	Aerochem wet/dry collector	1 day^{-1}
Precipitation Chemistry		
pH	Fisher model 805 meter	1 day^{-1} (GMCC); 1 wk^{-1} (NADP)
Conductivity	Beckman model RC-16C meter	1 day^{-1} (GMCC); 1 wk^{-1} (NADP)
Cooperative Programs		
CO_2, ^{13}C, N_2O (SIO)	5-L evacuated glass flasks	3 flasks wk^{-1}
GAGE project: CFC-11, CFC-12, N_2O, CH_3CCl_3, CCl_4 (OGC)	HP5880 gas chromatograph	1 h^{-1}
Various trace gases (OGC)	Stainless steel flasks	3 flasks wk^{-1} (3 flasks set^{-1})
^{13}C, ^{18}O, CO_2 (CSIRO)	5-L glass flasks	1 pair mo^{-1}
^{13}C (USGS)	10-L stainless steel flasks	2 pair mo^{-1}
Wet-dry deposition (NADP)	HASL Chemetrics wet-dry collector	1 wk^{-1}, wet; discrete, dry
Bulk deposition (EML)	Plastic bucket	Continuous (1 bucket mo^{-1})
Hi-vol sampler (EML)	High-volume sampler	Continuous (1 filter wk^{-1})
Hi-vol sampler (SEASPAN Project)	High-volume sampler	Continuous (1 filter wk^{-1})
CO_2, CH_4, trace gases (NCAR)	Evacuated stainless steel flasks	1 pair wk^{-1}
^{13}C, $^{13}CH_4$ (Argonne Lab.)	30-L evacuated steel cylinders	1 pair discrete
^4He (U.S. Bureau of Mines)	1-L pressurized steel cylinder	2 yr^{-1}

Meteorology

The meteorology program continued with the same instruments as in 1987. In July 1988, a period of 11 consecutive months of below-normal precipitation finally ended. December 1988 was the rainiest month in the 12-year Samoa record.

Precipitation Chemistry

In March the funnel/bottle collector was replaced with an Aerochem wet/dry collector. Following this change, rain samples had much lower average conductivities and the average pH rose from 4.8 to 5.2.

Cooperative Programs

The complement of cooperative programs conducted at Samoa remained unchanged in 1988.

The largest cooperative project at SMO is OGC's GAGE gas chromatography program. A new PC for data acquisition was installed in February, and it experienced some downtime from the utility power problems later in the year. A replacement terminal was installed on the HP5880 chromatograph in May.

The DOE/EML high-volume pump was replaced late in 1988 with a new unit. Filter collection continued on an uninterrupted basis all year.

2.4. SOUTH POLE

R. POSTON

2.4.1. OPERATIONS

SPO is operated in cooperation with NSF at the Amundsen-Scott South Pole Station. Located on the Polar Plateau at an elevation greater than 2.8 km above sea level and only 150 m from the geographic South Pole, GMCC's CAF samples what is probably the cleanest and most constant air mass on earth. Because of the 6-mo long day and 6-mo long night, the air shows no signs of diurnal variations in its constituents, and except for total ozone, only slight indications of seasonal variations.

Transportation of supplies and personnel to and from the South Pole is provided by the U.S. Navy Operation Deep Freeze VXE-6 squadron, which uses ski-equipped LC-130 Hercules aircraft for its polar operations. Because of the intense cold, the aircraft operations can only be maintained during the austral summer, approximately late October through mid February. As a training mission, the U.S. Air Force provides a mid-winter airdrop of materials, fresh food, and personal mail to the crew of approximately 20 winter-over personnel who otherwise spend 8.5 months of the year in seclusion from the rest of the world. The GMCC program, staffed by a two-person crew, is only one of several programs operating continuously at the South Pole.

The raising of the CAF last year has proved to be helpful in the constant battle against drifting snow accumulation around the building. The drifting and blowing snow is now far less impeded by the building's presence, and although there is still some accumulation of snow downwind of the building, most of the accumulation is now 5-10 m downwind, and not right next to the building. Also, although there is a net buildup of snow directly underneath the building, occasional shifts in wind direction actually scour this area somewhat, thus significantly slowing the accumulation there.

A new steel deck and stairway were installed in January and February. The deck provides storage space for crates of air sample flasks, calibration gas cylinders, and empty crates and boxes. These items had previously been stored on the roof, inside the building, or in the cargo storage area 0.4 km away. The lower section of stairway was originally intended to be raised when not in use and lowered as needed, but the counterbalance provided was not the correct weight. The stairs had to therefore be made fixed, instead. The upper section of stairway goes from the CAF main level to the roof, where an increasing number of experiments and apparatus are located.

Lack of good, clean power was responsible for some loss of data and equipment downtime. Power brownouts were a common occurrence, and complete blackouts occurred twice. Fluctuations in power frequency of +0.5 to +1.0 Hz caused station clocks to run fast all year, and caused some equipment failures and decreased performance. Installation of new power plant facilities are tentatively scheduled for 1990-91.

Satellite data transmissions did not always go smoothly. Because of the severely limited ATS-3 satellite window available at the South Pole and because of the many projects that require satellite data transmissions, competition for satellite time is quite keen. Only 2 years ago there was more than enough satellite time to satisfy the needs of all the research projects there, but because of the South Pole's rapidly growing popularity as a desirable location for atmospheric and astronomic research, the satellite time available has quickly become insufficient. Also contributing to the difficulty of data transmission are the problems of static noise from dry air, blowing snow, and daily aurora activity, all of which interfere with the transmission antennas. GMCC began compressing data files and sending raw binary data as a more economical data format. A new LES-9 satellite data link, scheduled to begin operation in 1989, should immensely improve this situation.

The CAMS units are still being improved each year, and there were very few problems with them this year. The major problem, occasional AUTORESTARTing of the system, was anything inherent to CAMS itself, but was caused by periodic static discharge in the dry air during periods of high winds.

2.4.2. PROGRAMS

Table 2.5 summarizes the programs at SMO. Further discussion of some of the programs follows:

Carbon Dioxide

Data acquisition with the continuous analyzer was interrupted several times by equipment failures. The most common failures were of the rubber diaphragms in the sampling pumps. The old pumps were replaced with new Air-Cadet pumps after airdrop; they proved much less prone to failure, only failing once in 4 months. The rubber diaphragms of all sampling pumps have shortened life spans at the South Pole because of the severely dry air. Another kind of failure was of the heating/cooling units inside the analyzer case. These older units were also replaced with newer versions after airdrop.

11

TABLE 2.5. Summary of Sampling Programs at SPO in 1988

Program	Instrument	Sampling Frequency
Gases		
CO_2	URAS-2T IR analyzer	Continuous
CO_2, CH_4	0.5-L glass flasks, through analyzer	1 pair twice mo^{-1}
	0.5-L glass flasks, P^3	1 pair twice mo^{-1}
Surface O_3	Dasibi ozone meter	Continuous
Total O_3	Dobson spectrophotometer no. 82	3 day^{-1}
Ozone profile	Balloonborne ECC sonde	1 wk^{-1} summer, autumn, winter
		1 (3 day)$^{-1}$ spring
N_2O, CFC-12, CFC-11, CH_3CCl_3, CCl_4	Shimadzu automated mini-2 gas chromatographs	1 sample (3 h^{-1})
	300-mL stainless steel flasks	1 pair wk^{-1} summer
CFC-12, CFC-11, N_2O	300-mL stainless steel flasks	3 wk^{-1} summer
	Shimadzu manual GC	2 analyses wk^{-1} (discontinued February 1988)
Aerosols		
Condensation nuclei	Pollak CNC	2 day^{-1}
		G.E. CNC Continuous
Optical properties	Four-wavelength nephelometer	Continuous
Carbon aerosols	Aethalometer	Continuous
Solar and Terrestrial Radiation		
Global irradiance	Eppley pyranometers with Q and RG8 filters	Continuous, summer
Direct irradiance	Eppley pyrheliometer with Q, OG1, RG2,	Discrete, summer and RG8 filters
Turbidity	Sunphotometers with 380-, 500-, 778-,	Discrete, summer and 862-nm narrowband filters
Albedo	Eppley pyranometers with Q and RG8	Continuous, summer filters, downward-facing
Terrestrial (IR) radiation	Eppley pyrgeometers, upward- and	Continuous downward-facing
Meteorology		
Air temperature	Platinum resistor, 2- and 20-m heights	Continuous
Snow temperature	Platinum resistor, 0.5 cm	Continuous
Pressure	Capacitance transducer	Continuous
	Mercurial barometer	2 times wk^{-1}
Wind (speed and direction)	Bendix Aerovane	Continuous
Frost-point temperature	Hygrometer	Continuous
Cooperative Programs		
CO_2, ^{13}C, N_2O (SIO)	5-L evacuated glass flasks	2 mo^{-1} (3 flasks sample^{-1})
Total surface particulates (DOE)	High-volume sampler	Continuous (4 filters mo^{-1})
Aerosol physical properites (SUNYA)	Pollak CNC with diffusion battery	Discrete
	Nuclepore filters	Continuous
Various trace gases (OGC)	Stainless steel flasks	Twice mo^{-1} (3 flasks set^{-1})
$^{13}C/^{12}C$, CH_4 (USGS)	10-L stainless steel cylinder	1 mo^{-1} (2 cylinders sample^{-1})
^{14}C (NOAA/ARL)	3,000 psi spheres	500 psi day^{-1}
Snow acidity (NOAA/ARL)	125-mL Nalgene flasks	1 (2 wk)$^{-1}$
Interhemispheric $^{13}C/^{14}C$ (CSIRO)	5-L glass flasks	1 or 2 flasks mo^{-1}
NO_2, O_3 (NZARP)	Spectrophotometer, data logger	Continuous for 6 wk at sunrise and sunset, and control periods in summer
CH_4, CO_2, CO (NCAR)	2.5-L steel flasks	Daily (seasonally)
Ultraviolet radiation (NSF)	UV radiometer, data logger	Discrete
NO_2 and O_3 (Univ. of Rome)	Optical lidar	Twice day^{-1}

GMCC 0.5-L flasks and SIO 5-L flasks were filled concurrently twice each month outdoors using the P³ apparatus and, on alternate weeks, they were filled using the indoor analyzer plumbing.

Surface Ozone

Dasibi no. 1328 was installed in November 1987 and worked continuously throughout 1988 without mishap. An occasional problem did occur, however, with the parallel-to-serial converter. The converter box was apparently responsible for sporadicly locking up the weekly automated calibration program. When the converter box was unplugged then plugged back in, the program would continue.

Total Ozone

Dobson spectrophotometer no. 82 was used throughout 1988 with no problems. The battery-operated clock drive was replaced with an electric driven clock in July. A minor problem that arose from the dirty station power was unstable output power from the mercury lamp. During monthly calibrations with the mercury lamp the microammeter would oscillate by ±0.5 μA, thus requiring visual averaging for the recorded reading. The oscillation could sometimes be cured by plugging the lamp power supply into another electrical outlet.

Ozone Profiles

Fifty-two successful ozonesonde flights were made; most were concentrated in September and October. Balloon tracking was limited to approximately 10 mb during the second half of the year because of a bad connection on the GMD pre-amp unit. It was originally thought that the pre-amp itself had malfunctioned, but was later determined that the problem was in a soldered connection that had vibrated loose.

Nitrous Oxide and Halocarbons

The only change in any of the GMCC projects was the implementation of automated gas chromatographs by the NOAH group, which replaced the previously manually operated system. It was discovered that drastic room temperature variations have most likely been responsible for the unacceptable spread in analysis results for the halocarbons over the past few years. An effort will be made during the 1989 summer season to correct the wide swings in room temperature.

Aerosols

The aerosol programs were kept online all year. The Pollak CNC was operated twice daily to provide calibration points for the automatic CN counter. Daily checks were performed on the G.E. CNC and calibrations were performed weekly. The four-wavelength nephelometer operated throughout the entire year with the time constant set at 7.3 hours.

Solar Radiation

The solar radiation measurements continued as usual, but experienced some problems from blown pre-amps and broken cables. Both problems seem to be common occurrences at the Pole, where the pre-amps are affected by the high static electricity and the signal cables become very brittle from the cold temperature. In addition this year, the temperature-compensated channel on the albedo pyrgeometer malfunctioned, requiring replacement of the instrument.

Meteorology

This program continued as usual, but it was not possible to correctly calibrate the frost-point hygrometer. Brittle, broken signal cables were also a problem and resulted in several days of temperature data loss on at least three different occasions.

Cooperative Programs

Two new cooperative programs required access holes to be cut into the roof of the CAF. The first was the University of Rome optical lidar. Its main purpose is to record the presence of polar stratospheric clouds during the Antarctic winter and spring. The receiving telescope for the lidar required a 1-m² hole with a chimney-like hatch above the roof. The lid of the hatch is swung open from above when the lidar is in operation. The chimney blocks much of the blowing snow from entering the hatch, and also provides a slightly warmed airspace that slows frost accumulation on the glass pane that separates outside air from room air. It was originally thought that an air-blowing system would be required to prevent frost buildup on the glass, but in practice it was discovered that no blower is needed as long as the outside lid is kept closed while the lidar is not in use.

The lidar's Nd-YAG laser operates at the 53.2 nm wavelength. Combined with a 0.5-m-diameter reflecting telescope, the lidar produces 30-m resolution at the lower levels and 75-m resolution at the upper levels to approximately 20 km above sea level. In its first year of operation the instrument recorded the presence of polar stratospheric clouds throughout most of the austral winter and into the early spring.

The other new program that required a roof access was the NSF-sponsored UV-B monitoring program. The instrument detector is housed in a 1.2 m × 1.5 m × 1.5 m rooftop enclosure that provides "crawl space" access by station personnel for maintenance. The purpose of this project is to monitor the flux of UV-B radiation, particularly during the period of ozone depletion.

The other cooperative programs continued as in the past and without notable incident (Table 2.5).

2.5. REFERENCES

Bodhaine, B. A., and R. M. Rosson (Eds.), *Geophysical Monitoring for Climatic Change, No. 16: Summary Report 1987*, 110 pp., NOAA Environmental Research Laboratories, Boulder, CO, 1988.

3. Aerosols and Radiation Monitoring Group

B.A. BODHAINE (Editor), J.J. DELUISI, E.G. DUTTON, D.U. LONGENECKER, D.W. NELSON, P. REDDY, AND R. STONE

3.1. CONTINUING PROGRAMS

3.1.1. SURFACE AEROSOLS

The aerosol monitoring program at BRW, MLO, SMO, and SPO continued during 1988 as in previous years. CN concentration was measured continuously with a G.E. CN counter, and daily calibration points were provided by a Pollak CN counter at each station. Aerosol scattering extinction coefficient (σ_{sp}) at the 450-, 550-, 700-, and 850-nm wavelengths was measured continuously at each station with a four-wavelength nephelometer.

Additions to the routine aerosol monitoring program during 1988 included an aethalometer for the continuous measurement of carbon aerosol at BRW, and a new TSI alcohol-based CN counter at MLO. An aethalometer has been operating at SPO since December 1986, and another instrument will be installed at MLO in 1989. New alcohol-based CN counters will be installed at BRW, SMO, and SPO in 1989. After a 1-yr overlap of the new CN counter with the G.E. CN counter at each station, the G.E. CN counters will be retired.

Figure 3.1 shows daily geometric means of CN concentration (lower portion of each plot), σ_{sp} (middle portion of each plot), and Angstrom exponent α (upper portion of each plot) at the GMCC stations for 1988. Three independent values of Angstrom exponent were calculated from the σ_{sp} data using the relation $\alpha = -\Delta \log \sigma_{sp} / \Delta \log \lambda$. The interpretation of α in terms of aerosol size distribution was discussed by *Bodhaine and DeLuisi* [1985]. Monthly geometric means of the 1988 aerosol data are listed in Table 3.1. A graphical presentation of the monthly geometric means of the entire data record for the four stations is shown in Figure 3.2.

The BRW data in Figure 3.1 show a σ_{sp} maximum of about 2×10^{-5} m^{-1} at the beginning of April, typical of the well-known springtime Arctic haze. However, chronic problems with the BRW nephelometer during some of 1988 produced a rather sparse data set. The BRW long-term record shown in Figure 3.2 clearly shows this annual cycle in σ_{sp}. The BRW CN record shows a more variable semiannual cycle, having a maximum that usually coincides with the maximum in σ_{sp} and another maximum in about September.

The MLO σ_{sp} data shown in Figure 3.1 are atypical because of the unusually low values in April and the unusually high values in fall and winter. A maximum is expected in April, as well as in May, that is caused by the long-range transport of Asian desert dust in the upper troposphere to the vicinity of

TABLE 3.1. Monthly Geometric Means of CN Concentration (cm^{-3}) and σ_{sp} (m^{-1}) at 450, 550, 700, and 850 nm, for BRW, MLO, SMO, and SPO During 1988

	Jan.	Feb.	March	April	May	June	July	Aug.	Sept.	Oct.	Nov.	Dec.
BRW												
CN	168	220	363	318	127	389	462	592	490	132	78	138
σ_{sp} (450)	8.07-6	1.29-5	1.81-5	1.81-5	5.54-6	3.47-6	5.70-6	2.61-6		1.60-5	9.25-6	1.35-5
σ_{sp} (550)	7.24-6	1.17-5	1.59-5	1.54-5	4.51-6	2.97-6	5.10-6	2.39-6		1.60-5	7.76-6	1.22-5
σ_{sp} (700)	4.98-6	8.11-6	1.04-5	9.71-6	2.80-6	1.99-6	3.74-6	1.72-6		1.29-5	4.89-6	8.19-6
σ_{sp} (850)	3.58-6	5.88-6	7.13-6	6.49-6	1.82-6	1.52-6	2.91-6	1.36-6		1.13-5	3.29-6	6.01-6
MLO												
CN	211	201	221	155	222	189	250	254	241	302	196	189
σ_{sp} (450)	1.83-6	2.43-6	2.49-6	1.96-6	3.56-6	1.41-6	1.94-6	1.48-6	2.47-6	3.04-6	2.80-6	
σ_{sp} (550)	1.37-6	1.85-6	1.91-6	1.46-6	2.86-6	1.10-6	1.38-6	1.01-6	1.80-6	2.13-6	1.98-6	
σ_{sp} (700)	9.30-7	1.29-6	1.38-6	1.01-6	2.18-6	8.20-7	9.18-7	6.55-7	1.18-6	1.35-6	1.24-6	
σ_{sp} (850)	8.48-7	1.11-6	1.26-6	9.21-7	1.98-6	7.55-7	7.80-7	5.43-7	9.60-7	1.13-6	1.04-6	
SMO												
CN	237	334	305	282	255	221	240	238	268	304	243	292
σ_{sp} (450)	1.56-5	1.54-5	2.02-5	1.42-5	1.93-5	1.60-5	2.41-5	2.01-5	2.22-5	1.54-5	1.14-5	1.66-5
σ_{sp} (550)	1.51-5	1.49-5	1.95-5	1.39-5	1.90-5	1.57-5	2.45-5	2.03-5	2.23-5	1.47-5	1.09-5	1.59-5
σ_{sp} (700)	1.52-5	1.50-5	1.95-5	1.41-5	1.94-5	1.61-5	2.59-5	2.12-5	2.32-5	1.46-5	1.07-5	1.57-5
σ_{sp} (850)	1.60-5	1.58-5	2.07-5	1.49-5	2.04-5	1.72-5	2.81-5	2.31-5	2.50-5	1.53-5	1.12-5	1.65-5
SPO												
CN	146	95	91	37	18	17	17	16	39	86	90	147
σ_{sp} (450)			2.74-7	3.20-7	2.31-7	2.63-7	5.17-7	6.58-7	4.56-7	4.55-7	6.00-7	3.47-7
σ_{sp} (550)			1.46-7	2.04-7	1.45-7	1.75-7	3.92-7	5.08-7	3.20-7	2.89-7	3.86-7	2.27-7
σ_{sp} (700)			7.08-8	1.09-7	7.67-8	9.42-8	2.33-7	3.41-7	2.15-7	1.80-7	2.23-7	1.19-7
σ_{sp} (850)			5.70-8	7.03-8	4.75-8	5.58-8	1.57-7	2.53-7	1.84-7	1.05-7	1.42-7	9.23-8

A compact exponential format is used for σ_{sp} such that 8.07–6 = 8.07×10^{-6}.
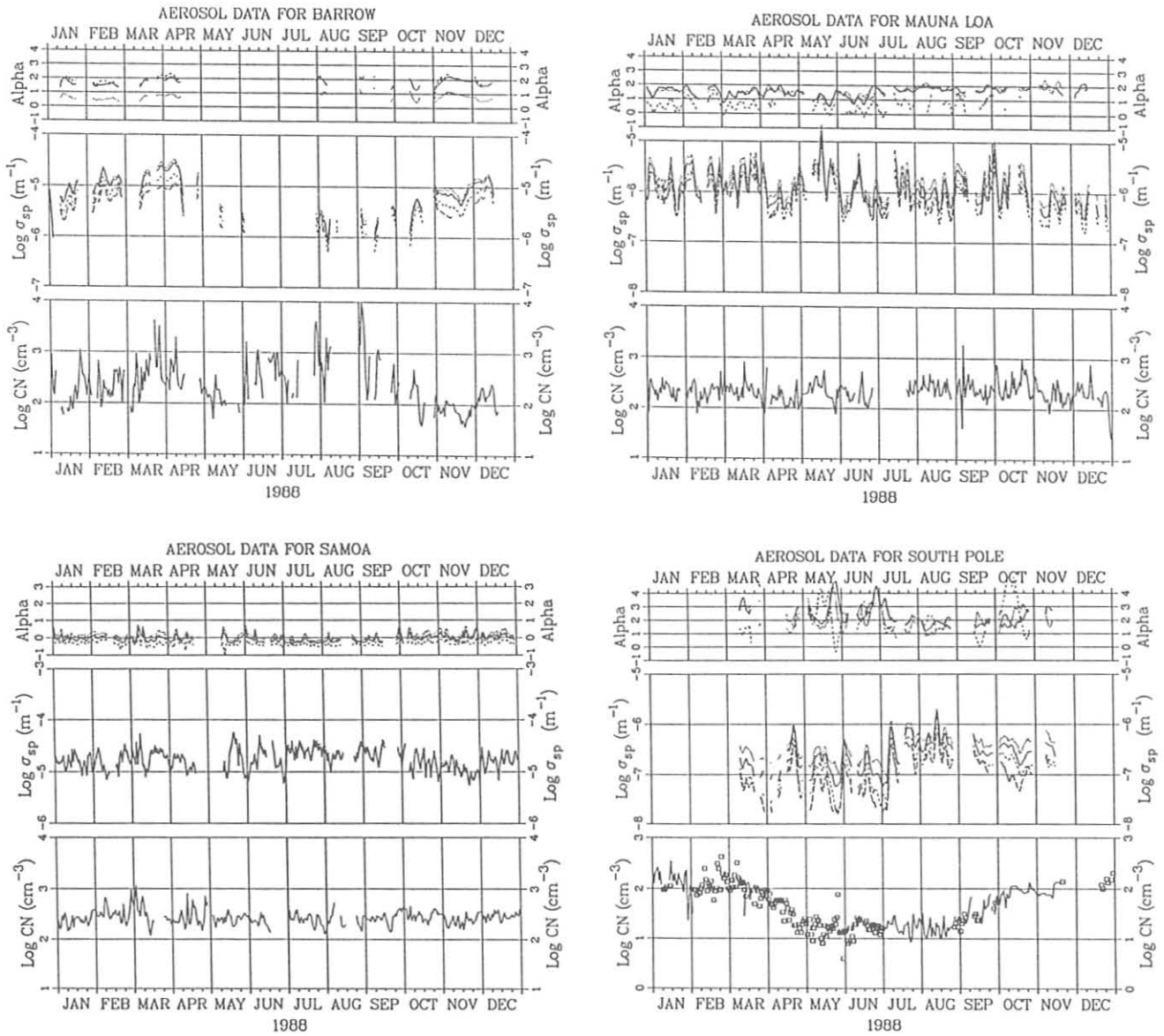
Fig. 3.1. Daily geometric means of σ_{sp} and CN data, and Angstrom exponents, at BRW, MLO, SMO, and SPO, for 1988. Data for MLO are included only for 0000-0800 LST. For each station, CN concentration (bottom) is shown as a solid line; σ_{sp} data (middle) are shown for 450 (dotted), 550 (solid), 700 (dashed), and 850 nm (long-dashed); Angstrom exponents (alpha, top) were calculated from 450- and 550-nm (dotted), 550- and 700-nm (solid), and 700- and 850-nm (dashed) σ_{sp} data. The σ_{sp} data for 850 nm and Angstrom exponent data for 700-850 nm are not shown for MLO. The CN data represented by squares for SPO are from the Pollak CN counter.

Hawaii. The σ_{sp} values have been generally higher since the installation of the new nephelometer in 1985, and have not reached the low values expected in winter. An experiment is being planned in which a high-sensitivity nephelometer will be located at MLO during winter months for a comparison with the MLO instrument. This should help determine if the new MLO instrument is less sensitive than the old one or if σ_{sp} has generally increased at MLO. The MLO CN annual geometric mean for the data shown in Figure 3.1 is 216 cm^{-3}, probably representative of the background midtroposphere in that region.

The SMO σ_{sp} and CN data continue as in previous years with no significant annual cycle or long-term trend. The SMO 1988

annual mean is about 1.68×10^{-5} m^{-1} for σ_{sp} (550) and about 266 cm^{-3} for CN concentration, representative of the background marine boundary layer in that region. A detailed analysis of the entire SMO data record was presented by *Bodhaine and DeLuisi* [1985].

The SPO CN data (Figure 3.1) show a strong annual cycle, reaching a maximum of about 200 cm^{-3} in the austral summer and a minimum of about 10 cm^{-3} in the winter. Because of severe instrument problems with the SPO G.E. CN counter, the missing CN data were filled with daily means from the Pollak CN counter. Instrument problems with the SPO nephelometer caused loss of data for the entire months of January, February,
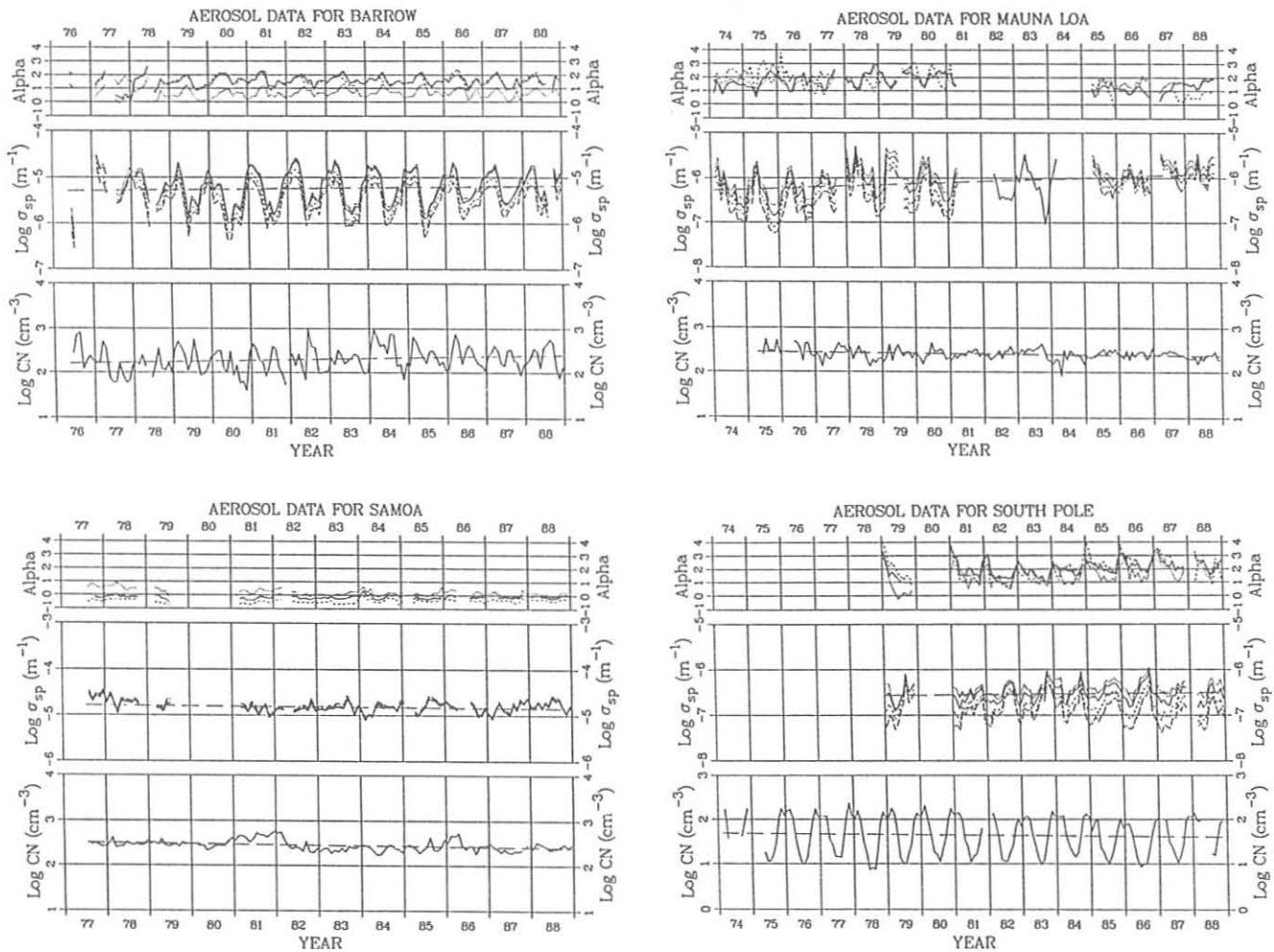
15

Fig. 3.2. Monthly geometric means of σ_{sp} and CN data, and Angstrom exponents, for the entire data record. Details of the trend lines are given in Table 3.2.

December. However, the σ_{sp} cycle, strikingly different from the CN cycle, is still evident. The σ_{sp} data generally show intermediate values in the austral summer, a minimum in May, and large events, sometimes exceeding 10^{-6} m^{-1}, in late winter. These large aerosol events (such as occurred in early July and late August in Figure 3.1) are caused by the transport of sea salt in the upper troposphere from stormy regions near the Antarctic coast to the interior of the continent. Analyses of the SPO data were presented by *Bodhaine et al.* [1986, 1987].

The least-squares trend lines shown in Figure 3.2 were calculated using the common logarithms of the monthly means of the entire data record, and the results are given in Table 3.2. Similar trend lines have been calculated and presented in previous *GMCC Summary Reports*. The long-term trends are still not statistically significant compared with the standard error about the regression line, suggesting that there is no long-term trend in the background aerosol measured at these four stations.

3.1.2. SOLAR AND THERMAL RADIATION

Introduction

Surface radiation budget, atmospheric transmission, and aerosol remote sensing measurement projects at the four GMCC observatories continued through the year, and only minor modifications were made in the measurement systems. Table 3.3 shows the current observatory radiation projects. Another ongoing project is the surface radiation budget measurements made at the top of the 300-m BAO tower near Erie, Colorado. Also, a new temporary surface radiation measurement project was planned for the island of Kwajalein in the Marshall Islands. Processing and analysis of the data acquired during the year is well under way. Results of these and other ARM radiation projects during past and previous years have been used in numerous studies of surface radiation budget characteristics, light-sensitive atmospheric

TABLE 3.2. Least-Squares Trend Analysis of the Common Logarithms of the Data Shown in Figure 3.2*

TABLE 3.2. Least-Squares Trend Analysis of the Common Logarithms of the Data Shown in Figure 3.2*

	Parameter	Slope	Intercept	S.E.	Trend (% yr^{-1})
BRW	CN	0.0156	1.01	0.288	3.66
	σ_{sp}	0.00896	−5.98	0.365	2.08
MLO	CN	−0.00624	2.93	0.125	−1.43
	σ_{sp}	0.0255	−8.17	0.313	6.5
SMO	CN	−0.00964	3.25	0.110	−2.20
	σ_{sp}	−0.00554	−4.36	0.118	−1.27
SPO	CN	−0.00593	2.14	0.429	−1.36
	σ_{sp}	0.00660	−7.10	0.189	1.53

*The time axes in Figure 3.2 are in fractional years, with a data point centered at the center of a month; e.g., Jan. 1974 = 74.042; Feb. 1974 = 74.125.

TABLE 3.3. Current Radiation Measurements at GMCC Observatories

	SWD	SWU	LWD	LWU	RG8D	DIRQ	FWNIP	SPHTM	MISC
BRW	X	X	X	X	X	X	X	X	O
MLO	X	O	O	O	X	X	X	X	X
SMO	X	O	O	O	X	X	X	X	O
SPO	X	X	X	X	X	X	X	X	X

X, measurements made; O, measurements not made; SWD, shortwave downward solar irradiance; SWU, shortwave upward (reflected) solar; LWD, longwave downward (sky emitted); LWU, longwave upward (earth emitted); RG8D, downward solar (RG8 filter, 0.7 to 3.0 μm) irradiance; DIRQ, direct solar; FWNIP, filter wheel normal incidence pyrheliometer (discrete observations, four solar bands); SPHTM, multiwavelength sunphotometer; MISC, miscellaneous—MLO: global diffuse solar, downward solar (OG1 filter, 0.53 to 3.0 μm), 2-channel sunphotometer (water vapor), 3-channel sunphotometer (calibration standard); SPO: RG8 albedo, direct sun (RG8 filter).

chemical reactions, satellite algorithm verification, climatic impact of volcanic eruptions, climatic trends and variability, errors in ozone remote sensing, surface optical properties, cloud optical properties, radiative transfer calculation verification, instrument development and improvement, and solar energy assessment and utilization. All acquired data from these studies are available in the form of various reports and publications and/or directly from the ARM radiation project leader.

Observatory Activities

At BRW improvements were made to the forced-air system used to prevent ice buildup on the pyranometer domes. The print and stripchart quality of the HP backup data system was improved by adding a moisture source in the vicinity of the printer head, thus making the charts and daily summary reports more reliably legible. The solar instruments were returned to Boulder during the sundown months for recalibration and inspection.

The MLO diffuse pyranometer no. 12502 failed in March during a lightning storm and was replaced in April by pyranometer no. 11749. The automated solar tracking dome, in which continuous recording sunphotometers are housed, operated precariously during the year with occasional unexplained failures, but it still captured about 90% of the useful data periods including unattended operation on the weekends.

SMO continues to be a severe testing site for radiation instrumentation, where weather-tight instruments absorb moisture, spectral filter material provides a culture for various fungal and bacterial decay, and calibration constants drift three to four times faster than specifications. Nonetheless, the program is maintained with relatively frequent instrument exchanges and calibration corrections.

At SPO upward-facing pyranometer no. 12271 was replaced by no. 12272 in January 1988. Pyranometer no. 12271 had demonstrated an extremely steady calibration over the past decade, but the base plate had become warped, making leveling impossible. The downward-facing pyrgeometer no. 23215 was

replaced by no. 24333 in November 1988, after the battery-powered circuit failed. Because the pyrgeometer provides the field personnel with "quick look" quality control capability, it was replaced even though the battery circuit is not used in the final data analysis. The rack on which the downward-facing instruments are located, about 90 m grid NE of the CAF, was replaced in December 1988 with a very sturdy, newly designed unit. The rack unit should overcome earlier problems due to unstable instrument mounting points and great difficulty in constantly raising the rack to maintain a constant height above the snow surface. The new rack is designed to keep the instruments 2-2.5 m above the surface.

Example Results

For the past 8 years, nominally once a month, a comparison has been made between direct solar beam measurements made by an ACR and those made by the on-line continuous tracking pyrheliometer (NIP) at MLO. The ratio of NIP/ACR data is shown in Figure 3.3. Each point results from the average of 12 ACR observations made 15 seconds apart and a simultaneous 3-min average NIP observation. If more than one 3-min comparison is made within a month, all results are averaged to obtained the plotted point for the month. The long and short dashed lines indicate the mean and ±2 standard deviations of the data excluding the three very low points in 1984-1985. Although several rather large excursions are seen in the record, the long-term stability of the relative calibration of the two instruments is indicated to better than ±0.1%. Some of the larger excursions in the record are related to electrical measurement problems with the ACR.

The relative transmission of the atmosphere over MLO, commonly called "apparent transmission," is monitored using a procedure developed by *Ellis and Pueschel* [1971]. The record since 1957 has been shown to be very sensitive to small changes in the absolute atmospheric transmission and reveals the effects of many volcanic eruptions and other aerosol events, as discussed by *Mendonca et al.* [1978]. The most recent published account of the MLO relative transmission record, its water vapor sensitivity, and its physical interpretation was given
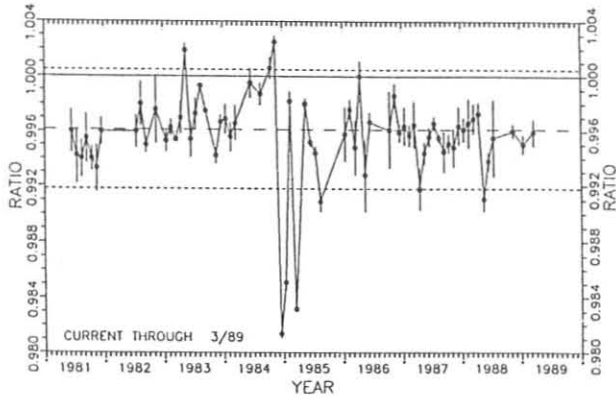
17

Fig. 3.3. Time series of the ratio between the continuous tracking NIP and the ACR determinations of the direct solar beam at MLO. The comparisons were made sporadically; each plotted point represents an average for a given month. The mean and 2 standard deviations of all the points, excluding the three lowest, are represented by the dashed lines.

by *Dutton et al.* [1985]. The complete record through 1988 is given in Figure 3.4. The dramatic effect of the 1982 El Chichòn eruption and the long recovery are evident in Figure 3.4. The effects of the El Chichòn aerosol on the different components of solar radiation (direct, diffuse, and total) at MLO were given by *Dutton and DeLuisi* [1987].

3.1.3. SOLAR RADIATION FACILITY

Delivery of the final complement of new solar trackers for the NOAA network was completed during the first quarter. Installation of the first tracker was completed during February, at Grand Junction, Colorado. The second unit was sent to Columbia, Missouri. By the end of the year, approximately one-third of the network was equipped with the new units.
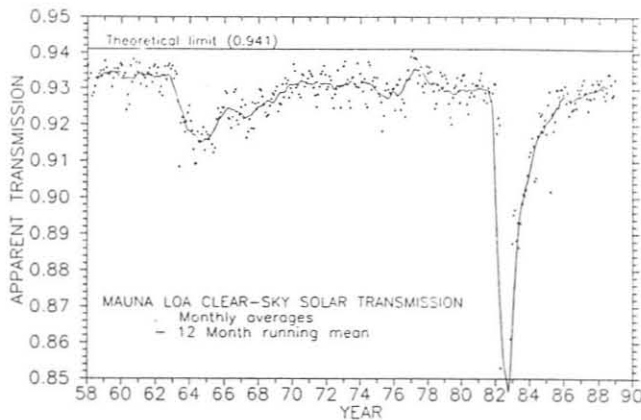

Fig. 3.4. Time series of the MLO apparent atmospheric transmission. The theoretical limit is determined from a LOWTRAN modeled case with no aerosol and average MLO water vapor and ozone. The theoretical limit could be exceeded for a very dry and low aerosol case.

Initial installation sites were selected on the basis of minimal facilities modification requirements, and coordination with NWS regional facilities offices delayed installation of subsequent units. All new trackers are operated in Boulder prior to field site shipment, and records of tracking performance are created for each unit's permanent file. Tracking accuracy of the new units has been excellent.

In addition to the new tracker checkout and installation activities, usual SRF support of the NOAA SOLRAD network was maintained throughout the year. Replacement sensors were provided when required, and support of the older equatorial mount trackers was continued.

The Boulder SOLRAD sensors and data acquisition system operated the entire year, as did the sensors and acquisition hardware for the entire network. The year 1988 represented the first complete year of SOLRAD network data acquisition using the new PC-based data acquisition system. Dial-up access to the on-line SOLRAD network data residing on the Climate Analysis Center computers was established in August 1988, and plotting software developed in Boulder allows plotting of daily network data for AFOS-equipped sites. Non-AFOS sites are collecting data for monthly periods on floppy disks.

Plots of 1988 Boulder SOLRAD global and normal incidence (direct beam) radiation as daily sums are shown in Figure 3.5. A plot of the 1988 daily sums for the diffuse component is also shown.

Standards activity during 1988 involved comparisons of SRF ACRs for repeatability of historical ratios, intercomparisons with the SERI reference ACRs, and examination of historical ratios. No significant drifts were noted. A WMO-sanctioned Region IV pyrheliometer comparison is scheduled for April 1989 in Ensenada, Mexico, and the NOAA reference, TMI no. 67502 will be taken there for comparison with a reference ACR from the world standard group in Davos, Switzerland.

SRF calibration efforts for pyranometers focused on developing data analysis software for more thorough examination of sensor characteristics. Complete characterization data can be obtained for any sensor for any day, and plots can be generated to illustrate any sensor response curve. In addition, a complete bench-top electronic calibration system was acquired for future use as a DC voltage reference standard for the facility.

3.1.4. TURBIDITY

The number of monitoring sites in GMCC's United States Turbidity Network declined from 17 to 16. [The terms turbidity and aerosol optical depth are used interchangeably in this text, and both refer to the base e formula for aerosol optical depth.] The NWS closed its station at Salem, Illinois, in November. Twelve of the remaining 16 stations continued to send data to GMCC in Boulder for reduction and processing. Sunphotometers at Sterling, Madison, Raleigh, and Lander, however, were used primarily for quality control of pyrheliometric data. Turbidity measurements also continued at the four GMCC baseline stations. In addition, a five-channel Mainz II handheld sunphotometer was put into service at Poker Flat, Alaska, during March. Poker Flat is the third ADN station
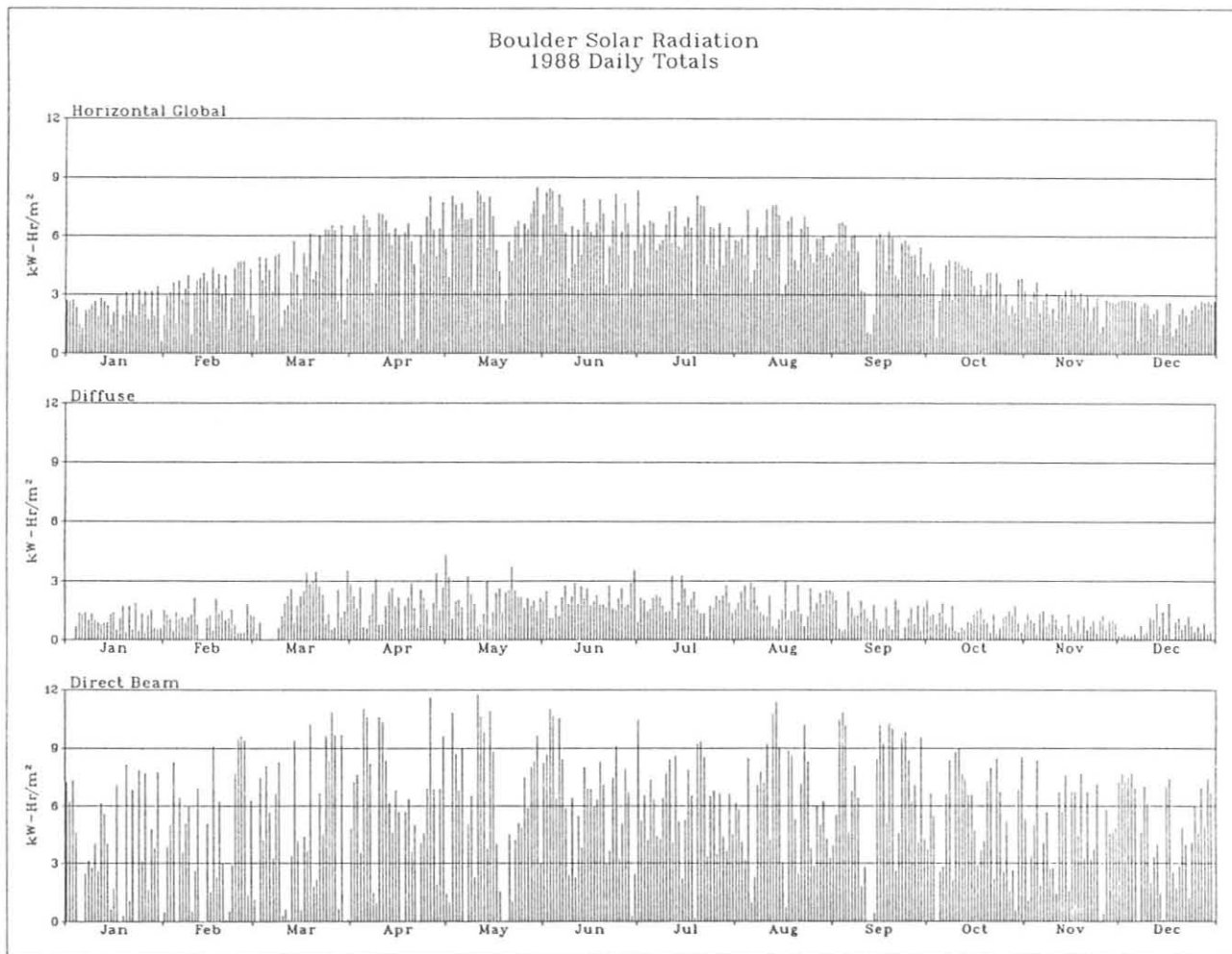
Fig. 3.5. Daily totals for global, diffuse, and direct beam irradiance at SRF in Boulder during 1988. A pyranometer, a continuously shaded pyranometer, and a pyrheliometer were used, respectively, to collect the data.

to be equipped with a sunphotometer. Another Mainz II instrument was shipped to Australia in November for eventual installation at the ADN station at Perth. Table 3.4 lists the 23 stations and the wavelengths at which turbidity was measured.

GMCC also collected turbidity data in conjunction with five experiments conducted during 1988. These experiments are listed in Table 3.5. Most of the data from these experiments have been processed. A plot of aerosol optical depths measured on the NOAA/RITS/CO_2 cruise is presented in Figure 3.6. The data show higher levels of turbidity in the northern hemisphere and very low levels in the intertropical convergence zone and the southern hemisphere. Analysis of data from these studies continues.

Approximately 184 sunphotometer calibrations were completed in 1988; 61 were performed in the mountains west of Boulder, Colorado, and 123 at MLO. All calibrations were by the Langley plot method and were conducted at elevations of 2.8 and 3.4 km above sea level. Boulder Turbidity Project staff participated in the MLO calibration activities during March and

April. During this time, it was noted that sunphotometers frequently experienced a temperature increase of 10° to 25°C during the course of Langley plot observations. Subsequent analyses have indicated that this can result in a bias of about −1% to −1.5% for 380-nm calibrations and −0.5% for calibrations at 500 nm. Efforts to correct past MLO calibrations and the data sets based on these continued at the time this report was prepared. Instrument temperatures are now more carefully controlled during MLO Langley plot observation sessions.

Four Mainz II sunphotometers were returned to the plant in Germany for warranty repairs and remained there for most of the year. Mainz II problems contributed to delays in installing sunphotometers at the remaining ADN stations.

GMCC had 65 sunphotometers on hand in 1988. Because of the need for improved instruments, the aging of J-series sunphotometers, and difficulties with 9 Mainz II sunphotometers, work continued on the design and construction of 10 K-series sunphotometers. A prototype was built and tested during the summer. Most of the design and construction of the

TABLE 3.4. GMCC Turbidity Monitoring Sites and Filter
Wavelengths for Sunphotometers Used at Each Site

Station	Sunphotometer Wavelength (nm)
Barrow, AK*	380, 500, 778, 862
Mauna Loa, HI*†	380, 500, 778, 862
Samoa*	380, 500, 778, 862
South Pole*	380, 500, 778, 862
Alamosa, CO*	380, 500
Atlantic City, NJ	380, 500
Boulder, CO	380, 500, 778, 862
Bismarck, ND	380, 500
Caribou, ME*	380, 500
Ely, NV	380, 500
Haute Provence, France†	380, 412, 500, 675, 862
Huron, SD	380, 500
Lander, WY‡	380, 500
Las Vegas, NV	380, 500
Madison, WI‡	380, 500
Meridian, MS*	380, 500
Poker Flat, AK†	380, 412, 500, 675, 862
Raleigh, NC‡	380, 500
Salem, IL*§	380, 500
Salt Lake City, UT	380, 500
Sterling, VA‡	380, 500
Tallahassee, FL	380, 500
Victoria, TX*	380, 500

*BAPMoN stations.
†ADN stations.
‡Not yet reporting data as part of the Turbidity Network.
§Closed in November 1988.

TABLE 3.5. Experiments Incorporating GMCC
Sunphotometer Observations

Experiment	Description/Turbidity Project Involvement
NOAA/RITS/CO$_2$ Cruise	North-south cruise from the North Pacific to the South Pacific. Turbidity measurements were made to complement ocean aerosol studies and aid in ground-truthing of satellite observations of aerosol optical depths.
Esperanza del Mar Hospital Ship Spain Cruise	Cruise in the area of the Canary Islands off the northwest coast of Africa. Turbidity measurements were made to aid in ground-truthing of satellite observations of aerosol optical depths. NOAA/NESDIS staff performed measurements.
NOAA *Mt. Mitchell* Global Cruise	Cruise circumnavigating the North Atlantic. Turbidity measurements were made to complement ocean aerosol studies and aid in ground-truthing of satellite observations of aerosol optical depths.
Chesapeake Bay Cruise	Brief cruise of the Chesapeake Bay. Turbidity measurements were made to aid in ground-truthing of satellite observations of aerosol optical depths. NOAA/NESDIS staff performed measurements.
Yellowstone Fire Smoke Study	Extensive sunphotometer observations made in Boulder (and east of Boulder) during August and September to characterize smoke aerosols from forest fires in Yellowstone National Park and in Boulder County.

mechanical parts for 10 K-series instruments had been finished by the end of 1988. A full-scale circuit had been assembled, tested, and corrected by the end of the year. Fifty-five EG&G detector-filter-amplifier modules to be used in the sunphotometers were returned for warranty repairs in the fall of the year.

A summary of station data processed to date is given in Figure 3.7. A major improvement in instrument quality and calibration accuracy occurred from 1982 through 1984. Most of the data collected prior to 1982 are of unknown quality, but are expected, in many cases, to be of low accuracy. For example, reconstruction and reanalysis of Boulder data for 1978-1980 and MLO data for the 1970's indicated it to be of generally poor quality.

Data for Boulder (see Figure 3.8) and most other continental U.S. stations continue to show a clear annual cycle with maxima in the spring or summer months and minima during November, December, or January. The impact of the El Chichòn eruption in 1982 is evident at many stations. Data for most GMCC stations in the northern hemisphere indicate that the El Chichòn stratospheric aerosol cloud had an optical depth of approximately 0.10 (at 380, 500, 778, and 862 nm) during early 1983. The decay of the El Chichòn signal appears as a slow downward trend in optical depths since the beginning of the record in early 1983, and this decay continued in 1988. The elevated optical depths associated with smoke from forest fires in Yellowstone and in Colorado are evident in the expanded view of Boulder data for 1988 in Figure 3.9.

BRW data are presented in Figure 3.10. It is believed that BRW data have a maximum bias of about 0.01 to 0.015 at 380 nm because of a temperature-dependent bias in calibrations obtained at MLO. The temperature dependent bias is believed to be negligible at 778 nm. Arctic haze events in the spring shift the maximum in the annual cycle to early spring.

As indicated in the 1987 Summary Report [*Bodhaine and Rosson*, 1988], the SPO staff formerly made sunphotometer observations through an open window in the CAF. Cold air pouring into the heated room caused density discontinuity waves in the air around the window. Sunlight was apparently focused in some areas of the wave field, and the peak-hold feature of the sunphotometer stored the maximum signal received within the measurement period. This resulted in an artificially high reading and correspondingly low computed optical depth. This phenomenon has been duplicated at Boulder during observations made in subfreezing weather near a building air exit vent on the roof of the ERL building. The 1988-1989 SPO crew took one observation from outside the open window of the CAF for each
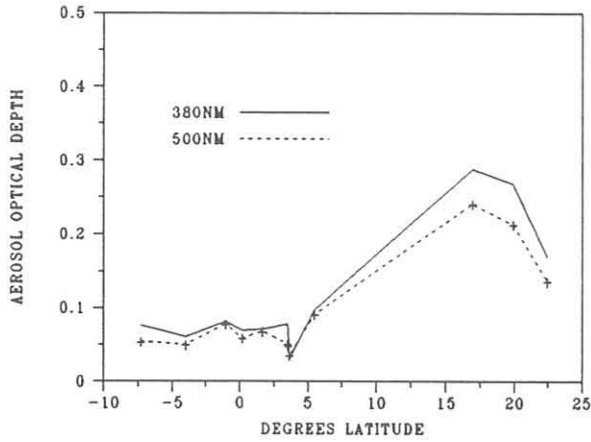
Fig. 3.6. Aerosol optical depths at 380 nm and 500 nm measured on the NOAA/RITS/CO$_2$ cruise.

observation taken from inside the building. Figure 3.11 shows a sample of aerosol optical depths computed from these observation pairs. The data appear to confirm the hypothesis that readings from within the CAF are often elevated and yield erroneous, lower optical depths. About half of the data obtained from within the building compare well with those obtained from outside. This distribution of apparently valid and erroneous optical depths for measurements made inside suggests a method for reconstructing the SPO record for years when readings were made from within the CAF.
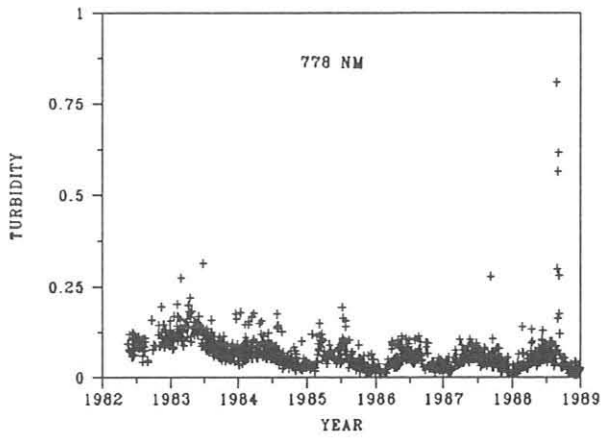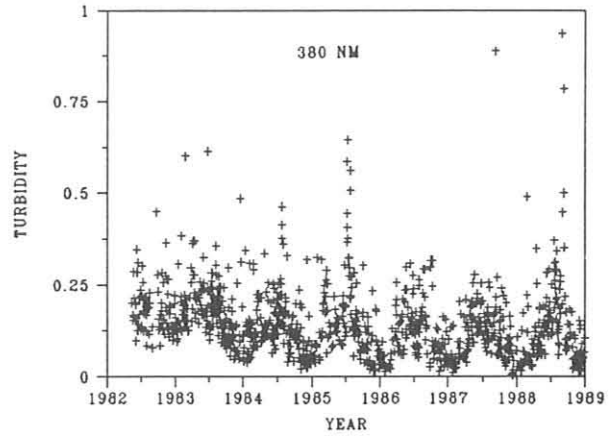
Fig. 3.8. Daily average aerosol optical depths at 380 nm (upper) and 778 nm (lower) for Boulder during 1988.

Fig. 3.7. Status of turbidity data from the U.S. network and GMCC baseline stations.

Fig. 3.9. Daily average aerosol optical depths at 380 nm for Boulder during 1988, showing forest fire smoke events in August and September.

Fig. 3.10. Daily average aerosol optical depths at Barrow for 380 nm (left) and 778 nm (right).
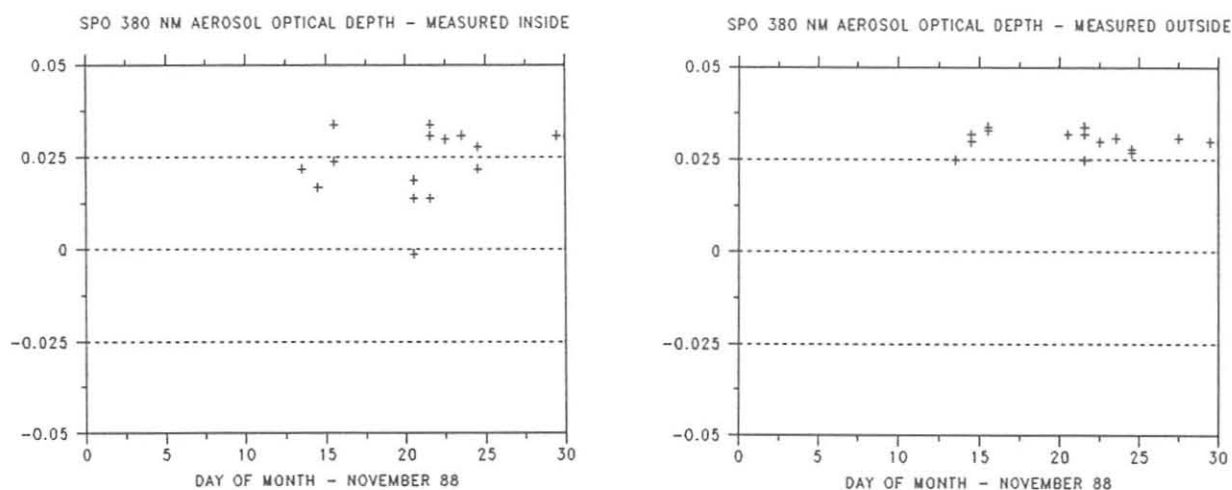
Fig. 3.11. SPO 380-nm aerosol optical depths measured from within the CAF through an open window and from outside the CAF.

3.2. SPECIAL PROJECTS

3.2.1. SPO AEROSOL MEASUREMENTS DURING 1987

Introduction

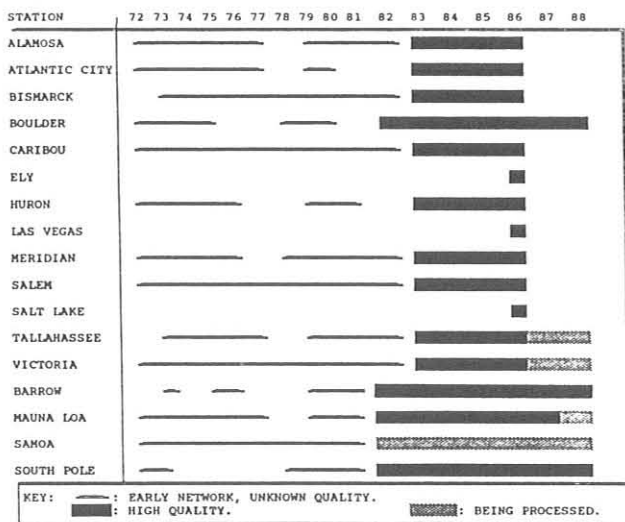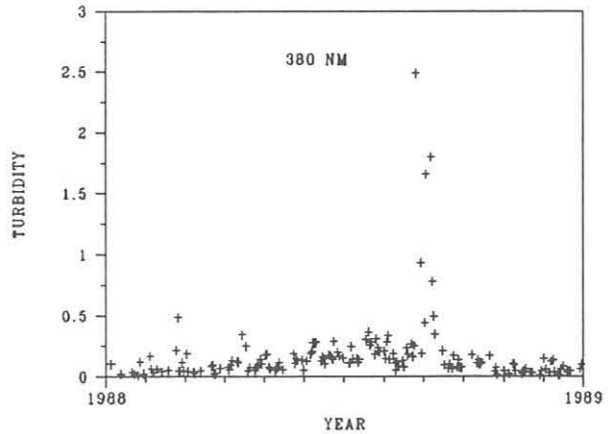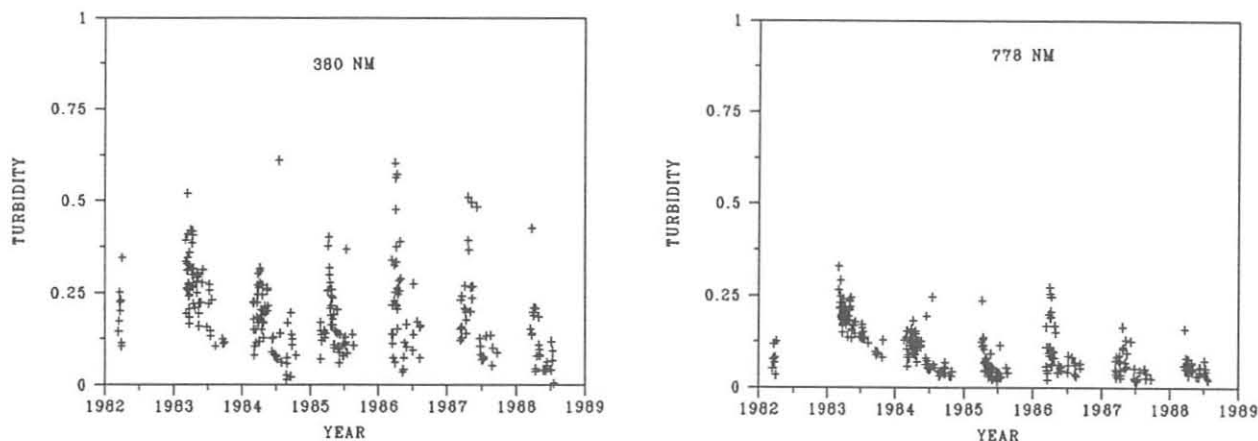The first year of σ_{sp} data from SPO, presented by *Bodhaine and Bortniak* [1981], showed an annual cycle strikingly different from the CN record, being dominated by sea salt events in the austral winter. An aerosol chemistry experiment was conducted during 1982, and the results were presented by *Bodhaine et al.* [1986, 1987].

In 1987 a more extensive aerosol experiment was conducted that included aerosol filter samples for PIXE analysis, aerosol size distribution measurements in the Aitken size range, and aerosol black carbon measurements. Results of the 1987 experiment are presented here.

Instrumentation

CN concentration is measured continuously with a G.E. automatic CN counter [*Skala*, 1963]. Calibration points for the automatic CN counter are obtained twice daily with a Pollak CN

counter [*Metnieks and Pollak*, 1959]. The operation and calibration of the automatic instrument at the South Pole were discussed by *Bodhaine and Murphy* [1980].

A four-wavelength nephelometer similar in design to that of *Ahlquist and Charlson* [1969] measures σ_{sp} continuously with approximately 4-h time resolution at the wavelengths 450, 550, 700, and 850 nm. The σ_{sp} measurements are most sensitive to particles having diameters in the 0.1- to 1.0-μm diameter range (the accumulation mode) whereas CN concentrations tend to be dominated by particles smaller than 0.1-μm diameter (the Aitken mode). Since particles in the 0.1- to 1.0-μm range tend to dominate the total background atmospheric aerosol mass, σ_{sp} is often representative of aerosol mass. The CN measurements provide a good indication of any local pollution events that could interfere with the routine monitoring program.

Aerosol size distribution in the Aitken size range was measured using a Nuclepore-filter diffusion battery instrument constructed at GMCC. Six airflow paths consisting of four paths through 8-, 5-, 2-, and 1-μm-pore-diameter Nuclepore filters, one path through an absolute filter, and one straight-through path, were activated sequentially by motor-driven ball

22

measurements and the inversion method to recover the size distributions were described by *Twomey* [1975] and reviewed by *Heidam* [1981].

The black-carbon component of the aerosol was measured with an aethalometer constructed at Lawrence Berkeley Laboratory [*Hansen et al.*, 1982]. This instrument was described in detail by *Bodhaine et al.* [1989]. Since carbon is by far the dominant absorber in the atmospheric aerosol, the measurement of light absorption using this instrument is essentially a carbon measurement [*Rosen et al.*, 1978].

An HP-71 computer and HP-3421 data acquisition and control unit were used to control the diffusion battery and acquire all data from the instruments. Data were stored on cassette tapes with a time resolution of 1 hour.

Results

Daily geometric means of CN concentration and σ_{sp} for 1987 were presented by *Bodhaine and Rosson* [1988]. The month of July was chosen to examine relationships among the various measured variables because the first half of the month appears to be representative of background conditions and the second half is dominated by large events that may contain sea salt. Figure 3.12 shows σ_{sp}, CN concentration, black carbon concentration, and fraction of CN penetrating a Nuclepore filter for July 1987. The general level of σ_{sp} during the last half of the month is nearly a factor of 10 higher than during the first half of the month, and seems to be dominated by individual events. The major peaks in CN coincide with the peaks in σ_{sp}; however, the overall level for CN is relatively not as high as for σ_{sp}, suggesting an influx of larger particles during the last half of the month.

The major peaks in aerosol carbon generally coincide with those in σ_{sp} and CN, and occasionally exceed 1 ng m^{-3}. The two carbon peaks on July 28 probably were caused by local pollution; the cause of the large carbon peak on July 30 is unknown.

The fraction of CN penetrating a Nuclepore filter with 2-μm-diameter pores (Figure 3.12, bottom) suggests a shift in size distribution toward larger sizes during the last half of July. Although the CN-fraction data are somewhat noisy, it is apparent that the major CN-fraction peaks tend to coincide with the major σ_{sp} peaks. Again, this suggests that an additional shift toward larger sizes occurs during large σ_{sp} events.

Figure 3.13 shows a time-height cross section of temperature for July calculated from South Pole rawinsonde data. The strong, shallow surface temperature inversion is persistent during the entire month. However, on July 17, the time of the transition in aerosol data, the strength of the inversion decreased dramatically and a warm air mass moved in at about the 600-mb level. Trajectories typical of the first and last halves of July are shown in Figure 3.14. The direct, rapid transport, evident on July 23 near the maximum of the warm event, arrived from the Weddell sea in less than 2 days. The July 12 trajectories were slow moving and remained over the continent for up to 7 or 8 days back.
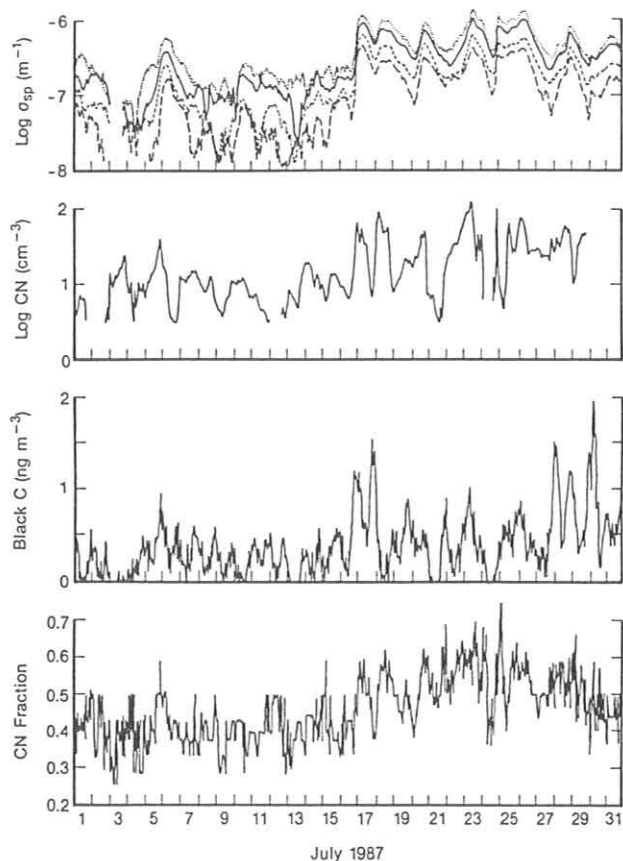

Fig. 3.12. SPO aerosol data for July 1987: σ_{sp} for 450 (dotted), 550 (solid), 700 (dashed), and 850 nm (long-dashed); CN concentration; black-carbon concentration; and fraction of CN penetrating a 2-μm-pore-diameter Nuclepore filter.
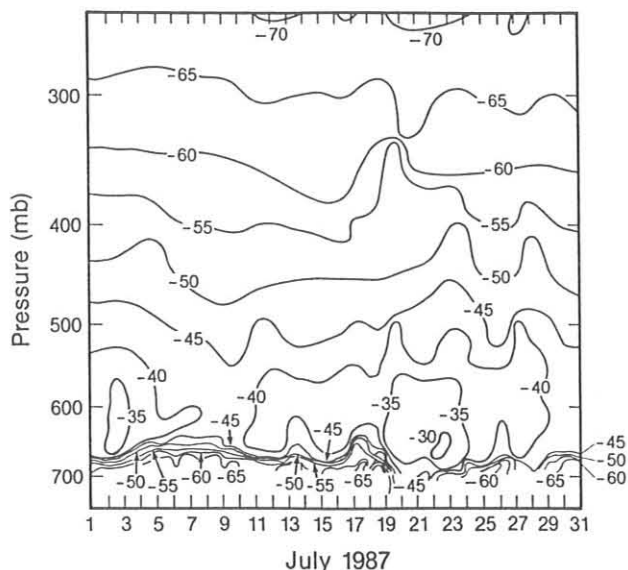

Fig. 3.13. Time-height cross section of temperature (°C) for July 1987 at SPO.
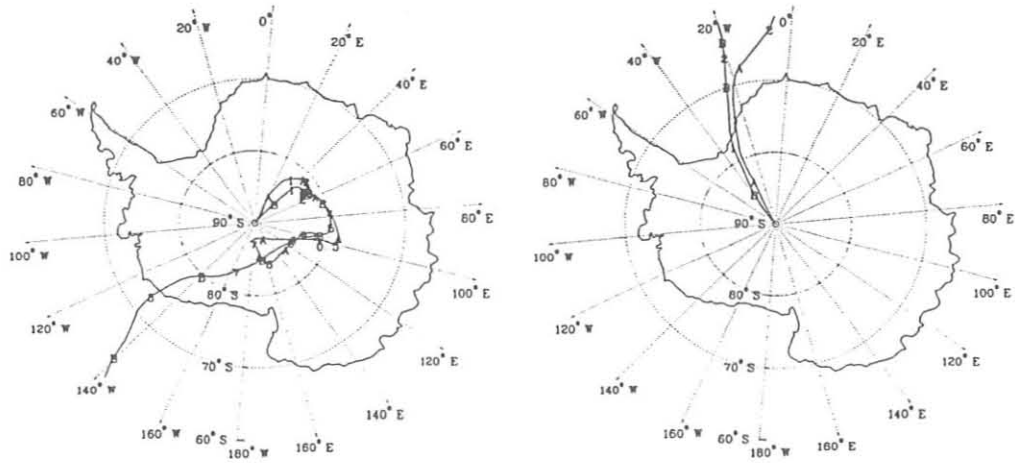
Fig. 3.14. Isobaric trajectories calculated backward from the South Pole at 0000 UTC (A) and 1200 UTC (B) on July 12 (left) and July 23 (right), 1987, at the 500-mb level. The numbers on the trajectories indicate the number of days back.

The black carbon data for the entire experiment are shown in Figure 3.15. Maximum values of about 2-3 ng m^{-3} occurred during the austral summer and minimum values less than 0.1 ng m^{-3} occurred in about April-May. This annual cycle resembles the annual cycle in σ_{sp} data, suggesting that the aerosol carbon may be related to long-range transport from oceanic regions or from lower latitudes in general.

Conclusions

Surface-based aerosol measurements at the South Pole clearly show annual cycles in CN concentration, σ_{sp}, and black carbon concentration. Large-scale back trajectories show that rapid transport paths can exist from the coast of Antarctica to the interior, during which large events occur in the aerosol data. Large-scale transport in the troposphere and mixing to the surface during periods of weakened surface temperature inversion are responsible for events in the surface aerosol data.
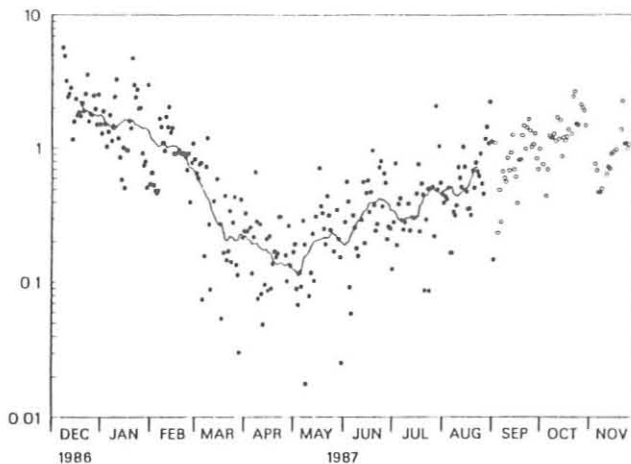
Fig. 3.15. Black carbon concentration (ng m^{-3}) at SPO during 1987. The solid circles represent data calculated from hourly data; the open circles are data from the operator's daily checks.

3.2.2. SURFACE RADIATION AND TEMPERATURE VARIATIONS ASSOCIATED WITH CLOUDINESS AT THE SOUTH POLE

Introduction

Results from ERBE indicate that although clouds have a net cooling effect on the surface of the earth on a global scale, they may contribute to anomalous surface heating in high-latitude snow-covered regions [*Ramanathan et al.*, 1989]. Past trajectory analyses show that upper-level intrusions of warm, moist air and cloud condensation nuclei frequently reach the South Pole from the Weddell Sea, producing a variety of cloud types [*Ohtake*, 1978]. Preliminary analysis of the 1986-1987 SPO data presented here relates surface warming to enhancements of longwave downward radiation associated with such transitory cloud systems.

Data

Daily mean values of "surface" temperature measured at 2 m (T_s), longwave downward radiation (LWD), and the direct-beam irradiance (DB) from *Dutton et al.* [1989] are analyzed. These quantities are correlated with daily mean total sky cover (SC) estimates. Figure 3.16 is a time series for 1 year, beginning September 1986, of T_s, LWD with SC, and DB, respectively. The smooth curves represent empirically determined clear-sky conditions for the peak sunlit months, November-January (NDJ, dashed), and the dark winter months, April-August (AMJJA, dotted). Refer to *Stone et al.* [1989] for a detailed description of how these curves were fitted.

Clear-sky conditions are typically characterized by a weak, steady flow of cold air from higher terrain and a strong, persistent temperature inversion in the lower troposphere. Transitory disturbances are characterized by cloudy skies, a dramatic decrease in DB, an increase in T_s, and a weakening of the inversion and an enhanced LWD signal as is evident by departures from the smoothed clear-sky curves in Figure 3.16.

Analysis

Scatter plots of T_s versus LWD for months NDJ and AMJJA are shown in Figure 3.17. Each plot is fitted with a quadratic

24
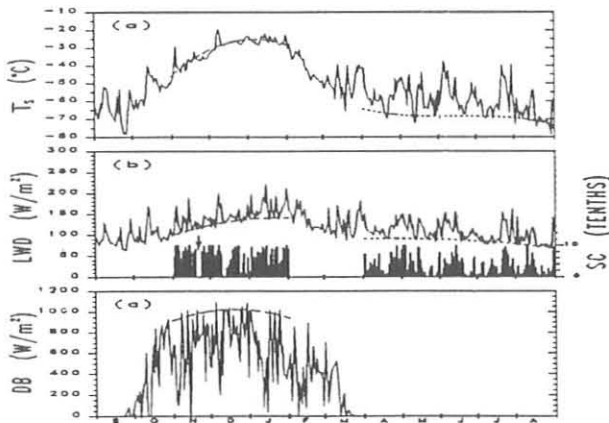
Fig. 3.16. Time series of (a) surface temperature, (b) longwave downward irradiance (line referenced to left scale) and sky cover (bars, right scale), and (c) direct-beam irradiance, at SPO for 1 year beginning September 1986. The smooth curves represent clear-sky conditions described in the text. The inverted arrow in b indicates missing sky cover data.

Fig. 3.17. Scatter plots of SPO surface temperature vs. longwave downward irradiance for (a) November-January 1986-87 and (b) April-August 1987, fitted with quadratic functions. RSD is the residual standard deviation of fit, and COR is the correlation coefficient.
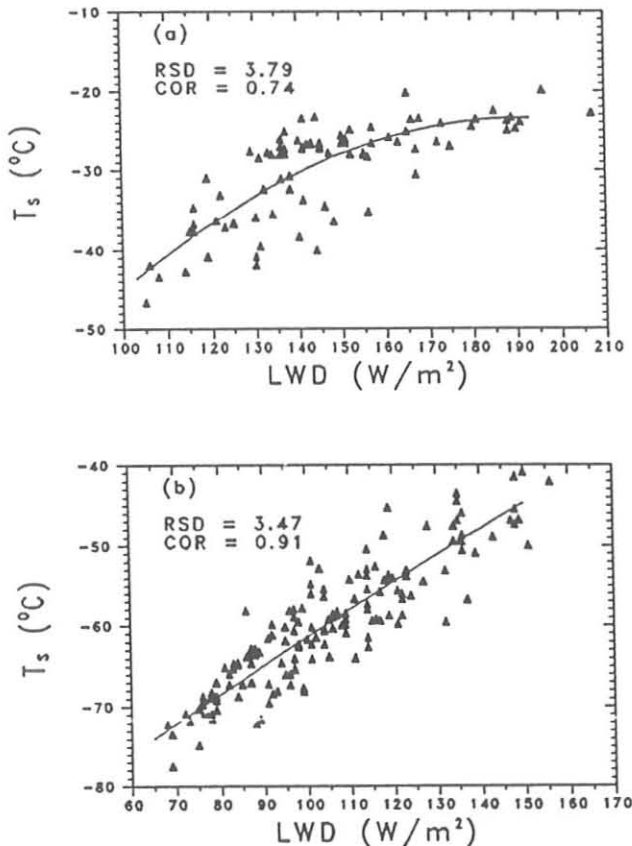
function. The residual standard deviation (RSD) of fit and correlation coefficient (COR) are given in each figure. Note (in Figure 3.16) that the range of clear-sky temperatures during AMJJA is only about 10°C, whereas the total observed range is close to 40°C; the warmest temperatures correlate with enhanced values of LWD. Because clouds over the pole tend to form in the warmest layers near the top of the inversion and are more emissive than clear air, thermal emissions from clouds are normally greater than thermal emissions from the relatively cool, dry subcloud layers. Thus, observed enhancements of LWD are mostly attributed to cloud "greenhouse" effects.

To quantify the relationship between departures of temperature from clear-sky conditions and the observed LWD enhancements, ratios of observed LWD values to corresponding predicted clear-sky values were computed to estimate the fractional LW-radiative forcing (LWRF) associated with clouds. The largest values of LWRF correspond to optically thick clouds. It is hypothesized that during the initial stages of a warming event, when clouds are decoupled from the surface by a strong intervening inversion layer, LWRF is dominated by warm cloud emissions. As radiative exchanges between the cloud base and the surface occur, and turbulent and advective processes progress, dynamic forces are increasingly important in controlling the surface temperature field. On the basis of the available data, only the relationship between LWRF and the observed temperature perturbations, expressed in terms of temperature differences, $\Delta T = T_s$ (measured) $-T_s$ (clear), is presented here. This relationship is shown for the months NDJ and AMJJA in Figures 3.18a and b, respectively.

During the winter months, positive temperature differences are highly correlated with LWRF, but during NDJ there is virtually zero correlation for small LWRF and increasingly positive correlation as LWRF increases (i.e., for optically thicker clouds). It is likely that shortwave albedo effects involving multiple reflections (not yet accounted for in our analysis) may compete with, or add to, the LW (thermal) effects, thus greatly complicating the determination of the net radiative forcing caused by thin, broken or scattered clouds during the summer months.

Conclusions

Preliminary analyses of the 1986-1987 SPO data indicate that positive LW radiative forcing may occur whenever clouds of sufficient optical depth and sky cover are present. Under such conditions the surface actually tends to warm, supporting the preliminary analysis of the ERBE data. These results suggest that transitory clouds may have a potentially important role as a source of heat for the Antarctic Plateau and, as such, must be accounted for to improve model simulations of the total surface energy budget for that region. Detailed case studies involving analyses of the physical and optical properties of clouds and the components of the surface energy budget in conjunction with studies of synoptic and local dynamical mechanisms are necessary to understand further the effects clouds have on the temperature field at the South Pole.
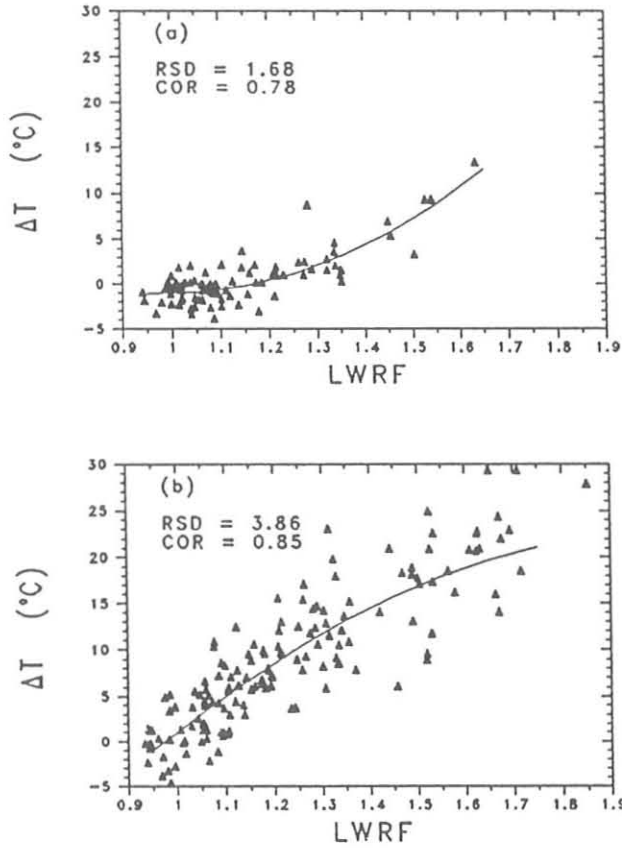
Fig. 3.18. Scatter plots with quadratic fits of observed temperature differences versus longwave radiative forcing for (a) November 1986-January 1987 and (b) April-August 1987, at SPO. RSD and COR values are as noted.

3.2.3. CALIBRATION OF THE SBUV USING UMKEHR MEASUREMENTS

Introduction

Experience has shown that the diffuser plate calibration of the SBUV satellite does not remain stable with time and that the total ozone and ozone profile data deduced from the SBUV albedo measurements have displayed significant drifts with time when compared with ground-based observations [*Fleig et al.*, 1981; *Cebula et al.*, 1988]. Attempts to correct the SBUV calibration drift independently of any external reference have not been satisfactory. *Fleig et al.* [1988] showed that a drift in total ozone and profile ozone still existed after a first-order diffuser plate correction had been applied.

Results are described here of an investigation that directly relates a ground-based UV measurement to backscattered intensities, which can be used to monitor the calibration of the SBUV. For UV measurements the Umkehr method was used because of the abundant data that are available for the time that the SBUV was in operation. The method developed eliminates the need to estimate ozone profiles and instead directly relates the Umkehr measurement to the albedo measurement from the satellite-borne SBUV. The SBUV and Umkehr wavelengths are shown in Table 3.6.

TABLE 3.6. SBUV Satellite Instrument and Umkehr Wavelengths

Satellite (nm)	Umkehr (nm)
273.5	305.5
283.0	311.4
287.6	317.6
292.2	325.4
297.5	332.4
301.9	
305.8	
312.5	
317.5	
331.2	

Relating the Umkehr to the SBUV

The C wavelength pair was used as the Umkehr vector, and a linear regression T matrix was constructed from 62 samples. The least-squares solution is given by

$$T\Delta\underline{u} = \Delta\hat{\underline{a}}$$

where $\Delta\underline{u}$ is the Umkehr vector, $\Delta\hat{\underline{a}}$ is the predicted SBUV albedo expressed as departures from the mean, and $\wedge$ denotes predicted values. The mathematical forms of the $\underline{u}$ and $\underline{a}$ vectors are

$$\underline{u} = 100 \log_{10}[I(332.4)/I(311.4)]$$

$$- 100 \log_{10}[F_0(332.4)/F_0(311.4)]$$

$$\underline{a} = \log_{10}[I_s(\lambda)/F_0(\lambda)]$$

where I is zenith sky intensity, F_0 is extraterrestrial solar flux, $I_s(\lambda)$ is intensity going back to space seen by the satellite, and λ is wavelength in nm. Ozone profiles used to calculate $\underline{u}$ and $\hat{\underline{a}}$ were obtained from SAGE II data for 1985 and 1986 at 40°N latitude. The elements of the $\underline{u}$ and $\hat{\underline{a}}$ vectors are N-values. Randomly distributed errors for the Umkehr ($\varepsilon_u = \pm 0.5, \pm 1.0$, and ± 3.0 N-units) and for the SBUV ($\varepsilon_a = \pm 0.7\%$) were applied to simulate measurement uncertainty under idealized clear atmospheric conditions.

Results

Figure 3.19 shows the root-mean-square errors (σ_a) obtained by comparing the predicted $\hat{\underline{a}}$ with "truth" $\underline{a}$ for the Dobson C wavelength pair for an SBUV solar zenith angle of 30°; random errors (constant over the interval) of $\pm 0.5, \pm 1.0$, and ± 3.0 N-units for the Umkehr data; and random error of $\pm 0.7\%$ for the SBUV measurements. In this figure, the plot on the right is the error for all SBUV albedo data. This plot represents the first-guess statistics. The other plots represent the improvement (in terms of error reduction) provided by the information contained in the Umkehr measurements. The plot in which $\varepsilon_u = 3.0$ represents a
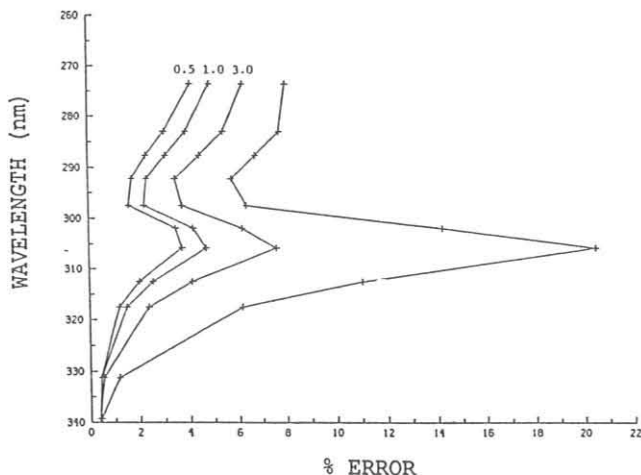
Fig. 3.19. Estimated SBUV albedo errors (+; $\sigma_{\hat{a}-a}$ in the text), shown as wavelength versus percent root-mean-square error of estimation. The conventional Umkehr C pair was used for the estimation. The three plots on the left are the Umkehr errors in terms of N-values, 0.5, 1.0, and 3.0. The plot on the right is the standard deviation for all SBUV data. The SBUV solar zenith angle was 30°.

Fig. 3.20. Estimated SBUV albedos using Umkehr A-C-D pair data (dashed lines) and simulated "truth" SBUV albedos (solid lines) for a period of 1 year. The simulated Umker $\hat{a}$ A-C-D pair error is ±1.0 N-unit. Ordinate values are in terms of the fractional departure from the algorithm mean value a_0 (see text). The abscissa is year and fraction of that year. SBUV wavelength is 283.0 nm.

severe-error case. An error of 1 N-unit is more likely to be encountered with the Umkehr measurement. Re-examination of the figures shows that the C pair provides reasonably good error reduction $\sigma_{\hat{a}-a}$ in the estimation of the albedos. Even in the $\sigma_{\hat{a}-a}$ severe case, there is reasonably useful error reduction. The values seen in the two longest wavelengths (for total ozone) are small because ozone absorbs weakly at these wavelengths, and there is virtually no ozone profile information. SBUV total ozone is determined from these wavelengths, but normalization of the Umkehr at a solar zenith angle of 60° essentially removed most of its total ozone information. The SBUV 305.8-nm wavelength shows the largest variation because it optimally senses ozone profile information in the region of the ozone maximum, where the absolute total ozone changes are also a maximum.

Plots are shown of simulated SBUV albedos and Umkehr-estimated SBUV albedos in Figure 3.20 to illustrate the capability of our method for sensing the annual variation of SBUV albedos. The ordinate is in terms of $\hat{a}$, the fractional departure from the mean a_0. The dashed line connecting points gives the Umkehr-estimated SBUV albedos at 283.0 nm using the A-C-D pairs. The abscissa is the year and fraction of that year. The solid line connecting the points gives the simulated SBUV albedos. The Umkehr error was set at ±1.0 N-value. This figure reveals an expected annual variation, in accordance with the SAGE II observations, which formed the basis of the a priori ozone profile information used in the retrieval algorithm.

Conclusion

The preliminary results of the present investigation suggest a potentially advantageous retrieval method of using ground-based UV measurements to track the calibration drift of an SBUV satellite. Dobson standard or short Umkehr measurements with verifiable calibrations can be used as the ground-based measurements for the present investigation because of their availability and potential stability. The GMCC Automated Dobson network will provide ample Umkehr data for comparisons.

The satellite SBUV albedo-estimation procedure indicates that the retrieval random errors are about ±5% or less for an Umkehr error of ±1.0 N-unit. These errors are believed to be close to the tolerances required for the validation of mathematical methods devised to correct the calibration drift of the SBUV.

An error analysis that includes instrument errors, biases, and stratospheric aerosol interference errors was not done in the present investigation but is suggested as a future research topic. More work is required to develop a general algorithm to account for more SBUV solar zenith angles and latitudes.

3.3. REFERENCES

Ahlquist, N.C., and R.J. Charlson, Measurement of the wavelength dependence of atmospheric extinction due to scatter, *Atmos. Environ., 3*, 551-564, 1969.

Bodhaine, B.A., and J.C. Bortniak, Four wavelength nephelometer measurements at South Pole, *Geophys. Res. Lett., 8*, 539-542, 1981.

Bodhaine, B.A., and J.J. DeLuisi, An aerosol climatology of Samoa, *J. Atmos. Chem., 3*, 107-122, 1985.

Bodhaine, B.A., and M.E. Murphy, Calibration of an automatic condensation nuclei counter at the South Pole, *J. Aerosol Sci., 11*, 305-312, 1980.

Bodhaine, B.A., and R.M. Rosson, *Geophysical Monitoring for Climatic Change, No. 16: Summary Report 1987*, pp. 16-19, NOAA Air Resources Laboratory, Boulder, CO, 1988.

Bodhaine, B.A., J.J. DeLuisi, J.M. Harris, P. Houmere, and S. Bauman, Aerosol measurements at the South Pole, *Tellus, 38B*, 223-235, 1986.

Bodhaine, B.A., J.J. DeLuisi, J.M. Harris, P. Houmere, and S. Bauman, PIXE analysis of South Pole aerosol, *Nucl. Instr. Meth., B22*, 241-247, 1987.

Bodhaine, B.A., E.G. Dutton, J.J. DeLuisi, G.A. Herbert, G.E. Shaw, and A.D.A. Hansen, Surface aerosol measurements at Barrow during AGASP-II, *J. Atmos. Chem., 9*, 213-224, 1989.

Cebula, R. P., H. Park, and D. F. Heath, Characterization of the Nimbus-7 SBUV radiometer for the long-term monitoring of the stratospheric ozone, *J. Atmos. Oceanic Technol., 5*, 215-227, 1988.

Dutton, E.G., and J.J. DeLuisi, Measurements of solar radiation at Mauna Loa observatory, 1978-1985, with emphasis on the effects of the eruption of El Chichòn, *NOAA Data Rep. ERL ARL-13*, 35 pp., NOAA Air Resources Laboratory, Boulder, CO, 1987.

Dutton, E.G., J.J. DeLuisi, and A.P. Austring, Interpretation of Mauna Loa atmospheric transmission relative to aerosols, using photometric precipitable water amounts, *J. Atmos. Chem., 3*, 53-68, 1985.

Dutton, E.G., R.S. Stone, and J.J DeLuisi, South Pole surface radiation measurements, April 1986 to February 1988, *NOAA Data Rep. ERL ARL-17*, 49 pp., NOAA Air Resources Laboratory, Boulder, CO, 1989.

Ellis, H.T., and R.F. Pueschel, Solar radiation: Absence of air pollution trends at Mauna Loa, *Science, 172*, 845-846, 1971.

Fleig, A.J., K.F. Klenk, P.K. Bhartia, K.D. Lee, C.G. Wellemeyer, and V.G. Kaveeshwar, Vertical ozone profile results from Nimbus-4 BUV data, Proc. Fourth Conf. on Atmospheric Radiation, Toronto, Ontario, June 16-18, 1981, pp. 20-26, American Meteorology Society, Boston, 1981.

Fleig, A.J., D.S. Silberstein, C.G. Wellemeyer, P.K. Bhartia, and J.J. DeLuisi, An assessment of the SBUV/TOMS ozone data quality, based on comparison with external data, *Atmospheric Ozone*, International Ozone Commission, in press, 1989.

Hansen, A.D.A., H. Rosen, and T. Novakov, Real-time measurement of the absorption coefficient of aerosol particles, *Appl. Opt., 21*, 3060-3062, 1982.

Heidam, N.Z., Review: Aerosol fractionation by sequential filtration with Nuclepore filters, *Atmos. Environ., 15*, 891-904, 1981.

Mendonca, B.G., K.J. Hanson, and J.J. DeLuisi, Volcanically related secular trends in atmospheric transmission at Mauna Loa, Hawaii, *Science, 202*, 513-515, 1978.

Metnieks, A.L., and L.W. Pollak, Instruction for use of photo-electric condensation nucleus counters, *Geophys. Bull. No. 16*, School of Cosmic Physics, Dublin Institute for Advanced Study, Dublin, Ireland, 1959.

Ohtake, T., Atmospheric ice crystals at the South Pole in summer, *Ant. J. U. S., 13*, 174-175, 1978.

Ramanathan, V., R.D. Cess, E.F. Harrison, P. Minnis, B.R. Barkstrom, E. Ahmad, and D. Hartmann, Cloud-radiative forcing and climate: Results from the Earth Radiation Budget Experiment, *Science, 243*, 57-63, 1989.

Rosen, H., A.D.A. Hansen, L. Gundel, and T. Novakov, Identification of the optically absorbing component in urban aerosols, *Appl. Opt., 17*, 3859-3861, 1978.

Skala, G.F., A new instrument for the continuous measurement of condensation nuclei, *Anal. Chem., 35*, 702-706, 1963.

Stone, R.S., E.G. Dutton, and J.J. DeLuisi, Surface radiation and temperature variations associated with cloudiness at the South Pole, *Ant. J. U. S.*, in press, 1989.

Twomey, S., Comparison of constrained linear inversion and an iterative nonlinear algorithm applied to the indirect estimation of particle size distributions, *J. Comp. Phys., 18*, 188-200, 1975.

4. Carbon Cycle Group

T.J. CONWAY (Editor), K.W. THONING, L.P. STEELE, P.C. NOVELLI, L.S. WATERMAN,
P.P. TANS, D.G. KITZIS, P.M. LANG, R.C. MARTIN, AND K.A. MASARIE

4.1. CONTINUING PROGRAMS

4.1.1. CONTINUOUS IN-SITU AND FLASK SAMPLE CARBON DIOXIDE MEASUREMENTS

The in-situ NDIR continuous measurements of CO_2 at the four GMCC observatories were made in 1988 as in previous years. Preliminary monthly and annual mean CO_2 values are shown in Table 4.1, expressed in the WMO 1985 mole fraction scale (X85). Calibration procedures for CO_2-in-air reference gas tanks remained the same as in previous years. Only minor modifications in sampling methodology occurred in 1988. Second parallel sampling lines were installed at SMO and MLO in March and April, respectively. Air is sampled for 25 minutes of each hour from each of the two lines. The remaining 10 minutes of the hour are used for measurement of calibration gases. The dual sampling lines will allow better quality control of the CO_2 measurements. Comparison of the results from one line to the other will make it possible to spot problems in a line or pump and to have a backup in case one sampling line system fails. There will also be an overlapping check on sampling line integrity when a line is replaced, since only one line will be changed at a time.

The NOAA/GMCC cooperative flask sampling network continued to provide whole air samples for the measurement of atmospheric CO_2 and methane (CH_4) concentrations. In 1988 the network consisted of the 26 sites listed in Table 4.2. Provisional mean CO_2 concentrations are also given in Table 4.2. Sampling was begun at Ragged Point, Barbados, and sampling at Cosmos, Peru, was discontinued because of intractable logistical problems.

The measurement of atmospheric carbon monoxide (CO) concentration was begun using samples collected in flasks equipped with Teflon O-ring stopcocks at a few selected network sites (see Section 4.1.5). Extensive field and laboratory testing have shown that Teflon O-ring stopcocks will be a suitable replacement for the greased ground-glass type currently in use. This is significant because the greased stopcocks are unacceptable for CO measurements. The problem of frequent breakage of Teflon O-ring stopcocks has now been resolved.

A new CO_2 flask analysis apparatus was put into service in December 1988. The previous analysis system, described by *Komhyr et al.* [1983], did not have the capacity for handling the large number of flasks that are currently being analyzed (more than 7000 samples in 1988). The analysis system is shown schematically in Figure 4.1. In general, 12 sample flasks are connected by two-way solenoid valves to a central manifold. Four reference gases (W, X, Y, and Z) are also connected to the manifold so that the reference gases flow through the same analysis path as the flask samples. A diaphragm vacuum/pressure transfer pump pulls the air from the flasks or the reference gas cylinders and momentarily compresses the air into

Table 4.1. Provisional Monthly and Annual Mean CO_2 Concentrations (ppm, Relative to Dry-Air X85 Mole Fraction Scale) from the 1988 Continuous Analyzer Data

	BRW	MLO	SMO	SPO
Jan.	354.87	350.19	349.24	348.06
Feb.	356.23	351.50	349.70	347.92
March	356.56	352.11	349.35	347.98
April	357.40	353.51	350.27	348.18
May	356.83	354.16	349.63	348.28
June	355.27	353.60	349.66	348.50
July	348.43	352.61	349.94	348.89
Aug.	343.10	350.32	349.81	349.33
Sept.	345.87	348.81	348.94	349.59
Oct.	350.59	348.96	349.26	349.70
Nov.	354.28	350.09	349.72	349.53
Dec.	357.86	351.32	350.58	349.23
Annual	353.11	351.43	349.68	348.76

Table 4.2. Provisional 1988 Annual Mean CO_2 Concentrations From the Flask Network Sites

Code	Station	CO_2 (ppm)
ALT	Alert, N.W.T., Canada	352.8
AMS	Amsterdam Island	[ ]
ASC	Ascencion Island	350.3
AVI	St. Croix, Virgin Islands	351.3
AZR	Terceira Island, Azores	351.4
BRW	Barrow, Alaska	353.2
CBA	Cold Bay, Alaska	352.1
CGO	Cape Grim, Tasmania	348.8
CHR	Christmas Island	351.1
CMO	Cape Meares, Oregon	352.5
GMI	Guam, Mariana Islands	351.9
HBA	Halley Bay, Antarctica	[ ]
KEY	Key Biscayne, Florida	352.6
KUM	Cape Kumukahi, Hawaii	351.3
MBC	Mould Bay, Canada	352.7
MID	Midway Island	352.8
MLO	Mauna Loa, Hawaii	351.1
NWR	Niwot Ridge, Colorado	351.8
PSA	Palmer Station, Antarctica	349.4
RPB	Ragged Point, Barbados	351.4
SEY	Mahé Island, Seychelles	350.2
SGI	South Georgia Island	[ ]
SHM	Shemya Island, Alaska	352.5
SMO	American Samoa	350.0
SPO	South Pole, Antarctica	348.8
STM	Station M	352.1

Square brackets indicate insufficient data to calculate annual mean.
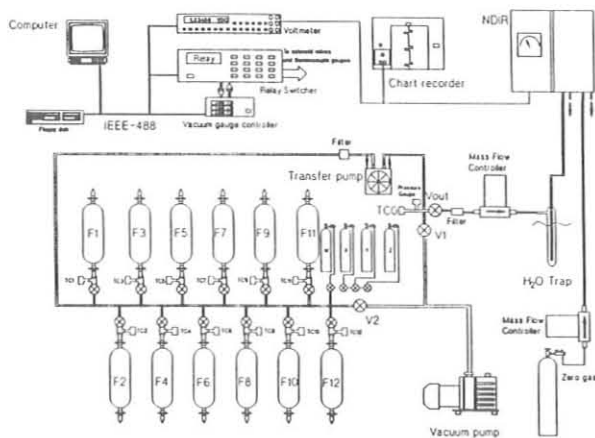
29

Fig. 4.1. The new semiautomatic flask analysis apparatus.

a small volume between the pump and the outlet solenoid valve (V_{out}). The solenoid valve is then opened, and the sample is pushed through a particle filter, a mass flow controller, a cold trap for removing water vapor, and into the CO_2 NDIR analyzer. The response of the analyzer is measured with a digital voltmeter, and the results are transferred to the computer. Timing and sequencing of events are controlled by the computer, which sends commands to a relay switching unit for activating devices. A two-stage direct-drive vacuum pump evacuates the system between samples when the two solenoid valves V1 and V2 are open.

For the analysis of flask samples, two reference gases, approximately 10 ppm apart in concentration, are chosen from the four available to bracket the expected concentrations of the flask samples. These gases are analyzed, followed by 12 flask samples. The two reference gases are again analyzed to allow correction for drift and sensitivity changes in the analyzer. Results of tests performed on the system show that under optimum conditions, the short-term (1 day) precision of the analysis system is better than 0.05 ppm. Longer term precision over several months, based on test flasks filled from a calibrated compressed air tank, is about 0.07 ppm. This value includes uncertainties due to filling and analyzing flasks, as well as to uncertainties in the calibration system used for assigning CO_2 concentrations to reference gas tanks.

The new CO_2 flask analysis system has a number of advantages over the analysis system used previously by GMCC. The system has been configured to analyze up to 180 flasks per analysis day. In practice, about 100 to 120 are analyzed, which takes approximately 6 hours to complete. The old system had a capacity of 60 flasks per day, so fewer analysis days will now be required to analyze the same number of flasks. A slight decrease in the amount of reference gas used is expected, since more flasks are analyzed for each reference gas sample. Extensive tests with flasks filled from calibrated cylinders showed that no systematic offsets are present. It is expected that the new system will be able to handle, for several years, the ever-increasing number of samples required for determining the global distribution of CO_2 concentration in the atmosphere.

Concentrations of atmospheric CO_2 in 1988 showed a larger than normal increase from the previous year. Annual means of CO_2 concentration from the flask sampling network for 1981-1988 are shown as a function of sine of latitude in Figure 4.2. A relatively large increase from 1987 to 1988 can be seen. The average difference of annual means from 1987 to 1988 for 20 sites was 2.6 ppm. This compares with an average of about 1.5 ppm yr^{-1} for the 7 previous years. It also appears that the magnitude of the North Pole-to-South Pole difference in CO_2 concentration is larger in 1988 than in the prior 7 years. This is seen more clearly in Figure 4.3, which shows the latitudinal gradient for 1988 along with the average gradient for 1981-1987. The curves are third-degree polynomials fitted to the annual means; both curves are forced through 0 at the South Pole. The North Pole-to-South Pole difference was 3.7 ppm for 1988, compared with an average of 2.8 ppm for 1981-1987. This result implies either a larger source/smaller sink of CO_2 in the northern hemisphere, a larger sink/smaller source of CO_2 in the southern hemisphere, or a combination of the two. The first of these two possibilities is much more likely, since the anomalously high growth rate from 1987 to 1988 suggests an increased source rather than a smaller sink. Model studies of CO_2 transport in the atmosphere are required to determine more precisely the cause of the large latitudinal gradient in 1988.
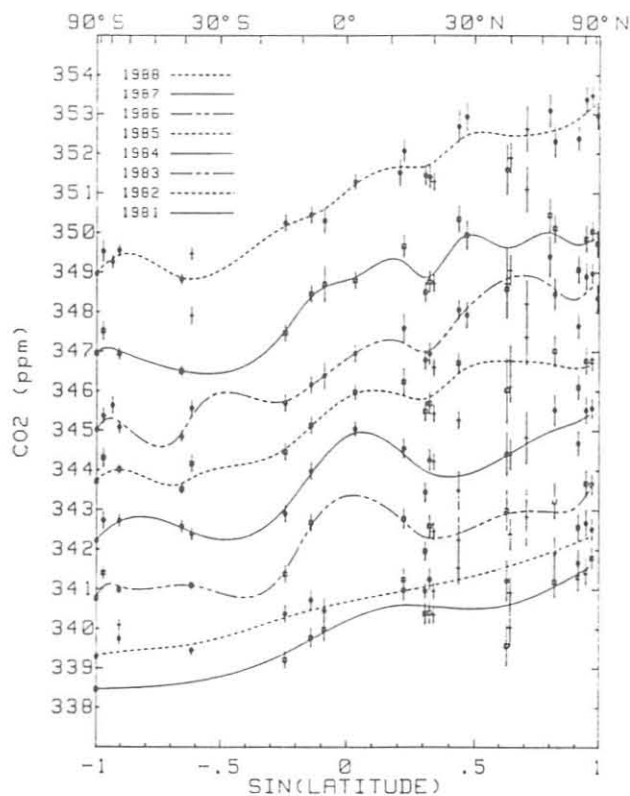

Fig. 4.2. Annual mean CO_2 concentrations vs. latitude for 1981 (bottom) through 1988 (top) flask network data. The vertical lines represent the 1-σ statistical uncertainty of the annual mean, as described by *Conway et al.* [1988]. The curves are cubic splines fitted to the data.
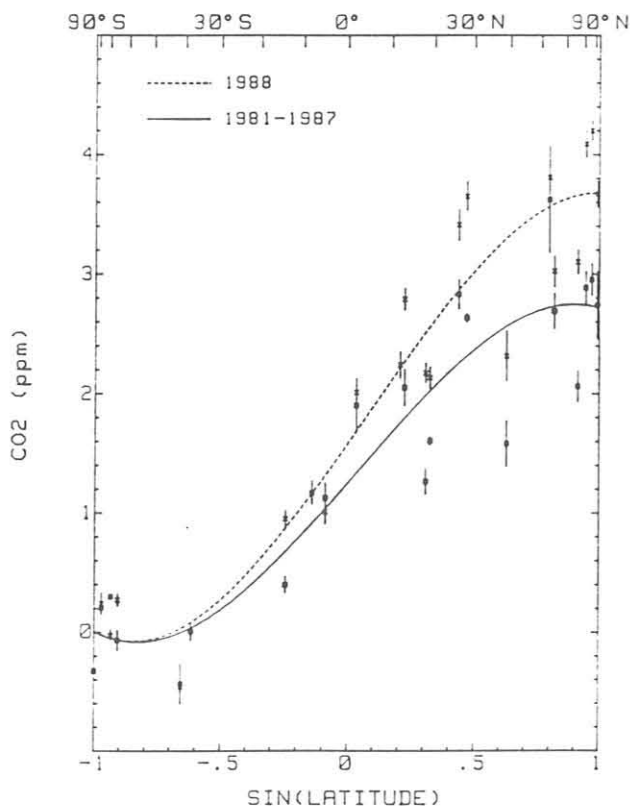
30

Fig. 4.3. A comparison of the 1988 CO_2 latitude gradient (top), determined from flask network data, with the mean gradient for 1981-1987 (bottom). The curves are third-degree polynomials fitted to the means; both curves are forced through 0 at the South Pole.

consistent with previous ENSO events, in which high CO_2 growth rates followed minima in the Southern Oscillation Index by approximately 6 months, and the CO_2 growth rate was correlated with sea surface temperatures (see, for example *Bacastow*, 1976; *Komhyr et al.*, 1985; *Elliott and Angell*, 1987; *Conway et al.*, 1988; and *Thoning et al.*, 1989). Figure 4.4 also shows a peak in the growth rate in 1983, following the strong ENSO event of 1982. Preliminary results from 1989 show a return to more typical growth rates of about 1.5 ppm yr^{-1}.

4.1.2. FLASK SAMPLE METHANE MEASUREMENTS

The program to measure the global distribution of atmospheric CH_4 from flask samples collected at sites in the NOAA/GMCC cooperative flask sampling network continued in 1988. Results from this program for the calendar years 1984-1988 are summarized in the three-dimensional (3-D) representation shown as Figure 4.5. The way in which data from the individual sites are treated in order to generate Figure 4.5 is described by *Steele et al.* [1987]. Data from the high-altitude sites of MLO and Niwot Ridge are not used in Figure 4.5. The globally averaged linear growth rate of atmospheric CH_4 over the period May 1983 to December 1988 is 12.24 ± 0.08 ppb yr^{-1}.

A significant improvement was implemented during the year with the installation of a fully automated system for the analysis of flask samples. Up to eight flasks at a time may be mounted on a carousel that is computer controlled. Each flask is analyzed in turn, and a sample of calibration gas is analyzed between each flask aliquot. Once analysis is initiated, the system will run unattended for about 4 hours, thus making flask analysis a less labor-intensive activity than it was previously.

In addition to the flask samples obtained from the sites in the flask sampling network, many flask air samples have been collected aboard ships and also analyzed for CH_4. The shipboard data set was treated as an independent record in order to compare it with the data obtained from the network sites, by using the 3-D representation shown in Figure 4.5. The sample date and latitude of each shipboard flask sample were used to perform a straight-forward interpolation on the 3-D surface in Figure 4.5 to obtain the CH_4 concentration at the same date and latitude as each

The global CO_2 growth rate was determined by averaging the growth rates, weighted by latitude, from each of the flask network stations. The result is shown in Figure 4.4. A maximum in the growth rate of close to 3 ppm yr^{-1} occurred in late 1987, and 1988 had a mean growth rate greatre than 2 ppm yr^{-1}. Growth rates for individual sites ranged from 2.0 to 3.9 ppm yr^{-1}. This peak in the growth rate is associated with the ENSO event in 1987. The pattern of the growth rate variation in 1987-1988 is

Fig. 4.4. The globally averaged CO_2 growth rate determined from the flask network data for 1981-1988.
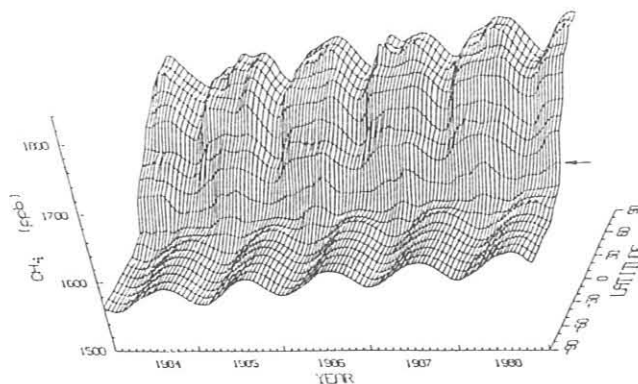

Fig. 4.5. Three-dimensional representation of atmospheric CH_4 in the marine boundary layer for 1984-1988. Grid spacing is 10° in latitude and 0.5 months in time. The arrow indicates the position of the equator.

31

shipboard flask sample. This was done for all flask samples taken on ships between May 1983 and December 1988. The result of the comparison is shown in Figure 4.6, where ΔCH_4 (shipboard CH_4 − interpolated network CH_4) is plotted against the latitude of the shipboard flask. It is clear that the overall comparison is very good; the mean value of ΔCH_4 is −0.06 ppb (σ = 13.92 ppb). The degree of scatter in the results for the southern hemisphere, particularly south of 10°S, is noticeably less than that for the northern hemisphere. This is consistent with observations of less scatter in the records of the southern hemisphere network sites [*Steele et al.*, 1987]. The good agreement indicated in Figure 4.6 provides further proof that the current flask sampling network yields a realistic description of atmospheric CH_4 in the marine boundary layer. In addition, since most of the shipboard flask samples have been collected by using evacuated 3-L flasks fitted with an O-ring stopcock, they provide a useful check on the sampling procedures and the 0.5-L pressurized flasks used at most of the network sites.

4.1.3. IN-SITU METHANE MEASUREMENTS AT MLO

These measurements continued during 1988. Some minor technical problems were experienced, but quick remedies kept data losses to a minimum. The data were edited to flag those periods when the gas chromatographic system was not functioning satisfactorily, then daily average concentrations were calculated. The results for 1987 and 1988 are shown in Figure 4.7. Note that at this stage, no data selection has been applied. The daily average data continue to show the types of fluctuations that have been noticed in earlier versions of these results. A thorough analysis of these variations is currently under way.

Since flask air samples are routinely collected at MLO each week and analyzed for CH_4 at the Boulder laboratory, we have an opportunity to compare the in-situ data with the flask results. In Figure 4.8 the flask sample data are plotted versus the hourly average in-situ CH_4 value for the hour during which the flask sample was collected. It is clear that during 1987 and 1988 agreement between the flask and in-situ measurements of CH_4 at MLO was excellent.

4.1.4. IN-SITU METHANE MEASUREMENTS AT BRW

This program continued through 1988. A major breakdown of the system occurred in June when both of the internal valves of the gas chromatograph failed. They were promptly replaced, resulting in a loss of only 10 days of data in June and 10 days in July. At the time of this repair, the gas chromatographic data system was also upgraded significantly. New ambient air intake lines that run from the observatory building to the top of the meteorological tower were installed. Consequently the chromatograph was working normally during the period of the ABLE-3A experiment, part of which was carried out in the vicinity of BRW in July (see Section 4.2.2).

Considerable effort has been devoted to the development of robust procedures for the processing of the gas chromatographic CH_4 data. The first and most critical need was for an objective computer algorithm to be applied to the raw data (i.e., peak areas, retention times, etc.) to assess the instrumental performance.
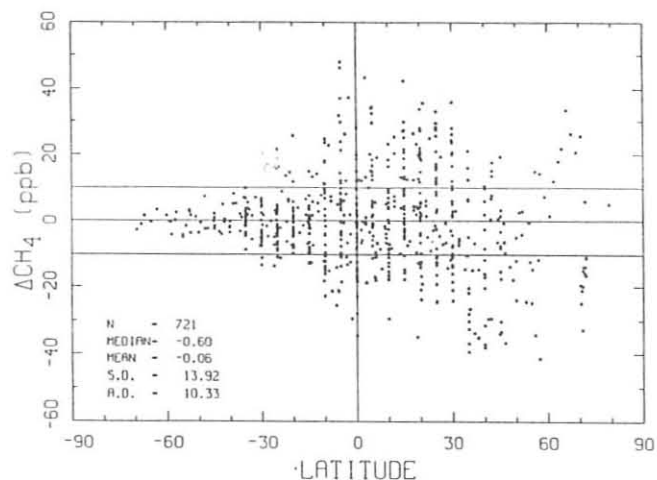
Fig. 4.6. Comparison between atmospheric CH_4 values measured in flask samples collected onboard ships and the CH_4 values interpolated for the same date and latitude from the 3-D surface shown in Figure 4.5; ΔCH_4 is shipboard CH_4 minus interpolated network CH_4 (see text). Values of ΔCH_4 are plotted at the latitude of the shipboard sample.
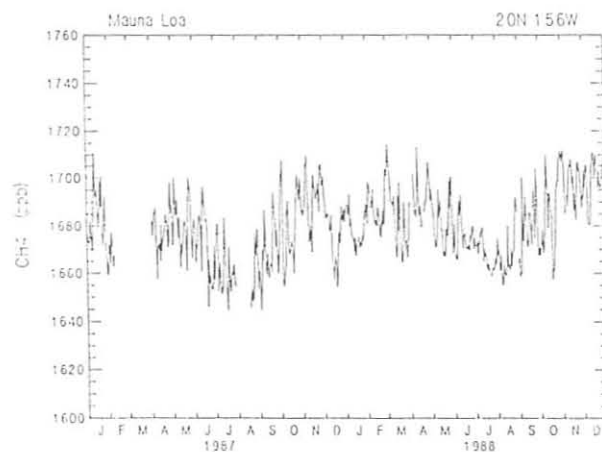
Fig. 4.7. Daily average CH_4 concentrations at MLO for 1987 and 1988. The gaps in the record are due to instrument malfunctions.

This has been achieved and allows for ready identification of those periods when the chromatograph was not functioning satisfactorily. The objective algorithm was assessed by carrying out an intensive comparison between the results of its decisions and those from a subjective evaluation of the chromatographic data. The effect of this objective algorithm on the in-situ CH_4 data obtained at BRW can be seen by comparing the first two panels of Figure 4.9. The first panel shows all of the CH_4 concentrations obtained from the system, and the second panel shows only those values obtained when the system was judged to be operating satisfactorily. The most significant feature of the second panel is the absence of the large downward "spikes" in concentration.
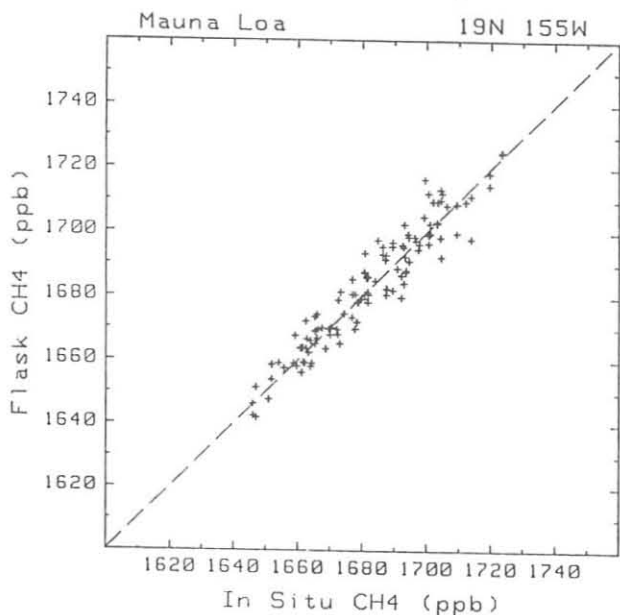
Fig. 4.8. Scatter plot of the atmospheric CH₄ concentration at MLO found from flask samples vs. the corresponding hourly-average in-situ CH₄ concentration at MLO. The period covered by this comparison is April 1987 to December 1988. The dashed line is the 1:1 line representing perfect agreement between the two types of measurements.

Further assessments of the BRW in-situ CH₄ data were carried out with the aid of the MUSIC software package developed by the Carbon Cycle Group for use on Hewlett-Packard work stations. Extensive modifications and improvements to this package have been made. The third panel of Figure 4.9 shows the result of the application of this package to 3 years of in situ data. Whereas the second panel shows all of the acceptable data, the third shows only those data obtained when both the hourly average wind speed was greater than 3 m s⁻¹ and the hourly average wind direction was in the sector 20°-110°. These meteorological constraints were applied for both the current and preceding hour (i.e., for a CH₄ concentration in any 1-h period to be accepted, the meteorological constraints must be satisfied for both that hour and the preceding one). The effect of this particular choice of constraints to "select" the data is quite dramatic, indicating that much of the observed short-term variability of CH₄ at BRW is associated with local human activities to the south and west of the observatory site.

4.1.5. FLASK SAMPLE CARBON MONOXIDE MEASUREMENTS

A program to measure the global variations of atmospheric CO concentration was begun in 1988. The activities of this project during 1988 were to (1) assemble an analytical system capable of making precise measurements of CO, (2) evaluate the stability of various flask types with respect to CO, (3) prepare gravimetric standards as the basis for an absolute CO concentration scale, and (4) begin measuring CO in flask samples collected at GMCC sites.
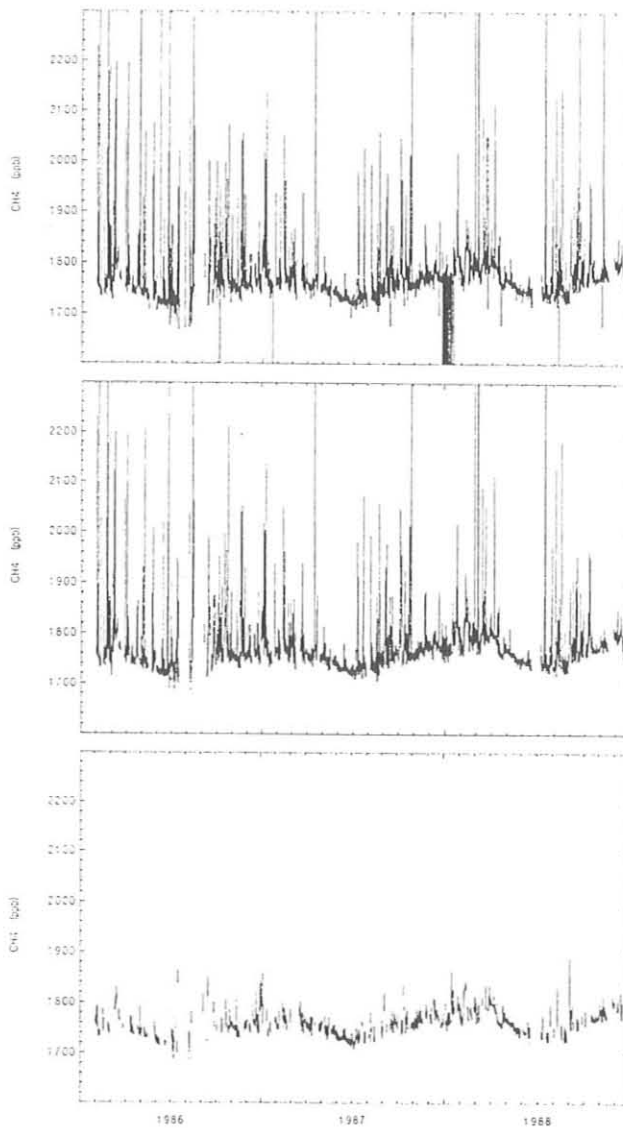
Fig. 4.9. In-situ hourly-average CH₄ measurements at BRW for 3 years, 1986-1988. The top panel shows all the data. The second panel shows the acceptable data after the application of an objective algorithm designed to identify periods of time when the gas chromatograph was not functioning satisfactorily. The third panel shows the data "selected" for the clean-air sector (see text).

The analytical system was developed using a gas chromatograph equipped with a Trace Analytical Reduction Gas Detector that measures CO by a mercuric oxide reduction technique. Gas sampling is controlled by a Hewlett-Packard integrator, along with an interface loop and a sample event controller. Precision at 100 ppb is typically ±0.5%. Cylinders of chemically dried air collected at Niwot Ridge, Colorado, were used as working standards. The CO content of this air was determined by calibration against GMCC gravimetric standards (described later in this section).

The geographical coverage offered by the GMCC flask network can be used for CO measurements only if a type of flask is found in which CO concentrations do not change over time. Currently, air samples collected at GMCC flask network sites are not routinely dried. Laboratory tests were performed to evaluate the stability of various metal and glass flasks filled with both wet and dry natural air. These tests showed that dry air in flasks was more stable than wet air, and that samples in glass flasks were more stable than in metal. Glass flasks with Teflon O-rings were found to be the most suitable for measurement of CO in undried air samples. Carbon monoxide concentration was stable to within 1 ppb for storage periods of up to 2 weeks in 0.5-L flasks, and up to 6 weeks in 3-L flasks. However, samples in glass flasks must be protected from exposure to sunlight because CO is known to be produced during the photochemical oxidation of some organic compounds. Flasks exposed to direct sunlight for even a few minutes have exhibited increased CO concentrations.

In collaboration with the GMCC Nitrous Oxide and Halocarbons Group, the Carbon Cycle Group began preparing gravimetric standards to define an absolute CO calibration scale. Experiments had shown that 0.8 m^3 aluminum cylinders purchased from Scott-Marrin Inc., were stable for CO to within 1%, for at least 6 months. These cylinders were used to prepare a 250-ppm mole fraction CO standard. From this parent, three daughter-standards were made in the concentration range found in the remote background troposphere: 45.22, 110.8, and 189.2 ppb. Based on these three standards, a preliminary relationship of area response versus CO concentration was defined (Figure 4.10). The CO concentrations reported here are referenced to these standards.

Air samples collected in the boundary layer, in 0.5-L flasks fitted with Teflon O-rings, were analyzed for CO as part of the ABLE-3A mission in July 1988 (see Section 4.2.2.). In October, air sampling in Teflon O-ring 0.5-L flasks was begun at BRW as part of the weekly flask sampling program for carbon cycle gases. Sample takers were advised to avoid exposing the flasks to sunlight by keeping the P^3 sampling units closed and by keeping the flasks in their containers except when filling them. In fall 1988, weekly sampling in Teflon O-ring 0.5-L flasks was also initiated at SMO.

Preliminary CO concentrations at BRW (Figure 4.11) show a strong seasonal variation, with CO ranging from 85 to 160 ppb (GMCC concentration scale). The lowest CO levels were observed in July and the highest were in December. This relatively smooth increase in CO concentration from summer to winter is similar to that observed in previous years at BRW [*Rasmussen and Khalil*, 1982]. In contrast, the CO concentrations at SMO show more scatter from week to week. In addition, concentrations at SMO fall into a much narrower range than at BRW; CO levels were typically between 75 and 100 ppb (Figure 4.11). The apparent attenuation of seasonal variation at SMO compared with BRW is believed to reflect such factors as the smaller variation in seasonal solar radiation intensities at SMO compared to BRW, and stronger anthropogenic influences at BRW in the winter.
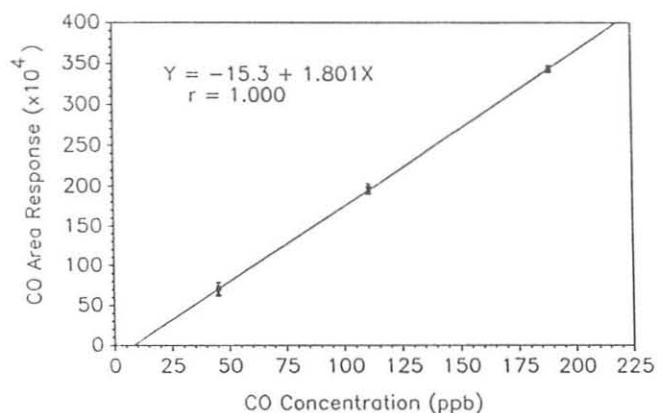
Fig. 4.10. Gas chromatographic peak area response vs. concentration for three GMCC gravimetrically prepared CO standards.
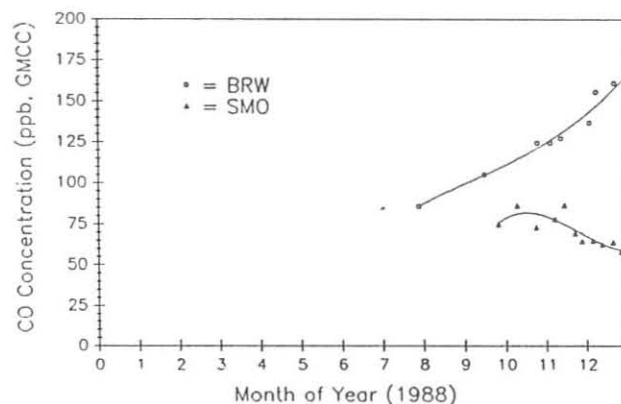
Fig. 4.11. Flask sample CO measurements for BRW and SMO during 1988. Each point represents the average of several measurements of a single flask sample. The 1-σ uncertainty is shown when it is larger than the point.

4.2. SPECIAL PROJECTS

4.2.1. SHIPBOARD AIR SAMPLING: OPERATION PACIFIC AIR

This shipboard flask sampling project, begun on December 14, 1986, continued through 1988; 12 voyages of the *Southland Star* were completed between Los Angeles and Auckland, New Zealand. The 358 samples collected in 3-L evacuated flasks were analyzed for CO_2 concentration. One sample from each pair was analyzed for CH_4. In an attempt to determine how well this series of samples collected in 5° latitude bands at 3-week intervals characterizes Pacific open-ocean background conditions, a project to measure atmospheric CO_2 continuously, in situ, was carried out on voyage 159 during July 1988.

A Siemens ULTRAMAT-3 infrared analyzer, programmable switching unit, stripchart recorder, magnetic tape data logger, and gas handling system were installed aboard the *Southland Star*. Air lines were strung forward to both the starboard and port bridge wings of the navigation bridge. The vessel sailed from Terminal Island, California, on July 10 and arrived at Auckland on July 24. Continuous measurements of atmospheric CO_2 were made throughout the voyage: 50 minutes of ambient air and 5 minutes each of two reference gases every hour. The hourly average concentrations are plotted versus latitude in Figure 4.12.

The regular flask sampling routine was followed throughout the voyage by the ship's deck officers, who collected pairs of samples every 5° of latitude. A member of the Carbon Cycle Group participated in all the flask sampling on this voyage, observing the technique and providing suggestions for improvement when appropriate. In several instances, near-simultaneous samples were collected on the forecastle deck (bow) of the vessel while the deck officers sampled air from the usual bridge locations.

Nineteen pairs of samples were collected. The pair difference was less than 0.1 ppm for 14 pairs and less than 0.3 ppm for 5 pairs. The difference between the flask samples and the infrared analyzer continuous record for the hour when the sample was collected ranges from -0.71 to +0.84 ppm. The average difference is +0.30 ppm ($\sigma = 0.36$), the flask values being higher than the continuous record. These preliminary (pending final reference gas calibration) results support the concept of a shipboard flask sampling program. Careful collection of flask samples by ship personnel will provide better resolution of the CO_2 and CH_4 latitude gradients over the Pacific Ocean than is possible from the land-based flask network.

4.2.2. ABLE-3A MISSION

During July and August the NASA GTE program carried out the ABLE-3A mission. The NASA Electra aircraft was extensively instrumented to make airborne observations of atmospheric properties, and a ground measurement site was set up within a remote tundra ecosystem near Bethel, Alaska [*Harriss and Wofsy*, 1989]. Several of the aircraft flights were in the vicinity of BRW. One of the objectives during ABLE-3A was to compare, under field conditions, some different techniques for measuring the major atmospheric carbon containing trace species. On the NASA Electra, a fast-response tunable diode laser instrument was operated to provide simultaneous measurements of CH_4 and CO [*Sachse et al.*, 1989], while an NDIR analyzer was used for CO_2 measurements [*Wofsy et al.*, 1988]. On several flights in the vicinity of BRW, the Carbon Cycle Group collected approximately 170 flask air samples that were returned to Boulder for analysis of CO_2, CH_4, and CO. To provide the best possible chances for a successful intercomparison experiment, NOAA/GMCC supplied the other participants in the experiment with tanks of calibration air. Preliminary comparisons of the onboard and flask measurements indicate excellent agreement between the different techniques [*Sachse et al.*, 1989].

4.3. REFERENCES

Bacastow, R.B., Modulation of atmospheric carbon dioxide by the Southern Oscillation, *Nature, 261*, 116-118, 1976.

Conway, T.J., P.P. Tans, L.S. Waterman, K.W. Thoning, K.A. Masarie, and R.H. Gammon, Atmospheric carbon dioxide measurements in the remote global troposphere, 1981-1984, *Tellus, 40B*, 81-115, 1988.

Elliott, W.P., and J.K. Angell, On the relation between atmospheric CO_2 and equatorial sea-surface temperature, *Tellus, 39B*, 171-183, 1987.

Harriss, R.C., and S.C. Wofsy, The Arctic Boundary Layer Expedition (ABLE-3A), *EOS, 70*, 282, 1989.

Komhyr, W.D., L.S. Waterman, and W.R. Taylor, Semiautomatic nondispersive infrared analyzer apparatus for CO_2 air sample analyses, *J. Geophys. Res., 88*, 1315-1322, 1983.

Komhyr, W.D., R.H. Gammon, T.B. Harris, L.S. Waterman, T.J. Conway, W.R. Taylor, and K.W. Thoning, Global atmospheric CO_2 distribution and variations from 1968-82 NOAA/GMCC CO_2 flask sample data, *J. Geophys. Res., 90*, 5567-5596, 1985.

Rasmussen, R.A., and M.A.K. Kahlil, Atmospheric trace gases and Arctic haze at BRW, in *Geophysical Monitoring for Climatic Change, No. 10: Summary Report 1981*, B.A. Bodhaine and J.M. Harris (eds.), NOAA Air Resources Laboratory, Boulder, CO, 1982.

Sachse, G.W., K.B. Bartlett, R.C. Harriss, G.F. Hill, L.O. Wade, L.G. Burney, J.E. Collins, and L.P. Steele, Airborne measurements of methane and carbon monoxide during ABLE-3A, *EOS, 70*, 282, 1989.

Steele, L.P., P.J. Fraser, R.A. Rasmussen, M.A.K. Khalil, T.J. Conway, A.J. Crawford, R.H. Gammon, K.A. Masarie, and K.W. Thoning, The global distribution of methane in the troposphere, *J. Atmos. Chem., 5*, 125-171, 1987.

Thoning, K.W., P.P. Tans, and W.D. Komhyr, Atmospheric carbon dioxide at Mauna Loa Observatory. 2. Analysis of the NOAA GMCC data, 1974-1985, *J. Geophys. Res., 94*, 8549-8565, 1989.

Wofsy, S.C., R.C. Harriss, and W.A. Kaplan, Carbon dioxide in the atmosphere over the Amazon basin, *J. Geophys. Res., 93*, 1377-1387, 1988.
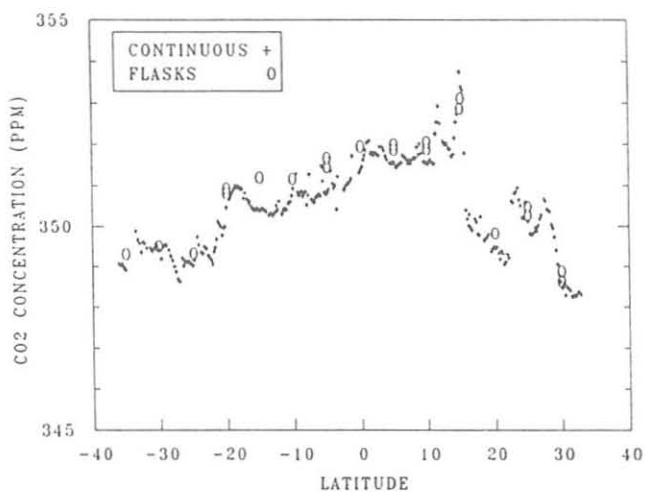
SOUTHLAND STAR JULY 1988

Fig. 4.12. Continuous analyzer and flask sample data vs. latitude from voyage 159 of the *M/V Southland Star* during July 1988. The plus symbols (+) represent 1-h averages of continuous analyzer data, and the circles (o) represent averages of flask pairs. Data associated with instrumental problems were edited from the plot.

5. Ozone Group

W. D. Komhyr (Editor), S. J. Oltmans, R. D. Grass, , R. D. Evans, and R. K. Leonard

5.1. Continuing Programs

5.1.1. Total Ozone Observations

Routine total O_3 observations with Dobson O_3 spectrophotometers were continued in 1988 at four GMCC stations, four foreign cooperative stations, three domestic cooperative stations, four NWS stations, and GMCC headquarters in Boulder. Table 5.1 lists the 16 stations, observing time periods for which data are available, instrument numbers, and agencies responsible for making the observations. Table 5.2 lists

provisional monthly mean total O_3 amounts for 1988.

The year was unusual in that poleward transport of O_3 in the southern hemisphere from the tropical stratospheric O_3 source region, during the second half of the year, was stronger than normal. O_3 values at SMO reverted to those last observed there in the mid-1970s. O_3 depletion in Antarctica was substantially less severe than it had been in recent years; polar vortex breakdown occurred relatively early, as did O_3 recovery. The mean SPO total O_3 for October 15-31 was 251 D.U. (Figure 5.1), which is comparable with total O_3 amounts observed at SPO during the same period in 1966, 1969, 1975, and 1977.

TABLE 5.1. U.S. Dobson Ozone Spectrophotometer Station Network for 1988

Station	Period of Record	Instrument No.	Agency
Bismarck, ND	Jan. 1, 1963-present	33	NOAA
Caribou, ME	Jan. 1, 1963-present	34	NOAA
Wallops Is., VA	July 1, 1967-present	38	NOAA; NASA
SMO	Dec. 19, 1975-present	42	NOAA
Tallahassee, FL	May 2, 1964-present	58	NOAA; Florida State Univ.
Boulder, CO	Sept. 1, 1966-present	61	NOAA
Poker Flat, AK	March 6, 1984-present	63	NOAA; Univ. of Alaska
Lauder, New Zealand	Jan. 29, 1987-present	72	NOAA; DSIR
MLO	Jan. 2, 1964-present	76	NOAA
Nashville, TN	Jan. 2, 1963-present	79	NOAA
Perth, Australia	July 30, 1984-present	81	NOAA; Australian Bureau Meteorology
SPO	Nov. 17, 1961-present	82	NOAA
Haute Provence, France	Sept. 2, 1983-present	85	NOAA; CNRS
Huancayo, Peru	Feb. 14, 1964-present	87	NOAA; IGP
BRW	June 6, 1986-present	91	NOAA
Fresno, CA	June 22, 1983-present	94	NOAA

TABLE 5.2. Provisional 1988 Monthly Mean Total Ozone Amounts (m-atm-cm)

| Station	Jan.	Feb.	March	April	May	June	July	Aug.	Sept.	Oct.	Nov.	Dec.
Bismarck, ND	342	350	380	360	355	316	324	309	295	283	314	315
Caribou, ME	362	391	398	385	372	384	336	330	319	332	304	372
Wallops Is., VA	316	327	352	369	369	356	336	314	303	315	281	303
SMO	255	256	251	252	253	268	270	269	272	274	268	262
Tallahassee, FL	292	290	295	325					273	285	272	291
Boulder, CO	306	321	357	327	339	311	303	295	297	272	286	306
Poker Flat, AK			447	427	380	350	331	315	312	305		
Lauder, New Zealand	291	292	277	274	284	303	325	360	361	387	322	304
MLO	229	241	265	279	288	276	276	266	259	266	261	253
Nashville, TN	314	323	345	355	369	360	333	319	298	312	281	290
Perth, Australia	283	282	271	275	282	289	307	325	328	325	312	296
SPO	283	262			246	246	256	241		251	342	333
Haute Provence, France	329	345	364	369	362	360	326	320	313	285	280	321
Huancayo, Peru	254	253	251	248	252	253	254	255	264	262	260	257
BRW			468	447	399	353	330	310	338			
Fresno, CA	283	300	334	353	346	338	317	310	302	276	281	303
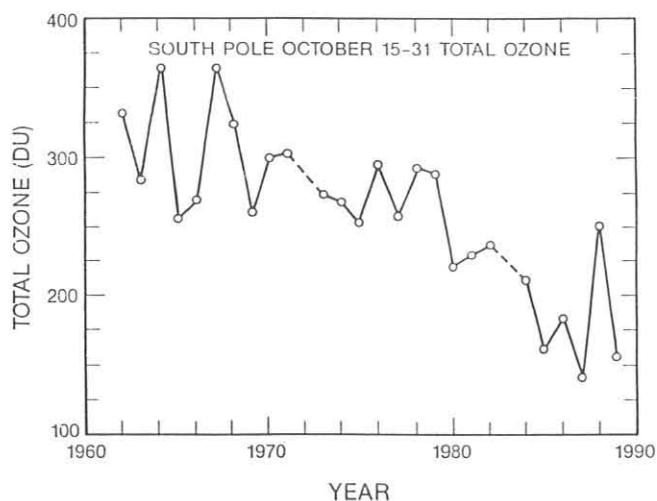
Fig. 5.1. Mean October 15-31 South Pole, Antarctica, total O_3 amounts for 1961-1988, determined from Dobson spectrophotometer observations.

5.1.2. UMKEHR OBSERVATIONS

Umkehr observations with Dobson O_3 spectrophotometers were continued during 1988 in Boulder, Colorado (40°N, 105°W); Mauna Loa, Hawaii (20°N, 156°W); Haute Provence Observatory, France (44°N, 6°E); Poker Flat, Alaska (65°N, 148°W); Perth, Australia (32°S, 116°E); and Lauder, New Zealand (45°S, 169°E). A total of 1458 usable O_3 profiles were obtained. All provisional data have been archived at the WMO World Ozone Data Centre, Atmospheric Environment Service, Downsview, Canada.

Umkehr observations at Huancayo were not made during most of the year because of failure of the Huancayo instrument to operate in the automatic mode. Total O_3 observations were continued manually, however. The International Affairs Office of NOAA helped arrange a visit to Boulder in June by the Chief of Meteorology and Electronics at the Huancayo Observatory. While in Boulder, he was trained in operation and repair of the instrument. However, because he was unable to repair the automated instrument completely, a decision was made to abandon attempts at repair, and manual Umkehr observations were commenced in November 1988. Operations at the observatory are being increasingly adversely affected by activities of the "Shining Path" guerilla armies.

The Perth automated Dobson instrument malfunctioned in October when an optical wedge band broke. The instrument was recalibrated relative to World Primary Standard Dobson Spectrophotometer no. 83 in November.

5.1.3. DOBSON SPECTROPHOTOMETER CALIBRATIONS

GMCC continued its program of upgrading and calibrating Dobson O_3 spectrophotometers of the global Dobson instrument network. Instruments worked on are listed in Table 5.3. Calibrations were performed relative to Dobson spectrophotometer no. 83.

Table 5.3. Dobson Spectrophotometers Calibrated in 1988

Country	Station	Instrument No.
U.S.S.R.	Leningrad	108
U.S.S.R.	Moscow	107
Australia	Perth	81
New Zealand	Lauder	72
U.S.A.	Bismarck	33
U.S.A.	Boulder (SPO)	80
U.S.A.	Boulder (Secondary Standard)	65
Australia	Melbourne (Regional Standard)	105

Of the three domestic instruments calibrated, instrument no. 80 was destined for shipment to SPO, to replace instrument no. 82 that has been in use at the South Pole since 1984. Instrument no. 65 was calibrated for use as a secondary standard. Instrument no. 33 remained in Bismarck.

Preliminary calibration of U.S.S.R. secondary standard Dobson instrument no. 108 showed that O_3 values obtained with it agree with those of instrument no. 83 to ±0.15%. U.S.S.R. instrument no. 107 was modernized electronically, opitcally aligned, and calibrated for the first time.

In November-December 1988, the automated Dobson instruments at Perth, Australia, and Lauder, New Zealand, were calibrated. Calibrations were performed in the total O_3 and Umkehr modes. Recalibration of the Perth instrument was needed following repair of the instrument's optical wedge in October. The Lauder spectrophotometer was found to be in good calibration.

5.1.4. VALIDATION OF TOMS AND SBUV SATELLITE OZONE DATA AT MLO WITH DOBSON SPECTROPHOTOMETER NO. 83

Since 1979, when the TOMS and the SBUV O_3 instruments were launched aboard the Nimbus-7 satellite, calibration checks have been performed during most years at MLO on World Primary Standard Dobson Instrument no. 83. The Dobson instrument total O_3 data have been compared with the TOMS and SBUV overpass data as a check on the calibration drift of the satellite O_3 sensors. Figure 5.2 shows the comparison results. Note that the calibration drifts of the TOMS and SBUV instruments, caused by deterioration of a diffuser plate common to both instruments, are nonlinear and amount overall to about 5% in 9 years. Satellite data for the comparisons were provided by NASA [see *McPeters and Komhyr*, 1989]. A similar calibration drift for the TOMS and SBUV satellite O_3 sensors is indicated by data from 39 select stations of the global Dobson instrument network [*Fleig et al.*, 1986]. The network instruments have been calibrated relative to instrument no. 83 since the mid-to-late 1970s.

The long-term O_3 measurement precision of instrument no. 83. has been maintained to within ±0.5% since 1962 [*Komhyr et al.*, 1989a]. Instrument No. 83 data are presented in Figure 5.2 on an absolute scale, indicating that when the satellite O_3
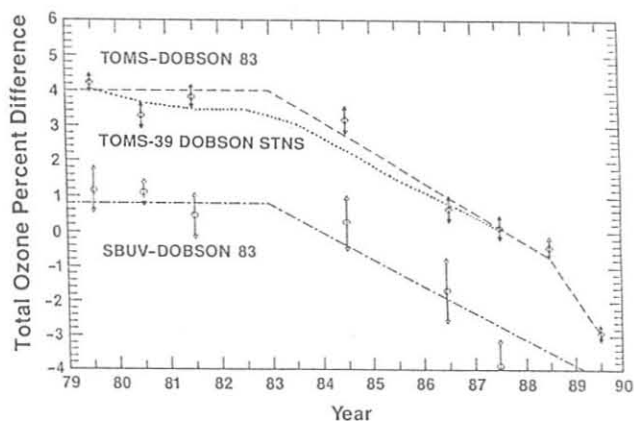
37

Fig. 5.2. Calibration drift of the TOMS and SBUV satellite O_3 instruments during 1979-1988 relative to World Primary Standard Dobson instrument No. 83, and relative to 39 stations of the global Dobson spectrophotometer network.

Fig. 5.3. Annual surface O_3 amounts for the June-November season at BRW, for the month of January at MLO, and for the December-January-February season at SMO and SPO. The trends are the linear least-squares fit to the data. The uncertainties are the 95% confidence interval, based on a two-tailed t test.

instruments first began operating in 1979 the TOMS instrument measured total O_3 amounts too high by 4% while the SBUV instrument measured O_3 values too highly by 1%.

5.1.5. TROPOSPHERIC OZONE

Observations of O_3 near the surface have been made for 15 years at the GMCC observatory at BRW. Records approaching this length have been obtained at the other GMCC sites. In October 1988, as part of the AEROCE, a surface O_3 monitoring program was begun in Bermuda. Installations are planned during 1989 for Barbados; Mace Head, Ireland; and Tennerife, Canary Islands. This network is designed to measure fluxes from the continental regions surrounding the North Atlantic to the ocean region. These sites are more likely to record alterations in the background levels of O_3, as a result of reactive nitrogen compounds emitted by human activity, than are the more remote GMCC sites.

At BRW the marked summer and autumn increases have continued (Figure 5.3) with a highly significant linear trend of $1.39 \pm 0.57\%$ yr^{-1}. This is in contrast to the remainder of the year (not shown) when no change has been detected over the 15-year record. During the summer months sufficient solar insolation allows for O_3 generation, if necessary precursor gases such as nitrogen oxides are present. Recent summertime aircraft measurements as part of the NASA ABLE-3A experiment indicate rather low reactive nitrogen amounts for Alaskan continental regions [*Chen et al.*, 1989] except during forest-fire related episodes. The O_3 flux to the surface during this time of year is also large. Long-term changes in this flux could also produce changes in the seasonal surface O_3 amount.

At MLO, surface O_3 increases have been confined to the winter months, primarily January (Figure 5.3). Large O_3 amounts were noted in late 1982 and early 1983 at the level of MLO (680 mb). The continuing series of ozonesonde measurements from Hilo show that although tropospheric values at the level of the observatory were high in 1983 relative to
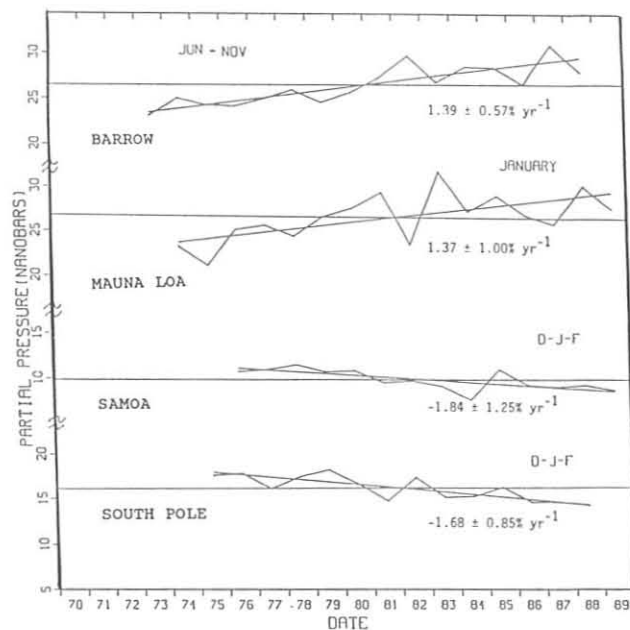
subsequent years (Figure 5.4), upper tropospheric values (above 300 mb) were much reduced. A similar pattern was seen in the spring of 1987 (Figure 5.5) in which O_3 in the upper troposphere was much reduced. In both December-January-February 1983 and March-April-May 1987 tropopause heights were higher than normal. In both cases this period is the minimum in the SOI, which is indicative of an El Niño event. During such an event, Pacific Ocean temperatures are above normal, and enhanced convection produces higher tropopauses in the region. This seems to be reflected in reduced O_3 amounts in the upper troposphere. It is not clear, however, why the troposphere below about 8 km has above-normal O_3 amounts under such conditions. Although tropospheric circulation patterns are altered during an El Niño event [*Quiroz*, 1983], it is difficult to specify how such changes affect the O_3 circulation at a particular location without detailed model calculations.

At both SMO and SPO, there has been a significant decrease in the near-surface O_3 concentration during the austral summer months (Figure 5.3). In both cases, this is the season of the minimum in the annual cycle.

The minimum occurs during this season rather uniformly throughout the southern hemisphere at locations unaffected by local pollution sources. Under the very low NO_x ($NO_2 + NO$) conditions that probably predominate throughout the southern hemisphere lower troposphere, the oxidation of CH_4 and CO produces a net loss of O_3 [*Crutzen*, 1988]. Although no long-term changes of CO have been noted in the southern hemisphere [*Fraser and Coram*, 1988], CH_4 concentrations
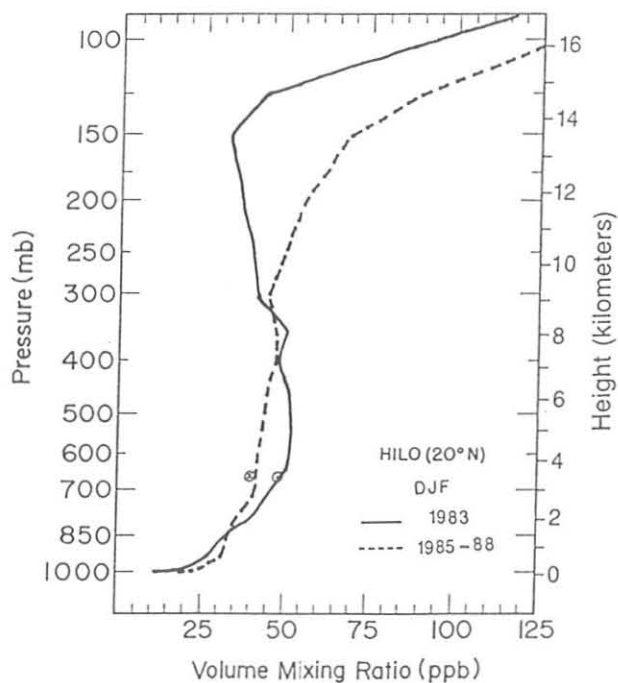
Fig. 5.4. Season average (December-January-February) O_3 profile from ozonesondes at Hilo, Hawaii, for 1983 (solid curve) and 1985-88 (dashed curve). The ⊗ is the 1983 value measured at MLO with the surface monitor. The ⊙ is the MLO data for 1985-88. The MLO data are plotted at the approximate altitude of the observatory.

Fig. 5.5. Season average (March-April-May) O_3 profile from ozonesondes at Hilo, Hawaii, for 1987 (solid curve) and 1983-88 (dashed curve). There were no observations in 1984.

have continued to rise [*Bodhaine and Rosson*, 1988]. The summer months, having abundant solar insolation and higher water vapor amounts, give greater OH concentrations [*Crutzen*, 1988]. This in turn should lead to lower O_3 amounts through the oxidation of CH_4. Determining whether the gradual decline in summertime southern hemisphere O_3 concentrations is related to the buildup in atmospheric CH_4 requires additional modeling of this chemistry.
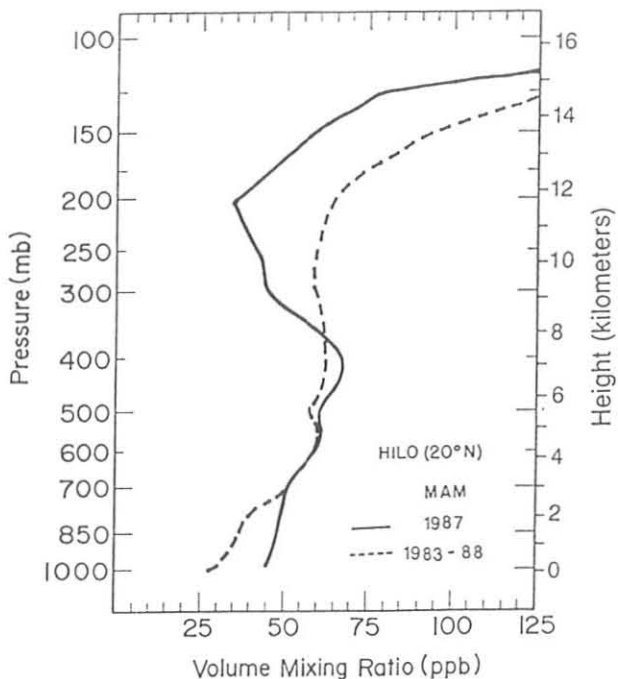
5.1.6. OZONESONDE OBSERVATIONS

ECC ozonesonde observations were continued at Boulder, Colorado, and Hilo, Hawaii; soundings were made at weekly intervals. Similar observations were made throughout the year at SPO, but at a frequency of one sounding every 2-3 days during the Antarctica springtime.

As indicated earlier, O_3 depletion in Antarctica during September and October 1988 was much less pronounced than in 1987 [*Komhyr et al.*, 1989b]. Figure 5.6 contrasts O_3 and temperature profiles over SPO on October 12, 1987, and October 10, 1988, days during the 2 years when maximum O_3 depletions were observed at pressure altitudes of 100-30 mb (centered at about 17 km). Note that in 1987 the O_3 at 17 km was virtually completely depleted, whereas in 1988 the depletion amounted to only about 60%. Stratospheric temperatures colder than -78°C, at which polar stratospheric clouds occur, persisted in 1987 till the end of October. In 1988 the temperatures became warmer than -78°C about 2 weeks earlier. Rapid stratospheric warming occurs at the time of polar vortex breakdown and the influx of O_3-rich air into Antarctica from lower latitudes. In 1987, the winter and early spring Antarctica circumpolar vortex was of large areal extent, and SPO was situated approximately centrally within it. In 1988 the vortex was much smaller, and its center during September and October was generally displaced from SPO in the direction of the Palmer Peninsula.

5.1.7. STRATOSPHERIC WATER VAPOR

With 8 years (1981 through 1988) of water vapor profiles in the stratosphere, it is possible to look for the longer term variations that might be suggested by the rising trend in CH_4 in the atmosphere. The photolysis of CH_4 in the stratosphere is expected to be a major source of H_2O vapor in this region. The average growth rate in CH_4 over the past several years is about 0.012 ppmv yr[1], based on observations at the GMCC flask sampling network [*Bodhaine and Rosson*, 1988]. If a similar increase is taking place in the stratosphere, then a maximum increase in H_2O vapor of about 0.024 ppmv yr[1] might be expected if all the CH_4 was eventually photolyzed.

At 50 mb (20 km) the seasonal variability of H_2O vapor is small [*Schnell and Rosson*, 1987], making this an appropriate level to check for longer term changes. It is also a level that is usually attained in the balloon sounding and where instrument performance is good. Volume mixing ratios at 50 mb for each successful sounding are shown in Figure 5.7. The trend line is a linear least-squares fit to the data. The trend and 95% confidence interval based on the two-tailed t test is 1.26 ± 0.67%

OZONAGRAM

SITE: SOUTH POLE   TOTAL O3: 147.
DATE: 12 OCT 87   SONDE O3: 160.
TIME: 0204 Z   C.F.: .917
INST: ECC 4A2613

0.1 ATM-CM

OZONAGRAM

SITE: SOUTH POLE   TOTAL O3:
DATE: 10 OCT 88   SONDE O3: 197.
TIME: 0850 Z   C.F.:
INST: ECC 4A3680

0.1 ATM-CM
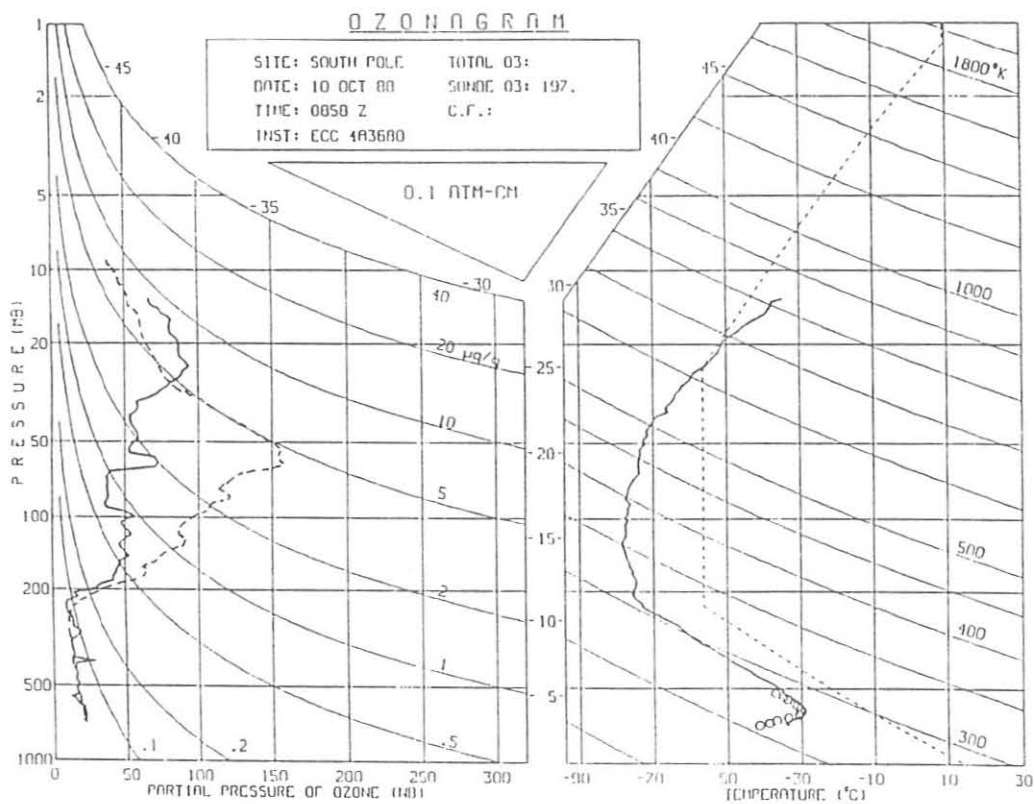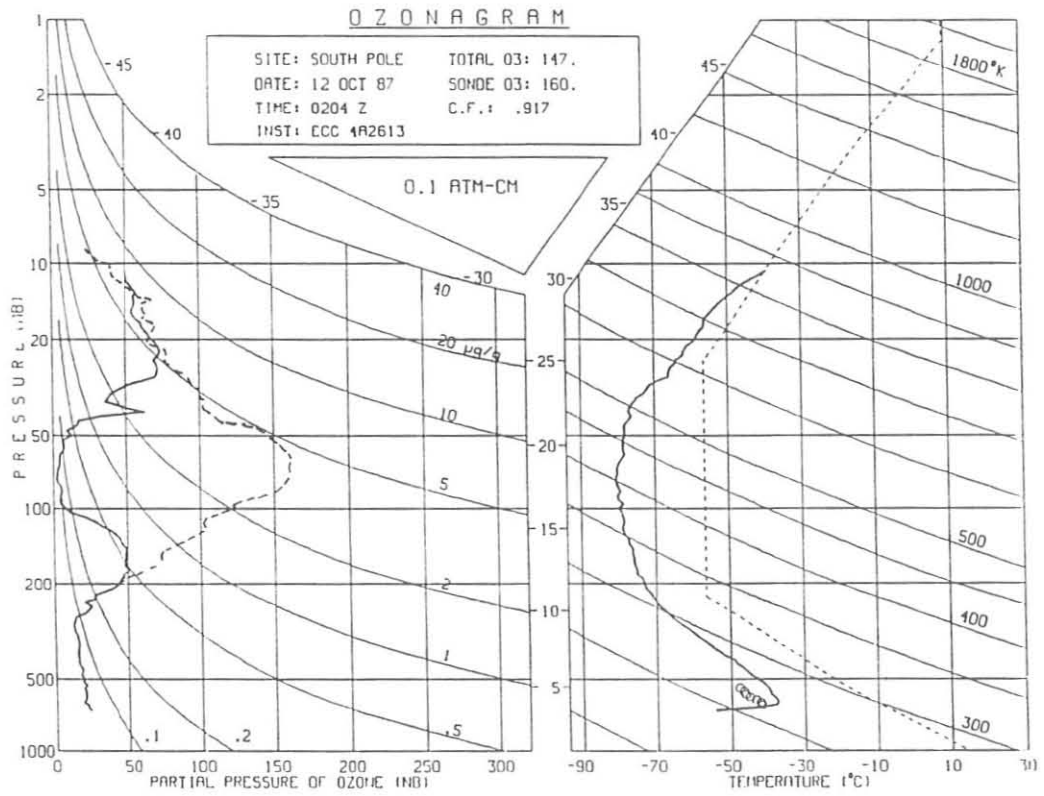
Fig. 5.6. O₃ and temperature profiles (solid curves) over South Pole, Antarctica, on days in October 1987 and 1988 when maximum O₃ depletions were observed between 100 and 30 mb. The dashed O₃ curves are August 24, 1987, and August 21, 1988, profiles obtained prior to the onset of O₃ depletion processes. (The dashed temperature curves represent standard atmosphere temperatures.)
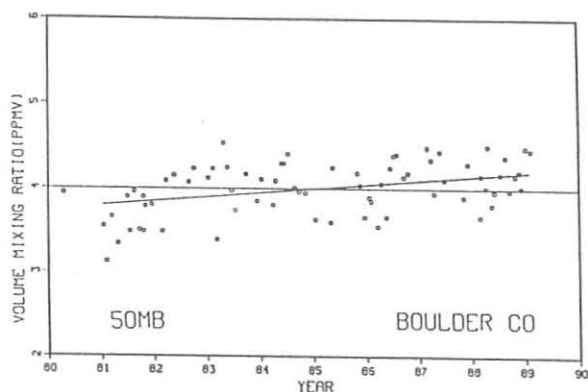
40

Fig. 5.7. Water vapor volume mixing ratio (ppmv) at 50 mb from balloonborne frost-point hygrometer soundings at Boulder, Colorado. The trend line is a linear least-squares fit to the data.
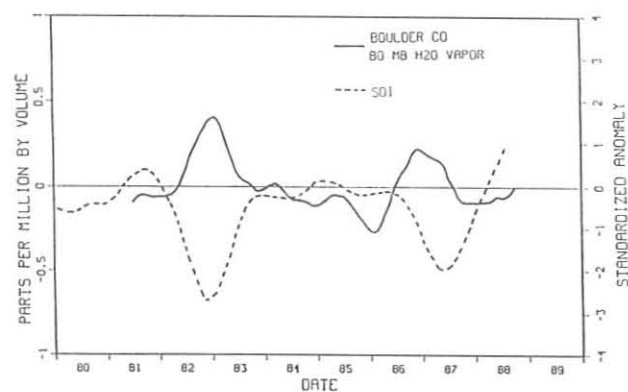

Fig. 5.8. The smoothed water vapor volume mixing ratio (ppmv) at 80 mb at Boulder, Colorado (solid curve), and smoothed SOI (dashed curve).

yr^{-1}. This is an increase of about 0.05 ppmv yr^{-1}, which is more than expected for CH$_4$ increase. From Figure 5.7, it is clear that most of the trend can be attributed to the low values in 1981. The sensors used in 1981 and the first half of 1982 were calibrated at the Naval Research Laboratory in Washington, D.C. Since 1982, the sensors have been calibrated at a GMCC laboratory. The two laboratories' temperature measurement systems were intercompared and found to be in close agreement [*Harris and Nickerson*, 1984]. Unfortunately no sensors used during 1981-82 are still available to verify the earlier calibrations.

At lower altitudes in the stratosphere, the seasonal variation dominates. The strong springtime minimum is thought to be related to the very cold tropopause temperatures in the tropical western Pacific and to subsequent poleward transport of this dry air [*Brewer*, 1949]. Meteorological variations on longer time scales such as those of the ENSO, which are centered in the tropical Pacific, might be reflected in the lower stratospheric water vapor pattern at Boulder. In Figure 5.8 the smoothed

water vapor anomalies at 80 mb in Boulder are shown with the smoothed values of the SOI. The two ENSO events of 1982-1983 and 1987 shown in the SOI are perhaps reflected in above-average water amounts seen during this time at Boulder. If this relationship holds up over longer measurement periods, it suggests that during ENSO events, additional water vapor reaches the stratosphere. This might be the result of the enhanced convection associated with warmer ocean temperatures. Data from Washington, D.C., from 1964 to 1976 suggests that a similar relationship held, although the year-to-year variations in water vapor are much larger than those at Boulder.

5.2. SPECIAL PROJECTS: OBSERVATIONS INDICATING POSSIBLE OZONE DESTRUCTION DURING THE ANTARCTIC POLAR NIGHT

Since the discovery of the springtime Antarctic O$_3$ depletion, a great deal of attention has been given to processes related to aerosol formation and heterogeneous chemistry at low temperatures. Polar stratospheric clouds (PSCs) are frequent features of the southern winter atmosphere, and provide a site for heterogeneous reactions that lead to O$_3$ destruction in the presence of sunlight. Models have been proposed for the formation of PSCs based on the condensation of HNO$_3$.

An aerosol lidar instrument from the University of Rome "La Sapienza," Physics Department, Rome, Italy, operated at SPO during the 1988 polar night, indicated the presence of PSCs [*Fiocco et al.*, 1989]. O$_3$ profile measurements, made quasi-simultaneously with ECC sondes during June and July months, showed sharp O$_3$ concentration minima in the vicinity of the PSCs. The correspondence between the aerosol layers and the O$_3$ minima is shown in Figure 5.9, which depicts four half-hour-average aerosol profiles for June 21-24 (all taken at about 2230 UTC), and O$_3$ and temperature profiles for June 23, 0255 UTC. (For reference, Figure 5.9 also shows an average O$_3$ profile derived from ozonesonde measurements made in June.) The O$_3$ minima occur at about 14.5, 15.6 and 16.9 km. Less than a day later (curve c), intense stratifications at about 14.4, 15.8, and 17.4 km were seen by lidar.

Definitive information is unavailable for unambiguous interpretation of the results. The simultaneous presence of the O$_3$ and aerosol features may, however, be ascribed to several possible mechanisms: (1) Air masses with low O$_3$ content and appreciable amounts of condensable matter, possibly water, reach the SPO stratosphere, structured in thin (1-km) layers. No chemical interaction between the constituents is implied; the lower O$_3$ amounts are related to the origin of the air masses. (2) Air masses carrying PSCs pass in and out of darkness through sunlit regions where photochemical O$_3$ destruction may occur. Thus, O$_3$ may also be destroyed in Antarctica during winter and not only during springtime. (3) O$_3$ can be destroyed in the absence of sunlight through reaction with NO$_2$ to form N$_2$O$_5$ and then condensable HNO$_3$. However, this process is unlikely to occur at the magnitude implied by the measurements. (4) O$_3$ is destroyed catalytically by reaction on the PSCs.

41
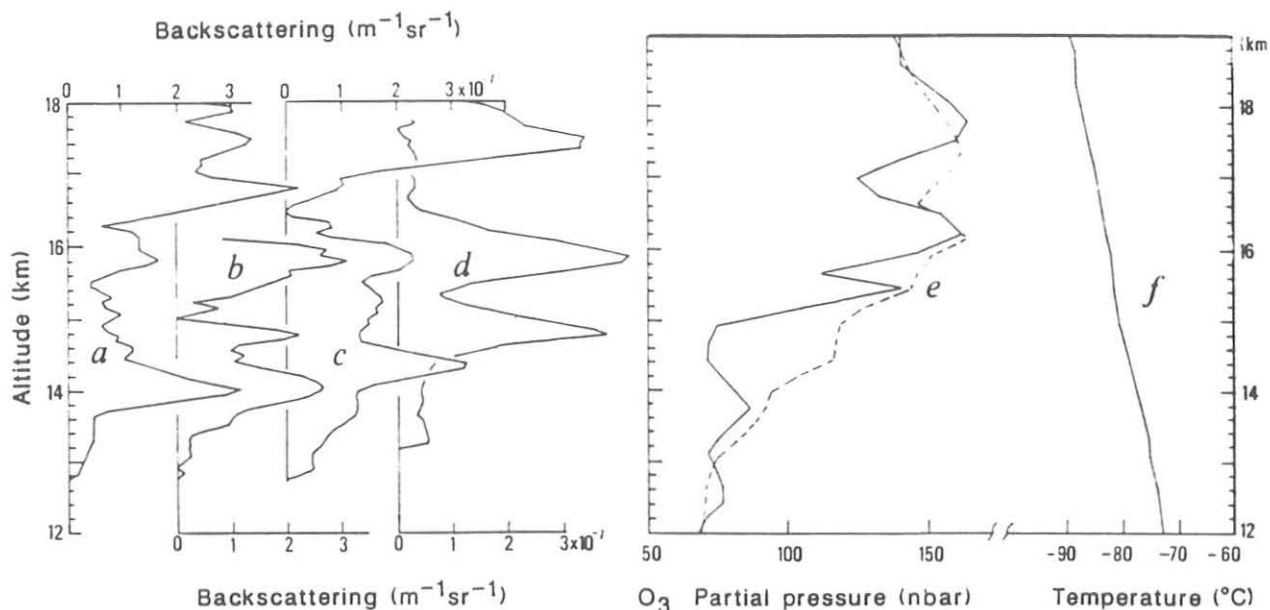
Fig. 5.9. (a)-(d) Aerosol backscattering profiles for June 21-24, respectively, derived from averaged half-hour lidar observations made at about 2230 UTC, (e) O_3 partial pressure profile and (f) temperature profile, for June 23, 0255 UTC (solid curves). The dashed curve is the average O_3 profile derived from five ECC ozonesonde measurements made in June.

5.3. REFERENCES

Bodhaine, B.H., and R.M. Rosson (Eds.), *Geophysical Monitoring for Climatic Change No. 15, Summary Report 1987*, 110 pp., NOAA Environmental Research Laboratories, Boulder, CO, 1988.

Brewer, A.W., Evidence for a world circulation provided by measurement of helium and water vapor in the stratosphere, *Q. J. R. Meteorol. Soc., 75*, 351-363, 1949.

Chen, G., S. Sandholm, J. Schendel, D. Davis, and J. Bradshaw, High latitude distributions of reactive odd-nitrogen components NO, NO_2, and NO_y observed during GTE/ABLE-3A, *EOS, 70*, 291, 1989.

Crutzen, P.J., Tropospheric ozone: An Overview, in *Tropospheric Ozone*, edited by I.S.A. Isaksen, pp. 3-32, D. Reidel, Dortrecht, 1988.

Fiocco, G., W.D. Komhyr, and D. Fuá, Is ozone destroyed during the Antarctic polar night in the presence of polar stratospheric clouds? *Nature, 341*, 426-427, 1989.

Fleig, A.J., P.K. Bhartia, C.G. Wellemeyer, and D.S. Silberstein, An assessment of long term drift in the SBUV total ozone data based on comparison with the Dobson network, *Geophys. Res. Lett., 13(12)*, 1359-1362, 1986.

Fraser, P.J., and S. Coram, Atmospheric methane, carbon monoxide, and carbon dioxide by gas chromatography, 1986, in *Baseline 86*, edited by B.W. Forgan and P.J. Fraser, pp. 65-66, Bureau of Meteorology, Australia, 1988.

Harris, J.M., and E.C. Nickerson (Eds.), *Geophysical Monitoring for Climatic Change, No. 12: Summary Report 1983*, 183 pp., NOAA Environmental Research Laboratories, Boulder, CO, 1984.

Komhyr, W.D., R.D. Grass, and R.K. Leonard, Dobson spectrophotometer 83: A standard for total ozone measurements, 1962-1987, *J. Geophys. Res., 94(D7)*, 9847-9861, 1989a.

Komhyr, W.D., J.A. Lathrop, R.W. Poston, and T.O. Mullen, ECC ozonesonde observations at South Pole, Antarctica, during 1988, *NOAA Data Rep. ERL ARL-18*, 277 pp., NOAA Air Resources Laboratory, Silver Spring, MD, 1989b.

McPeters, R.D., and W.D. Komhyr, Long-term changes in SBUV/TOMS relative to the World Standard Dobson Ozone Spectrophotometer, *Proceedings of the 1988 Ozone Symposium*, University of Göttingen, Federal Republic of Germany, A. Deepak, Hampton, VA., in press, 1989.

Quiroz, R.S., Seasonal climate summary: The climate of the El Niño winter of 1982-83-A season of extraordinary climatic anomalies, *Mon. Weather Rev., 111*, 1685-1706, 1983.

Schnell, R.C., and R.M. Rosson (Eds.), *Geophysical Monitoring for Climatic Change, No. 15: Summary Report 1986*, 155 pp., NOAA Environmental Research Laboratories, Boulder, CO, 1987.

6. Acquisition and Data Management Group

J. HARRIS (Editor), G. HERBERT, AND J. McCUTCHEON

6.1. CONTINUING PROGRAMS

6.1.1. STATION CLIMATOLOGY

Measurements of meteorological variables are necessary for the interpretation of measured values of aerosols, trace gases, and turbidity. More than 10 years of meterological data at the four baseline stations have produced climatologies typical of the polar and tropical atmospheres. Surface weather data include the measurements of wind direction, wind speed, station pressure, air and dewpoint temperature, precipitation amount, and a determination of boundary layer stability. The current sensors used at GMCC stations were selected to withstand the extreme conditions of the environment at the two polar stations. WMO-recommended standards for exposure are used wherever possible. *Nickerson* [1986] gave a complete list of the sensors, model numbers, and heights.

In 1984 the CAMS data acquisition systems were installed at all stations; this improved the consistency of the data acquisition hardware and reduced the quantity of missing data. The meteorological data are printed as hourly average values in a Daily Weather Report (DWR), and are checked against real-time observations by station personnel. The DWRs are then sent to Boulder, where they are edited and microfiched. An edited computer file of these data will be stored in the Boulder meteorology archive. *Herbert et al.* [1986a, b] presented a detailed discussion on the individual parameters contained in the DWR and other CAMS printouts.

Barrow

Descriptions of the BRW site, its surroundings, and climate are given in previous *GMCC Summary Reports* [e.g., *DeLuisi*, 1981]. Wind roses of hourly average resultant wind direction and speed are presented in 16 direction classes and 4 speed classes (Figure 6.1). The distribution of wind by direction for 1988 is almost identical to the 11-year climatology. A higher percentage of calm hours (1.2%) was reported in 1988. The predominant wind direction is again from the "clean-air sector," northeast-southeast (60%), and all other directions except north-northeast are less than 5%. The east-southeast direction logged the year's peak gust of 25 m s^{-1} on January 2, and this set a new January record for the station (Table 6.1).

The average temperature and pressure for 1988 were consistent with the long-term averages, although there were anomalous values during the year. The minimum temperature for 1988 of −41°C occurred on February 22, and the maximum temperature of 17°C occurred on August 5. February was a month of extreme variability in pressure and temperature. On February 3 a new all-time-high pressure record was set at 1057 hPa. The minimum pressure for 1988 of 986 hPa was first recorded on February 24. In March, the pressure again reached the all-time high set in February. BRW's climate in August had extremes in temperature, missing the 1925 August record low of −7°C by 1°C based on the NWS climate record. In the same month BRW logged the year's maximum temperature (17°C). Climatologically, August receives the majority of BRW's precipitation, as it did in 1988.
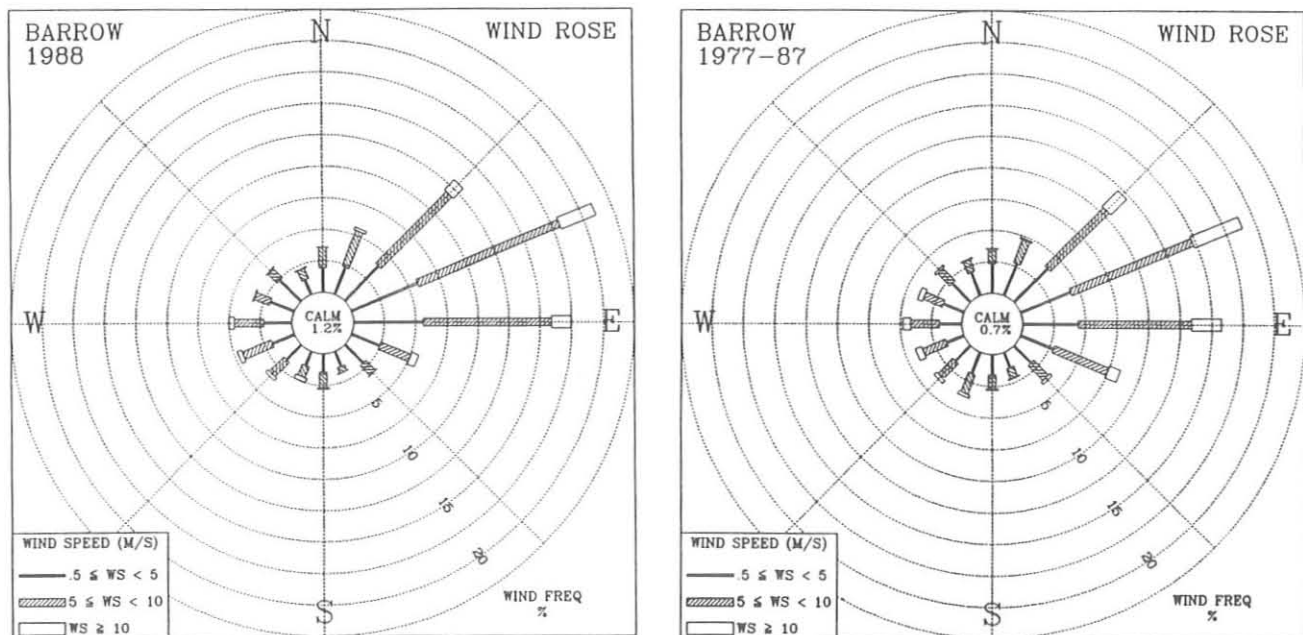

Fig. 6.1. Wind rose of surface winds for BRW for 1988 (left) and 1977-1987 (right). The distribution of the resultant wind direction and speed are in units of percent occurrence for the year and 11-year period, respectively. Wind speed is displayed as a function of direction in three speed classes.

	Jan.	Feb.	March	April	May	June	July	Aug.	Sept.	Oct.	Nov.	Dec.	1988
Prevailing wind direction	ENE	E	ENE	E	ENE	E	E	ENE	NE	E	ENE	ENE	ENE
Average wind speed (m s $^{-1}$)	6.7	5.4	5.2	5.9	7.2	5.1	5.5	6.1	6.1	5.9	6.7	5.7	6.0
Maximum wind speed* (m s^{-1})	21	16	14	13	14	13	13	17	20	14	18	16	21
Direction of max. wind* (deg.)	113	80	27	72	73	118	230	232	204	206	56	99	113
Average station pressure (hPa)	1014.6	1015.7	1019.4	1016.6	1018.8	1013.4	1011.6	1007.5	1010.3	1017.7	1018.4	1008.6	1014.4
Maximum pressure* (hPa)	1038	1057	1057	1031	1036	1025	1024	1019	1022	1036	1034	1038	1057
Minimum pressure* (hPa)	996	986	989	998	1008	997	988	986	987	1000	1002	988	986
Average air temperature (°C)	−23.8	−25.5	−24.9	−16.9	−6.5	0.2	3.1	1.5	−2.3	−16.2	−24.9	−22.4	−12.9
Maximum temperature* (°C)	−1	−7	−10	0	4	6	14	15	5	0	−12	−13	15
Minimum temperature* (°C)	−40	−41	−38	−36	−21	−9	−2	−6	−12	−27	−33	−40	−41
Average dewpoint temperature (°C)									−4.2	−16.5	−25.3	−23.5	−19.4
Maximum dewpoint temperature* (°C)									2	−1	−12	−13	2
Minimum dewpoint temperature* (°C)									−12	−27	−33	−41	−41
Precipitation (mm)	0	1	0	0	1	7	25	34	4	0	0	1	72

Instrument heights: wind, 17 m; pressure, 9.5 m (MSL); air and dewpoint temperature, 3 m. Wind and temperature instruments are on a tower 25 m northeast of the main building. 1 hPa = 1 mb.

*Maximum and minimum values are hourly averages.

The measurement of dewpoint temperature began again in September with the installation of a new dewpoint hygrometer (hygrothermometer, model 1063, Technical Services Laboratory, Fort Walton Beach, Florida).

Mauna Loa

Descriptions of MLO and its general climatology are given in previous *GMCC Summary Reports*. The topography of Mauna Loa redirects stronger, predominantly easterly or westerly winds aloft down the slope resulting in a more southerly component. A new anemometer was installed at a height of 39 m on February 17, 1988. The new configuration now permits the comparison of winds at different heights.

The year's minimum temperature (−4°C) and pressure (671 hPa) occurred on December 18 during one of 1988's tropical storms. The next day the year's peak gust (25 m s^{-1}) was recorded, accompanied by 51 mm of snow. The maximum temperature for 1988 was 19°C on September 21. MLO had a dry summer that was relieved by a relatively wet November and December. May was an anomalous month, having light winds from the north 11% of the time. High pressure was persistent, and only a trace of precipitation was measured. The precipitation total for the year was 410 mm (Table 6.2), which is slightly below normal.

The climatology of MLO is often considered as two separate regimes, because of the bimodal distribution of the wind direction, which depends on the time of day. The day/upslope period (0600-1800 LST) and the night/downslope period (1800-0600 LST) define the two regimes. The 11-year day and night wind roses illustrate the two distinct wind patterns (Figure 6.2). Strong west-southwest and east-southeast winds in the 11-year roses can be attributed to large synoptic-scale storms. In the 1988 day/night wind roses (Figure 6.3) those anomalous winds were not observed.

Day regime. The 11-year day wind rose indicates that light wind speeds in the northwest-northeast sector were observed 47% of the time. The day regime had calm winds 2.8% of the time. The 1988 day wind rose shows an increase, compared with the long-term average, in light northerly upslope winds, and medium-strength southeast winds. Wind speeds of less than 10 m s^{-1} from the south-southeast were observed 28% of the time, compared with the normal of 16%. The characteristic pattern of the winds for 1988 was an increase in the frequency of upslope/downslope flow. The dewpoint temperature reflects the upslope/downslope events in that upslope flow brings moist tropical air from below the trade inversion to the observatory.

Night regime. The 11-year night wind rose shows that 75% of all winds observed were from the southwest-southeast sector.

TABLE 6.2. MLO 1988 Monthly Climate Summary

	Jan.	Feb.	March	April	May	June	July	Aug.	Sept.	Oct.	Nov.	Dec.	1988
						Day							
Prevailing wind direction	NNW	N	NNW	NNE	N	SE	N	NNE	NNE	N	SE	SSE	N
Average wind speed (m s^{-1})	4.0	3.8	3.8	3.8	3.9	4.9	4.4	3.8	3.2	3.7	5.6	5.4	4.2
Maximum wind speed* (m s^{-1})	13	10	10	8	11	12	13	10	9	11	15	15	15
Direction of max. wind* (deg.)	210	133	174	139	153	137	150	158	172	153	182	172	172
Average station pressure (hPa)	679.4	678.9	680.2	679.8	681.0	681.8	681.1	680.8	680.4	680.2	680.4	679.2	680.3
Maximum pressure* (hPA)	684	683	684	683	685	684	684	683	683	684	684	683	685
Minimum pressure* (hPa)	674	675	676	677	678	679	678	678	678	678	674	671	671
Average air temperature (°C)	7.3	6.9	8.0	9.0	10.4	12.1	10.9	11.5	10.9	9.6	7.6	6.1	9.2
Maximum temperature* (°C)	14	12	14	16	17	18	18	17	18	16	14	12	18
Minimum temperature* (°C)	−2	−1	0	0	2	3	3	5	2	3	1	−3	−3
Average dewpoint temperature (°C)	−8.2	−9.3	−10.7	−7.2	−5.0	−7.8	−4.5	−4.3	−3.3	−1.6	−1.6	−5.9	−5.8
Maximum dewpoint temperature* (°C)	6	5	4	6	7	8	6	9	9	7	7	6	9
Minimum dewpoint temperature* (°C)	−28	−33	−37	−26	−25	−27	−32	−29	−32	−26	−24	−40	−40
Precipitation (mm)	53	0	47	35	0	20	0	41	6	40	63	14	320
						Night							
Prevailing wind direction	SE	SE	SSE	SSE	SSW	SSE	SSE	SSE	SSE	SSE	SSE	SSE	SSE
Average wind speed (m s^{-1})	5.2	3.9	4.0	4.1	3.6	5.3	3.9	3.8	3.3	3.8	6.2	6.3	4.5
Maximum wind speed* (m s^{-1})	16	9	8	9	12	11	15	10	11	13	16	20	20
Direction of max. wind* (deg.)	215	144	164	161	152	149	151	168	151	150	178	149	149
Average station pressure (hPa)	679.5	679.0	680.2	679.7	681.1	681.8	680.9	680.8	680.3	680.2	680.5	679.4	680.3
Maximum pressure* (hPA)	684	683	684	683	685	685	684	683	683	683	683	683	685
Minimum pressure* (hPA)	674	675	675	677	678	679	678	678	678	678	675	671	671
Average air temperature (°C)	3.6	2.7	3.6	3.8	5.4	6.9	5.9	6.8	6.7	5.4	4.1	2.6	4.8
Maximum temperature* (°C)	9	9	9	11	12	14	14	13	13	10	7	9	14
Minimum temperature* (°C)	−1	−1	−1	−1	0	2	1	4	1	3	0	−4	−4
Average dewpoint temperature (°C)	−12.9	−14.0	−16.9	−13.2	−9.9	−11.5	−10.6	−11.6	−10.6	−6.8	−4.2	−9.6	−11.0
Maximum dewpoint temperature* (°C)	4	3	2	3	5	6	6	8	7	5	4	4	8
Minimum dewpoint temperature* (°C)	-23	-31	-36	-26	-25	-29	-29	-30	-32	-29	-20	-25	-36
precipitation (mm)	20	1	7	1	0	0	0	6	1	2	33	20	90

Instrument heights: wind, 8.3 m; pressure, 3399 m (MSL); air and dewpoint temperature, 2 m. Wind and temperature instruments are on a tower located 15 m southwest of the main building.
*Maximum and minimum values are hourly averages.

45

Fig. 6.2. Wind roses of the surface winds for MLO for 1977-1987 Day (left) and Night (right). The distributions of the resultant wind direction and speed are units of percent occurrence for the 11-year period. Wind speed is displayed as a function of direction in three speed classes.

Fig. 6.3. Wind roses of the surface winds for MLO for 1988 Day (left) and Night (right). The distribution of the resultant wind direction and speed are given in units of percent occurrence for the year. Wind speed is displayed as a function of direction in three speed classes.

At night calm conditions were observed 5.1% of the time. The 1988 average wind speed of the night regime of 4.5 m s⁻¹ is faster than the 4.2 m s⁻¹ average day speed (Table 6.2). The higher percentage of calm winds at night may be attributed to the inclusion of the transition periods at dusk when the flow is switching directions. In the night period, dry, mid-tropospheric air from above the trade inversion is advected over the station.

Samoa

A comparison of SMO's 1988 wind rose with that for the 11-year period shows a very similar distribution except for a 3% increase in north-northwest winds, and a 3% increase in south-southeast winds with speeds greater than 10 m s⁻¹ (Figure 6.4). The southeast sector accounted for 73% of all wind observations in 1988. The average wind speed (Table 6.3) for
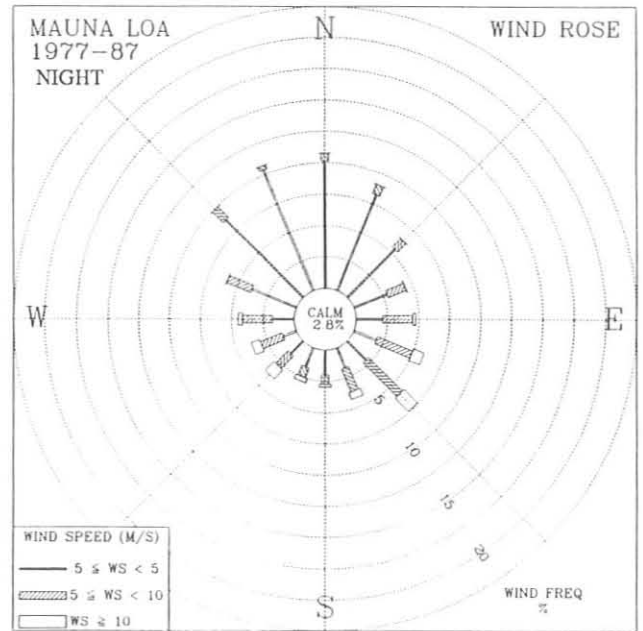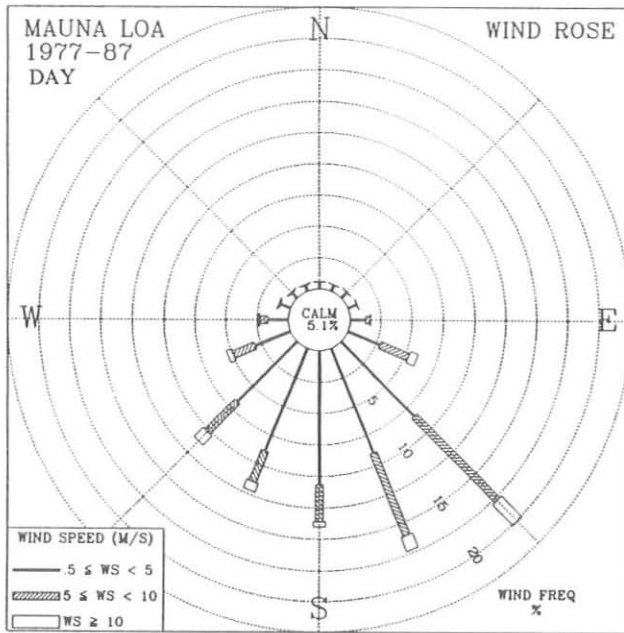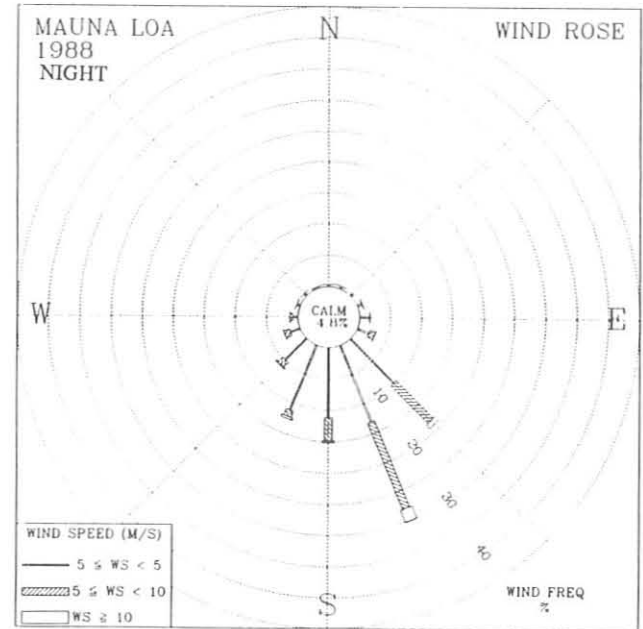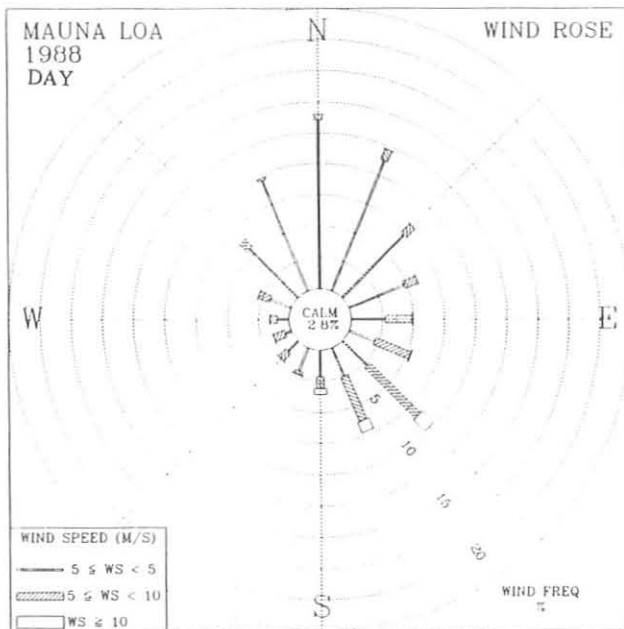
46

Fig. 6.4. Wind roses of the surface wind for SMO for 1988 (left) and 1977-1987 (right). The distributions of the resultant wind direction and speed are in units of percent occurrence for the year and 11-year period, respectively. Wind speed is displayed as a function of direction in three speed classes.

TABLE 6.3. SMO 1988 Monthly Climate Summary

	Jan.	Feb.	March	April	May	June	July	Aug.	Sept.	Oct.	Nov.	Dec.	1988
Prevailing wind direction	SSE	NNW	SE	NNW	SSE	SSE	SSE	SSE	SE	SE	NNW	NNW	SSE
Average wind speed (m s^{-1})	5.2	3.7	5.0	3.6	5.3	6.2	8.4	7.7	7.6	5.9	5.1	4.0	5.7
Maximum wind speed* (m s^{-1})	17	12	13	13	13	13	17	17	19	12	15	13	19
Direction of max. wind* (deg.)	330	333	292	333	147	159	159	155	89	128	119	327	89
Average station pressure (hPa)	999.7	997.9	1000.2	1000.1	1001.5	1003.3	1003.6	1004.5	1003.7	1001.7	1001.7	1000.0	1001.5
Maximum pressure* (hPA)	1005	1003	1005	1005	1005	1007	1007	1008	1008	1006	1006	1006	1008
Minimum pressure* (hPA)	994	992	994	996	997	1000	1000	1001	1000	998	998	994	992
Average air temperature (°C)	28.1	28.2	28.2	27.7	27.8	27.0	26.1	26.3	26.2	26.4	26.1	26.5	27.0
Maximum temperature* (°C)	33	33	32	33	33	32	29	30	29	31	31	31	33
Minimum temperature* (°C)	22	24	24	24	24	24	21	23	22	22	22	22	21
Precipitation (mm)	160	228	219	119	111	110	170	63	220	196	348	679	2623

Instrument heights: wind, 14 m; pressure, 30 m (MSL); air temperature, 9 m. Wind and temperature instruments are on Lauagae Ridge, 110 m northeast of the main building. Pressure sensors are in the main building. 1 hPa = 1 mb.

*Maximum and minimum values are hourly averages.

the year of 5.7 m s^{-1} was 3.2 m s^{-1} above the long-term average. July was the windiest month of the year; it had a 9 m s^{-1} average.

In 1987 and the first half of 1988, ENSO was in the low index phase. During the latter part of 1988, ENSO switched to the high index phase, characterized by below-normal sea surface temperatures, strong easterly surface winds, and enhanced precipitation in the equatorial Pacific [*WCP*, 1988].

Of the four GMCC baseline stations, SMO has a climate that is the most responsive to ENSO because of its location. There is a well-defined relationship between the phase of the ENSO event and the amount of precipitation the island receives [*WCP*,1988]. In 1988 a dry spring/summer and a wet, record-setting fall/winter were the result. December was the wettest month on record for the station, having 679 mm of recorded rain. The village of Tula was flooded when 254 mm of rain fell from December 7 to 9. The wind gusted to 28 m s^{-1} on the December 8 and 127 mm of precipitation was measured.

The 1988 maximum temperature of 34°C occurred on February 13, and the minimum temperature of 21°C occurred on July 10. The year's average temperature of 27°C was identical to SMO's long-term average. The strongest 10-min average wind speed of 22 m s^{-1} occurred on September 15. August had the year's highest pressure at 1008 hPa, and the highest monthly average at 1004.5 hPa. During this period of high pressure only 63 mm of rain fell, which was the lowest monthly total for the year.

South Pole

The distribution of the surface wind direction in 1988 at SPO is almost identical to that of the 11-year pattern (Figure 6.5).

The main difference is the shift to higher percentages of northerlies and easterlies. The predominant wind directions in 1988 were grid east-northeast and east (17%) as compared with the long-term prevailing north-northeast direction (19%). The peak gust for the year of 20 m s^{-1} occurred on October 9, from grid north. Wind speeds greater than 10 m s^{-1} were observed only 3% of the year, consistent with the climatological average.

The average temperature for the year was 0.7°C warmer than the 11-year average (Table 6.4). March had an anomalously warm average of −48.7°C, which was 5°C above the normal and set a new station record. March 23 set a monthly all time high (−28°C). August, which is usually the coldest month of the year, was 2°C above the normal for the month. May moderated the warm temperatures with the second coldest May average value of −60°C, compared with the 62°C recorded at the station in 1986. The year's maximum temperature of −19°C occurred on December 25, and the minimum of −78°C occurred on July 1. October logged the year's maximum pressure of 701 hPa and set the October record high-pressure average with a value of 688 hPa.

6.1.2. DATA MANAGEMENT

During 1988 the overall performance of the CAMS automated data acquisition system was good. From time to time, boards, batteries, tape drives, or power supplies were replaced, usually with spares available at the station. Such hardware failures were expected after 4 years of continuous operation.

Table 6.5 gives the CAMS operations summary for 1988. The number of data blocks missing increased from 1987, but at
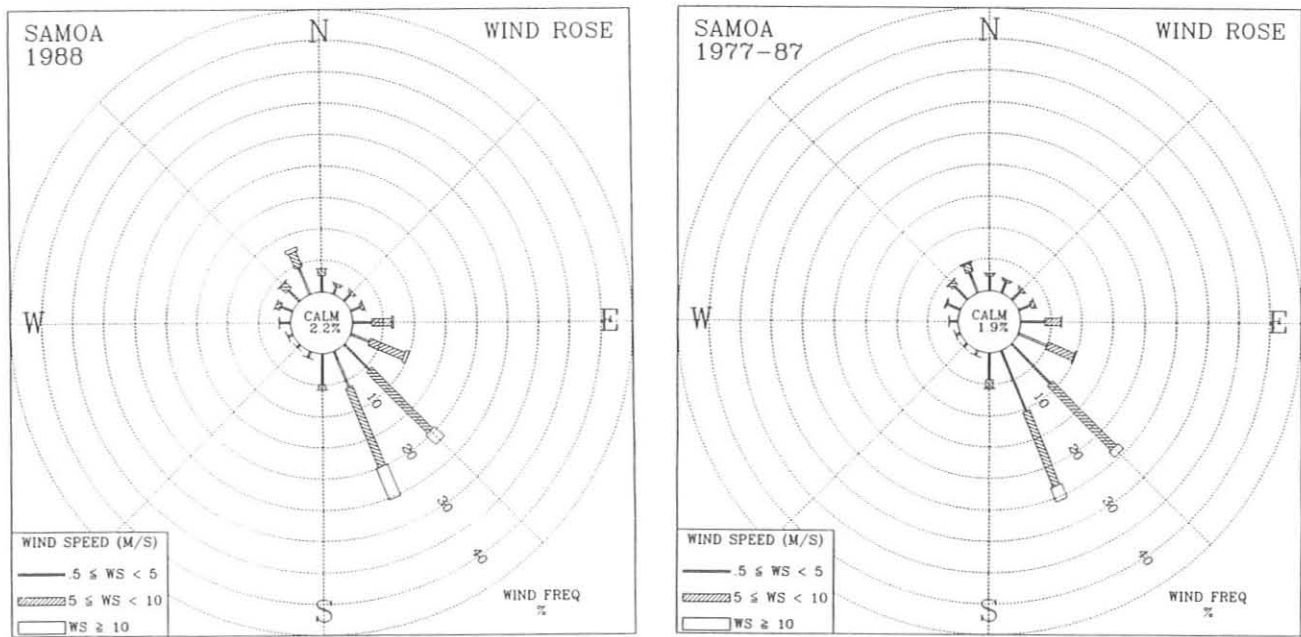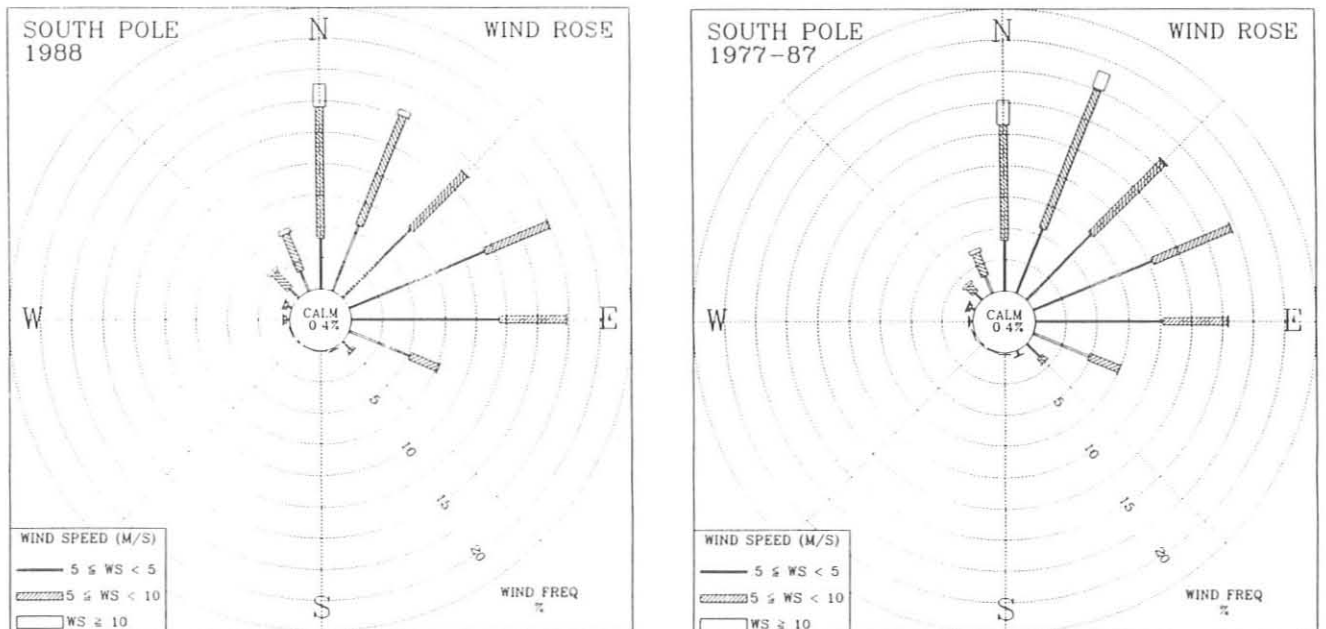

Fig. 6.5. Wind roses of the surface wind for SPO for 1988 (left) and 1977-1987 (right). The distributions of the resultant wind direction and speed are in units of percent occurrence for the year and the 11-year period, respectively. Wind speed is displayed as a function of direction in three speed classes.

TABLE 6.4. SPO 1988 Monthly Climate Summary

	Jan.	Feb.	March	April	May	June	July	Aug.	Sept.	Oct.	Nov.	Dec.	1988
Prevailing wind direction	N	ENE	NNE	ENE	E	NE	E	N	N	E	N	E	ENE
Average wind speed (m s^{-1})	4.8	4.8	6.2	5.6	5.1	6.5	5.7	6.1	5.9	5.7	4.3	3.9	5.4
Maximum wind speed* (m s^{-1})	9	11	12	12	9	13	12	13	14	16	11	8	16
Direction of max. wind* (deg.)	351	14	19	354	114	7	26	313	360	1	4	356	1
Average station pressure (hPa)	689.7	680.5	682.1	679.9	682.0	686.8	671.4	678.2	681.6	687.6	679.4	683.4	681.9
Maximum pressure* (hPA)	696	690	693	689	694	700	683	692	698	701	684	697	701
Minimum pressure* (hPA)	680	673	672	672	666	669	659	665	664	675	676	675	659
Average air temperature (°C)	−26.0	−42.0	−48.7	−58.5	−60.4	−57.3	−61.8	−57.1	−56.9	−49.4	−37.4	−26.3	−48.8
Maximum temperature* (°C)	−21	−27	−28	−40	−37	−35	−43	−37	−39	−33	−27	−19	−19
Minimum temperature* (°C)	−33	−53	−63	−68	−73	−75	−78	−77	−71	−65	−48	−32	−78

Instrument heights: wind, 12 m; pressure, 2841 m (MSL); air temperature, 2 m. The anemometer and thermometer are on a tower 100 m grid east-southeast of CAF. Pressure measurements are made inside CAF. 1 hPa = 1 mb.

*Maximum and minimum values are hourly averages.

TABLE 6.5. GMCC CAMS Operations Summary, 1988

Block Type	Description	Expected No. of Blocks 1988	Blocks Recorded and [Blocks Missing]			
			BRW	MLO	SMO	SPO
A	Hourly aerosol data	2196	2186 [10]	2188 [8]	2154 [42]	2193 [4]
B	Secondary aerosol data	Variable	1683	1565	9	0
H	Daily aerosol data	366	366 [0]	367 [0]	359 [7]	366 [0]
S	Hourly solar radiation data	8784	8743 [41]	8755 [30]	8617 [167]	8768 [17]
C	Hourly CO_2 data	Variable	7929 [421]	8317 [91]	8209 [218]	8187 [12]
D	Daily CO_2 data	366	346 [17]	365 [1]	358 [8]	366 [0]
E	Hourly CO_2 calibration data	Variable	356	375	355	552
F	CO_2 calibration report	52	48	53	48	71
M	Hourly meteorological data	4392	4215 [78]	4349 [44]	4382 [10]	4369 [29]
O	Daily ozone data	366	353 [13]	365 [2]	366 [0]	364 [3]
W	Daily meteorological data	366	353 [13]	364 [2]	366 [0]	364 [3]
I	Meteorological calibration	366	352 [14]	362 [4]	365 [1]	364 [2]
N	Ozone calibration	52	53	64	56	64

*Discrepancies between the expected number of blocks and blocks recorded + blocks missing are due to clock problems or autorestarts.

MLO and SPO it amounted to only a few percent at most. At BRW and MLO, there was significant loss of data. At BRW a faulty chopper motor on the CO_2 analyzer (not CAMS related) was responsible for several days of down time. At SMO the ASR CAMS had hardware problems that were difficult to diagnose, and caused this unit to be offline for a few days. During a large part of December, although surface ozone data were recorded at SMO, the values were not valid because of a bad interface board. The majority of missing CO_2 and MO3 data at BRW was the result of operator error in which good data were overwritten. Likewise, most of the CO_2 data missing for SMO was the result of data being overwritten. A memo was sent to all stations reemphasizing procedures for tape handling that will prevent data from being overwritten. These procedures have also been detailed at the annual meeting and during training for new observers.

Some program changes were made to CAMS. New CO_2 PROMs were installed in SMO and MLO to allow for two air line operations. Coding and testing of the new ASR PROMs was completed in Boulder by the end of the year. A

49

station-by-station conversion to the new ASR program was scheduled for 1989. Changes in the ASR program allow the computation of a daily summary of the past 24-hourly average values and a daily total for the solar radiation instruments. This information will be recorded at 1200 UTC every day in a new data block called a "T" record. The solar radiation values displayed on the front panel have been changed from 3-min averages to instantaneous values, as requested by the project leader. In addition, some of the functions (F2 and F6) were improved for ease of operation. A directory read from tape will have letter codes to identify the data records.

6.2. SPECIAL PROJECTS: ATMOSPHERIC TRAJECTORIES

The GMCC atmospheric trajectory models have been documented in previous *Summary Reports*. A description of the methodology for the isobaric program was given by *Harris* [1982] and the isentropic program by *Harris and Bodhaine* [1983].

Table 6.6 lists trajectories computed during 1988. These trajectories were provided for scientists within GMCC, as well as for cooperative scientists. Table 6.7 lists various experiments supported in 1988.

The two data sets available for trajectory calculations consist of analyzed grids of meteorological data from the NMC. Data on the northern hemisphere 65×65 grid cover the period 1975 to the present. Data on the global 2.5° latitude, longitude grids extend from 1977 to the present. Data are delivered from NCAR on a monthly basis and are available in house within 2 months of analysis time. In addition, this year a parallel gridded data set for 1980-1987 was obtained from the ECMWF. This data set was used in several comparison studies and will be used as input for a new three-dimensional model to be completed in 1989.

A new feature of the trajectory models is the ability to calculate trajectories to arrive at any specified hour, rather than just the routine 0000 or 1200 UTC. This feature is helpful for computing trajectories for aircraft sampling projects and ship cruises. Programs were written to unpack and reformat the European data set so that it could be used as input to the isobaric model.

The ECMWF parallel data set provided the opportunity to produce two sets of isobaric trajectories using the same model, the only differences being in the analyzed wind fields used as input. As background for this comparison, *Trenberth and Olson* [1988] directly compared selected grids from NMC and ECMWF. This study found fairly good agreement in the extratropics of the northern hemisphere, but considerable uncertainty elsewhere. For example, in July 1986 Trenberth and Olson report an RMS difference in the U component of more than 5 m s^{-1} in a large portion of the southern hemisphere.

The sensitivity of the isobaric model to these differences was investigated by computing trajectories to several sites around the globe using both input data sets. Except for SPO, where significant differences appeared between pairs of trajectories, agreement was better than expected, as in the case of trajectories to Katherine, Australia (Figure 6.6). After examining the raw input data, it was discovered that both data centers were storing

TABLE 6.6. GMCC Trajectories Calculated in 1988

Location or Project	Dates
Greenland	May 1988
Korolev cruise track	May- July 1987
Amsterdam Island	1986-1987
White Sands, NM	June 1988
BRW (ensembles)	March-April 1975-1988
Mediterranean	Selected dates 1982-1983
CURTAIN: Little Rock, St. Louis, Baton Rouge	Oct. 1988
Chile	Selected dates 1984-1988
SMO	Selected dates 1978, 1984, 1987
Miami, FL	June, July 1988, Oct 1988
Mojave, CA	Selected dates 1982-1988
Ny Alesund	March-April 1984-1988
Cape Pt. , South Africa	1986, 1987, Jan.-Oct. 1988
WATOX: Hampton, VA	July 17-21, 1988
CAPTEX	Sept.-Oct. 1983
Bermuda	1985, 1986, 1987
Tijuana, Mexico	1986, 1987
TOGA cruises	1986, 1987
Mt. Lemmon, AZ	Jan.-April 1987, Feb.-April 1988
AGASP-I, II	April 1983, 1986
SMO (ECMWF)	March, April 1986
MLO (isentropic)	May-June 1987
San Juan, Puerto Rico	March-April 1986, 1987
Barbados	March 1986
Hemsdy, England	1987, 1988
Gulf of Mexico	March 1988
TOGA-IV: South Pacific	Sept.-Oct. 1987
Mace Head, Ireland	1987
TOGA-V	April-May 1988
Lostock Dam, Australia	Selected Dates 1984, 1985, 1986
CASE flight track	July 1988
CASE/Leg II	July-Aug. 1988
SPO	Oct.-Dec. 1986,1987
CURTAIN	April-June 1988
REME, Cloudwater and Blue Ridge projects	Aug. 1988
Alert, Canada	Selected Dates 1988
Izana, Spain	June 1984-June 1985, Mar., Oct. 1987
Station M	Nov.-April 1981-1987
Grand Canyon, AZ	June 1984
Buffalo, NY	Nov.-Dec. 1979, 1983
South Pacific flight	Jan. 1987
Little Rock, AR	Jan. 1988
Baton Rouge, LA	Jan. 1988
St. Louis, MO	Jan. 1988
Adrigal, Ireland	1987
MLO	1987

wind data at the poles incorrectly. The problem is in the ECMWF data for 1980-1987 and in the NMC data for May 1986-November 1988. Correction code was written that averages valid wind data from 87.5° N and S and stores those values at the poles after orienting them with respect to longitude.

Kahl et al. [1989] compared three different trajectory models while employing three different input data sets. Trajectories were produced for Arctic locations using the GMCC isobaric, the GMCC isentropic, and the AES three-dimensional models.

TABLE 6.7. Experiments Supported During 1988

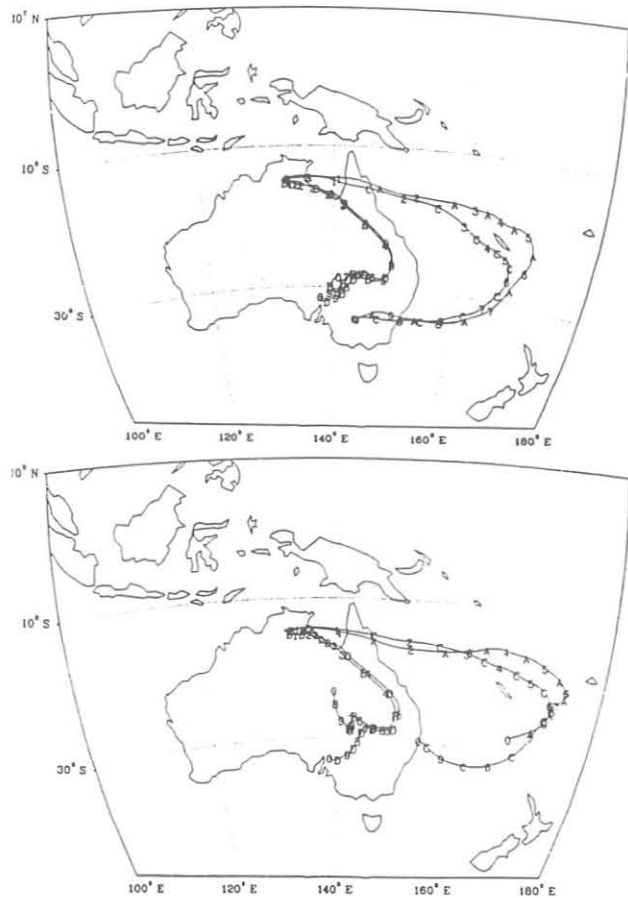| Experiment	Dates	Organization
WATOX	July 1988	GMCC, ARL
CAPTEX	1983	GMCC
Mojave	1982-1988	USGS
CURTAIN	April, June, Oct. 1988	GMCC
REME	Aug.-Sept. 1988	GMCC
Cloudwater	Aug.-Sept. 1988	GMCC
Blue Ridge	Aug.-Sept. 1988	GMCC
AGASP-I, II	March-April 1983, 1988	GMCC
TOGA-IV, V	Jan. 1986, July-Oct. 1987, April-May 1988	GMCC
GUFMEX	Jan.-March 1988	NSSL
SAGA-II	May-July 1987	GMCC, PMEL
GPCP	1983-1988	ARL, UVA
CASE	July-Aug. 1988	GMCC

Fig. 6.6. Back trajectories for Katherine, Australia, September 25, 1987, created using NMC (top) and ECMWF (bottom) analyzed grids. Numbers along each trajectory give the days back from Katherine. Letters identify the level and time--A: 850 mb, 0000 UTC; B: 700 mb, 0000 UTC; C: 850 mb, 1200 UTC; D: 700 mb, 1200 UTC.

The data sets were the NMC, ECMWF, and Canadian analyzed gridded fields. The authors found that sensitivity to the different data bases was at times greater than sensitivity to the three different methods of dealing with vertical motion. Although this type of study cannot lead to conclusions about absolute errors, it does give some measure of uncertainty. The median differences between 5-day endpoints in this study ranged from 800 to 1000 km.

Cluster analysis, a statistical multivariate technique, can be used to summarize a large data set or to explore structure within a data set. This spring a University of Virginia scientist gave a seminar about cluster analysis applied to trajectory data; after the seminar, members of our group developed procedures on the computer to employ this technique. The object of the clustering algorithm is to group trajectories of similar wind speed and direction so that those within each cluster represent a similar flow pattern. Cluster membership is determined by minimizing the within-cluster sum of squares of trajectory locations from the mean trajectory for the cluster. Each cluster may then be represented by its mean trajectory or cluster mean. Although exploration of different clustering procedures continues, some preliminary results are shown here, using a hybrid technique suggested in the seminar, which has worked well with trajectories. The technique uses Ward's hierarchical method to determine the number of clusters and an initial grouping. These clusters are then refined, using an iterative optimization algorithm (SPSS-X Quick Cluster).

For the first example, MLO 700-hPa, 5-day back trajectories for December 1987 through April 1988 were clustered. Figure 6.7 shows mean trajectories for the three clusters determined. The analysis discriminated two wind speed groups from the west, accounting for 35% for trajectories (clusters 2 and 3). The one easterly cluster accounts for the remainder of trajectories. To contrast with the warm season, trajectories for June-October 1988 were then clustered (Figure 6.8). The cluster means show only easterly flow, although 19% of the trajectories are represented by a mean trajectory with some anticyclonic curvature from the north.

Plots of cluster membership, which show all trajectories in each cluster on one page, were created to verify that the cluster mean is representative of trajectories in the cluster and to determine the variability within a cluster. Figure 6.9 is the cluster membership plot for cluster 1, Figure 6.8. Although not always readable, labels on each trajectory tell the month during which they occur. Note that this cluster contains 101 trajectories of roughly the same length and direction. None of these 5-day back trajectories travels over the North American continent.

Figure 6.10 shows four cluster means determined for SMO 1987 850-hPa trajectories. These indicate 79% of trajectories (clusters 1 and 4) are from the southeast Pacific tropical region, 11% from the region of the Australia-New Zealand anticyclone, and 10% from the northwest with possible northern hemisphere influence. These are the three source regions identified by *Halter et al.* [1988] in their study of CO_2 variability at SMO. The cluster membership plot for cluster 2 (Figure 6.11) shows more variability than the MLO example. There are many instances of cross-equatorial flow, the strongest of which are in January and February.
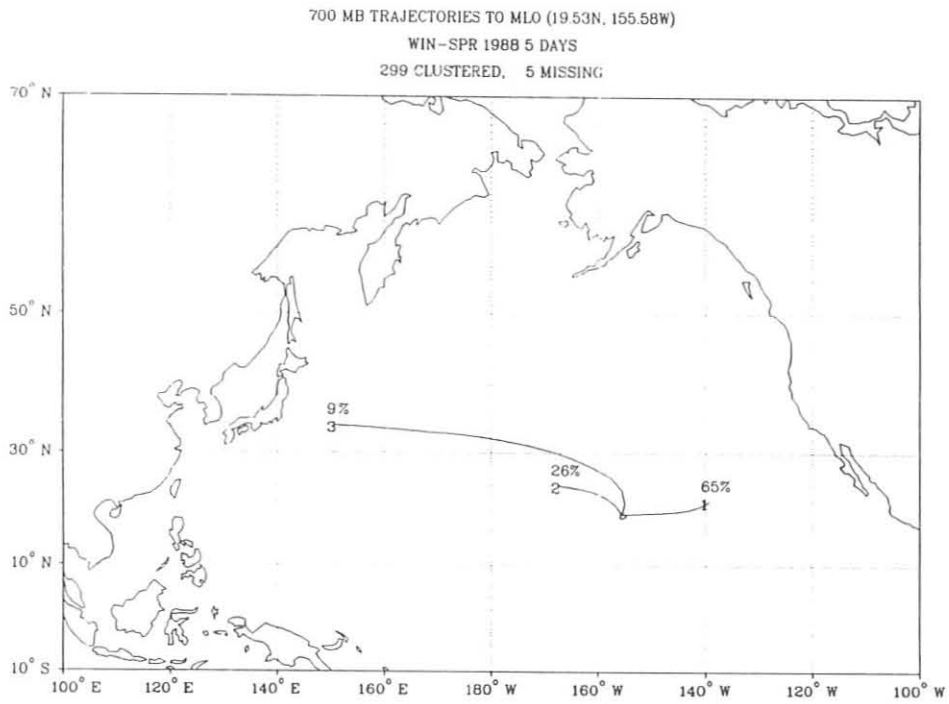
Fig. 6.7.   Mean trajectories for clusters formed from December 1987 to April 1988 700-hPa MLO 5-day back trajectories, showing percent of total trajectories in each cluster.   The numbers are cluster numbers for identification only.

700 MB TRAJECTORIES TO MLO (19.53N, 155.58W)

SUM–FAL 1988 5 DAYS

306 CLUSTERED,   0 MISSING

Fig. 6.8.   Mean trajectories for clusters formed from June to October 1988 700-hPa MLO 5-day back trajectories, as in Figure 6.7.

Fig. 6.9. Cluster membership for cluster 1, Figure 6.8. Numbers at the end of each trajectory tell the month of occurrence.

850 MB TRAJECTORIES TO SMO (14.25S, 170.56W)
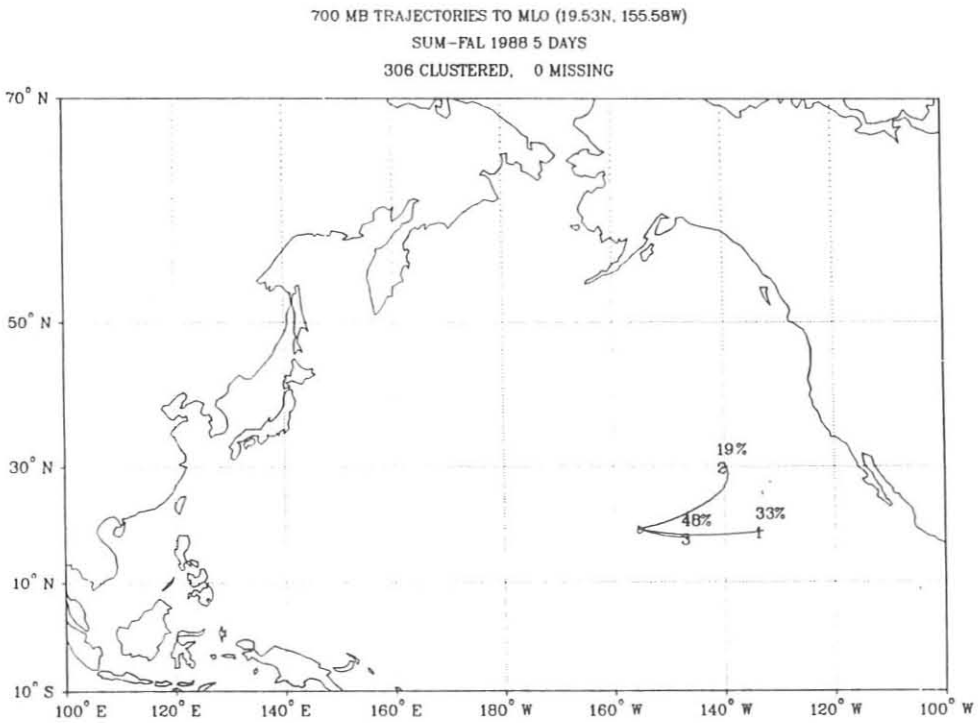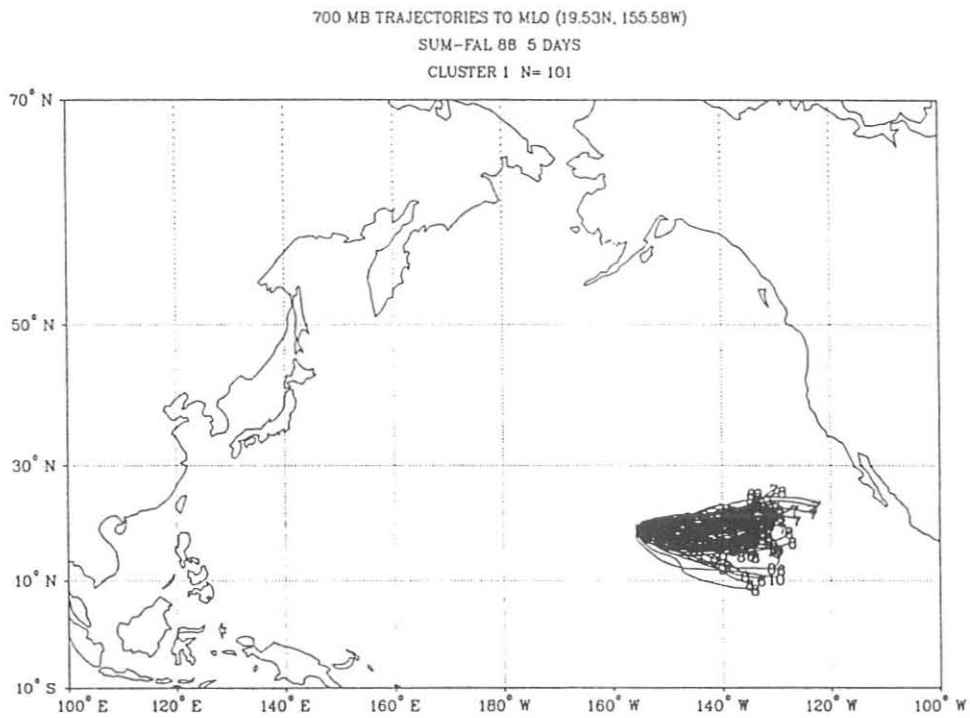
ALL OF 1987 5 DAYS

691 CLUSTERED. 21 MISSING

Fig. 6.10. Mean trajectories for clusters formed from 1987 850-hPa SMO 5-day back trajectories, as in Figure 6.7.

Fig. 6.11. Cluster membership for cluster 2, Figure 6.10. Numbers at the end of each trajectory tell the month of occurrence.
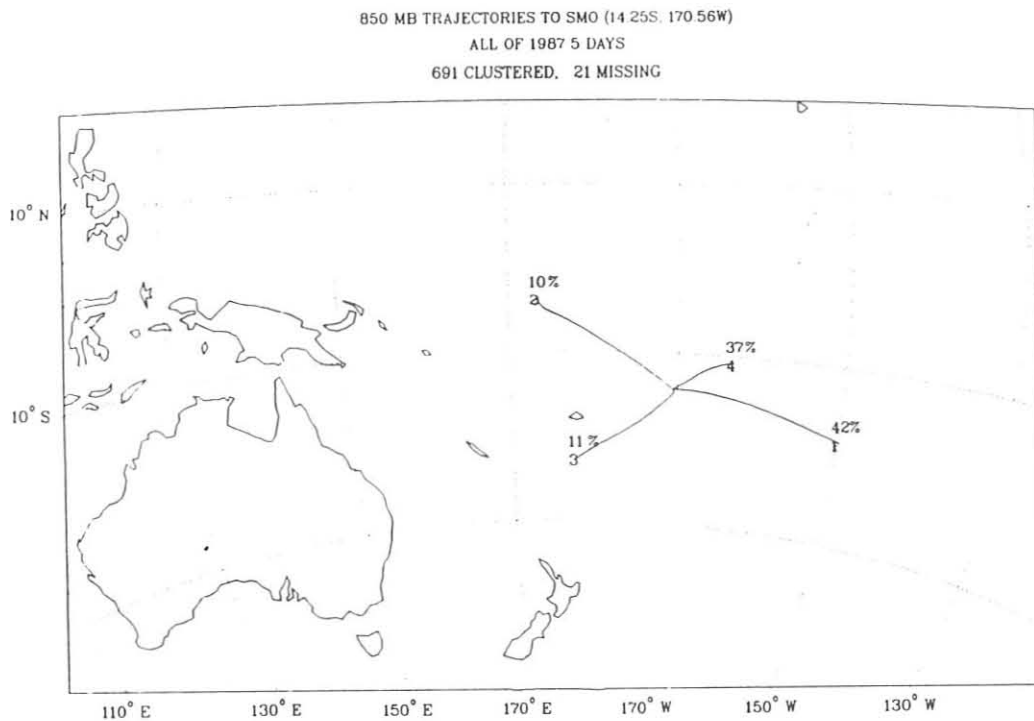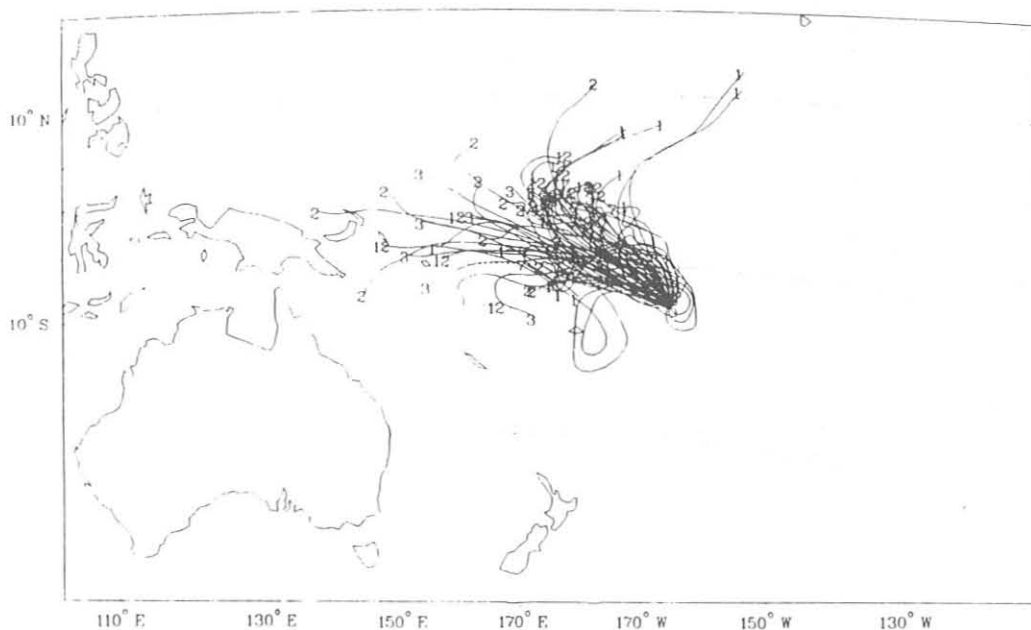
6.3. REFERENCES

DeLuisi, J.J. (Ed.), *Geophysical Monitoring for Climatic Change, No. 9: Summary Report 1980*, 163 pp., NOAA Environmental Research Laboratories, Boulder, CO, 1981.

Harris, J.M., The GMCC atmospheric trajectory program, NOAA Tech. Memo. ERL ARL-116, 30 pp., NOAA Environmental Research Laboratories, Boulder, CO, 1982.

Harris, J.M., and B.A. Bodhaine (Eds.), *Geophysical Monitoring for Climatic Change, No. 11: Summary Report 1982*, pp. 67-75, NOAA Environmental Research Laboratories, Boulder, CO, 1983.

Herbert, G.A., E.R. Green, J.M. Harris, G.L. Koenig, and K.W. Thaut, Control and monitoring instrumentation for the continuous measurement of atmospheric CO_2 and meteorological variables, *J. Atmos. Ocean. Technol. 3*, 414-421, 1986a.

Herbert, G.A., E.R. Green, G.L. Koenig, and K.W. Thaut, Monitoring instrumentation for the continous measurement and quality assurance of meteorological observations, *NOAA Tech. Memo. ERL ARL-148*, 44 pp., NOAA Environmental Research Laboratories, Boulder, CO, 1986b.

Kahl, J.D., J.M. Harris, G.A. Herbert, and M.P. Olson, Intercomparison of three long-range trajectory models applied to Arctic haze, *Tellus, 41B*, 524-536, 1989.

Nickerson, E.C. (Ed.), *Geophysical Monitoring for Climatic Change, No. 13: Summary Report 1984*, 111 pp., NOAA Environmental Research Laboratories, Boulder, CO, 1986.

Trenberth, K.E. and J.G. Olson, Intercomparison of NMC and ECMWF global analyses: 1980-1986, *NCAR Tech. Note, NCAR/TN 301+STR*, 81 pp., National Center for Atmospheric Research, Boulder, CO, 1988.

WCP (World Climate Programme), *Climate System Monitoring Monthly Bulletin, 1988, Vol. 10*, 42 pp., World Meteorological Organization, Geneva, Switzerland, 1988.

7. Air Quality Group

Y. KIM (Editor), J.F. BOATMAN, H. SIEVERING, J. RAY, C. VAN VALIN, AND L. GUNTER

7.1. CONTINUING PROGRAMS

7.1.1. INTRODUCTION

AQG research during 1988 had four objectives: (1) to improve understanding of the acidic deposition phenomenon; (2) to determine the amount and fate of various trace species that are advected eastward from North America; (3) to provide an observational data base to validate the acid deposition models; and (4) to gain a better understanding of the concentration of acid-causing agents within clouds. AQG acquired data to satisfy these objectives using the NOAA King Air research aircraft (Figure 7.1). Table 7.1 summarizes the research flights made by the King Air in support of our activities during 1988.

7.1.2. GLOBAL CHANGE EXPEDITION AND COORDINATED AIR-SEA EXPERIMENT

CASE was conducted during the 1988 GCE. The NOAA King Air was deployed over the western North Atlantic Ocean to sample certain pollutant gases (on a real-time basis) and

Fig. 7.1. The NOAA King Air C-90, configured for research.

aerosol particulate matter (by filter packs) in a coordinated effort with the NOAA ship *Mt. Mitchell* during leg I of GCE. CASE sampling and analysis has provided intercomparison data on O_3, SO_2, and NO_y gas concentrations; on fine- and coarse-fraction particulate matter; on sulfate, nitrate, chloride, sodium, and other ion concentrations; and on a number of elemental concentrations in the total particulate matter. Meteorological data obtained from the King Air are being compared with sounding data obtained from shipboard radiosonde releases [*Boatman et al.*, 1989a]. CASE aircraft flights took place on July 17, 18, 19 and 21, 1988, off the coast of Cape Hatteras, and July 26, 27, and 28, 1988, upwind of Bermuda. The flight pattern provided sufficient time for free troposphere (2600 m) and lower marine boundary layer (150 m) filter pack sampling and one additional altitude (600 to 900 m) for 5-10 min time averaging of the real-time gas analysis data.

An additional feature of the CASE program was the careful sampling and analysis of particle size distribution using the Knollenberg optical sizing probes and previous experimental empirical formulas for aerosol water. This work has enabled AQG to determine aerosol water volume and mass fractions. This work also identifies the contributions of the (1) predominantly anthropogenic accumulation mode, (2) soil intermediate mode, and (3) sea salt coarse mode volume and mass to the total observed volume [*Kim et al.*, 1989]. This latter aspect will prove invaluable because the fine- and coarse-fraction particulate matter determinations from aircraft and shipboard sampling are compared.

Excess sulfate (XSO_4, after subtracting sea salt sulfate) was found to be remarkably high in the Bermuda area, ~1 µg m^{-3}. The aircraft 150-m-level Bermuda-area average XSO_4 of 1.03 µg m^{-3} was very close to the three shipboard Bermuda-area average XSO_4 values of 1.06 µg m^{-3}, 1.09 µg m^{-3}, and 1.03 µg m^{-3}, using three distinct filter pack systems.

The coarse-fraction XSO_4 was observed to be greater aboard the aircraft (~30%) than aboard ship (~20%). This discrepancy is considered to be due to a smaller particle size cut for the cyclone separator aboard the aircraft than for the cascade impactor aboard the ship: 0.6-0.9 µm diameter versus 1-1.5 µm diameter [*Sievering et al.*, 1989].

A large chloride deficit (i.e., relative to the sea water Cl$^-$/Na$^+$ ratio of 1.165) was found to be very strongly correlated with the sum of nitrate and excess sulfate. This suggests that the heterogeneous conversion of SO_2 to sulfate in and on sea salt aerosol is an important contributor to the total excess sulfate observed in the remote North Atlantic marine boundary layer [*Sievering et al.*, 1989].

7.1.3. CENTRAL U.S. RADM TEST AND ASSESSMENT INTENSIVES

The 2-year CURTAIN program was completed in 1988. Seasonal observations of trace gases, aerosols, and meteorological parameters were obtained in the south-central
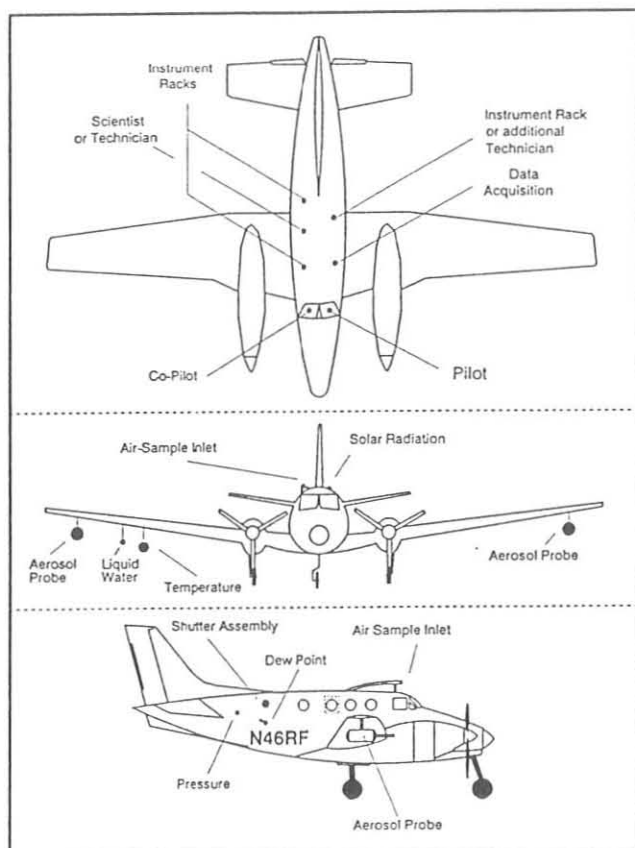
TABLE 7.1. NOAA King Air Research Flights During 1988

Date 1988	Start	End	Date 1988	Start	End
CURTAIN Project, Little Rock, AR			*ACID-MODES Study, Harrisburg, PA*		
	(CST)	(CST)		(UTC)	(UTC)
Jan. 22	1337	1745	Aug. 21 (1)	1430	1845
Jan. 23 (1)	1135	1547	Aug. 21 (2)	1949	2206
Jan. 23 (2)	2021	2441	Aug. 22 (1)	1426	1830
Jan. 25	1150	1550	Aug. 22 (2)	2015	2330
Jan. 26 (1)	1128	1530	Aug. 26	1657	2039
Jan. 26 (2)	2300	0313	Sept. 1 (1)	1347	1800
	(CDT)	(CDT)	Sept. 1 (2)	1943	2219
Apr. 21	1208	1625			
Apr. 22 (1)	1025	1442	*Yellowstone Smoke Flight, Boulder, CO*		
Apr. .22 (2)	2214	0233		(MDT)	(MDT)
Apr. 24	1016	1430	Sept. 7	2200	2344
Apr. 25	2217	0231			
Apr. 26	1110	1523	*GCE/CASE, Newport News, Va. and Bermuda*		
June 19 (1)	0031	0442		(UTC)	(UTC)
June19 (2)	1117	1528	July 17	1251	1733
June 20	0912	1322	July 18	1250	1718
June 21	0905	1322	July 19	1405	1818
June 22 (1)	0922	1332	July 21	1235	1653
June 22 (2)	2212	2624	July 26	1151	1609
	(CST)	(CST)	July 27 (1)	1054	1502
Oct. 18	1136	1602	July 27 (2)	1700	2117
Oct. 19 (1)	1120	1541	July 28	1125	1524
Oct. 19 (2)	2153	0212			
Oct. 21	1145	1613	*BAO Tower Flyby, Erie, CO*		
Oct. 22 (1)	1028	1441		(MDT)	(MDT)
Oct. 22 (2)	2205	0222	Oct. 13	1355	1519
Blue Ridge Flights, Harrisburg, PA			*CFC Instrument Test flight, N.E. CO*		
	(EDT)	(EDT)		(MST)	(MST)
Aug 16 (1)	1027	1355	Dec. 6	0800	1200
Aug 16 (2)	1505	1822			
			Ozone Instrument Test Flight, Boulder, CO		
Cloud Water Flights, Harrisburg, PA				(MST)	(MST)
	(UTC)	(UTC)	Dec. 16	10225	1300
Aug 18	1231	1442			
Aug 19	1433	1757	*Nephelometer Test Flight, Boulder, CO*		
Aug 20	1436	1710		(MST)	(MST)
Aug 29	1347	1647	Dec. 16	1524	1709
Sept. 4	1435	1826			

United States. Research aircraft flights using the NOAA King Air were made from a base site in Little Rock, Arkansas, north and south along the 91°30′W meridian. A climatological data base was established by making seasonal field observations in February, April, July, and October, during 1987, and in January, April, June, and October, during 1988. The purpose of the studies was to make observations for comparison with RADM, a model that covers the eastern half of the United States. In the future, the observational data base will be an aid in the model initialization along the RADM western boundary.

Each field intensive mission included six flights, consisting of a repeating series of two day flights and a night flight. Day flights alternated between northward to Missouri and southward to the Gulf of Mexico. Night flights had shorter flight legs but included both north and south segments from the Little Rock

base. During each flight, two altitudes 1450 and 2450 m above sea level, were flown. A stepwise profile was added to the flight plans in 1988. All flights attempted to sample only in clear air.

Hydrogen Peroxide Measurements

Instruments to measure ambient H_2O_2 on a continuous basis have become available only recently [*Lazrus et al.*, 1986]. H_2O_2 is an important photochemically produced oxidant that is a by-product of the OH radical oxidation of nonmethane hydrocarbons. It is formed by a termination reaction of HO_2 radicals, and as such is an indicator of recent concentrations of free radicals in the atmosphere. H_2O_2 is thought to be important in the oxidation of SO_2 to H_2SO_4 in aqueous-phase reactions. Several researchers have reported aircraft-based measurements

of H_2O_2 [*Van Valin et al.*, 1987; *Heikes et al.*, 1987; *Barth et al.*, 1989; and *Boatman et al.*, 1989*b*].

Measurements of H_2O_2 made during CURTAIN show a strong annual cycle. Mean and standard deviations for seasonal field programs are shown in Figure 7.2*a*. Winter mean H_2O_2 values are near 0.2 ppbv whereas summer mean values are near 4.0 ppbv. The winter to summer increase of a factor of 20 is most likely due to increased solar radiation and to greater water mixing ratios in summer. There is a linear relationship between water mixing ratio (WMR) and H_2O_2 concentrations (H_2O_2 = 0.327 * WMR − 0.380, R^2 = 0.89) when mean values for each field program are compared. Individual flights, however, show poor statistical correlations. This most likely reflects the difference in time coefficients for the production and loss of H_2O_2 compared with humidity. In addition, the detailed structure in the measurements during flights is indicative of meteorological influences and changing precursor concentrations.

Altitude profiles were made in 1988 field programs in addition to the two level-flight-altitude segments. *Heikes et al.* [1987] reported that H_2O_2 generally increased with altitude in measurements made in the eastern United States during the fall of 1984. AQG observations during 1987 at two altitudes indicated a general decrease in H_2O_2 with altitude; for 1988, the H_2O_2 profiles were highly variable, each flight being different (Figure 7.3). In winter there was very little variation in H_2O_2 with altitude. Spring and summer had generally decreasing H_2O_2 with altitude, and fall had increasing H_2O_2 with altitude up to about 2000 m. Computer models [*Kleinman*, 1986] have suggested that H_2O_2 should increase with altitude in the boundary layer. *Logan et al.* [1981] modeled H_2O_2 to higher altitudes and concluded that H_2O_2 should decrease with altitude. Only more measurements and updated models will clarify this situation.

Computer models also predict a daily cycle for H_2O_2, having maximum concentrations in late afternoon. In CURTAIN a day-night difference in H_2O_2 was observed, but with the higher values at night. The night/day ratio varied from 1.15 to 2.7 and did not appear to follow a seasonal cycle. The data validate the prediction of a daily cycle but not the times for the minimum and maximum. The night maximum may be explained partly by the timing of the measurements. Daytime flights were centered around noon, and night flights were centered about midnight. Hence, day flights were during the buildup period well before the predicted maximum. The night flights occurred before significant losses and well before the early morning predicted minimum. Thus, daily maximum H_2O_2 concentrations are predicted to be greater than the measured nighttime values and the reported means are not the "true" mean that would be obtained by more frequent measurement of the daily cycle.

Other Trace Gases

O_3 was also measured during the CURTAIN program. Figure 7.2*b* shows 2 years of seasonal data. The annual cycle for O_3 was clearly observed, although the seasonal maximums were different for the 2 years. The difference in O_3 concentrations at the two altitudes was not consistent. Mean winter values for 1988 were 52 ppbv, and mean summer values were 80 ppbv. The standard deviation for the summer was relatively large, which was a reflection of the large differences seen between different flights.

As indicated in Figure 7.2*c*, SO_2 did not appear to have an annual cycle in the south-central United States. Also, compared with the northeast United States, the SO_2 values are low. Figure 7.4 shows the ratios of H_2O_2/SO_2 for 1987-1988. A ratio above 1 indicates oxidant in excess of that needed for complete conversion of SO_2 to H_2SO_4 in cloud water. The boundaries of the hatched surfaces indicate the upper and lower altitudes measured in the CURTAIN flights. The 2 years are very

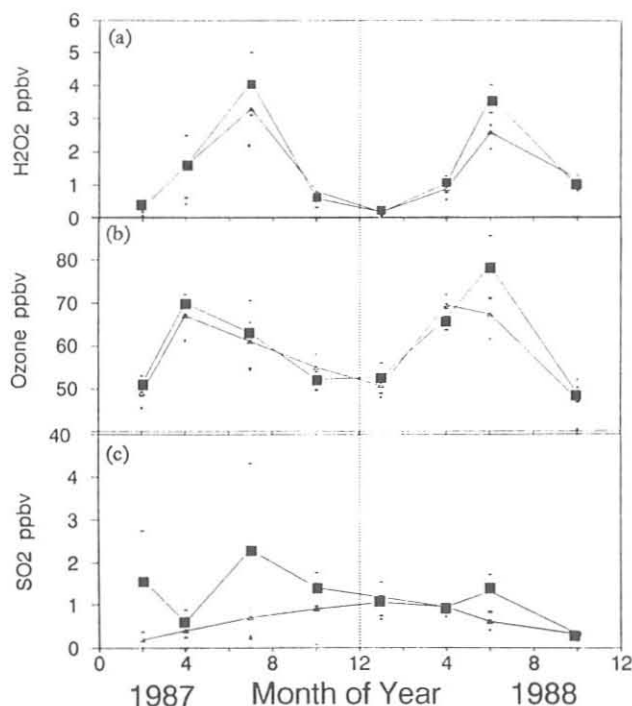Fig. 7.2. CURTAIN data for 1987-1988. Squares are upper altitude values, and triangles are lower altitude values. Dashes and dots are the ± standard deviations. H_2O_2 and O_3 had annual cycles, but SO_2 did not.
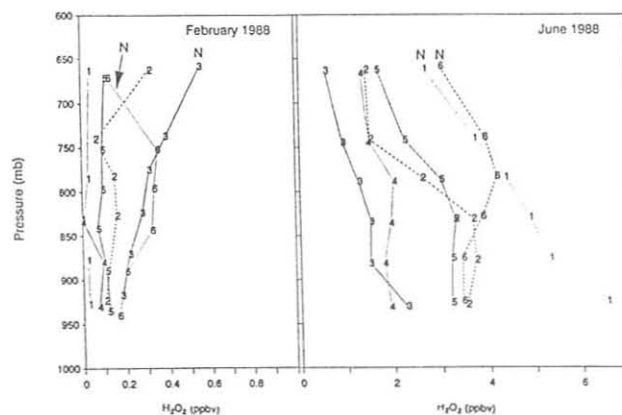
Fig. 7.3. Profiles for H_2O_2 for February and June, 1988. The summer flights show greater flight-to-flight variations. Largest values are for the night (N) flights in both seasons.
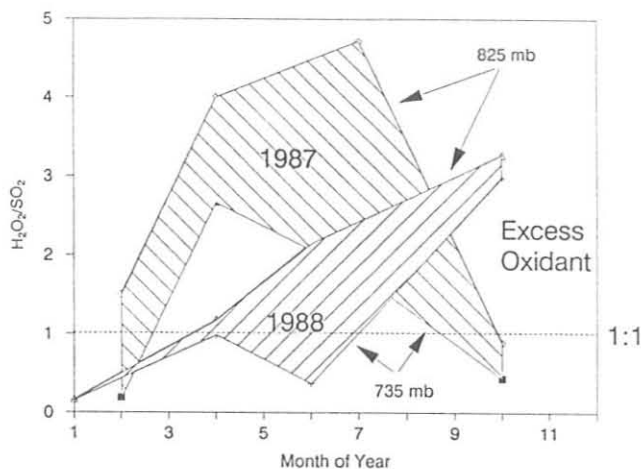
Fig. 7.4. The ratio of H_2O_2/SO_2 for both altitudes at which data were collected, for 1987 and 1988. Excess oxidant was available for most of each year.

Fig. 7.5. The mean aerosol number concentration at high and low altitudes during each of the CURTAIN field periods.

different, which is primarily due to the irregular concentrations of SO_2. Winter generally has a limited amount of oxidant, and the rest of the year has an excess of oxidant. Thus, acid formation would be expected to occur rapidly in the spring and summer in this region but to be limited by the lower available SO_2.

Aerosols

Figure 7.5 shows the seasonal variation of average small-particle (0.1-3 μm diameter) aerosol number concentration obtained using the ASASP at low and high altitudes [*Kim et al.*, 1988]. It shows that small-particle concentrations at both altitudes and during day or night are maximized in spring and summer and minimized during fall and winter. This supports the results of *Mueller et al.* [1980]. High-altitude concentrations during both day and night are smaller than those at low altitude. At least four processes affect the seasonal aerosol cycle. First, anthropogenic aerosol production may be higher during the heating and cooling seasons (winter and summer). Second, during the snowy months when substantial areas of frozen ground exist, soil-derived particles are minimized [*Gillette and Hansen*, 1988]. Third, photochemical and wet conversion of SO_2 to SO_4^{2-} is faster during summer [*Meagher et al.*, 1983]. Fourth, natural emissions of isoprene and hydrocarbons increase in spring and summer.

7.1.4. RADM EVALUATION EXPERIMENT

Two aircraft, the NOAA King Air and a Battelle Pacific Northwest Laboratories DC-3, made three coordinated research flights on June 24 and June 30, 1987 (Figure 7.6). Each flight was along a track from Columbus, Ohio, to Pittsburgh, Pennsylvania, to Pennsylvania State College, Pennsylvania (36°N), to Binghamton, New York, to Utica, New York, to Saranac Lake, New York. The DC-3 flew in the planetary boundary layer at an altitude of 1.1 km (3500 ft) above sea level. The King Air flew in or above the planetary boundary
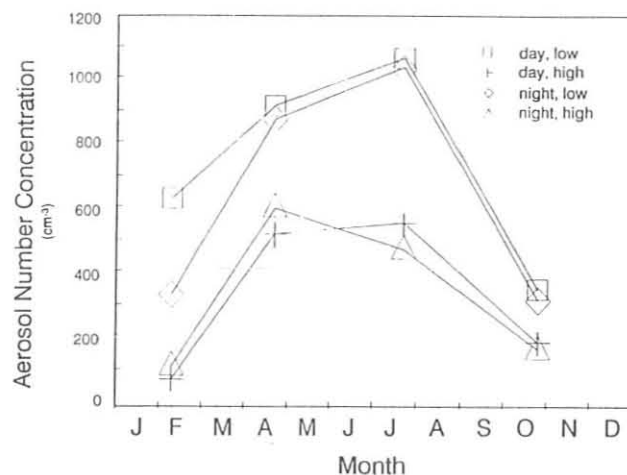
layer at altitudes between 2.4 and 3.4 km (8000-11000 ft) above sea level. The two aircraft began and ended the flights together, each flying along its same flight tracks on each flight. The relationships between selected acid precursors were evaluated along the flight tracks, in concert with the known meteorological conditions.

The primary purpose of this study was to gain a better understanding of the concentrations of acid precursors present above the northeastern United States during summer. Two secondary purposes were to use this new understanding in evaluating the RADM [*Chang et al.*, 1987] and in designing additional field studies for the EPA's ACID-MODES program. Figures 7.7a-d show the patterns of selected trace gases observed with the aircraft.

A large patch of SO_2 having concentrations as high as 10 ppbv was evident in the planetary boundary layer above Pittsburgh. A second weaker patch (2 ppbv) was present in the free troposphere above Columbus. The fact that this patch was observed both in the morning and afternoon suggests its origin to be stable surface emissions.

In the planetary boundary layer, the H_2O_2 concentration field (Figure 7.7b) was similar in the two flights. However, in the free troposphere, the concentration pattern both expanded and intensified during the second flight. Peak concentrations in the free troposphere rose from 2.5 ppbv to 3.0 ppbv. These changes definitely suggest the secondary production of H_2O_2 during the day.

It is interesting that the region of expansion and intensification was mostly in the free troposphere. *Luria et al.* [1989] showed that H_2O_2 is formed in the presence of ultraviolet light through chemical reactions involving NO_y, O_3, and the OH radical. These reactions are accelerated in the presence of water vapor. Ultraviolet light is more abundant at higher altitudes. Conversely, the water vapor concentration decreases with altitude. The speculation is that the region of maximum H_2O_2 production was achieved at an altitude balanced between these two competing factors. The peak in the H_2O_2 pattern above

58

Fig. 7.6. Flight tracks flown during the RADM Evaluation Experiment. See text for locations.

Columbus is associated with enhanced O_3, NO_y, and probably hydrocarbons.

The peak O_3 concentration observed in the afternoon flight (Figure 7.7c, 110 ppbv) was 30 ppbv higher than that of the morning flight (80 ppbv). The enhancement also expanded in size to cover much of the lower troposphere between Columbus and Pittsburgh. The obvious explanation for these observations is strong photochemical production in a polluted region on a clear summer day. This rate of O_3 increase (4 ppbv h^{-1}) may be near the maximum attainable for this region.

NO_y concentrations (Figure 7.7d) were generally less than 2 ppbv, except in a patch in the planetary boundary layer above Pittsburgh. The peak NO_y concentration increased from 5 ppbv to >8 ppbv in this patch between the two flights. This could have been due to NO_y production or to sampling in a different part of the plume above Pittsburgh on the two flights. The former suggestion is more plausible, but the latter cannot be ruled out.

The following conclusions were drawn from this work:

(1) The concentrations of both SO_2 and H_2O_2 were higher during the flights of June 30, 1987, than during the flight of June 24, 1987. A cold front had passed through the area within 24 hours of the June 24 flight. The June 30 flight was through a stagnant warm-air mass of subtropical origin.

(2) SO_2 concentrations averaged 1-2 ppbv within the planetary boundary layer and <1 ppbv in the free troposphere. Superimposed on these background concentrations were surface source regions having elevated concentrations as high as 14 ppbv.

(3) H_2O_2 concentrations averaged 2-4 ppbv. The highest values were observed near the top of the planetary boundary layer.

(4) The ratio between H_2O_2 and SO_2 was greater than 1, except in the lower planetary boundary layer and in the vicinity of surface SO_2 source regions. The ratio was much less than 1 in the latter regions. Further studies are necessary to confirm whether this is a typical summer condition in those regions.

(5) Two daytime flights were made on June 30, 1987. The patterns of both SO_2 and H_2O_2 remained substantially the same. An increase in the concentrations of SO_2 and H_2O_2 was observed in the second flight.

7.1.5. ACID-MODES EXPERIMENT

During August and early September, 1988, AQG participated in the EPA-sponsored ACID-MODES experiment, centered in Pennsylvania. One purpose for our participation was to measure the acidity and the acid-causing agents within clouds using the NOAA King Air aircraft. Our working hypothesis was the following:

Both H_2O_2 and SO_2 are readily absorbed by cloud water, where they quickly react to form sulfuric acid. Therefore, in a

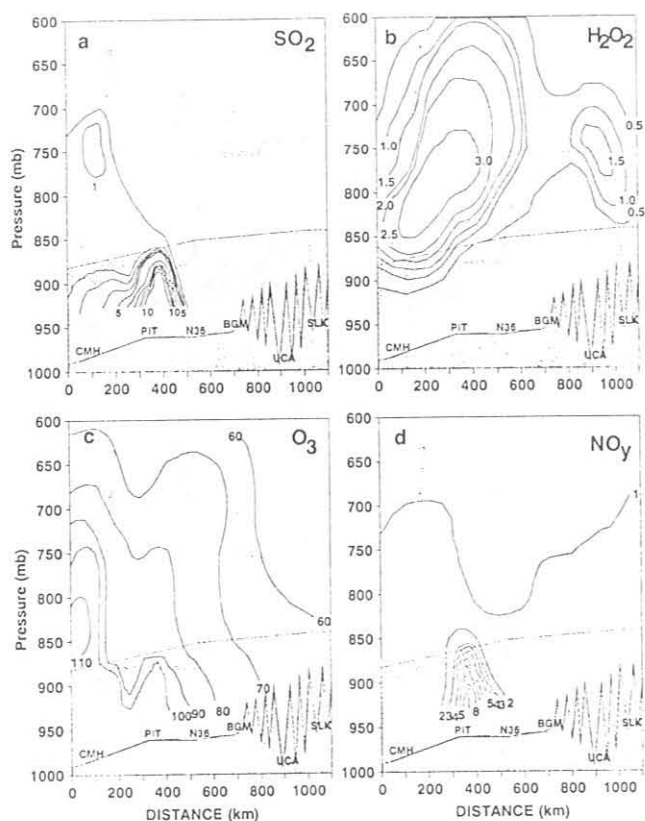Fig. 7.7. Concentration profiles of selected trace gases observed with the NOAA King Air aircraft on June 30, 1987: (a) SO_2 concentrations contoured at 1 ppbv intervals, (b) H_2O_2 concentrations contoured at 0.5 ppbv intervals, (c) O_3 concentrations contoured at 10 ppbv intervals, and (d) NO_y concentrations contoured at 1 ppbv intervals. Dotted lines represent the flight altitude (ambient pressure).

polluted cloud, the concentrations of H_2O_2 (oxidant) and SO_2 (oxidizer) in the air between cloud drops are mutually exclusive.

AQG collected cloud water samples and made interstitial air measurements on five occasions. Each sampling flight lasted long enough to collect 10 cloud water samples and to measure the H_2O_2 and SO_2 concentrations simultaneously within the clouds. All flights were made during daylight hours in extensive stratiform cloud layers.

On August 19, 1988, the King Air flew within a non-precipitating stratus cloud above central Pennsylvania for about 1.5 hours. During this time 10 cloud water samples were collected while cloud liquid water content, SO_2 concentration, H_2O_2 concentration, and O_3 concentration were being measured.

Figure 7.8 shows the isobaric back trajectories for 1200 UTC on August 19, 1988, with termination at Harrisburg, Pennsylvania. The 1000 mb (L) and 850 mb (M) trajectories suggest that the air at these levels arrived from the north or northwest. The 700 mb (U) trajectory suggests that air at this altitude arrived from the west-northwest.

Figure 7.9 summarizes the salient features of the data from the August 19 flight. The flight altitude, liquid water content, SO_2 concentration, H_2O_2 concentration, and O_3 concentration are plotted versus time. Also shown is the pH of each cloud water sample collected.

The aircraft remained within the clouds for about 1.5 hours. The cloud layer was thin, extending between 900 and 850 mb (depth = 600 m). The 1-min average liquid water content hovered near 0.2 g m^{-3}, a low but reasonable value for a summer stratiform cloud. The SO_2 concentration was between 2 and 4 ppbv, a value typical of polluted summer conditions [*Boatman et al.*, 1989*b*]. The H_2O_2 concentration was less than 0.2 ppbv with the cloud. This is an order of magnitude lower than that typical of polluted summer conditions [*Boatman et al.*, 1989*b*]. The O_3 concentration was between 45 and 68 ppbv. The pH

Fig. 7.9. Temporal variation of flight altitude (ambient pressure) and pH of cloud water samples, liquid water content, SO_2 concentration, H_2O_2 concentration, and O_3 concentration within the clouds during the flight of August 19, 1988.

Fig. 7.8. Isobaric back trajectories (L: 1000 mb, M: 850 mb, V: 700 mb) for 1200 UTC on August 19, 1988, with termination at Harrisburg, Pennsylvania. Numbers are positioned at 1-day intervals along the trajectories.

measurements from the 10 cloud water samples varied between 2.3 and 3.1. Such values are very acidic, suggesting active acid formation within the cloud drops.

The following conclusions were reached on the basis of the results from this and the other four flights:

(1) The concentrations of interstitial H_2O_2 and SO_2 were mutually exclusive, except in one unpolluted case.

(2) In the polluted cases, H_2SO_4 was forming in the clouds. These clouds had pH values as low as 2.3:

(3) Trajectory analysis showed that the polluted air observed in clouds over Pennsylvania had lingered over the Ohio River basin or the Canadian province of Ontario. In contrast, trajectories for the unpolluted case showed that air masses lingered above the western Atlantic Ocean.

7.2. Special Projects

7.2.1. Sulfur Monitoring at MLO

AQG began a sulfur gas monitoring project at MLO in March, 1988. This study was set up to test the following hypotheses:

(1) Atmospheric sulfur is a surrogate for volcanic contamination at MLO.

(2) The background atmospheric sulfur concentration in the free troposphere can be successfully measured at MLO.

A CSI real-time total sulfur gas monitor was installed at MLO in March 1988, and a TECO real-time SO_2 gas monitor was installed in November 1988. The CSI device measures all sulfur gases, has a detection limit of 1 ppbv for 1-min samples, and has a response time of 10 seconds. The TECO device measures only SO_2, has a detection limit of 0.1 ppbv for 1-min samples, and a response time of 1 minute. The two instruments are described by *Boatman et al.* [1988].

Figure 7.10 shows the history of volcanic sulfur events at MLO from June 1988 to January 1989 as measured by the CSI device. No significant seasonal trend was evident. The following conclusions were reached with regard to hypothesis 1:

(1) Sulfur gas events with a volcanic origin occurred 32 times between June 1988 and January 1989, an average of one event every 7.7 days.

(2) These events began about 2200 UTC and ended after several hours.

(3) The largest 1-h-average sulfur concentration observed during any event was 34 ppbv. The largest event-average sulfur concentration was 18.1 ppbv.

(4) Nearly all the sulfur events were associated with northerly winds and small dew point depressions. This suggested that the events were occurring when marine boundary layer air reached the observatory.

Figure 7.11 shows the sulfur gas concentration observed with the CSI instrument and the SO_2 concentration observed with the

TECO instrument during December 1988. Also shown is the ratio between the concentrations measured with the two devices. The CSI trend is characterized by occasional volcanic events interspersed between long periods of quiescent cyclic behavior. The TECO trend is characterized by occasional volcanic events interspersed between long periods of nearly flat signal. The following conclusions were reached with regard to hypothesis 2.

(1) The TECO SO_2 gas monitor, installed in November 1988, measured concentrations of 0.1-0.3 ppbv, except during volcanic events.

(2) The CSI total sulfur gas monitor, installed in March, 1988, measured concentrations of 0.1 to nearly 3 ppbv, except during volcanic events.

(3) The ratio between SO_2 and total sulfur approached 1 during volcanic events.

(4) When air was sampled from above the marine boundary layer, SO_2 concentrations remained between 0.1 and 0.3 ppbv. However, total sulfur increased dramatically. This resulted in the SO_2 to total sulfur ratio being <0.1 at times in the free troposphere.

Fig. 7.10. History of volcanic sulfur events at MLO from June 1988 through January 1989.

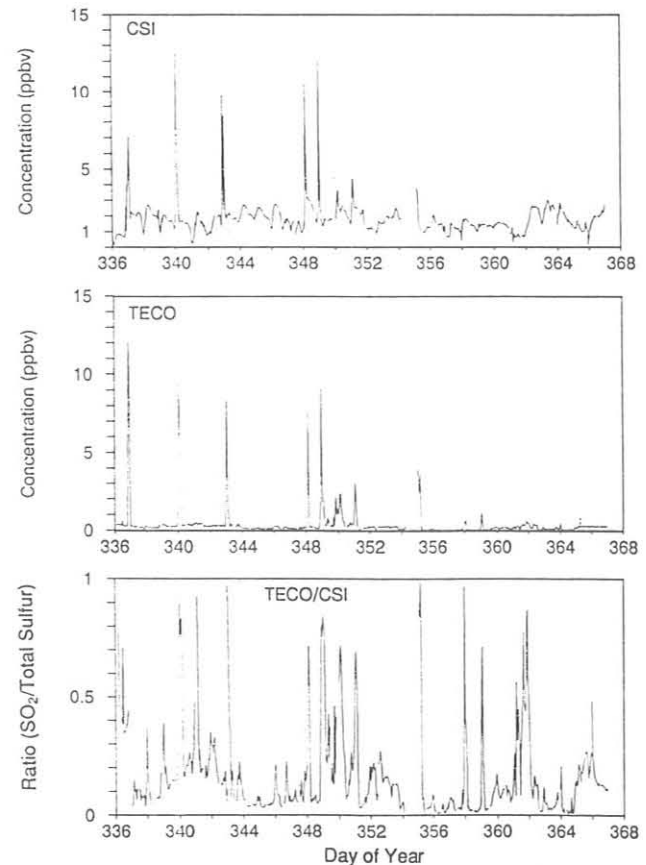Fig. 7.11. Sulfur gas concentration observed with the CSI instrument and SO_2 concentration observed with the TECO instrument, and the ratio between them, during December 1988.

7.2.2. Blue Ridge Flights

In connection with the AQG's participation in the Aircraft Monitoring for Diagnostic Model Evaluation project in the northeastern United States in August 1988, a sub-project was undertaken to provide some comparison between aircraft and surface measurements. Two flights were made on August 16, 1988, with the NOAA King Air aircraft. These flights included traverses at 2400-3000 m above sea level between the aircraft base at Harrisburg, Pennsylvania, and surface research sites from two projects (ECP and MCCP) from central Pennsylvania to northern Georgia.

Vertical profiles were flown over each of the five sites, the lowest altitude at each location being about 152 m above ground level. The sites were (1) Scotia (ECP), near State College, Pennsylvania, operated by the NOAA/AL, (2) Shenandoah (MCCP), in the Shenandoah National Park, Virginia, operated by the University of Virginia, (3) White Top Mountain (ECP), in southwest Virginia, operated by the Tennessee Valley Authority, (4) Mt. Mitchell (MCCP), near Asheville, North Carolina, operated by North Carolina State University, and (5) Brasstown Bald (ECP), in northern Georgia, operated by the Georgia Institute of Technology. In addition, vertical profiles were flown over the Scotia site during flights on August 21, 22, and 26.

Measurements from the surface sites were found to be generally lower in the concentrations of O_3, SO_2, H_2O_2, and NO_y. Detailed analyses have been made of the data from the Scotia site. The best comparison between ground samples and aircraft data is expected to be obtained by comparing atmospheric secondary products (O_3, H_2O_2, sulfate, and nitrate). These species are produced in the atmosphere and have formation times of about 2-50 hours. This time is long with respect to the usual boundary layer mixing times; thus the concentrations within the planetary boundary layer should be fairly uniform. Comprehensive comparison of aircraft and surface data at Scotia was possible only with O_3; H_2O_2 measurements aboard the aircraft provided supplemental information.

O_3 concentrations aloft were, with few exceptions, higher by 3-25 ppbv than those measured at the surface. The lowest altitude aircraft measurements were 3-5 ppbv higher than those at the surface during three of the four sampling flights over the Scotia site (August 16, 22, and 26); on August 21, O_3 levels measured from the aircraft at the lowest flight altitude were nearly 10 ppbv higher than those at ground level. Slightly higher concentrations at the lowest aircraft sampling altitude can be related to deposition of O_3 to the surface, especially during the day when convective activity was at a maximum.

On each of the four flights, O_3 concentrations were nearly uniform within the planetary boundary layer. Fluctuations measured at the two lowest aircraft profile altitudes were less than 5 ppbv around the mean; O_3 time series for the surface and the two lowest aircraft altitudes for each of the four sampling flights showed no break in the O_3 trace between the lower sampling level (950 mb) and the upper part of the mixed layer (approximately 890 mb). This observation suggests that the ground-level data provide a good indication of the O_3 distribu-

tion within the planetary boundary layer during the day.

Again with the exception of the profile taken on August 21, O_3 concentrations in the free troposphere (above 850 mb) were higher, occasionally by as much as 30 ppbv, than those observed inside the mixed layer. Likewise, H_2O_2 concentrations were higher in the free troposphere, compared with the mixed layer, on all flights, in spite of the fact that the dew points were much lower at those altitudes. The high O_3 levels in the free troposphere did not correlate with primary pollutants (SO_2, NO_y, and hydrocarbons), which were significantly lower at the higher altitudes. Thus the elevated concentrations of the secondary pollutants (O_3 and H_2O_2) in the free troposphere may have been related to aged pollution parcels (one or more days), in which all primary pollutants had already been oxidized.

On August 21, boundary layer O_3 concentrations measured by aircraft were about 70 ppbv, approximately 10 ppbv greater than those measured at the surface or in the free troposphere. These boundary layer concentrations were also the highest values measured during the four profile flights, and were correlated with elevated boundary layer SO_2 levels (approximately 5 ppbv); this indicates that relatively fresh anthropogenic pollution was present, in which O_3 generation was occurring. The difference between the surface and aircraft measurements was greater than that observed on the other flights, indicating that boundary layer mixing was not as complete as at the other times.

7.3. References

Barth, M.C., D.A. Hegg, P.V. Hobbs, J.G. Walega, G.L. Kok, B.G. Heikes, and A.L. Lazrus, Measurements of atmospheric gas-phase and aqueous-phase hydrogen peroxide concentrations on winter on the east coast of the United States, *Tellus, 41B*, 61-69, 1989.

Boatman, J.F., M. Luria, C.C. Van Valin, and D.L. Wellman, Continuous atmospheric sulfur gas measurements aboard an aircraft: A comparison between the flame photometric and fluorescence methods, *Atmos. Environ., 22(9)*, 1949-1955, 1988.

Boatman, J.F., R. Artz, L. Gunter, and H. Sievering, Intercomparison of AQG-aircraft and AOML-ship chemical and meteorological data during CASE/WATOX, *Proceedings GCE/CASE/WATOX Data Workshop*, Miami, FL, September 11-15, NOAA/ERL/AOML, 1989a.

Boatman, J.F., D.L. Wellman, C.C. Van Valin, R.L. Gunter, J.D. Ray, H. Sievering, Y. Kim, S.W. Wilkison, and M. Luria, Airborne sampling of selected trace chemicals above the central United States, *J. Geophys. Res., 94(D4)*, 5081-5093, 1989b.

Chang, J.S., R.A. Brost, I.S.A. Isaksen, S. Madronich, P. Middleton, W.R. Stockwell, and C.J. Walcek, A three-dimensional Eulerian acid deposition model: Physical concepts and formulation, *J. Geophys. Res., 92*, 14,681-14,700, 1987.

Gillette, D., and K. Hansen, Spatial and temporal variability of dust emissions in the United States, *J. Geophys. Res., 94*, 2197-2206, 1988.

Heikes, B.G., G.L. Kok, J.G. Walega, and A.L. Lazrus, H_2O_2, O_3, and SO_2 measurements in the lower troposphere over the eastern United States during fall, *J. Geophys. Res., 92*, 915-931, 1987.

Kim, Y.J., H. Sievering, and J. Boatman, Airborne measurement of atmospheric aerosol particles in the lower troposphere over the central United States, *J. Geophys. Res., 93*, 12,631-12,644, 1988.

Kim, Y., H. Sievering, J. Boatman, and S. Wilkison, Determination of water mass and dry mass composition of CASE/WATOX marine aerosols, *Proceedings, GCE/CASE/WATOX Data Workshop*, Miami, FL, September 11-15, NOAA/ERL/AOML, 1989.

Kleinman, L.I., Photochemical formation of peroxides in the boundary layer, *J. Geophys. Res., 91*, 10,889-10,904, 1986.

Lazrus, A.L., G.L. Kok, J.A. Lind, S.N. Gitlin, B.G. Heikes, and R.E. Shetter, Automated fluorimetric method for hydrogen peroxide in the air, *Anal. Chem., 58*, 594-597, 1986.

Logan, J.A., M.J. Prather, S.C. Wofry, and M.B. McElroy, Tropospheric chemistry: A global perspective, *J. Geophys. Res., 86*, 7210-7254, 1981.

Luria, M.L., C.C. Van Valin, J.D. Ray, and J. Boatman, The relationship between ozone and hydrogen peroxide: Field observation and model evaluation, *Proc. of the Quadrennial Ozone Symposium, August 8-14, 1988, Göttingen, FRG*, A. Deepak Publishing Co., Hampton, VA, 1989.

Meagher, J.F., E.M. Bailey, and M. Luria, The seasonal variation of the atmospheric SO_2 to SO_4^{2-} conversion rate, *J. Geophys. Res., 88*, 1525-1527, 1983.

Mueller, P.K., G.H. Hidy, K. Warren, T.F. Lavery, and R.L. Baskett, The occurrence of atmospheric aerosols in the northeastern United States, *Ann. N.Y. Acad. Sci., 338*, 463-482, 1980.

Sievering, H., G. Ennis, E. Gorman, and C. Nagamoto, Size distributions of excess sulfate, nitrate, and chloride deficit during CASE/WATOX: A case for the heterogeneous conversion mechanisms, *Proceedings, GCE/CASE/WATOX Data Workshop, Miami, FL, September 11-15*, NOAA/ERL/AOML, 1989.

Van Valin, C.C., J.D. Ray, J.F. Boatman, and R.L. Gunter, Hydrogen peroxide during winter in air over the south-central United States, *Geophys. Res. Lett., 14*, 1146-1149, 1987.

8. Nitrous Oxide and Halocarbons Group

J. Butler (Editor), J.W. Elkins, T.M. Thompson, B.D. Hall, and C.M. Brunson

8.1. Continuing Programs

8.1.1. Flask Samples

Sampling and Instrumentation

During 1988, air samples were collected in pairs of 0.3-L, Summa-treated, stainless steel cylinders each week at BRW, NWR, MLO, and SMO. The samples at SPO were collected each week only during January, November, and December, when the Antarctic interior was accessible by aircraft. In addition, a new flask sampling effort was instituted at the Alert (ALT) station of the Canadian Atmospheric Environment Service, in the Northwest Territories, where flask pairs were filled with air on a 1-2 week schedule beginning in February. All flask samples were shipped to our central laboratory in Boulder, Colorado, where they were analyzed by EC-GC for N_2O, CFC-12 (CCl_2F_2), and CFC-11 (CCl_3F).

Primary calibration tank no. T3088 was retired from service in December 1987 and was replaced by aluminum cylinder 62631 that had been treated with Aculife (Scott Specialty Gases, Plumsteadville, Pennsylvania) and filled with dried air from NWR. N_2O, CFC-12, and CFC-11 concentrations in the new tank were compared with those in T3088 in September and October 1987, and again in May 1988. No significant drift was apparent from these intercomparisons.

An automated flask analysis system was designed, and construction of it was begun in 1988. In the past, each flask was analyzed manually on one GC system, but with this new system, up to 10 flasks can be analyzed in any sequence, and reference gases can be interspersed as needed. Three GCs will be used to analyze N_2O (affected by CO_2), N_2O (unaffected by CO_2), CFC-12, CFC-11, CFC-113 (CCl_2F-$CClF_2$), chloroform ($CHCl_3$), methylchloroform (CH_3CCl_3), and carbon tetrachloride (CCl_4). A desk-top computer will be used to control the chromatographic system as well as to collect, analyze, and store the data. The hardware has been purchased, and most of the controlling software has been written.

Some unusual samples were collected or reported in 1988. The first came from the second boat pit of Khufu's pyramid in Egypt in October 1987. *Tans et al.* [1988] explained the air sampling procedure and measurement results. It was hoped that the chamber would contain ancient air, but the halocarbon composition showed that the pit was not sealed with respect to the outside atmosphere. A stability study was initiated using various types and sizes of containers (aluminum and stainless steel) to find a suitable generic flask for all compounds measured by GMCC for ambient levels of CO_2, CH_4, N_2O, CFC-11, and CFC-12 over time. The electropolished stainless steel and aluminum flasks were stable for ambient levels of CFC-11 and CFC-12 for storage under 35 days, but all other compounds showed significant loss or gain with time for these unusually wet samples [*Tans et al.*, 1988].

The second set of unusual samples was collected at SPO on January 24, 1988. The samples in two 1.0-L flasks were pressurized to 150 kPa, returned to Boulder, and sealed in a time capsule in the foundation of the new CIRES building on the University of Colorado campus. These samples will be recovered in 50-100 years for reevaluation of their contents.

Results

Data from flasks collected at BRW, NWR, MLO, SMO, and SPO from 1977 through 1988 show a mean, global growth rate of 0.68 ppb yr^{-1} for N_2O (Figure 8.1), 16.1 ppt yr^{-1} for CFC-12 (Figure 8.2), and 9.8 ppt yr^{-1} for CFC-11 (Figure 8.3). Preliminary 1988 monthly mean data are tabulated in Table 8.1. The CFC-11 and CFC-12 data show that concentrations are rising over the past few years at a rate stronger than that seen in the earlier record. Since calibration gas standards have been changed in this period and insufficient time has gone by to determine calibration tank long-term stability or drift characteristics, it is uncertain whether the stronger rise is real, being a response to increased chemical usage and release into the atmosphere, or a vagary of the new standard.

Data from flasks collected at ALT were often erratic; many pairs did not match well. This was worse for CFC-11 than it was for CFC-12. Consequently, only flask pairs with concentrations that agreed have been retained for subsequent analysis. Results from ALT compare favorably with those from BRW, although there are slight differences (Figure 8.4). These differences can be ascribed to the large distance between the stations and the different air masses that move in and across the Arctic basin.

8.1.2. RITS Continuous Gas Chromatograph Systems at GMCC Baseline Stations

Sampling and Instrumentation

In-situ measurements of CFC-11, CFC-12, CFC-113, N_2O, CH_3CCl_3, and CCl_4 were made 8 times per day at three GMCC baseline stations, BRW, MLO, and SMO, and 12 times per day at SPO. Instrumental precision has consistently been better than 0.3% for N_2O and between 0.5 and 2% for the rest of the compounds. In mid-1987 measurements of N_2O were begun using a Porapak Q column, and the precision has been greatly improved because there is no known CO_2 effect, and no interfering peaks on the chromatogram (Figure 8.5).

In November 1988, the MLO and SMO systems were modified so that all three columns could be backflushed. Previously, only the N_2O GC was equipped for backflush operation. The backflush modifications at BRW will be completed in early 1989. Backflushing the columns should improve the precision of the measurements by allowing 30-min runs instead of 60-min runs. Along with the backflush modifications, an HP hierarchical filing system was installed to speed up data storage. It is anticipated that 30-min runs will begin early in 1990.
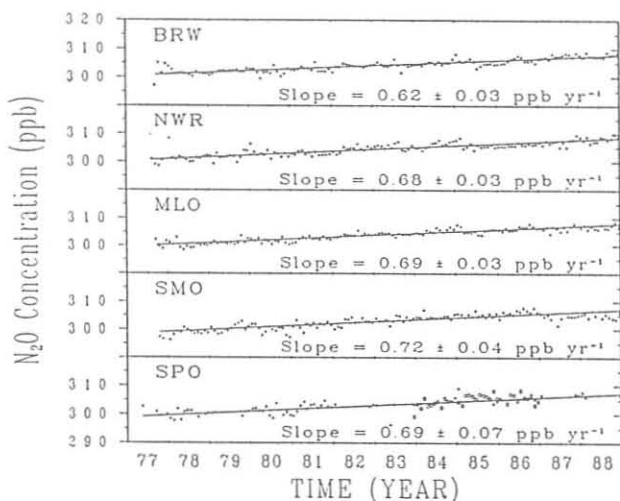
Fig. 8.1. Monthly mean concentrations of N_2O from the NOAA/GMCC flask (+) network (CO_2 and H_2O corrected). The SPO plot also shows monthly means (o) from the old GMCC in-situ GC. The trends and ±2 standard deviations are also shown.
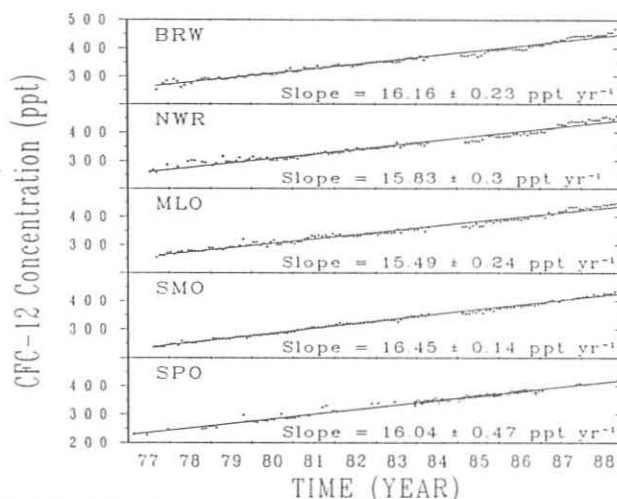

Fig. 8.3. Monthly mean concentrations of CFC-11 from the NOAA/GMCC flask (+) network. The SPO plot also shows monthly means (o) from the old GMCC in-situ GC. The trends and ±2 standard deviations are also shown.

Fig. 8.2. Monthly mean concentrations of CFC-12 from the NOAA/GMCC flask (+) network. The SPO plot also shows monthly means (o) from the manually operated GMCC in-situ GC. The trends and ±2 standard deviations are also shown.
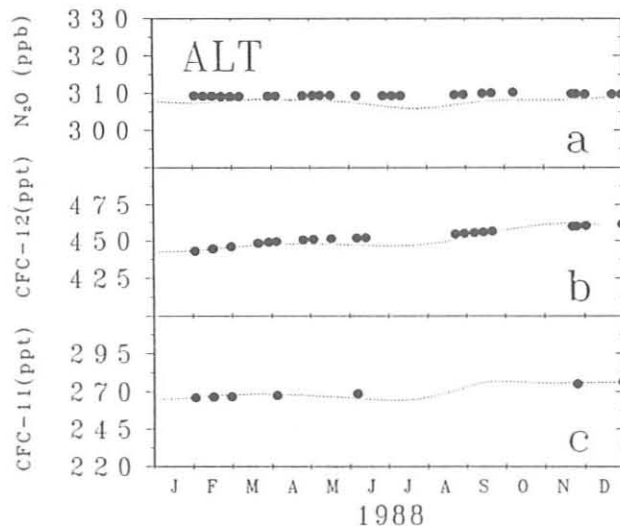
Fig. 8.4. Average concentrations for (a) N_2O, (b) CFC-12, and (c) CFC-11 from flask pairs collected at ALT. The dotted line is a spline fit to BRW flask data for comparison.

New regulators were purchased and installed in 1988, solving many of the contamination problems. A contaminant still elutes between CH_3CCl_3 and CCl_4 on the SP2100 GC column in one of the BRW standards, and one of the MLO standards has a large amount of CFC-113. The major problem with the contaminants is that they make it difficult to integrate the chromatogram peaks consistently, and the precision suffers as a result. The precision can be improved for CH_3CCl_3 and CCl_4 by calculating concentrations from peak heights instead of from peak areas. In the future, both peak heights and peak areas will be computed and stored for all components measured by the RITS GC system, and old data will be reintegrated and both areas and heights will be stored.

A modified RITS GC was set up and tested at SPO in February. The system consisted of two Shimadzu Mini-2 GCs that measure the concentrations of N_2O, CFC-12, CFC-11, CH_3CCl_3, and CCl_4 on an hourly basis. An IBM XT clone computer was set up to allow automated data transfer from the two HP3390 integrators to a floppy disk. Data from the disk are then transferred weekly via satellite to Boulder.

Results

In 1987 an apparent increase of 18 ppt yr^{-1} was reported for CFC-12 at BRW (Figure 8.6a). It is now apparent that this was the result of seasonal fluctuations in the CFCs, perhaps from European air masses. The seasonal variation at BRW is also more apparent in the CFC-11 data (Figure 8.6b).

65

TABLE 8.1. 1988 Monthly Mean Concentration for N$_2$O (ppb by mole fraction in dry air), CFC-12 (ppt), and CFC-11 (ppt) from Flask Pairs Collected at BRW, NWR, MLO, SMO, and SPO

1988	N$_2$O					CFC-12					CFC-11				
	BRW	NWR	MLO	SMO	SPO	BRW	NWR	MLO	SMO	SPO	BRW	NWR	MLO	SMO	SPO
Jan.	308.7	309.5	307.2	305.4	308.0	443.9	440.9	428.3	415.7	405.1	263.5	260.3	248.8	242.7	
Feb.	308.1	308.3	308.1	305.8	306.4	444.2	437.2	433.1	418.8		265.3	258.5	254.2	243.9	
March	309.8	309.8	306.5	304.3		446.6	447.8	430.9	415.4		266.3	263.5	250.3	238.0	
Arpil	308.6	307.5	308.0			447.8	444.6	438.1	424.1		268.5	262.1	256.2	247.0	
May	308.4	308.1	307.2	305.1		443.8	445.8	438.3	421.3		265.6	269.4	256.9	243.7	
June	308.1	307.7	306.8			446.8	445.6	438.6			266.1	263.8	257.9		
July	307.5	309.2	308.3	304.3		446.8	454.2	442.8	426.9		265.6	267.9	257.7	246.2	
Aug.	306.9	309.0	307.0	305.5		448.6	455.4	442.0	426.8		267.3	270.0	259.1	249.2	
Sept.	308.9	308.1	306.7	304.6		457.0	450.9	445.7	427.3		268.6	264.5	261.8	245.8	
Oct.	308.5	308.8	307.9	304.1		456.7	448.5	446.0	433.5		271.9	263.8	262.0	249.9	
Nov.	309.0	310.4	308.9	303.7		469.6	459.1	449.2	437.7	423.4	277.7	272.7	266.9	251.5	246.9
Dec.	309.6	309.6	307.3	306.2	307.1	462.0	451.2	453.7	434.0	423.1	277.3	268.0		258.3	244.6

These data are provisional, pending final calibration.

The year 1988 was the first complete year of CH$_3$CCl$_3$, and CCl$_4$ measurements from the GMCC baseline observatories. Although it has been possible to calculate crude atmospheric growth rates from this limited data set, the results should be considered tentative until measurements over a larger time span are obtained. Also, some analytical problems, which may have an effect on the overall accuracy of these numbers, are still being resolved.

On the basis of only 1 year of observations at MLO (Figure 8.7), the concentration of atmospheric CCl$_4$ does not appear to be increasing significantly; CH$_3$CCl$_3$, however, does seem to be growing at about 4% per year, a finding that is confounded by a contaminant interfering with the measurement of this com-

pound. As for the CFC-113 estimates, the estimated growth rates for CCl$_4$ and CH$_3$CCl$_3$ will be refined considerably as our in-situ systems remain on line long enough to collect a few years' data and as lingering contamination problems are resolved.

8.1.3. LOW ELECTRON ATTACHMENT POTENTIAL SPECIES

A temperature-programmable, dual-channel, EC-GC was purchased and installed for the measurement of LEAPS gases, specifically HCFC-22 (CHClF$_2$), CFC-113, and the Halons, H-1301 (CBrF$_3$) and H-1211 (CBrClF), in our Boulder laboratory. The GC was fitted with a programmable cryofocus-
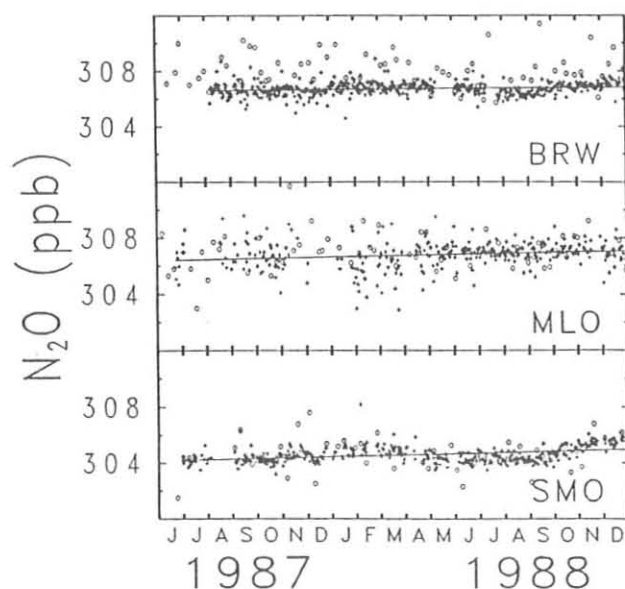

Fig. 8.5. N$_2$O concentrations from flask pair samples (o) and daily means from the in-situ RITS GC (+), at BRW, MLO, and SMO.
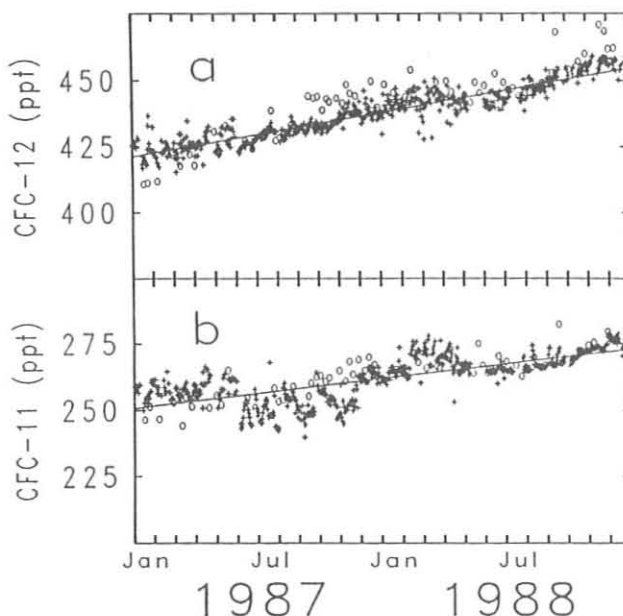

Fig. 8.6. (a) CFC-12 and (b) CFC-11 concentrations (ppt) at BRW from the in-situ RITS GC. Note the apparent elevation in CFC concentration from late October to late May.
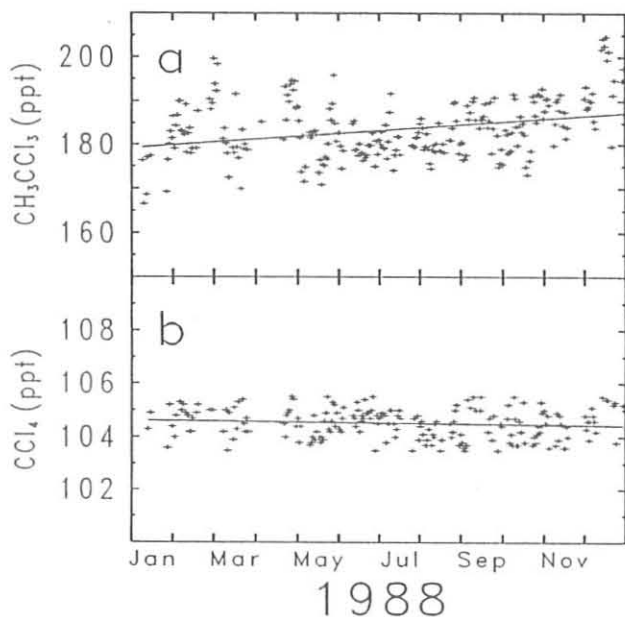
Fig. 8.7. (a) CH_3CCl_3 and (b) CCl_4 concentrations at MLO in 1988 from the in-situ RITS GC.

Fig. 8.8. Boiling point curve for the chromatographic separation of natural gases and halocarbons on a silicone oil-based, capillary column (Chrompack CP-Sil-5, 1.2μm; 0.53 mm × 50 m). Note similar retention times for proposed replacement halocarbons (CFC-134a and HCFC-123) and the compounds they are to replace (CFC-12 and CFC-11).

ing unit for concentrating and injecting atmospheric gases. This unit, designed for injecting gases adsorbed to packed tubes, was modified to allow the direct injection of up to 500 mL. As a result, electrophilic gases can be measured to levels as low as 1 ppt.

A number of standard gases were tested on the GC with a silicone oil column (Chrompack CP-Sil-5, 1.2 μm) set to a temperature range of -60°C to +110°C. The column eluted all gases of interest from H-1301 (boiling point = -59°C) to CCl_4 (boiling point = 77°C), with reasonable separation of peaks. Peaks were identified and response factors determined for N_2O, H-1301, HCFC-22, CFC-12, CH_3Cl, HFC-134a ($C_2H_2F_4$), H-1211, CFC-11, HCFC-123 (CF_3CHCl_2), CH_2Cl_2, CFC-113,

$CHCl_3$, CH_3CCl_3, and CCl_4 (Figure 8.8). Two of these gases, HFC-134a and HCFC-123, have been proposed as replacement halocarbons for CFC-12 and CFC-11.

The first air samples for LEAPS gases were collected from NWR in November, beginning our long-term monitoring program for the four LEAPS gases. The GC has also been used to measure the composition and contamination of industrial solvents used for cleaning regulators and fittings purchased by our laboratory, and to identify contaminants in cylinders of commercial carrier gas, "zero air" collected at NWR, and standard gases filled at NWR. Evaluating alternative, analytical columns and installing new, high-pressure pumps at the observatories to provide sufficient samples for replicate mea-

TABLE 8.2. Summary of GMCC Gravimetric Standards Prepared in 1988

Set	Compounds	Quantity	Concentration Range	Prepared for
1	CO_2, N_2O	5	ppm	NOAA/RITS
2	CFC-12	8	ppm, ppb, ppt	NOAA/RITS
3	CFC-12, CFC-11, CFC-113, CH_3CCl_3, CCl_4, $CHCl_3$	3	ppb, ppt	NOAA/RITS
4	CFC-12, CFC-11, CFC-113, CH_3CCl_3, CCl_4, CH_3Br	3	ppt	NOAA/RITS
5	CFC-113	3	ppm, ppb, ppt	NOAA/RITS
6	CFC-113, Halon-1211, CFC-22	1	ppb	NOAA/LEAPS
7	CH_4	5	0.1 %	NOAA/FT-IR/CC
8	HFC-134a	7	ppm	NOAA/FT-IR
9	HCFC-123	1	ppm	NOAA/FT-IR
10	CO_2	4	ppb	NOAA/GMCC
11	Benzene, isoprene, pentane, α-pinene, m-xylene, 2,2-dimethylbutane	1	ppm	NOAA/AL
12	Halon-1211	1	ppm	OGC
13	Halon-1211	1	ppm	NOAA/ARL/Idaho Falls

surement of LEAPS gases should lead to improvements in precision and accuracy of the LEAPS measurements.

8.1.4. GRAVIMETRIC STANDARDS

Our newly completed gravimetric standards laboratory is now capable of preparing gravimetric standards for a large variety of compounds at sub-percent, parts per million, parts per billion, and parts per trillion concentrations. Several sets of gravimetric standards were prepared for various projects such as RITS, LEAPS, and FT-IR, and other groups, including NOAA/ARL Idaho Falls, NOAA/AL, and OGC (Table 8.2).

Standard curves were constructed from gravimetric sets of N_2O, CFC-12, CH_3CCl_3, and CCl_4. The precision for these curves was 0.4 ppb, 1.6 ppt, 2.2 ppt, and 1.3 ppt, respectively, where precision is defined as the average difference between the gravimetric concentration and the concentration predicted by the standard curve (Figures 8.9-8.12). A set of CFC-11 and

CFC-113 standards will soon be prepared, and all RITS compounds will be reported on the NOAA scale. CFC-11 and CFC-12 are currently reported on the OGC scale of 1985. The nonlinear response of N_2O on an ECD was investigated by comparing N_2O gravimetric standards in a 290-ppb range. NIST SRMs and NOAA N_2O standards were used to construct a curve from 44 to 333 ppb (Figure 8.9). A linear extrapolation from a response of unity differed by as much as 12.5 ppb from the true curve in the 130 to 150 ppb range, but the difference was not as significant (less than 3 ppb) in the 280 to 320 ppb range.

Gravimetric standards of CFC-12 were prepared by two different methods. Pure CFC-12 gas was diluted to the parts per trillion level and compared with parts per trillion standards prepared from the dilution of pure CFC-12 liquid. Both sets of standards agreed within 1.6 ppt (Figure 8.10).

A dual-detector Shimadzu GC-8A with a flame ionization detector was purchased and will be used to compare standards at the parts per million levels. A Perkin-Elmer 3920B GC and a
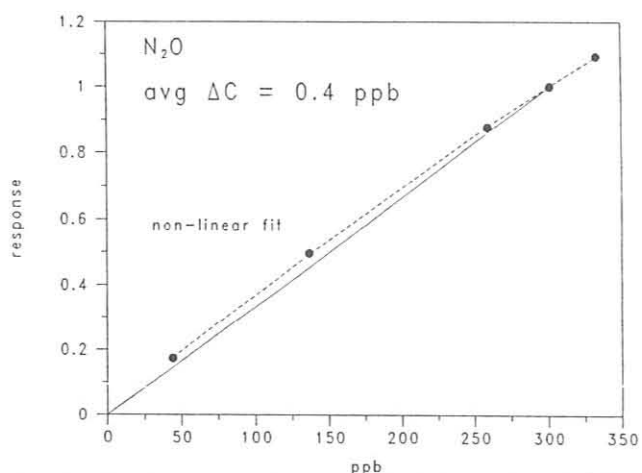
Fig. 8.9. N_2O standard curve prepared from NIST SRMs and NOAA gravimetric standards. A normalized detector response is plotted versus concentration.
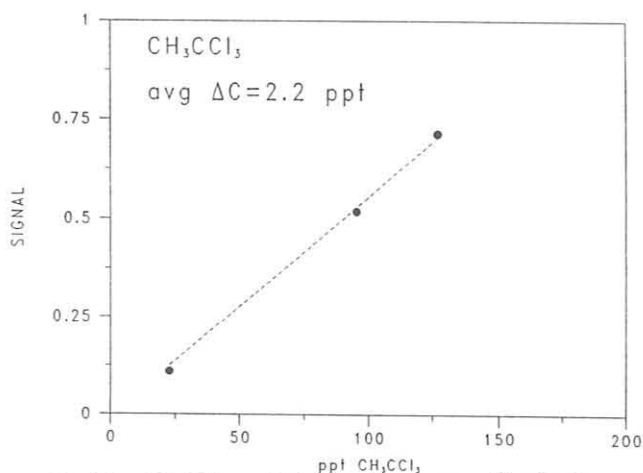
Fig. 8.11. CH_3CCl_3 standard curve for parts per trillion levels.
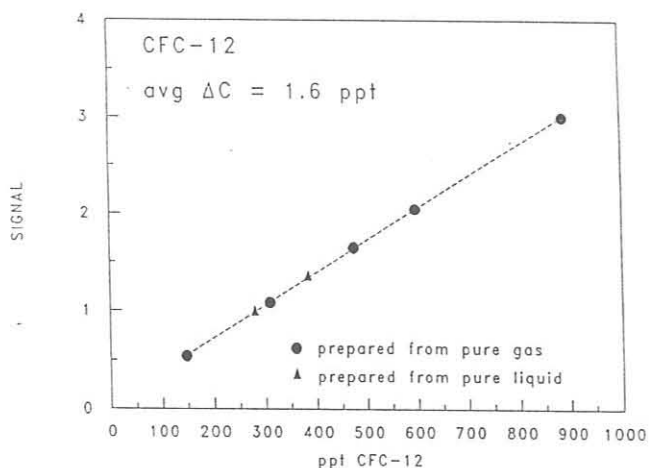
Fig. 8.10. CFC-12 standard curve for parts per trillion concentration levels, showing good agreement between two methods of preparation.
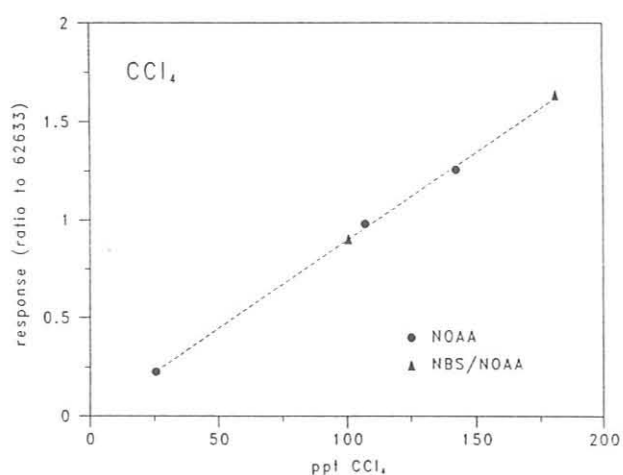
Fig. 8.12. CCl_4 standard curve for pats per trillion levels showing good agreement between NOAA and NIST standards.

Spectro-Physics SP7100 GC with electron capture detectors will be used to compare standards at parts per billion and parts per trillion level. This set of GCs will allow us to examine our standard sets more closely at each step in the dilution process.

8.2. SPECIAL PROJECTS

8.2.1. SOVIET-AMERICAN GAS AND AEROSOL EXPERIMENT II

SAGA II in 1988 emphasized filtering and reducing the CFC, N_2O, CO_2, and CH_4 data collected by automated GCs during the 3-month cruise. The results were evaluated and presented at professional meetings, and a data report describing our analytical methods, data reduction, and results was published in December [*Butler et al.*, 1988]. Manuscripts for publication in professional journals were begun once the data were finalized.

8.2.2. FT-IR SPECTROMETER ARCHIVE PROJECT

As discussed in section 8.1.1., the goal of finding a generic flask for all compounds measured by GMCC has been elusive. The FT-IR spectrometer permits archiving the IR absorption of atmospheric trace gases for future analysis of compounds not currently analyzed by GMCC. A solar tracker that permits the spectometer to follow the sun was designed in 1988. It is anticipated that the FT-IR archive project will begin in 1990.

The principal goal in 1988 was measuring laboratory spectra of many important RITS gases, including CH_4 and the new substitute CFCs. These spectra are required to calibrate the instrument for atmospheric measurements. The spectra were also useful in verifying our methods for the preparation of gas standards. Figure 8.13 shows a laboratory infrared spectrum between 600 and 1500 cm^{-1} for one of the proposed replacement halocarbons, HFC-134a, measured for a sample containing 1021 ppm in air in a 15-cm-long gas cell at 300 K. Figure 8.14 shows a Beer's law plot for the v_4 fundamental band of CH_4 at various temperatures, where the slope of the line yields the band strength value for the compound. For both CH_4 and HFC-134a,

Fig. 8.14. Beer's law plot of integrated absorbance versus pressure-pathlength for the v_4 band of CH_4 at various temperatures.

band strength values were not a function of temperature, but the band shape was definitely affected by temperature; the band was narrower and absorption greater at lower temperatures. Table 8.3 shows a summary of all band strength measurements in 1988. The GMCC band strength for the v_4 band of CH_4 is identical to the value of *Varanasi et al.* [1983]. The measured total band strengths for HFC-134a and HCFC-123 are comparable with total band strengths for the compounds that they are replacing, CFC-12 and CFC-11. Since the atmospheric lifetimes of the replacement CFCs are shorter (~15 years for HFC-134a and ~2 years for HCFC-123) than that of the CFCs (~100 years), the potential for the replacement CFCs to produce the greenhouse effect is greatly reduced.

TABLE 8.3. Summary of Band Strength Measurements for RITS Gases

Compound	Formula	Total Band Strength (cm^{-2} atm^{-1} at 300 K)	Reference
Methane			
v_4 band	CH_4	125	This report
v_4 band	CH_4	126	*Varanasi et al.*, 1983
CFC and Substitutes			
HFC-134a	$C_2H_2F_4$	3147	This report
CFC-12	CCl_2F_2	3271	*Elkins et al.* 1986
HCFC-123	$C_2HCl_2F_3$	2379	This report
CFC-11	CCl_3F	2417	*Elkins et al.*, 1986

Fig. 8.13. Infrared absorption by one of the proposed replacement halocarbons (HFC-134a).

8.2.3. AIRBORNE GAS CHROMATOGRAPH

A Shimadzu Mini-2 gas chromatograph was modified for use aboard the NOAA King Air research aircraft. The GC was designed for measuring halocarbons in the atmosphere at the parts per trillion level at 4-min intervals in a pressurized aircraft. The GC was configured with a 0.6-m Porasil B main column and a 0.3-m Porasil B backflush column. A carrier gas makeup stream and two absolute backpressure regulators were installed at the outlet of the detector to compensate for changes in atmospheric pressure.

One test flight was conducted over eastern Colorado on December 6, 1988. CFC-12 was measured at various altitudes, and flask samples were collected and compared with the GC data. Figure 8.15 shows CFC-12 as a function of altitude. This test flight provided valuable preliminary information regarding the capabilities and limitations of an airborne EC-GC.

Fig. 8.15. CFC-12 variation with altitude over eastern Colorado on December 6, 1988.

8.3. REFERENCES

Butler, J. H., J. W. Elkins, C. M. Brunson, K. B. Egan, T. M. Thompson, T. J. Conway, B. D. Hall, Trace gases in and over the west Pacific and east Indian Oceans during the El Niño-Southern Oscillation event of 1987, *NOAA Data Rep. ERL ARL-16*, 104 pp., NOAA Air Resources Laboratory, Boulder, CO, 1988.

Elkins, J.W., R.L. Sams, and J. Wen, Measurements of the temperature dependence on the inrared band strengths and shapes for halocarbons F-11 and F-12, *National Bureau of Standards (U.S.) Report 553-K-86*, 30 pp., Gaithersburg, MD, 1986.

Tans, P. P., J. W. Elkins, and D. R. Kitzis, Air sampling procedures and measurements of the air composition of the second boat pit of Khufu's pyramid, *NOAA Tech. Memo. ERL ARL-163*, 21 pp., NOAA Air Resources Laboratory, Boulder, CO, 1988.

Varanasi, P., L.P. Giver, and F.P.J. Valero, Thermal infrared lines of methane broadened by nitrogen at low temperaures, *J. Quant. Spectrosc. Rad. Trans*, 6, 481-490, 1983.

9. Director's Office

9.1. ALKALINE AEROSOLS PROGRAM: ALKALINE AEROSOLS INVENTORY

D. A. GILLETTE

9.1.1. INTRODUCTION

The NAPAP Interim Assessment [*Placet and Streets*, 1987] concluded that "emissions of alkaline substances can significantly influence precipitation acidity by neutralizing some fraction of the acids," and that alkaline emissions may have an especially substantial effect on the pH of wet deposition in the western United States. Because of the importance of alkaline materials to rain chemistry, we have attempted to estimate the emissions of these materials in the United States. In previous work [*Evans and Cooper*, 1980] the largest sources of alkaline aerosols have been estimated to be "open" sources (sources too great in extent to be controlled by enclosure or ducting). These sources are wind erosion of soils, including dust devil emissions; road dust generation by vehicles; and dust emission from tillage operations.

These estimates for the open sources of alkaline particles were used in this study to form an inventory for elemental alkaline emissions of calcium, potassium, magnesium, and sodium. Fluxes of the alkaline elements were expressed in terms of equivalent fluxes of hydrogen so that the alkaline fluxes could be easily compared with acid precursor fluxes. That is, elemental fluxes were divided by atomic weight and multiplied by valence; for example, calcium fluxes were divided by 20. The mapping of results is consistent with the mapping format of the RADM.

9.1.2. METHOD OF ESTIMATING ALKALINE DUST PRODUCTION

Wind Erosion Emissions

A physically based model of dust emissions was discussed in the 1987 *GMCC Summary Report* [*Bodhaine and Rosson*, 1988]. The model was used to compute expected total wind erosion dust emissions for soils of the United States. The alkaline emissions were then estimated from the total dust emission estimates by multiplying the dust emissions by the fraction of the soil mass for the alkaline elements calcium, potassium, magnesium, and sodium and by an enrichment factor. Average soil fractions for those elements were calculated using the soil composition data of *Boerngen and Shacklette* [1981]. The enrichment factor (a ratio of the percentage of an alkaline element in particles smaller than 10 μm to the percentage of alkaline composition for all sizes of the soil) was needed because only particles smaller than 10 μm were suspendable for long periods of time, and it is known that the composition of soil varies as a function of size. The enrichment factor was calculated by using the soil texture data in the USDA National Resources Inventory data base and composition-versus-size measurements of *Gatz et al.* [1986] that show that virtually all alkaline mass is associated with the silt and clay

fractions of the soil (that is, particles smaller than 50 so that the alkaline fluxes could be easily compared with acid precursor fluxes, μm).

Dust Devil Emissions

We estimated total suspension of alkaline material by dust devils [*Gillette and Sinclair*, 1990] by generalizing the aircraft measurements of *Sinclair* [1990]. In Sinclair's aircraft experiments, simultaneous measurements were made of particle concentration and vertical velocities in the updrafts of several dust devils at altitudes of 142 and 300 m. The product of the average particle concentration in the updraft times the average vertical velocity gives the mean vertical flux for the dust devil being sampled. Dust devils were classified into four different sizes (small, medium, large, and extra large), as was done by *Sinclair* [1975], and the means of the experimentally determined vertical mass fluxes were found for each of these dust devil classifications. These mean fluxes were then used to calculate total vertical fluxes of dust and vertical fluxes of dust smaller than 25 μm: the mean dust flux for dust devils of all four classes was multiplied by number of devils during the year for a 16 km by 16 km area near Tucson, Arizona [*Sinclair*, 1969], supplemented by the data of *Snow and McClelland* [1988] for a test area near Alamagordo, New Mexico.

These data were then generalized to areas in the United States as defined by climatic and vegetative classifications [for details, see *Gillette and Sinclair*, 1990]. Fluxes of alkaline elements calcium, potassium, magnesium, and sodium were estimated by multiplying the calculated fluxes specified for each of the climatic/vegetation areas by the appropriate elemental mass fraction of soil.

Road Dust and Field Tillage Emissions

Road dust emissions were evaluated by cooperative work by the Illinois State Water Survey; results were described by *Gillette et al.* [1990]. Mass fluxes from tillage were quoted from the work of *Evans and Cooper* [1980].

9.1.3. RESULTS

Mass production for suspended dust mass and the four alkaline elements Ca, Mg, K, and Na were summed for the contiguous United States. The results are shown in Table 9.1. The total mass of suspended dust of about 18.9×10^6 tonnes yr^{-1} is small compared with *D'Almeida's* [1986] estimate for Saharan wind erosion aerosol production of $(630-710) \times 10^6$ tonnes yr^{-1}. On an equivalent mass basis, clearly the most important alkaline element is calcium, which contributes 62.1% of the atmospheric aerosol alkalinity of the above four elements. Mg is second in contributions with 21.7% of the aerosol alkalinity.

Table 9.2 gives the percentages of alkaline aerosol fluxes for each of the four principal sources of suspended dust production. The largest producer of suspended dust mass is the wind action

Table 9.1. Total Mass Production Per Year, Total Equivalent Mass Production Per Year, and Percentage of the Combined Total Equivalent Mass Production for Four Alkaline Elements for Combined Road, Dust Devil, Wind Erosion, and Tillage Sources

	Ca	Mg	K	Na
Mass* (10^6 T yr^{-1})	1.16	0.25	0.31	0.17
Equivalent mass (10^6 eq. T yr^{-1})	0.058	0.02	0.0079	0.0072
Percentage of combined total equivalent mass	62.1	21.7	8.5	7.7

*Total mass production was 18.9×10^{12} g yr^{-1}.

Table 9.2. Percentages of Four Alkaline Elements and Total Aerosol Flux for Road Dust, Dust Devil, Wind Erosion, and Tillage

	Ca (%)	Mg (%)	K (%)	Na (%)	Total Mass (%)
Road dust	68.8	61.7	29.0	25.6	40.3
Dust devils	12.7	14.9	21.6	26.3	36.7
Wind erosion	17.0	21.1	47.1	40.5	19.1
Tillage	1.4	2.4	2.4	7.6	3.9

upon soils (55%). "Wind action" (dust devils plus wind erosion) is dominant mostly in the western United States excluding the nondesert part of California and much of the mountainous regions. "Open anthropogenic" (road dust plus tillage) sources account for 44% of the dust produced in the United States and are dominant east of 95°W longitude.

Because Ca is the dominant alkaline aerosol element, patterns of its emissions and deposition are representative of alkaline aerosols as a whole. For Ca, road dust is clearly dominant with almost 70% of total emission in the United States. The sum of all the open sources for Ca are plotted in Figure 9.1. Ca emission has maxima in a large tongue originating at the Big Bend area of Texas; the Sonoran, Mojave, and Great Basin Deserts; a band of states including Iowa, Illinois, Indiana, Ohio, and Pennsylvania; and Massachusetts.

9.1.4. COMPARISON WITH CALCIUM WET DEPOSITION DATA

Wet deposition data (that is, data from deposition collected in the wet deposition collectors) for the alkaline elements Ca, K, Mg, and Na from the NADP/NTN were made available to us by J. Gibson [personal communication, Ft. Collins, CO, 1988]. Wet deposition is only one pathway of atmospheric deposition. The other (dry deposition) is often thought to be of about equal effectiveness over a continental scale in removing particles from the atmosphere. Indeed, in dry regions as the southwestern United States, dry deposition is probably more effective in removing particles from the air because of the lack of rainfall.

When comparing wet deposition data to calculated emission rates, solubility must be considered. Because dissolved material will be reduced by the ratio of soluble material to total material, the calculated alkaline fluxes should be reduced by a solubility factor depicting that part of the road material that can dissolve in the rain. This factor for Ca is 0.94 (*Gatz et al.* 1984).

The wet deposition of Ca is shown in Figure 9.2. Total Ca emissions estimated in Figure 9.1 are higher than wet deposition shown in Figure 9.2. For the arid regions along the southwestern border of the United States, this probably reflects the lack of rainfall. The large source area described as the old "dust bowl" (the panhandles of Texas and Oklahoma, western Kansas, eastern Colorado) typically produces much of its dust during winds from the southwest. Transport of this dust to the Midwest could explain the maximum of deposition starting in this area and slanting to the northeast. Road dust in Iowa and northern
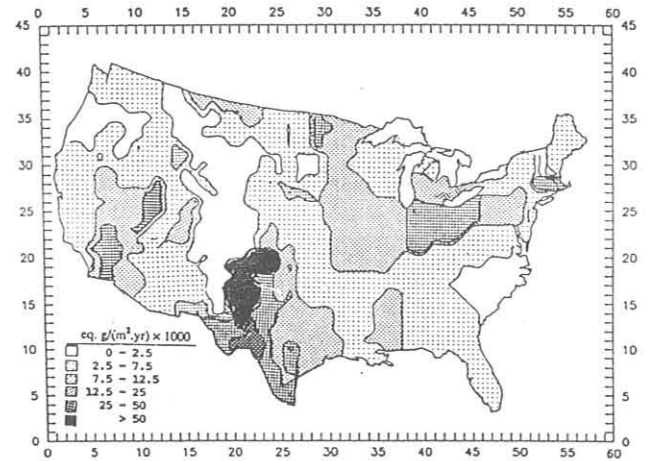

Fig. 9.1. Annual emissions of aerosol Ca. Units are equivalent grams per square meter per year times 1000.
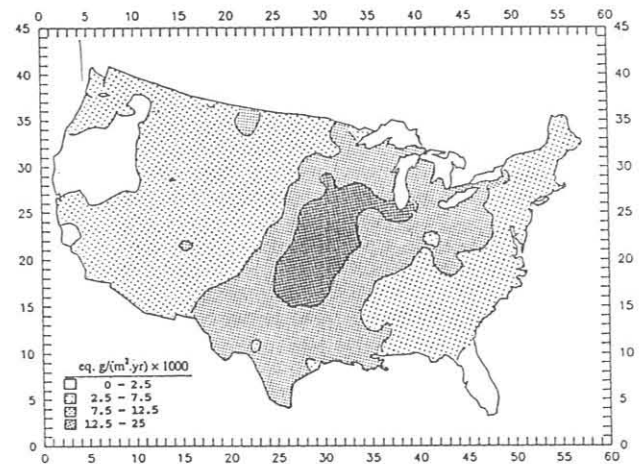

Fig. 9.2. Wet deposition of Ca determined for NADP/NTN. Units are as in Figure 9.1.
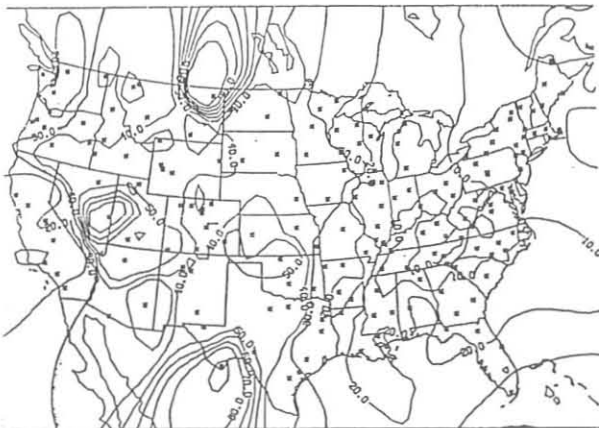
72

Illinois may also explain the northern part of this maximum of Ca deposition. Large road dust Ca sources in Ohio, Pennsylvania, and Massachusetts are not reflected in corresponding large Ca deposition in those states.

Emission estimates for the alkaline elements may be compared with the acid precursors SO_2 and $NO + NO_2$ ([for example in the NAPAP preliminary inventory by *Placet and Streets* [1987]). In general, the picture formed of comparing the equivalent mass emissions divides the contiguous United States into an eastern portion (east of 95°W latitude), where emissions of alkaline materials are overwhelmed by emissions of acid precursors, and a western portion (west of 95°W latitude), where emissions of alkaline materials are only slightly smaller than emissions of acid precursors.

This division is verified for the western United States by the *Young et al.* [1988] observation that 85% of the variance in sulfate is associated with variance of Ca, the dominant alkaline element found in our inventory. Another piece of evidence showing this division is a plot of the ratio of $Ca/(NO_3 + SO_4)$ in wet precipitation (where Ca, NO_3, and SO_4 are expressed as equivalents) from July 5, 1978, to February 4, 1986. The map (Figure 9.3) shows that for most of the western United States, except for the Pacific coastline, the ratio is greater than 0.3.

9.1.5. CONCLUSIONS

Total dust mass production for all open sources for the contiguous United States was used to generate emission rates and geographical patterns for alkaline emissions. Comparing the estimated sources of alkaline material given here with inventories of SO_2 and NO_x ($NO + NO_2$) by *Placet and Streets* [1987] gives the rough approximation that alkaline emission rates are only slightly less than the $SO_2 + NO_x$ emissions in the western United States but that they are much smaller than $SO_2 + NO_x$ in the eastern United States.

Fig. 9.3. $Ca/(NO_3 + SO_4)$ for wet deposition (%). Ca, NO_3, and SO_4 were expressed in equivalents. Data are from the NADP for July 5, 1978, to February 4, 1986.

9.2. ARCTIC GAS AND AEROSOL SAMPLING PROGRAM : LIDAR DETECTION OF LEADS IN ARCTIC SEA ICE

R. C. SCHNELL

9.2.1. INTRODUCTION

Downward-viewing lidar data that were collected in the Arctic winter by M.P. McCormick (NASA, Langley, personal communication, January 1984) were analyzed by AGASP scientists for the presence of haze layers. In some of the data, smoke-like plumes appeared to rise from open leads in the ice surface to heights in excess of 4 km. A second airborne lidar was used in the Arctic on the AGASP II mission, March-April 1986, to obtain additional information on these buoyant plumes. The overall results are presented here.

9.2.2. HYDROMETEOR PLUMES FROM OPEN LEADS

A hydrometeor plume rising from an open lead, and a plume streamer from another lead are shown in Figure 9.4; data are from the lidar flown on the NASA Electra, at about 83°-87°N, 70°W, on January 27, 1984. The rising plume (left side of figure) has an ice source, about 300 km north of Ellesmere Island, and reaches nearly 4 km altitude. The streamer to the south comes from a wide lead off Ellesmere Island, which is off the figure, but was observed on the return flight. This streamer extended downwind (northward) for about 250 km. The layer of aerosol observed at 3 km (1637 to 1650+ UTC) is Arctic haze air pollution.

In April 1986, as part of AGASP [*Schnell*, 1988], a research aircraft operated by the Cloud and Aerosol Research Group of the University of Washington, equipped with cloud physics instrumentation and a 1.06-µm downward-pointing lidar [*Radke et al.*, 1989], obtained cloud microphysical data over open leads in the Arctic. The lead-induced plumes were clearly associated with open-water regions.

The lidar system was also able to identify newly frozen leads. A flight made on April 18, 1986, off Baffin Island, Canada (Figure 9.5), shows both refrozen leads and a hydrometeor plume from an open lead. These lidar data were processed in a backscatter ratio color spectrum designed to highlight ice features. In Figure 9.5 the surface appears as a sharp boundary near the bottom edge; below the surface is a region of colors fading down the backscatter scale. Large areas with multiple leads, and single leads with dimensions greater than the horizontal resolution of the lidar (40 m) lack the gradual color gradient immediately "beneath" the surface. This gradient results from the following: when the laser beam from the lidar strikes the highly reflective snow surface, a strong return pulse saturates the receiver, which takes many nanoseconds to recover, thus producing a false signal below the surface. The less reflective surface of open and thinly covered leads produces no such saturation and thus no false signal. The "below surface" signal should be interpreted as a measure of reflectivity, not of ice thickness. The locations and presence of the open and refrozen leads were confirmed by photography and visual observations.
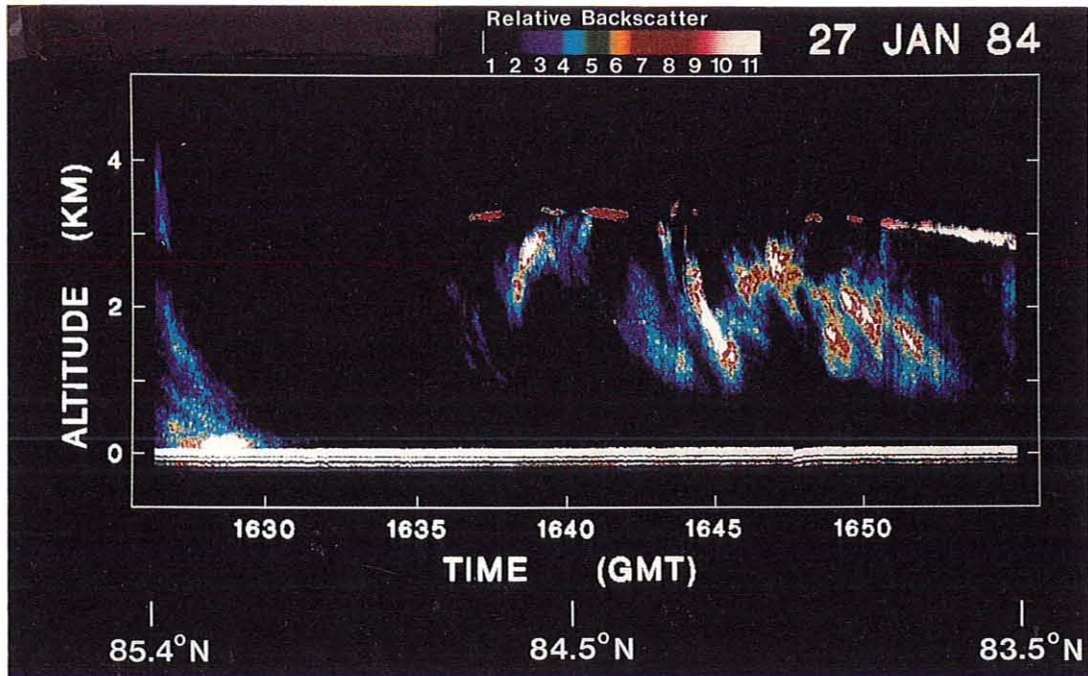
Fig. 9.4. Backscatter signal from a 0.6943-μm downward-viewing lidar flown on the NASA Electra north of Ellesmere Island, N.W.T., January 1984. White indicates maximum backscatter signal, decreasing linearly to black, which is indicative of scattering from gas molecules only. Shown are an apparent rising plume of hydrometeors (left) and a plume of aerosol (center and right) that had a surface origin at a near-shore lead 250 km to the south off of Alert, Ellesmere Island. The aerosol layer at 3 km is thought to be Arctic haze air pollutants.
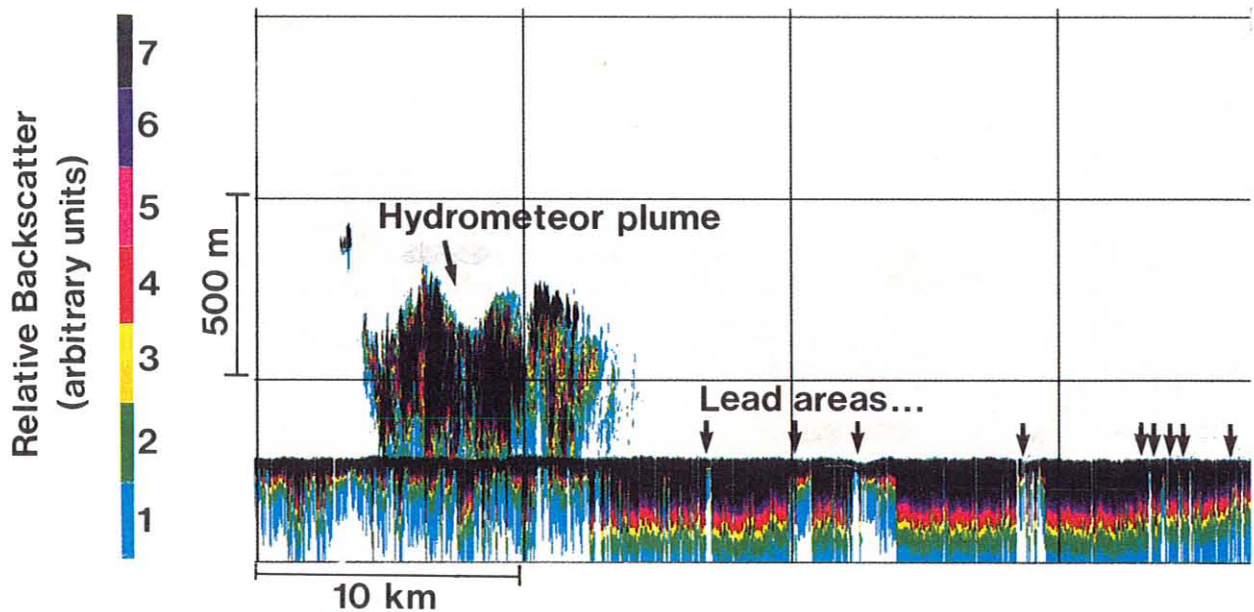

Fig. 9.5. False-color imagery of the relative backscatter signal from the lidar operated on the University of Washington aircraft. Colors indicate backscattering intensity from the lead-produced hydrometer plume and the ice surfaces. The signal is corrected and scaled to eliminate returns from gas molecules and aerosol particles. Lower backscatter beneath the ice surface indicates refrozen leads.

9.2.3. Role of Leads in the Arctic Heat Budget

Leads are of considerable interest to oceanographers and atmospheric scientists. Much of the heat lost from the Arctic in winter is converted into ice in the leads; the resulting salt rejection and brine drainage from the ice helps to maintain the Arctic Ocean halocline and may drive secondary circulations. Leads result from ice deformation, primarily under wind forcing, and have typical widths of 10-100 m. Analyses of aircraft photographs, LANDSAT imagery, and submarine sonar data on under-ice draft show that the size distribution of leads in Arctic sea ice follows a negative power law such that along a 100-km track one could expect to encounter 30 leads that are 50 m wide but only 3 that are 500 m wide. During winter in the absence of ice deformation or movement of frazil ice by the wind, leads rapidly refreeze, forming new ice within a few hours [*Badgley*, 1966]. Although areas of open water and of new ice represent only a few percent of the ice-covered Arctic Ocean in winter, they have a major role in turbulent heat transfer to the atmosphere [*Maykut*, 1982]. Refrozen leads with ice 0.2-0.8 m thick may account for more than half of the turbulent energy transfer from the ocean to the atmosphere in winter in the central Arctic [*Badgley*, 1966].

Previous field measurements [*Andreas* et al., 1981] of the turbulent scalar fluxes over leads suggest that the heat and moisture transferred to the atmosphere remain within the atmospheric boundary layer because of the strong low-level temperature inversion that dominates the lower Arctic troposphere in winter. Our observations show, however, that highly energetic plumes can penetrate to an altitude of at least 4 km.

The upper-air sounding from Alert, Ellesmere Island, for 1200 UTC January 27, 1984, 5 hours before the observations in Figure 9.4, shows an inversion of 8°C between the surface and 850 mb with an equivalent potential temperature (θ_e) at 4 km of 0°C. Since θ_e is conservative for adiabatic processes, to penetrate the inversion and reach 4 km, a plume originating at the surface must be warmed and moistened there to a θ_e of 0°C.

From the data, a CRREL scientist has calculated that the leads having plumes rising to 4 km must be roughly 10 km wide in order to warm and moisten the air flowing over it to a θ_e of 0°C. Realistically, however, this is the narrowest lead that could produce a plume that reaches 4 km for conditions in the Alert sounding. A plume will not rise adiabatically; through entrainment it will lose heat and moisture to the colder, drier ambient air. Therefore, to reach 4 km, the plume must have a surface θ_e value in excess of 0°C; a more sophisticated plume model, however, is necessary to predict how much in excess of 0°C θ_e must be. Although 10 similar major leads, estimated to be 5-10 km wide, are visible on Defense Meteorological Satellite Program infrared (2.7 km resolution) imagery along the flight path for January 27, 1984, only 3 produced plumes; the others had evidently recently refrozen.

9.2.4. Summary and Conclusions

It is not surprising that structures as extensive as these plumes have not been recognized before. They are not necessarily visible to the naked eye. Also, previous research has focused on relatively narrow open-water areas [*Badgley*, 1966]. Further, our data suggest that small leads are unable to warm and moisten the air enough to allow for vertical transport through a strong inversion.

Our observations are significant for three reasons. First, airborne lidar provides a capability for locating narrow leads that are smaller than the resolution of current satellite sensors. Recently refrozen leads are as easily detectable by lidar as the plumes from open leads. This capability is important for operational forecasting and for fuller understanding of ice dynamics. Second, the current view that turbulent fluxes from leads and polynyas affect only the boundary layer needs modifying. If heat and moisture from leads can regularly reach the midtroposphere, the role of the Arctic as a global heat sink may need reevaluating and climate models will require more realistic parameterizations of surface-atmosphere fluxes. Third, our results suggest that lead plumes may affect the radiation budget. Using observed ice crystal spectra, *Curry et al.* [1989] calculated a significant heating effect at the surface, due to the downward infrared radiation from the ice crystals. Thus, plumes will affect the radiation budget in their immediate vicinity and in large areas downwind.

9.2.5. Future Research

Airborne and satelliteborne lidar provide the potential for determining the impact of leads on the energy and moisture fluxes from the polar ocean to the atmosphere. Further research will focus on developing a climatology of lead occurrence and of plume frequency and distribution in the Arctic from lidar profiles and satellite data, identifying the phase of the plume moisture with lidar polarization measurements, and developing parameterizations to relate lidar backscatter to plume moisture content.

9.3. References

Andreas, E.L., R.M. Williams, and C.A., Paulson, Observations of condensate profiles over Arctic leads with a hot-film anemometer, *Q. J. R. Meteorol. Soc., 107*, 437-460, 1981.

Badgley, F.I., Heat budget at the surface of the Arctic Ocean, *Proceedings, Symposium on the Arctic Heat Budget and Atmospheric Circulation*, January 31-February 4, 1966, Lake Arrowhead, California, edited by J.O. Fletcher, pp. 267-277, Rand Corporation, Santa Monica, CA, (NTIS: PB-182 433), 1966.

Bodhaine, B.A., and R.M. Rosson (Eds.), *Geophysical Monitoring for Climatic Change, No. 16: Summary Report 1987*, 110 pp., NOAA Environmental Research Laboratories, Boulder, CO, 1988.

Boerngen, J.G., and H. T. Shacklette, Chemical analyses of soils and other surficial materials of the conterminous United States, *Open File Report 81-197*, 139 pp., U.S. Geological Survey, Denver, CO, 1981.

Curry, J.A., F.G. Meyer, L.F. Radke, C.A. Brock, and E.E. Ebert, Occurrence and characteristics of lower troposphere ice crystals in the Arctic, *Symposium on the Role of Clouds in Air Chemistry and Global Climate*, pp. 114-117, American Meteorological Society, Boston, 1989.

D'Almeida, G., A model for Saharan dust production, *J. Climate Appl. Meteorol., 25*, 903-916, 1986.

Evans, J.S., and D.W. Cooper, An inventory of particulate emissions from open sources, *J. Air Pollut. Control Assoc., 30*, 1298-1303, 1980.

Gatz, D.F., G.J. Stensland, M.V. Miller, and L.C. Chu, Alkaline aerosols: An initial investigation of their role in determining precipitation acidity, Final Report to NSF Grant ATM 77-24294, *Report No. 343*, 78 pp., Illinois State Water Survey, Champaign, IL, 1984.

Gatz, D.F., M.V. Miller, G.J. Stensland, and L.C. Chu, Evidence of element fractionation in fine particle size classes of highly erodible soils, *Proceedings of the Specialty Conference on Particulate Matter Fugitive Dusts: Measurement and Control in Western Arid Regions*, Tucson, Arizona, October 1986, *SWS Reprint 820*, pp. 39-51, Air Pollution Control Association, Tucson, 1986.

Gillette, D., and P. Sinclair, Estimation of suspension of alkaline material dust devils in the United States, *Atmos. Environ.*, submitted, 1990.

Gillette, D., G. Stensland, A. Williams, W. Barnard, D. Gatz, P. Sinclair, and T. Johnson, Emissions of alkaline elements, calcium, magnesium, potassium, and sodium from open sources in the contiguous United States, *Global Biochem. Cycles*, submitted, 1990.

Maykut, G.A., Large scale heat exchange and ice production in the central Arctic, *J. Geophys. Res., 87* (C10), 7971-7984, 1982.

Placet, M., and D.G. Streets, First interim assessment, National Acid Precipitation Assessment Program , Washington, DC, 1987.

Radke, L.F, C.A. Brock, J.H. Lyons, P.V. Hobbs, and R.C. Schnell, Aerosol and lidar measurements of hazes in midlatitude and polar air masses, *J. Atmos. Chem., 9*, in press, 1989.

Schnell, R.C., Arctic air chemistry, *Arctic Res., 2*, 39-41, 1988.

Sinclair, P.C., General characteristics of dust devils, *J. Appl. Meteorol., 8*, 32-45, 1969.

Sinclair, P.C., Vertical transport of desert particulates by dust devils and clear thermals, *Proceedings, Atmosphere-Surface Exchange of Particulates and Gaseous Pollutants, Energy Research and Development Center Series 38*, 497-527, Richland, Washington, 1975.

Sinclair, P.C., Dust devil dust transport features, *J. Appl. Meteorol.*, submitted, 1990.

Snow D.J.T., and T.M. McClelland, Dust devils at White Sands Missile Range, New Mexico, U.S.A. *J. Meteorol., 13*, 157-164, 1988.

Young J.R., E. Ellis, and G.M. Hidy, Deposition of airborne acidifiers in the western environment, *J. Environ. Qual., 17*, 1-28, 1988.

10. Cooperative Programs

Precipitation Chemistry

R. S. ARTZ

NOAA, Air Resources Laboratory, Silver Spring, Maryland 20910

1. INTRODUCTION

Precipitation chemistry measurement programs continued at the 4 GMCC stations and at the 14 regional stations. Several changes were instituted to reduce costs and to improve quality control. A cooperative project, instituted through the University of Virginia, continued with little change.

2. BASELINE MEASUREMENTS

Bimonthly chemistry measurements of snow samples continued normally at both BRW and SPO. At SMO collection of daily samples from the Aerochem Metrics sampler resumed and replaced funnel and bottle measurements at the conclusion of the drought.

Sampling on the Island of Hawaii continued at Hilo, 22 Mile Site, and at MLO. Suspected contamination from the funnel and bottle collectors was linked to the plastic tubing connecting several sections of the collector. Dry deposition is therefore no longer suspected as the primary cause of low pH values recorded at these stations. Preliminary results of a comparison between MLO funnel and bottle, and University of Virginia Aerochem Metrics measurements suggests that $SO_4^=$ measurements are of very high quality but that pH values are suspect.

NO_3^- and Cl^- measurements are also considered to be of high quality; however, the introduction of new Dionex columns should lower detection limits.

3. NADP REGIONAL AND BASELINE MEASUREMENTS

NADP measurements continued normally at MLO, SMO, and 12 regional stations. As a result of a statistical intercomparison conducted for stations in Maine and Texas last year, the Presque Isle, Maine, and Victoria, Texas, stations were closed. A similar study is planned for FY 1989 for two stations in Mississippi; one station will be closed at the termination of this project. A third station at Salem, Illinois, was closed in December 1988 when the NWS abandoned the site; a replacement station has been proposed for a nearby location.

4. MLO AND SMO 1980-1988 CHEMISTRY DATA

Precipitation chemistry data from MLO and SMO are presented in Figures 1-4 for the period from May 1980 through 1988. In Figures 1a and 1b, note that (unlike for regional sites) NO_3^- is proportionally very small relative to $SO_4^=$. Also note that $SO_4^=$ and H^+ (Figures 1a and 1b) track very closely, indicating that precipitation at both stations is primarily a very
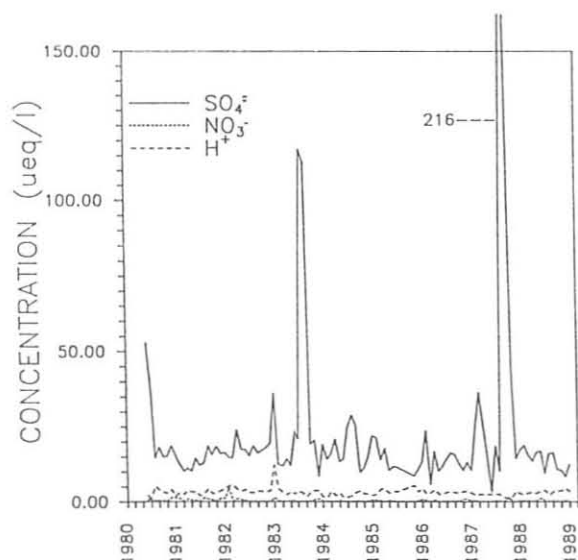

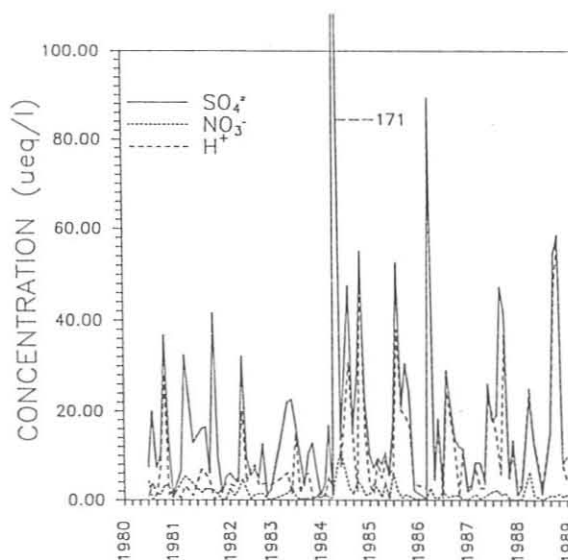Fig. 1a. Monthly volume-weighted $SO_4^=$, NO_3^-, and H^+ mean concentrations for MLO, 1980-1988.

Fig. 1b. Monthly volume-weighted $SO_4^=$, NO_3^-, and H^+ mean concentrations for SMO, 1980-1988.
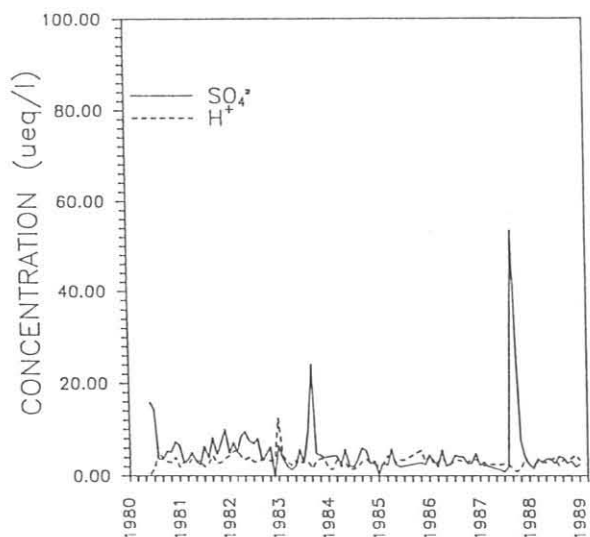
Fig. 2. Monthly volume-weighted non-seasalt $SO_4^=$ mean concentrations and H^+ mean concentrations for SMO, 1980-1988.

dilute solution of sulfuric acid. Figure 2 shows that monthly weighted non-seasalt $SO_4^=$ and H^+ means concentrations for SMO during 1980-1988 do not track as consistently as those in Figure 1. Figures 3a and 3b indicate that although seawater is the predominant source of material to SMO rain, other factors, probably volcanic and typically small relative to regional stations, affect MLO precipitation. Figures 4a and 4b indicate that most cases with high ion concentrations (Figures 1a and 1b) can be quickly correlated with low amounts of precipitation.
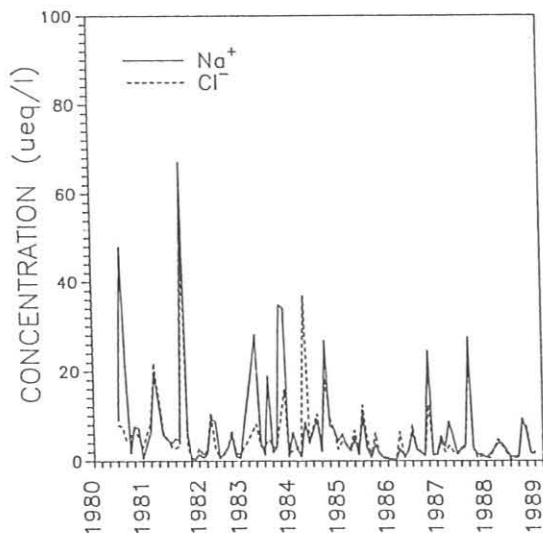

Fig. 3a. Monthly volume-weighted Na^+ and Cl^- mean concentrations for MLO.
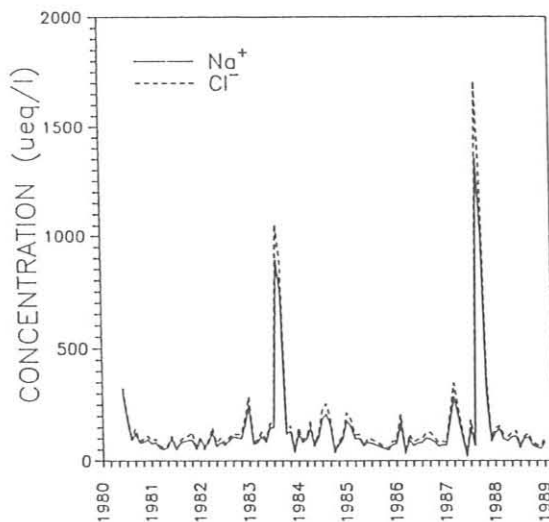

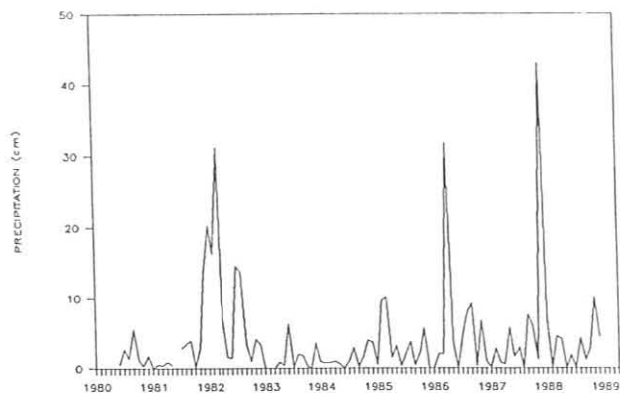Fig. 3b. Monthly volume-weighted Na^+ and Cl^- mean concentrations for SMO.

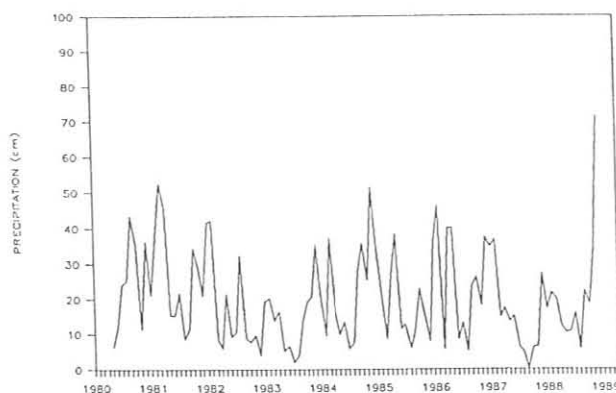Fig. 4a. Monthly precipitation for MLO, 1980-1988.

Fig. 4b. Monthly precipitation for SMO, 1980-1988.

The Mauna Loa Aerosol Backscatter Intercomparison Experiment (MABIE)

DAVID A. BOWDLE

University of Alabama in Huntsville, Johnson Research Center, Huntsville, Alabama 35899

MADISON J. POST AND R. MICHAEL HARDESTY

NOAA, Wave Propagation Laboratory, Boulder, Colorado 80303

ANTONY D. CLARKE

University of Hawaii, Hawaii Institute of Geophysics, Honolulu 96822

EDWARD M. PATTERSON

Georgia Institute of Technology, School of Geophysical Science, Atlanta, Georgia 30332

1. INTRODUCTION

The Fall 1988 MABIE-FALL was conducted at MLO November 14-December 12, 1988. MABIE-FALL involved intercomparisons of direct measurements of aerosol optical properties at visible and mid-infrared wavelengths, and Mie theory estimates of these properties derived from collocated measurements of aerosol physicochemical properties.

MABIE results are being used in the development of a global-scale model of aerosol backscatter properties for NASA's GLOBE [*Bowdle*, 1986]. GLOBE model results, in turn, are being used in the design of NASA's LAWS [*Curran*, 1987]. LAWS is intended to provide three-dimensional fields of horizontal vector winds on a global scale in the troposphere and lower stratosphere beginning in the late 1990s. LAWS measurement accuracy will be critically dependent on the typical magnitudes and variability of atmospheric aerosol backscatter coefficients at the LAWS operating wavelength [*Huffaker et al.*, 1984]. However, these aerosol parameters are currently not well characterized on a global scale, particularly in the middle and upper troposphere over the remote tropical oceans, where new wind measurements from LAWS are needed most.

MABIE-FALL is one of several GLOBE field programs designed to provide the necessary aerosol information in these data-sparse regions. MABIE-FALL operations were the most recent in a series of seasonally distributed MABIE programs (MABIE-SUMMER in 1986 [*Bowdle et al.*, 1987], MABIE-WINTER in 1988 [*Clarke*, 1988], MABIE-FALL-II in 1989, and MABIE-SPRING in 1990). MABIE-FALL was designed to (1) provide timely inputs on Pacific free-tropospheric aerosol properties to the incipient LAWS design effort, (2) evaluate instrumentation, sampling protocols, and analytical procedures for the Fall 1989 GLOBE Pacific Backscatter survey flight, (3) develop an internally consistent backscatter measurement and modeling data set, and (4) empirically link the MLO aerosol climatology to the GLOBE CO_2 backscatter climatologies. The instrumentation, experiment design, and some preliminary results for MABIE-FALL are described here.

2. INSTRUMENTATION

MABIE investigators provided three primary aerosol sensors. A trailer-mounted, hemispherically scanned, pulsed CO_2 Doppler lidar [*Post et al.*, 1989] was located north-northeast of MLO beside the MLO access road at 3.23 km altitude, with a 3.0 km clear-line-of-sight slant range to the MLO site at 3.4 km altitude. This lidar provided range-resolved measurements of radial wind velocity or of aerosol backscatter coefficient at 9.25 or 10.59 μm wavelength, every 300 m along the lidar line of sight. A modified high-resolution LOPC [LAS-X, Particle Measuring Systems, Boulder, Colorado] and CNC [Model 3760, ThermoSystems, Inc., Minneapolis, Minnesota], with computer-controlled sample preheating [*Clarke*, 1988], were located in a small shed ~50 m west of the main MLO instrument building. These instruments drew from a PVC sample stack with inside diameter of 10 cm and with sample inlet 8 m above ground (6.5 m above the roof of the shed). The LOPC provided size-segregated aerosol composition data, from direct measurements of aerosol size distributions as a function of preheater temperature, and an a priori knowledge of the volatility characteristics of typical MLO aerosols. A high-volume filter/impactor sampler in the shed drew out of the same sample stack. This unit provided bulk aerosol samples for conventional chemical analysis, and discrete particle samples for morphological and elemental analysis in an electron microscope.

Also available during MABIE were real-time outputs and daily summaries from the standard MLO multiwavelength integrating nephelometer, CNC, and surface meteorological observations [*Bodhaine and Rosson*, 1988]. These products were used to evaluate ongoing experimental operations and to provide supporting data for the aerosol measurement and modeling intercomparisons. Rawinsonde soundings for Hilo, Hawaii, ~50 km northeast of MLO, were obtained from the Hilo NWS office. Local and regional weather forecasts and hard-copy satellite imagery were obtained from the Honolulu NWS. Digital satellite imagery was collected during MABIE on the NASA Marshall Space Flight Center McIDAS. Isobaric and isentropic back trajectories from MLO were provided by

NOAA/GMCC. These local and regional meteorological data were used for long-range operational planning or for post-experiment analysis of air mass source conditions.

3. EXPERIMENT

MLO was selected for the operational site to allow for sampling of undisturbed, marine, free-tropospheric aerosols for extended periods, without the problems of airborne operation, and to take advantage of the long-term MLO aerosol climatology [*Bodhaine and Rosson*, 1988]. The well-known nocturnal downslope flow at MLO [*Bodhaine*, 1983] facilitates such sampling for aspirated sensors. The high altitude of the site improves the CO_2 lidar sensitivity in the middle and upper troposphere by reducing range-squared losses and water vapor absorption losses. Late fall was chosen for the operational period, to extend the seasonal coverage of the overall MABIE program, to increase the chances of encountering shallow marine boundary layers and very low free-tropospheric aerosol concentrations, and to provide timely input to the GLOBE/LAWS studies.

MABIE operations concentrated on intercomparisons of measured and modeled aerosol optical properties in nocturnal downslope flow conditions. Routine intercomparison studies involving the core MABIE instruments were normally scheduled every second night, weather permitting, from ~0600 to 1800 UTC. During typical intercomparisons, the LOPC and the filter/impactor sampled continuously for 1-3 hours, while the CO_2 lidar was pointed several meters above the MABIE sample stack and pulsed at 2 Hz. Considerable care was taken to ensure the validity of the intercomparisons. First, return signals from the well-collimated beam of the scanning CO_2 lidar were used in conjunction with a bore-sighted telescope to map out "ground clutter," such as terrain, buildings, towers, and guy wires, in the vicinity of the MABIE and MLO sample stacks. Scrupulous care was taken to avoid these easily identifiable obstacles in subsequent lidar sampling. Second, the lidar was used in a scanning mode to verify the uniformity of the aerosol population in the immediate vicinity of the MABIE sample stack, and also between the MABIE stack and the main MLO sample stack. Finally, intercomparison runs were terminated if cloud or fog developed in the vicinity, or if other meteorological, trace gas, or aerosol indicators began to vary rapidly.

Several other types of experiments were also performed during MABIE. The LOPC frequently operated continuously in an autonomous 3-h batch sampling mode for extended periods. The CO_2 lidar obtained vertical, off-zenith, and low-angle backscatter profiles; off-zenith cirrus backscatter time series; high-resolution wind profiles in upslope, downslope, and transitional flow conditions; and intercomparison runs with the MLO ruby lidar and with various satellite-based aerosol sensors.

4. RESULTS

Initial processing has been completed on most of the MABIE data. Three types of preliminary results are discussed here: (1) CO_2 backscatter statistics, (2) comparisons between measured and modeled aerosol optical properties, and (3) a 4-day dust plume event.

More than 250 vertical profiles of aerosol backscatter coefficients at 10.6-μm or 9.25 μm wavelength were obtained during MABIE. Comparisons of vertical and off-vertical profiles generally gave internally consistent results. Composites of sequential sets of vertical, off-vertical, and low-angle profiles generally showed (1) backscatter values of ~3-5 $\times$ 10^{-11} m^{-1} sr^{-1} near the 3.4-km MLO altitude, (2) steadily smaller values above MLO until about 6-km altitude, (3) fairly uniform values at ~1 $\times$ 10^{-11} m^{-1} sr^{-1} above 6 km, (4) slightly higher clear-air backscatter values above 10 km (these data should be interpreted cautiously, since they were near the lidar sensitivity limit for the longer ranges), and (5) more frequent visible and subvisible cirrus above 10 km. Minimal wavelength dependence was observed between backscatter values at 9.25- and 10.6-μm wavelength.

Under well-established downslope flow conditions, aerosol measurements at MLO should be representative of conditions near the Mauna Loa summit at ~4.5-km altitude. At this altitude, typical aerosol backscatter coefficients at 10.6-μm wavelength were ~2-4 $\times$ 10^{-11} m^{-1} sr^{-1}. Backscatter computations using Mie scattering theory with typical downslope LOPC data from MABIE generally give values about a factor of 2-3 higher than the direct measurements. Under these same conditions, typical nephelometer measurements gave aerosol scattering coefficients of ~2-4 $\times$ 10^{-7} m^{-1} at 0.55-μm wavelength. The resultant conversion factor of ~1 $\times$ 10^{-4} sr^{-1} is generally consistent with theoretical predictions from aerosol data in other remote regions. Refinements of these generally encouraging, but not conclusive, results should be available from the complete results of the lidar and stack intercomparisons.

An unusual aerosol plume was detected by the CO_2 lidar at ~2200 UTC November 30 and unambiguously detected by the MABIE and MLO surface samplers in downslope flow conditions at ~1200 UTC on December 2. All traces of the plume disappeared by ~0400 UTC December 4. During this event, lidar data showed spatially and temporally coherent backscatter enhancements up to at least 6-km and possibly 8-km altitude for several days (Figure 1). Filter samples showed a dust-like coloration. LOPC data showed a refractory component (at 300°C) in the size distribution between 5- and 10-μm diameter. Integrating nephelometer data showed minimal wavelength dependence in the aerosol scattering coefficient. Visual observations in all quadrants showed a dense whitish haze that filled the valley below MLO and extended well above MLO. Hilo rawinsonde profiles showed a deep dry layer encompassing the plume altitudes. Isobaric back trajectories at 700 and 500 mb showed 10-day origins near eastern China. Isentropic back trajectories terminating near 700 and 500 mb showed similar origins. Surface observations in the China desert showed a major event of blowing dust approximately 10 days before the plume was detected at MLO. Pulsed lidar observations in Japan showed a significant backscatter enhancement at about the time the China dust plume should have crossed Japan. These observations, taken together, point to an event of long-distance transport of super-micrometer-sized
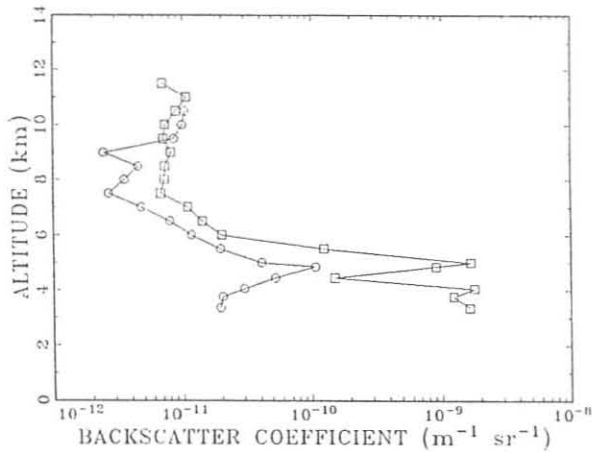
Fig. 1. Vertical profiles of aerosol backscatter at 10.6 μm wavelength obtained with a pulsed CO_2 Doppler lidar at MLO at 1506 UTC, December 2, 1988, during an event of long-distance mineral dust transport (squares) and at 0420 UTC, December 4, 1988, after the dust event (circles).

mineral dust particles from the China desert to the central-Pacific. Similar events in this region have been well documented, especially during the northern hemisphere spring. The MABIE event is remarkable, since it is the first such event in the central Pacific region to be investigated with a pulsed lidar, and since it documents the presence of mineral dust at altitudes well above 6 km, even after several days and several thousand kilometers of transport over the Pacific Ocean.

REFERENCES

Bodhaine, B.A., Aerosol measurements at four background sites, *J. Geophys. Res., 88*, 10753- 10768, 1983.

Bodhaine, B.A., and R.M. Rosson (Eds.), *Geophysical Monitoring for Climatic Change, No. 16: Summary Report 1987*, pp. 3-29, NOAA Environmental Research Laboratories, Boulder, CO, 1988.

Bowdle, D.A., A global-scale model of aerosol backscatter at CO_2 wavelengths for satellite-based lidar sensors, in *Preprint Volume, Second Conference on Satellite Meteorology/Remote Sensing and Applications*, May 13-16, 1986, Williamsburg, VA, pp. 303-306, American Meteorological Society, Boston, MA, 1986.

Bowdle, D.A., W.D. Jones, A.D. Clarke, S.A. Johnson, and D.E. Fitzjarrald, Mauna Loa Aerosol Backscatter Intercomparison Experiment (MABIE), in *Geophysical Monitoring for Climatic Change, No. 15: Summary Report 1986*, edited by R.C. Schnell and R.M. Rosson, pp. 137-139, NOAA Environmental Research Laboratories, Boulder, CO, 1987.

Clarke, A.D., Some characteristics of aerosol size distributions at MLO, in *Geophysical Monitoring for Climatic Change, No. 16: Summary Report 1987*, edited by B.A. Bodhaine and R.M. Rosson, pp. 87-89, NOAA Environmental Research Laboratories, Boulder, CO, 1988.

Curran, R.J. (Ed.), *Laws: Laser Atmospheric Wind Sounder, Earth Observing System Instrument Panel Report, Volume IIg*, 55 pp., National Aeronautics and Space Administration, Washington, DC, 1987.

Huffaker, R.M., T.R. Lawrence, M.J. Post, J.T. Priestley, F.F. Hall, Jr., R.A. Richter, and R.J. Keeler, Feasibility studies for a global wind measuring satellite system (Windsat): Analysis of simulated performance, *Appl. Opt., 23*, 2523-2536, 1984.

Post, M.J., R.E. Cupp, and R.M. Hardesty, NOAA's pulsed Doppler lidar: Performance characteristics, *Appl. Opt.*, accepted, 1989.

Fine Particulate Matter at Mauna Loa Observatory March 1988 to February 1989

T. A. CAHILL, L. K. WILKINSON, P. BEVEREDGE, AND T. TANADA

University of California, Davis , Crocker Nuclear Laboratory, Air Quality Group, Davis, California 95616

On March 2, 1988, the U.S. remote-area fine particulate network IMPROVE [*Eldred et al.*, 1989] initiated routine monitoring of fine (D_p < 2.5 µm) particulate matter at MLO. The IMPROVE protocols allow for a complete resolution of fine mass into its components for the purpose of predicting the effects of aerosols on the scattering and absorption of light, and the implications for visibility and the atmospheric radiation balance. Another IMPROVE station was initiated at about the same time at Hawaii Volcanoes National Park.

The protocols for MLO call for a continuous sample of approximately 3 days duration and a clean-air (downslope only) sample over the same 3-day period keyed by the Maryland System (W. Zoller et al., personal communication). Size segregation is accomplished through a nominally 2.5-µm cyclone (modified by altitude), and samples are collected on 25-mm stretched Teflon filters. Samples are mailed weekly to Davis, where analyses are done for (1) mass (gravimetric); (2) elemental content, Na to U (PIXE); (3) (PESA); and (4) H, Be, B, C, N, O, and Na (FAST) [*Cahill et al.*, 1984]. Data are provided in quarterly summaries, but neither all the analyses nor the MLO data protocols were completed at the time of this writing. Some results are presented here.

Figure 1 shows fine particulate mass from March 1988 to February 1989 for MLO1 (the continuous or average sample) and MLO2 (the downslope only). The two mass components were only weakly correlated (Figure 2). Fine mass is dominated by soil dust in April and May, and by sulfur (sulfates?) during much of the rest of the year (Figures 3 and 4).

Oceanic influences are easily seen by the presence of Cl with Na, but in the past 9 months only a few days showed oceanic
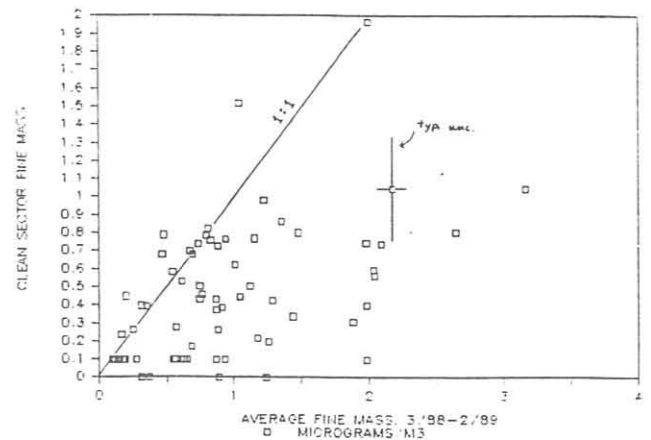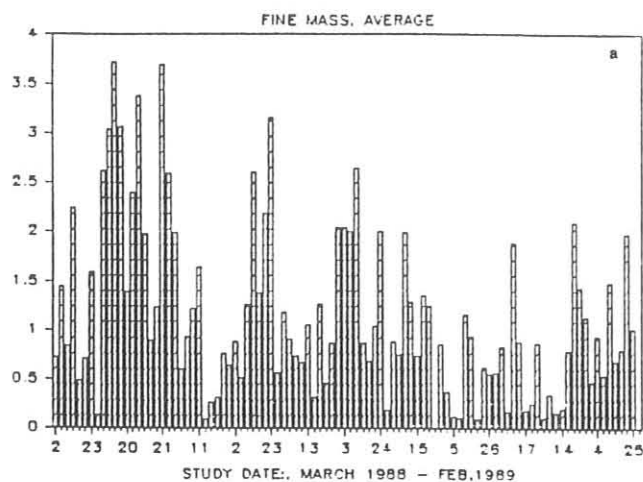
Fig. 2. Correlation between the two fine particulate masses (µg m⁻³) March 1988-February 1989 of the clear sector (MLO2) versus the average (MLO1). The typical uncertainty is shown.

influence in the average samples, and none for the clean-air samples. These data generally confirm and extend our earlier work [*Wang et al.*, 1982; *Cahill and Braaten*, 1983; *Braaten and Cahill*, 1986], although the spring S levels are higher than in earlier years. Full resolution of mass into elemental components will be attempted when the very-light-element analyses are completed.

In May and early June 1988, a detailed study was made of aerosols from the eruption of Kilauea at sites near the surface outbreak of lava very near the coast (VENT) and in the (now
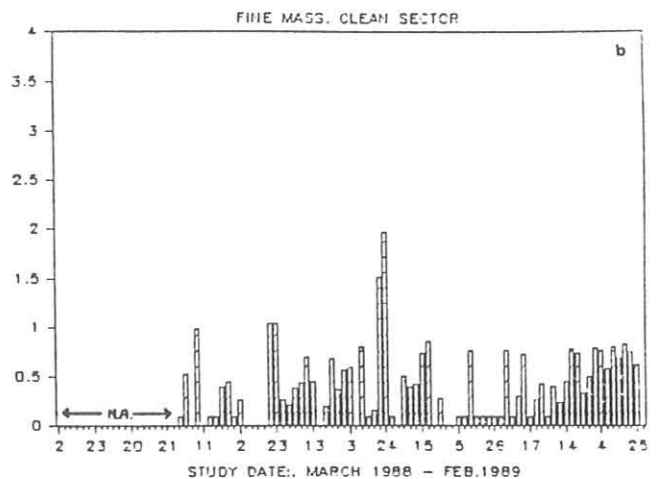
Fig. 1. Fine particulate mass (µg m⁻³) for (a) MLO1 (the continuous or average samples) and (b) MLO2 (the downslope only or clean samples), March 1983-February 1989.
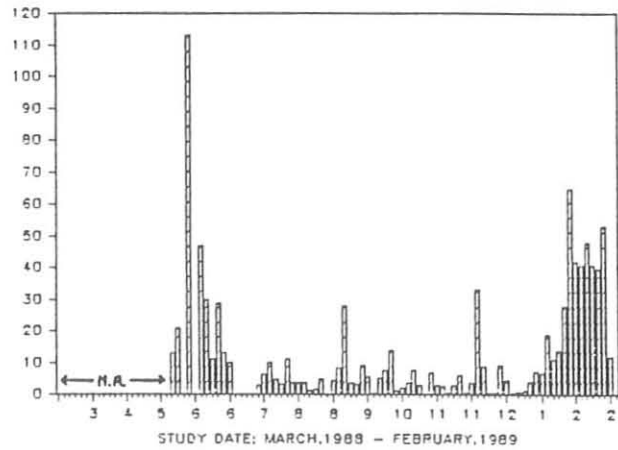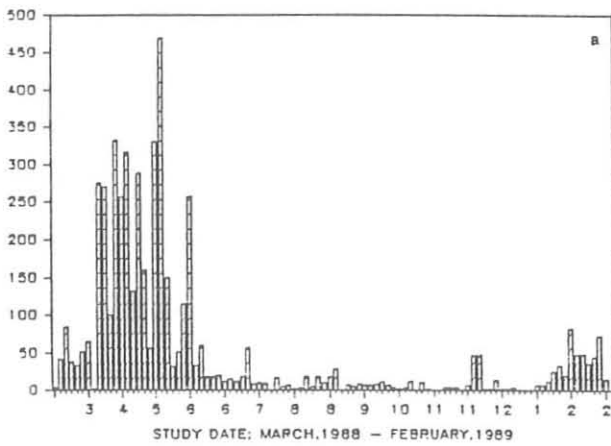
Fig. 3. Concentration (ng m⁻³) of silicon (soil dust) in the fine mass for the (*a*) average samples and the (*b*) clean samples, March 1988-February 1989.

Fig. 4. Concentration (μg m⁻³) of sulfur in the fine mass for the (*a*) average samples and the (*b*) clean samples, March 1988-February 1989.

Fig. 5. Concentration (ng m⁻³) of fine mass by site and date, May 4-June 16, 1988.

Fig. 6. Concentration (ng m⁻³) of fine particulate sulfur by site and date, May 4-June 16, 1988.

83

TABLE 1. Aerosol Composition (ng m^{-3}), Hawaii, May 1988

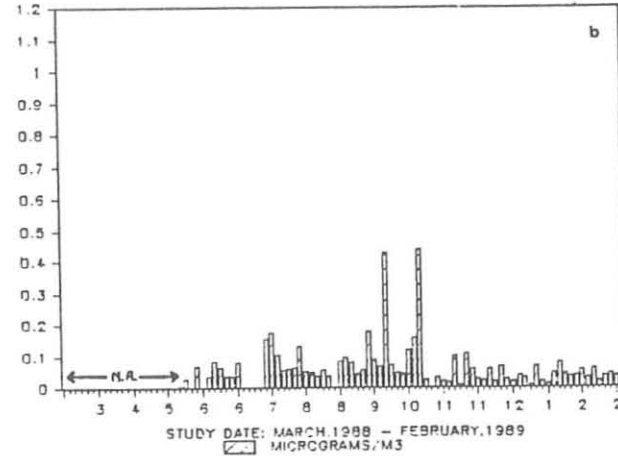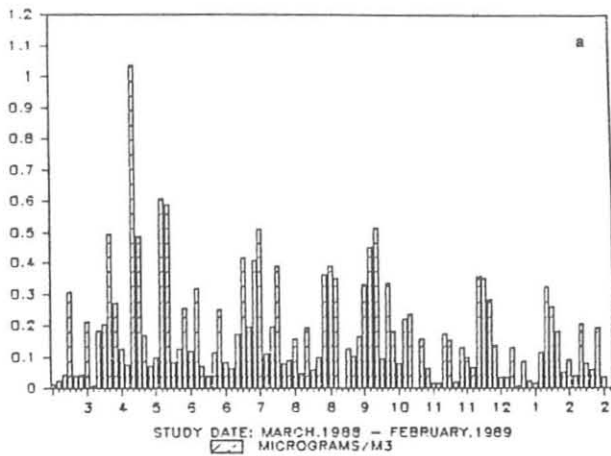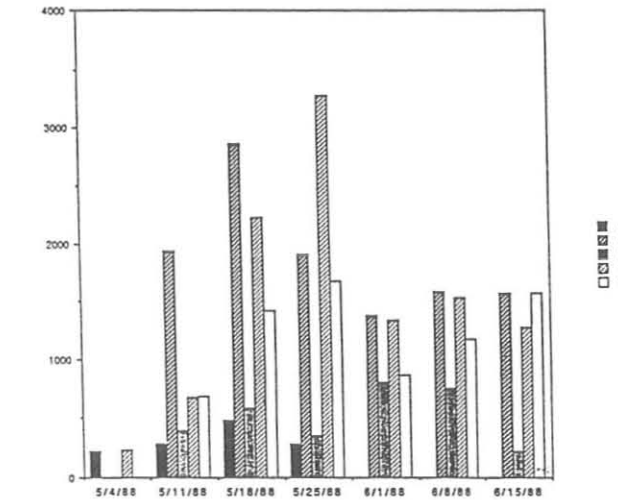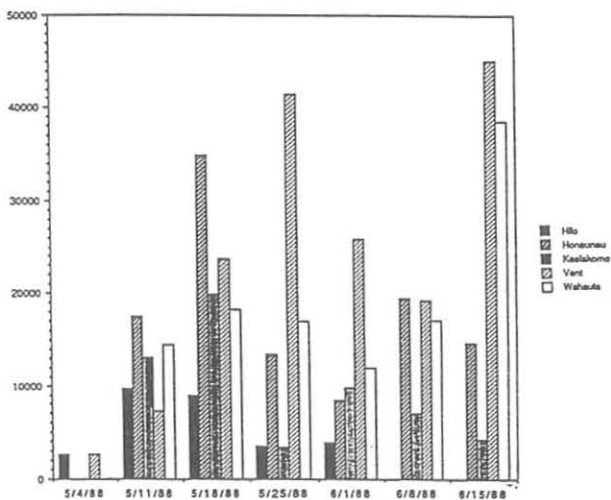| Location	Oceanic			Oceanic, Smoke, & Soil	Soil							Volcanic, Anthro.	Trace Elements						
	Na	Cl	Mg	K	Al	Si	Ca	Ti	Mn	Fe	Sr	S	V	Ni	Zn	Br	Se	Hg	Pb[†]
Upwind																			
Hilo (east coast)	86	196	24	32	51	109	29	4	1.8	31	*	317	7.1	3.4	1.8	2.0	0.4	<0.1	3.8
Near-Source																			
End, Lava Tube, at ocean	5660	6420	970	266	26	120	122	3	6.1	38	2.3	1507	3.6	3.8	9.4	6.6	2.4	3.2	8.3
Wahaula (about 1 km)[‡]	2020	2840	420	133	52	111	60	6	5.9	24	4.3	1234	6.5	2.8	7.5	3.7	3.0	2.4	*
Kealakomo (about 5 km)	69	238	45	30	109	127	18	19	2.6	28	*	521	5.5	4.0	2.8	1.9	6.3	4.9	7.9
Downwind																			
Hawaii Volcanoes National Park	*	*	*	37	26	70	33	2.5	*	23	*	631	*	*	1.8	1.7	4.4		3.9
Honaunau (Kona Coast)	66	*	9	38	32	76	16	*	1.4	11	0.5	1872	1.2	1.0	1.0	1.9	0.9	0.9	5.3
MLO	*	*	*	40	78	227	84	5	0.9	52	*	438	<0.2	≤0.05	0.4	0.3	≤0.2	*	0.4
U.S. Comparison Site (May 1988)																			
Crater Lake National Park	*	*	*	27	55	99	24	3	*	32	*	104	*	*	1.9	1.7	0.5	*	1.7
Shenandoah National Park	*	*	*	43	90	171	36	4	*	47	*	1805	*	*	8.3	3.3	1.1	*	6.2

*Not enough data to form an average.

[†]At levels below 2 ng m^3, Pb and As are not always distinguishable; if As, divide Pb by 3.

[‡]Destroyed by lava, spring 1989.

burned) Wahaula Visitor Center, at a site down the coast a few miles (Kealakomo), at Hilo, and at Honaunau on the Kona Coast [*Tanada et al.*, 1988; *Gill et al.*, 1989]. Figures 5 and 6 show the results of sampling between May 4, 1988, and June 1, 1988, for fine mass and S, and Table 1 shows mean elemental concentration at all sites. Surprisingly, but in conformance with qualitative local observations, fine particulate S often reached its highest levels on the Kona Coast (Figure 6). This might possibly be explained by the time delay between SO_2 emission at the cone and lava tubes and conversion into sulfates in the presence of sunlight and water. Lack of ammonia might favor an H_2SO_4 acidic aerosol. There is a large pool of fine sulfate aerosols ringing the MLO that may account for some of the S values on upslope winds.

REFERENCES

Braaten, D.A., and T.A. Cahill, Size and composition of Asian dust transported to Hawaii, *Atmos. Envron., 20*, 1105-1109, 1986.

Cahill, T.A., and D.A. Braaten, Size characteristics of Asian dust sampled at Mauna Loa Observatory, in *Geophysical Monitoring for Climatic Change, No. 11: Summary Report 1982*, edited by J.M. Harris and B.A. Bodhaine, 117-119, NOAA Air Resources Laboratory, Boulder, CO, 1983.

Cahill, T.A., R.A. Eldred, D. Shadoan, P.J. Feeney, B.H. Kusko, and T. Matsuda, Complete elemental analysis of aerosols: PIXE, FAST, LIPM, and mass, *Nucl. Instrum. Methods, B3*, 291-295, 1984.

Eldred, R.A., T.A. Cahill, L.K. Wilkinson, P.J. Feeney, and W. Malm, Particulate characterization at remote sites across the US: First year results of the NPS/IMPROVE Network 89-151.3, *Proc. of Annual Meeting, Air and Waste Management Association*, Anaheim, CA, 89-151.3, 1989.

Gill, T.E., T.N. Tanada, T.A. Cahill, D. Taylor, and H. Matsuura, Air quality on Hawaii island during a Kilauea eruption, *Proc. of Annual Meeting, Air and Waste Management Association*, Anaheim, CA, 89-66A.4, 1989.

Tanada, T.N., T.E. Gill, T.A. Cahill, and K.J. Bowers, The Hawaii '88 aerosol monitoring project, Report to National Park Service and State of Hawaii, Public Health, University of California, Davis, Crocker Nuclear Laboratory, 1988.

Wang, M., T.W. Winchester, T.A. Cahill, and R. Lixin, Chemical elemental composition of wind-blown dust, April 19, 1980, Beijing, *Dexue Tongbao (Science Bulletin), 27*, 1193-1199, 1982.

Artificial Windshielding of Precipitation Gauges in the Arctic

GEORGE P. CLAGETT

Soil Conservation Service, Anchorage, Alaska 99501

1. INTRODUCTION

Precipitation gauges can give a good measure of the water equivalent of snow precipitation, provided the gauge is protected or shielded from wind effects [*Brown and Peck*, 1962]. Unfortunately, there is little that is "standard" to the science of collecting snow precipitation. Gauges located in exposed and windy areas may be totally unshielded, partially shielded by one or more buildings, or equipped with one of several types of artificial shields. The various shielding options in common use, therefore, produce a wide range of gauge catch efficiency. Also, the various studies of artificial shields in the United States and Canada have produced a wide range of results. This must be, in part, due to the wide range of weather conditions under which the various studies have been conducted. A lingering question is whether the results can be appied to the local conditions of Alaska's tundra regions.

2. THE PROBLEM

The gauge catch efficiency for snowfall is known to change with increasing wind speed in exposed areas [*Benson*, 1982; *Goodison*, 1978]. At speeds of 5 m s^{-1} (11 mph), unshielded gauge catches are known to drop to 20-30% of the true amount, and even as low as 6% for an entire winter of abnormally windy conditions [*Clagett*, 1988]. One solution to the exposed gauge problem is to calibrate gauge catch efficiency with wind speeds and then record wind speeds at the gauge height in order to apply the correction. Another solution is to apply the "dual gauge" approach, that is, to use two adjacent gauges, one shielded and the other one unshielded, which provides a relationship with increasing wind speeds to calculate total solid precipitation [*Hamon*, 1973; *Hanson*, 1988]. Both of these solutions best fit individual sites, but are not generally practical for large networks.

Artificial windshielding of the precipitation gauge is yet another option. Three artificial windshields have significant use in North America: (1) The Alter shield is known to increase the snowfall catch of an unshielded gauge by about 30% [*Alter*, 1937; *Warnick*, 1953]. (2) The Nipher shield was developed by the Canadian government in the late 1970s and was subsequently adopted as the Canadian national standard shield for precipitation gauges. It provides a snowfall catch that is not significantly different from the total or "true" snowfall amount [*Goodison et al.*, 1983]. The one-piece Nipher shield also is the most affordable of the various shield options. It costs one-half as much as an Alter shield, is easy to install, and is relatively maintenance free. Its only drawback is that it easily caps over during wind-free storms and may cap over if wind velocity is below 2 m s^{-1}. Therefore, its use is limited to staffed locations. But at most sites, it is the most practical solution to the exposed precipitation gauge problem. (3) The Wyoming shield was developed by the University of Wyoming in the early 1970s [*Rechard and Larson*, 1971]. Several studies found that it provides a snowfall catch that is about 85-95% of the total snowfall [*Benson*, 1982; *Brown and Peck*, 1962; *Goodison*, 1975; *Goodison et al.*, 1983; *Rechard*, 1975]; however, a U.S. Forest Service study found the gauge caught only 48% of that of a "control" gauge located in a forest opening [*Sturges*, 1984]. The drawbacks of a Wyoming shield are numerous. Its size--6 m in diameter--is much larger than other shields, it costs five times as much as a Nipher shield, and it requires occasional maintenance. Its use is generally limited to unstaffed locations. Although the studies cited establish a relative catch efficiency for the various windshields, the range of variation is quite wide when the unshielded, Alter-shielded, Nipher-shielded, and Wyoming-shielded catches are related to each other. One reason for the variation is likely to be the wide range of wind and snow conditions under which the various studies were conducted.

Another problem that further compounds the issue and that is not uncommon in Alaska's Arctic coastal region is rime accumulation. Rime is an opaque coating of ice particles caused by the freezing of supercooled water droplets or fog on impact with an object, including the ground or snow surface. NWS does not consider rime as true precipitation. Ground fog is a phenomenon that always occurs under clear skies. Consequently, with a frequent gauge-servicing interval, NWS is able to separate riming events from precipitation events and eliminate the accumulation of rime inside the orifice of a precipitation gauge from entering the record. Obviously, this is not always possible at unstaffed sites. Furthermore, whether or not to count rime as precipitation is a debatable issue; rime certainly adds to the moisture reaching the ground. A comparison of 12 years of dual records at BRW and Barter Island, Alaska, between unshielded and Wyoming-shielded gauges indicates the Wyoming shield allows a snowfall catch slightly greater than 3 times the unshielded catch over the 9-month winter period [*Clagett*, 1988]. However, Wyoming gauges were never serviced more than twice monthly at BRW, and often not for several months in a row at Barter Island. Therefore, rime accumulation creates a potentially significant source of bias in that comparison.

3. THE SOLUTION

A study of the windshield alternatives, at a staffed location, under the unique conditions of Alaska's Arctic coastal region, is vitally important for measuring accurate precipitation amounts. Results of the study will reflect on an expanded future network of shielded precipitation gauges on the North Slope, western, and southwestern tundra regions of Alaska. Most of these potentially new sites are in rural villages, where they may be semi-staffed, but will need to operate independently for the most

part. Will the Nipher shield operate under these conditions? What will be the comparison of the Nipher shield record against the longer-term records of unshielded and Wyoming shielded gauges? What is the significance of rime and its effect on the various windshields? A study to answer these questions will begin in August 1989 at BRW.

The snowfall catch from five storage precipitation gauges will be compared the first year, three shielded and two unshielded: (1) Wyoming shielded; (2) Nipher shielded; (3) Alter-shielded; (4) unshielded and serviced on an event basis, the same as the three shielded gauges; and (5) unshielded but treated as if it were a remote gauge, allowing rime to build up and dissipate naturally to see what effects it has on the overall catch. All storage cylinders will be 20.3 cm diameter × 100 cm tall, mounted with the orifice 2 m above the normal ground surface. Recording precipitation gauges will replace the storage gauges the second year of operation.

WMO began an international study of artificial windshielding in 1986 [*Goodison et al.*, 1985]. Several additional shields in common usage in Europe and Russia will be evaluated simultaneously along with the other five, including the unshielded standard gauge of the United States. The BRW study will allow us to tie in the results from North Slope's unique conditions with those from the broader WMO study being conducted in snowy regions around the world.

REFERENCES

Alter, S.C., Shielded storage precipitation gages, *Mon. Weather Rev., 65*, 262-265, 1937.

Benson, C.S., Reassessment of winter precipitation on Alaska's Arctic slope and measurement on the flux of wind blown snow, *Report UAG R-288*, 26 pp., Geophysical Institute, University of Alaska, Fairbanks, 1982.

Brown, M.J., and E.L. Peck, Reliability of precipitation measurements as related to exposure, *J. Appl. Meteorol., 1*, 203-207, 1962.

Clagett, G.P., Snowfall measurements in the Arctic, *Geophysical Monitoring for Climatic Change, No. 16: Summary Report 1987*, edited by B.A. Bodhaine and R.M. Rosson, pp. 90-92, NOAA Air Resources Laboratory, Boulder, CO, 1988.

Goodison, B.E., Snow studies at Cold Creek: Testing and evaluation of gages used in Canada for fresh snowfall measurement, *Proc. Canadian Hydrology Symposium, 75*, Winnipeg, National Research Council of Canada, Winnepeg, 26-35, 1975.

Goodison, B.E., Accuracy of Canadian snow gauge measurements, *J. Applied Meteorol., 17(10)*, 1542-1548, 1978.

Goodison, B.E., V.R. Turner, and J.E. Metcalfe, A nipher-type shield for recording precipitation gauges, *5th Symposium on Meteorological Observations and Instrumentation*, Toronto, Ontario, Canada, pp. 21-26, American Meteorological Society, Boston, 1983.

Goodison, B., B. Sevruk, B. Dahlstron, and S. Klemm, International Organizing Committee for WMO Solid Precipitation Measurement Intercomparison, Norrkoping, Sweden, December 16-20, 1985, Final Report, World Meteorological Organization, Geneva, 1985.

Hamon, W.R., Computing actual precipitation, in *Distribution of Precipitation in Mountainous Areas, WMO No. 326,*Vol. 1, pp. 159-174, World Meteorological Organization, Geneva, Switzerland, 1973.

Hanson, C.L., Precipitation measured by gages protected by the Wyoming shield and the dual-gauge system, *Proc. 56th Western Snow Conference*, Kalispell, Montana, pp. 174-177, Colorado State University, Fort Collins, 1988.

Rechard, P.A., Measurement of winter precipitation in wind-swept areas, *Proc. Snow Management of the Great Plains*, Bismark, North Dakota, pp. 13-30, University of Nebraska, Lincoln, 1975.

Rechard, P.A., and L.W. Larson, The use of snow fences for shielding precipitation gages, *Proc. 39th Western Snow Conference*, Billings, Montana, pp. 56-62, Colorado State University, Fort Collins, 1971.

Sturges, D.L., Comparison of precipitation as measured in gages protected by a modified Alter shield, Wyoming shield, and a stand of trees, *Proc. 52nd Western Snow Conference*, Sun Valley, Idaho, pp. 57-67, Colorado State University, Fort Collins, 1984.

Warnick, C.C., Experiments with windshields for precipitation gages, *Trans-Am. Geophys. Union, 34*, 379-388, 1953.

UVB Monitoring Data from Mauna Loa and Rockville

DAVID L. CORRELL, CARL CLARK, RUSSELL GOODRICH, AND DOUGLAS HAYES

Smithsonian Environmental Research Center, P.O. Box 28, Edgewater, Maryland 21037

Our laboratory has been continuously monitoring surface irradiance in a series of eight 5-nm band passes in the UVB at various locations on the Earth's surface with high-precision, accurately calibrated, interference-filter spectral radiometers. Significant data sets have been collected at BRW (71°N); Rockville and Edgewater, Maryland (39°N); Tallahassee, Florida (30°N); MLO (19°N); Republic of Panama (9°N); and SPO (90°S). Long-term data sets are now being edited and analyzed for publication and archiving; these sets include data from 1976 to the present at Rockville and from August 1984 to the present at MLO.

Data editing includes checking for file consistency; screening for data processing and file maintenance errors by testing for unreasonable ratios between channels, times of sunrise and sunset, and effects of cloud cover; and correcting for calibration changes, and equipment malfunctioning, and altered equipment design.

Data from Rockville from 1976 through 1988 have now been edited and are archived on 9-track computer tapes. Extensive analyses of these data are in progress, and a few highlights are reported here. Requests for data or further information should be directed to David L. Correll, Director, at the above address.

A new-generation, 18-channel, interference-filter spectral radiometer is nearly ready for field operation. In the UVB it will have 2-nm band pass filters. This instrument features not only better spectral resolution and modern electronics, but also improved PC-based data acquisition and microprocessor-controlled choices of set gains over 3 orders of magnitude for different channels in the same operational instrument. Both the present radiometers and the radiometers under development operate as cosine collectors to measure global irradiance. We are currently surveying possible additional station sites in order to attain an optimal range of latitudes for future data collection.

Mean UV global irradiance in July at 39°N latitude were 76, 583, and 2311 J m^{-2} nm^{-1} d^{-1} at 300, 305, and 310 nm, respectively in 1976. These fluxes increased to 211, 1328, and 3676 in July 1983. UV radiation fluxes declined again in 1987 and 1988. When measured total daily fluxes (averaged monthly) are compared with those predicted by the "Green" model [*Johnson et al.*, 1976], the higher fluxes, such as those measured in 1983, are very similar (Figure 1). Thus it is the attenuation of the short-wavelength part of the UVB regions in periods of low irradiance, such as in 1976 (Figure 1), that is unexpectedly large.

Morning, clear-day secant = 2.5 fluxes had both annual and 11-year variations for the short-wavelength end of the UVB spectral region. Annual minima usually occurred in May, having a long-term average of 2.98 and 114 mJ m^{-2} nm^{-1} min at 300 and 305 nm, respectively. Annual maxima usually occurred in November and had a long-term average of 30.5 and 282 mJ m^{-2} nm^{-1} min^{-1} at 300 and 305 nm, respectively. Annual monthly average minima for morning, clear-day, secant = 2.5 fluxes at 305 nm (Figure 2) were lowest in 1978 (28.8 mJ m^{-2} nm min) and highest in 1985 (266 mJ m^{-2} nm^{-1} min^{-1}). The annual monthly average maxima at 305 nm were lowest in 1976 (109 mJ m^{-2} nm^{-1} min^{-1}) and highest in 1984 (546 mJ m^{-2} nm^{-1} min^{-1}). Thus, over a solar cycle annual minima at 305 nm varied ninefold, while maxima varied fivefold.

We believe that this large attenuation of the short-wavelength end of the UVB spectral irradiance during periods such as 1976-1978 and 1987-1988 is a response to increased O$_3$ concentrations in the stratosphere, which result from increased solar flare activity. Since almost all of the UVB global irradiance we measure is diffuse sky light [*Dave and Furukawa*, 1966; *Dave and Halpern*, 1976], the effective optical pathlength through the atmosphere is increased substantially over that of
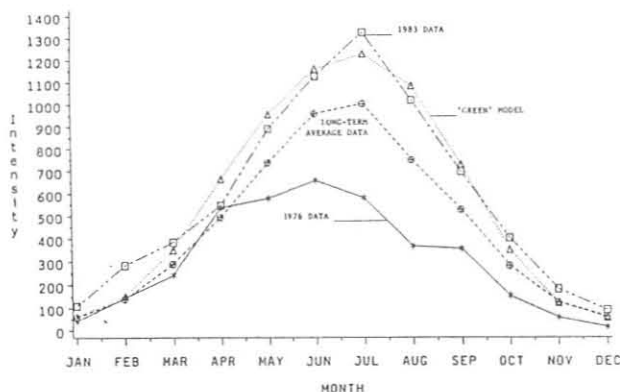
Fig. 1. Daily total irradiance fluxes (J m^{-2} nm^{-1} d^{-1} at 300 nm), averaged by month.
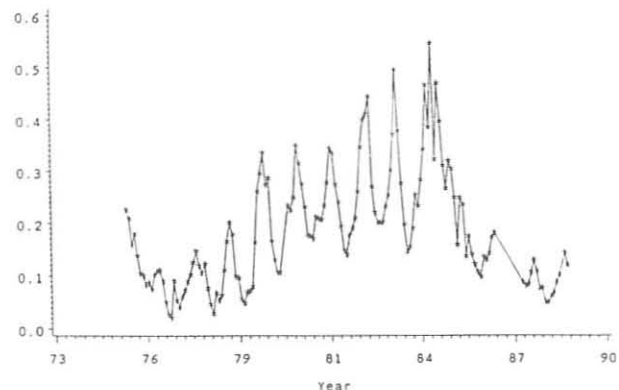
Fig. 2. Monthly averages for morning, clear-day, secant = 2.5 fluxes (J m^{-2} nm^{-1} min^{-1} at 305 nm).

direct sunlight. Therefore, relatively small changes in O_3 concentration cause large fluctuations in UV irradiance on the Earth's surface at wavelengths strongly absorbed by O_3. Certainly, the changes in global irradiance we are reporting are not due to significant changes in UVB radiation incident to the Earth's atmosphere [*Lean*, 1989].

REFERENCES

Dave, J.V., and P.M. Furukawa, Scattered radiation via the ozone absorption bands at selected levels of a Rayleigh atmosphere, *Meteorol. Monogr., 7*, 353 pp., American Meteorological Society, Boston, 1966.

Dave, J.V., and P. Halpern, Effect of changes in ozone amount on the ultraviolet radiation received at sea level of a model atmosphere, *Atmos. Environ., 10*, 547-555, 1976.

Johnson, F.S., T. Mo, and A.E.S. Green, Average latitudinal variation in ultraviolet radiation at the earth's surface, *Photochem. Photobiol., 28*, 179-188, 1976.

Lean, J. Contribution of ultraviolet irradiance variations to changes in the sun's total irradiance, *Science, 244*, 197-200, 1989.

Status of the Robertson-Berger UVB Monitoring Program, 1974-Present

GERALD F. COTTEN

NOAA, Air Resources Laboratory, Silver Spring, Maryland 20910

1. INTRODUCTION

MLO has served as one of the original 10 monitoring sites for the Robertson-Berger (R-B) Sunburning Meter network since its inception in 1974. An additional 24 sites, plus 11 non-U.S. sites, distributed unevenly worldwide, have operated with varying lengths of record. Until June 1989, the Skin and Cancer Hospital of Temple University has maintained the network functions, principally with contract support variously over the years from NIH, DOT, and EPA, with extensive field support by NOAA/ERL and NWS. The Skin and Cancer Hospital closed this year, so the operation of the network is currently being reviewed to determine whether measurements should be continued to overlap with measurements by more sophisticated instrumentation. The National Cancer Institute of NIH retains the data archive along with ancillary meteorological information.

2. INSTRUMENTATION AND DATA

The R-B meter was selected in the early 1970s as a UV-monitoring instrument at the surface for the Climatic Impact Assessment Program [*CIAP*, 1975] sponsored by DOT in reaction to concerns about possible climate impacts by the projected supersonic air transportation fleet. The instrument, described by *Berger* [1976], detects radiation in the UVB wavelength band, 295-330 nm. The meter response declines logarithmically such that the response at 330 nm is one-hudredth that at 295-300 nm. Although the R-B meter has always been accompanied by controversy, especially with respect to the wide UVB bandwidth and more recently with possible long-term instability (or drift) [*Scotto et al.*, 1988], it has proved to be a rugged, reliable instrument in the field. The Temple University staff maintained individual instrument calibrations that were performed annually through mid-1989 except for an unfunded period from mid-1983 to mid-1985. There were several comparisons of the R-B meter with more sophisticated instruments, obtaining side-by-side measurements over varying time periods [*Mo et al.*, 1975; *Machta et al.*, 1976; *Barton*, 1983; *Paltridge and Barton*, 1978]. In addition, *DeLuisi and Harris* [1983] performed an important though limited study of the meter behavior, providing under certain conditions estimates of the radiant energy of the somewhat arbitrary R-B sunburn unit of measurement. Finally, efforts have been made to modify the meter sensor in order to more nearly match the erythemal (McKinlay-Diffey action spectrum) response function. *Berger* [1989] prepared two "thin phosphor" instruments that were operated for approximately 1 year each at McMurdo and Temple University. These data are unavailable as of this writing. The published results of the CSIRO Australian network (1975-1981) include both types of instrumentation [*Barton*, 1983; *Paltridge and Barton*, 1978].

The period of record for each R-B observing sites is given in Table 1 (1974-1987), listing the number of complete years for each location. The data are retained as half-hourly sunburn units, which are archived as well as daily and monthly totals, along with observed daily and monthly Dobson ozone, percent sunshine, total cloudiness, and broad band solar radiation amounts where these are available. These data may be obtained from Joseph Scotto, NIH, National Cancer Institute, Public Health Service, Bethesda, MD 20892.

TABLE 1. Robertson-Berger Meter Network

Stations	No. of Complete Years	Start	End
United States			
Albuquerque, NM*	12	Jan. 1974	
Atlanta/Emory, GA*	7	Oct. 1977	Sept. 1987
Bismarck, ND	11	Jan. 1974	Feb. 1987
Burlington, VT*	2	Oct. 1985	
Concord, NH*	2	Oct. 1985	
Des Moines, IA	9	Jan. 1974	Dec. 1987
Detroit, MI*	10	Sept. 1977	
El Paso, TX*	13	Jan. 1974	
Ft. Worth, TX*	14	Jan. 1974	
Gainesville, FL	2	Jan. 1975	Aug. 1980
Honeybrook, PA	10	Jan. 1975	July 1985
La Jolla, CA	3	May 1979	March 1983
Lihue, HI*	0	Feb. 1987	
Mauna Loa, HI*	12	Jan. 1974	
Miami, FL*	0	May 1986	
Minneapolis, MN*	13	Jan. 1974	
New Orleans, LA*	4	Nov. 1977	
Oakland/Redwood City, CA*	12	Jan. 1974	
Philadelphia, PA*	14	Jan. 1974	
Pt. Barrow, AK*	8	Oct. 1978	
Rockville, MD	5	Sept. 1978	July 1985
Salt Lake City, UT*	9	Oct. 1977	
Seattle, WA*	9	Oct. 1977	
Tallahassee, FL	12	Jan. 1974	May 1986
Tucson, AZ*	6	Jan. 1980	
Non-United States			
Brisbane, Australia	7	Oct. 1974	Apr. 1981
Melbourne, Australia	11	Dec. 1974	Nov. 1986
Hamburg, Germany	5	Feb. 1976	June 1983
Hamilton, New Zealand*	3	May 1980	
Invercargill, New Zealand	2	Sept. 1981	Oct. 1985
Barro Colorado, Panama*	3	Nov. 1978	
Belsk, Poland*	11	May 1975	
Warsaw, Poland	1	June 1975	Sept. 1976
Nörrkoping, Sweden*	4	Oct. 1982	
Basel, Switzerland*	7	March 1980	
Davos, Switzerland*	13	Jan. 1975	

*Stations currently operational

REFERENCES

Barton, I.J., The Australian UV-B monitoring network, *Division of Atmospheric Physics Technical Paper No. 46*, CSIRO, Aspendale, Victoria, Australia, 1983.

Berger, D., The sunburning ultraviolet meter: Design and performance, *Photobiol., 24*, 587, 1976.

Berger, D., Product Brochure, Solar Light Co., Philadelphia, PA, 1989.

CIAP (Climatic Impact Assessment Program), *Impacts of Climatic Change on the Biosphere*, Final Report, *CIAP Monograph 5, DOT-TST-75-55*, Department of Transportation, Washington, DC, 1975.

DeLuisi, J., and J. Harris, A determination of the absolute radiant energy of a Robertson-Berger Meter Sunburn Unit, *Atmos. Environ. 17*(4), 751-758, 1983.

Machta, L., G. Cotton, W. Hass, and W. Komhyr, Erythemal ultraviolet solar radiation and environmental factors, Proc. of the Fourth Conference on the Climatic Impact Assessment Program, *DOT-TSC-OST-75-38*, 405-411, 1976.

Mo, T., A.T. Chai, and A.E.S. Green, An absolute calibration of the sunburn meter, in *Impacts of Climatic Change on the Biosphere, CIAP Monograph 5*, Appendix L, 2-247, Department of Transportation, , Washington, DC, 1975.

Paltridge, G.W., and I.J. Barton, Erythemal ultraviolet radiation distribution over Australia--Calculations, detailed results and input data, *Division of Atmospheric Physics Technical Paper No. 33*, CSIRO, Aspendale, Victoria, Australia, 1978.

Scotto, J., G. Cotton, F. Urbach, D. Berger, and T. Fears, Biologically effective ultraviolet radiation: Surface measurements in the United States, 1974-1985, *Science, 239*, 762-764, 1988.

The CSIRO Latitudinal Gradient Study of CO_2 Isotopes

ROGER FRANCEY, PAUL FRASER, AND GRAEME PEARMAN

CSIRO, Division of Atmospheric Research, Aspendale, Victoria, Australia 3195

1. INTRODUCTION

For long-lived atmospheric trace gases, zonal mixing suggests that a small number of carefully selected clean-air sites spanning latitudes from the north to south poles can provide a global perspective on the budget of each species. The gases of interest in this study are those influenced by human activity and implicated in environmental change by modification of the radiation balance of the atmosphere; specifically CO_2, CH_4, CO, N_2O, and some CFCs. The primary focus is on the stable isotopic composition of CO_2, measured as ratios $\delta^{13}C$ and $\delta^{18}O$ relative to the PDB (used here to describe reference CO_2 evolved from carbonate) standard. The $\delta^{13}C$ ratios, where

$$\delta^{13}C = \left[\frac{^{13}C/^{12}C_{sample}}{^{13}C/^{12}C_{PDB}} - 1 \right] \cdot 1000 \ (\text{per mil}) \quad (1)$$

are thought to characterize net atmosphere-surface exchanges involving the terrestrial biosphere (including biologically derived fossil fuel) and so can be used to distinguish CO_2 from this source compared with that from an oceanic source [*Keeling et al.*, 1980; *Pearman and Hyson*, 1986]. The $\delta^{18}O$ ratios, where

$$\delta^{18}O = \left[\frac{^{18}O/^{16}O_{sample}}{^{18}O/^{16}O_{PDB}} - 1 \right] \cdot 1000 \ (\text{per mil}) \quad (2)$$

in CO_2 are thought to involve gross CO_2 exchange with land plants [*Francey and Tans*, 1987]; they provide potentially useful new information on large-scale biological responses and/or atmospheric transport. Unlike other known global sampling networks, this network has the feature of pre-drying air, which may have implications for ^{13}C monitoring and is crucial for $\delta^{18}O$ in CO_2. The establishment and operation of the sampling network are described here. Brief reference is made to significant results emerging from analyses of the samples.

2. NETWORK DESCRIPTION

The CSIRO/DAR network was established at the end of 1983 with funding support from NERDDC and logistic support from NOAA/GMCC and CGBAPS. Monthly sample collections started at Cape Grim (41°S) and at the GMCC stations BRW (71°N), MLO (20°), SMO (14°S) and SPO (90°S). The Cape Grim observations constitute the foundation measurements, along with contiguous in-situ observations of all species of interest, including in-situ CO_2 extraction for isotopic ratios [*Francey and Goodman*, 1986]. At the GMCC stations, comparisons of flask CO_2 measurements with in-situ CO_2 observations are used as a basic quality control.

Sample collection has continued uninterrupted with both NERDDC and CSIRO financial support, and has expanded to include Alert (82°N, in cooperation with AES), Macquarie Island and Mawson (54°S and 68°S respectively, with logistic support from ANARE), and Niwot Ridge (NWR, 40°N, in cooperation with GMCC). Throughout, similar techniques have been employed to collect monthly samples from aircraft at about 4-km altitude over the ocean southeast of the Australian mainland.

3. METHODS

Sampling equipment at each collection site comprises a Teflon-diaphragm pump with an anhydrous magnesium perchlorate drying tower on the inlet, connected to the station air intake mast. The sample containers are 5-L-capacity glass flasks, fitted with two Teflon O-ring glass barreled taps, one connected to an internal flushing tube. In suitable conditions (typically winds greater than 4 m s^{-1} (9 mph), and from a "clean air" sector), flasks are connected to the pump unit one at a time, flushed for 15 minutes at about 2 L min^{-1}, then pressurized to 1 atm above ambient. Station operators record synoptic conditions and the preliminary in-situ CO_2 concentration.

Flasks are returned to Aspendale for analysis. The flask overpressure facilitates gas chromatographic analyses with a Hewlett-Packard 5890 Porasil column and ECD for N_2O, CCl_3F (CFC-11), and CCl_2F_2, (CFC-12) and with a CARLE Model 211S 5A molecular sieve column and FID for CO_2, CH_4, and CO. The remaining bulk of the air from the flask is then drawn through a cryogenic extraction line that collects the CO_2 for mass spectrometer analysis [*Francey and Goodman*, 1986]. A stable isotope ratio Micromass 602D mass spectrometer is used to determine the $\delta^{13}C$ and $\delta^{18}O$ ratios.

All measurements are made with respect to in-house working standards that are routinely calibrated against international standards. The gas chromatograph standards are tied to the OGC scale [*Rasmussen and Lovelock*, 1983] and NIST standards [*Rasberry and Reid*, 1984]. The mass spectrometer standard has been calibrated against the international PDB scale using NIST carbonate, and checked in a number of interlaboratory comparisons [*Francey and Goodman*, 1988].

4. RESULTS

Because of the relatively low sampling rate compared with other extensive overlapping networks (in particular the ALE/GAGE programs), the CFC-11 and CFC-12 data are used only for diagnostic purposes, and since 1987 they have not been routinely measured from those stations with in-situ programs. This is also the situation with N_2O, with the exception that the

N_2O mixing ratios are used to make a second-order correction for a mass 44 contribution to the CO_2 isotope ratios in the mass spectrometer measurements [*Mook and Jongsma*, 1987]; when data are not directly available from the flasks, a linear plus harmonic regression of the in-situ data from each station is used for this purpose.

The GC analysis of CO_2 is the main diagnostic for the assessment of integrity of the flask sample. For CO_2 of biological origin, mixing with the atmosphere is characterized by approximately 0.05% per ppm (by mole fraction) linear relationship, where the precision on an individual $\delta^{13}C$ analysis is 0.03-0.05%. This means that CO_2 determinations to better than 1 ppm are adequate for quality control; this is achieved with the CARLE GC.

Figure 1 shows the raw, flask CO_2 data (ppm) from the commencement of the records to the end of 1987. Solid lines connect the preliminary in-situ measurements reported at the measurements from 0.5-L glass flask samples using an NDIR
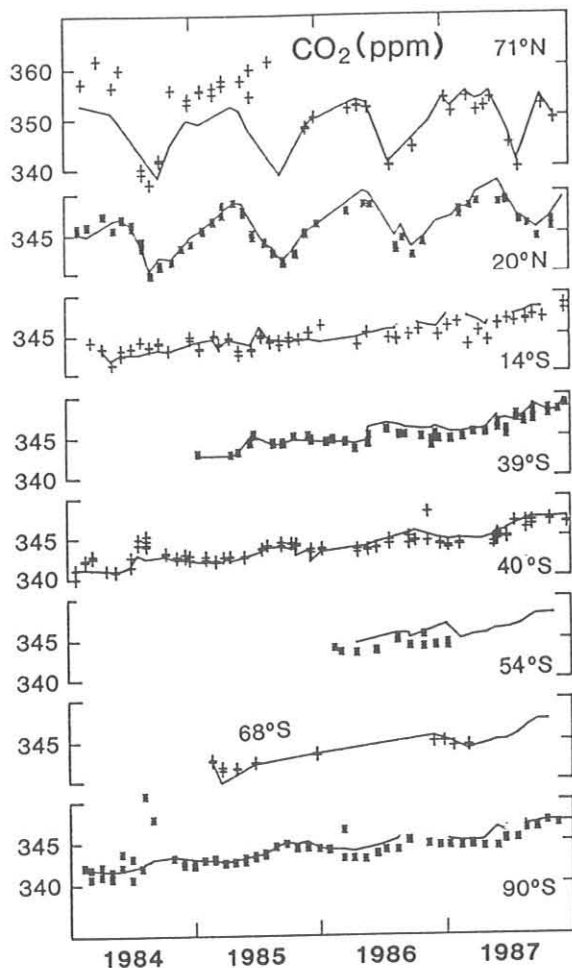
time of flask filling. When in-situ CO_2 data were not available--aircraft (39°S) and Mawson (68°S)--bracketing CO_2 analyzer [*Beardsmore* 1984] were used. The presentation of the raw data in this form serves to illustrate the following:

(1) The overall coverage and frequency of sampling. Typically, pairs of flask samples are collected at least every third month, and individual samples are collected during intervening months.

(2) Systematic errors, of varying seriousness, which appear from time to time. Examples include enhanced CO_2 at 71°N during most of 1984 and 1985, and occasionally at 41°S and 90°S, due to laboratory air from pump unit leaks; depleted CO_2 at 54°S in 1986 and at 14°S in early 1987, thought to be due to a saturated drying tower; a shift in GC calibratition around 1986; difficulties with preliminary in-situ values at 14°S and 90°S (normally, corrected monthly averages are available on these occasions).

The periods of affected data are limited, and it is evident from Figure 1 that the quantity and quality of data are approaching levels sufficient for the determination of latitudinal gradients, and of seasonality at most stations.

Only preliminary results for CH_4 [*Fraser et al.*, 1986a], CO [*Fraser et al.*, 1986b], and isotopes [*Francey and Tans*, 1987; *Francey et al.*, 1988] have been published; a more comprehensive summary of the isotope results [*Francey et al.*, submitted] will appear shortly. An assessment of flask performance is given by *Mansbridge et al.* [1988]. It is intended that this paper act as a general reference for specific results to be presented in future GMCC reports.

Fig. 1. Measured CO_2 in 5-L flasks (symbols) compared with preliminary in-situ values (lines) for the CSIRO network and aircraft (39°S). This illustrates the density of sampling and quality of sampling and storage.

REFERENCES

Beardsmore, D.J., G.I. Pearman, and R.C. O'Brien, The CSIRO (Australia) Atmospheric carbon dioxide monitoring program: Surface data, *Division of Atmospheric Research Technical Paper No. 6*, 115 pages, CSIRO, Aspendale, Victoria, Australia, 1984.

Francey, R.J., and H.S. Goodman, Systematic errors in, and selection of, in situ $\delta^{13}C$, *Baseline 1983-1984*, edited by P.J. Francey and B.W. Forgan, pp. 27-36, Australian Department of Science/Bureau of Meteorology in cooperation with CSIRO Division of Atmospheric Research, Aspendale, Victoria, Australia, 1986.

Francey, R.J., and H.S. Goodman, The DAR stable isoptope reference scale for CO_2, *Baseline 1986*, edited by B.W. Forgan and P.J. Francey, pp. 40-46, Australian Department of Science/Bureau of Meteorology in cooperation with CSIRO Division of Atmospheric Research, Aspendale, Victoria, Australia, 1988.

Francey, R.J., and P.P. Tans, Latitudinal variation in oxygen-18 of atmospheric CO_2, *Nature, 327*, 495-497, 1987.

Francey R.J., G.I. Pearman, and D.J. Beardsmore, A southern view of the global atmosphere, *Papers Proc. Roy. Soc. Tasmania, 122(1)*, 113-119, 1988.

Francey, R.J., F.J. Robbins, C.E. Allison, and N.G. Richards, The CSIRO global survey of CO_2 stable isotopes, edited by S.R. Wilson and G.P. Ayers, *Baseline 1988*, Bureau of Meteorology in cooperation with CSIRO Division of Atmospheric Research, Aspendale, Victoria, Australia, submitted, 1989.

Fraser P.J., P. Hyson, R.A. Rasmussen, A.J. Crawford, and M.A.K. Khalil, Methane, carbon dioxide and methylchloroform in the Southern Hemisphere, *J Atmos. Chem., 4*, 3-42, 1986a.

Fraser P.J, P.Hyson, S. Coram, R.A. Rasmussen, A.J. Crawford, and M.A.K. Khalil, Carbon monoxide in the Southern Hemisphere, *Proc. 7th World Clean Air Congress, 2*, 341-352, 1986b.

Keeling, C.D., R.B. Bacastow, and P.P. Tans, Predicted shift in the $^{13}C/^{12}C$ ratio of atmospheric carbon dioxide, *Geophys. Res. Lett., 7*, 505-508, 1980.

Mansbridge J.V, F.J. Robbins, and P.J. Fraser, Variation in measurements of methane, carbon dioxide and carbon monoxide from Cape Grim flask samples, *Baseline 1986*, edited by B.W. Forgan an P.J. Francey, pp. 27-34, Australian Department of Science/Bureau of Meteorology in cooperation with CSIRO Division of Atmospheric Research, Aspendale, Victoria, Australia, 1988.

Mook, W.G., and J. Jongsma, Measurement of the N_2O correction for $^{13}C/^{12}C$ ratios of atmospheric CO_2 by removal of N_2O, *Tellus, 39B*, 96-99, 1987.

Pearman, G.P., and P. Hyson, Global transport and inter-reservoir exchange of carbon dioxide with particular reference to stable isotopic distributions, *J. Atmos. Chem., 4*, 81-124, 1986.

Rasberry, S.D., and W.P. Reid, Reference materials and environmental analysis, *Environ. Int., 10*, 87-90, 1984.

Rasmussen, R.A., and J.E. Lovelock, The Atmospheric Lifetime Experiment, 2. Calibration, *J. Geophys. Res., 88*, 8369-8378, 1983.

Global Aurora Dynamics Campaign

K. HAYASHI

Geophysics Research Laboratory, University of Tokyo, Japan

1. INTRODUCTION

To study magnetospheric and ionospheric physics, a research group of the Geophysics Research Laboratory, University of Tokyo, has conducted campaigns of multistation observations in North America every 3-4 years for the last 15 years. Ground-based multistation observations provide two-dimensional, spatial and temporal, information, although the information is more or less spatially integrated and must be processed with remote sensing techniques. These observations also increase the chances of obtaining three-dimensional multipoint data when they are coordinated with satellite observations.

2. THE 1985-1986 CAMPAIGN

The last campaign, named Global Aurora Dynamics Campaign, was carried out from December 20, 1985, to February 3, 1986, at 43 stations (Figure 1). The research objectives of the campaign were to study (1) the global dynamics of auroras, (2) the generation and propagation of ULF-VLF waves in connection with auroral activities, (3) the relationships of simultaneous observations from the ground with those from satellites in the ionosphere and in the magnetosphere, (4) the energetics in the ionosphere-magnetosphere coupling system including wave- particle interactions, and (5) the propagation of ULF waves on the global scale, whether related to auroral activities or not. The campaign was organized by Geophysics Research Laboratory, University of Tokyo; the Department of Physics, Kyushu University; and the Department of Geophysics and Astronomy, University of Geophysics and Astronomy. It was supported by the members of the Data Analysis Center for Geomagnetism and Spacemagnetism, Kyoto University; Department of Engineering, Takushoku University; Upper Atmospheric Division, National Institute of Polar
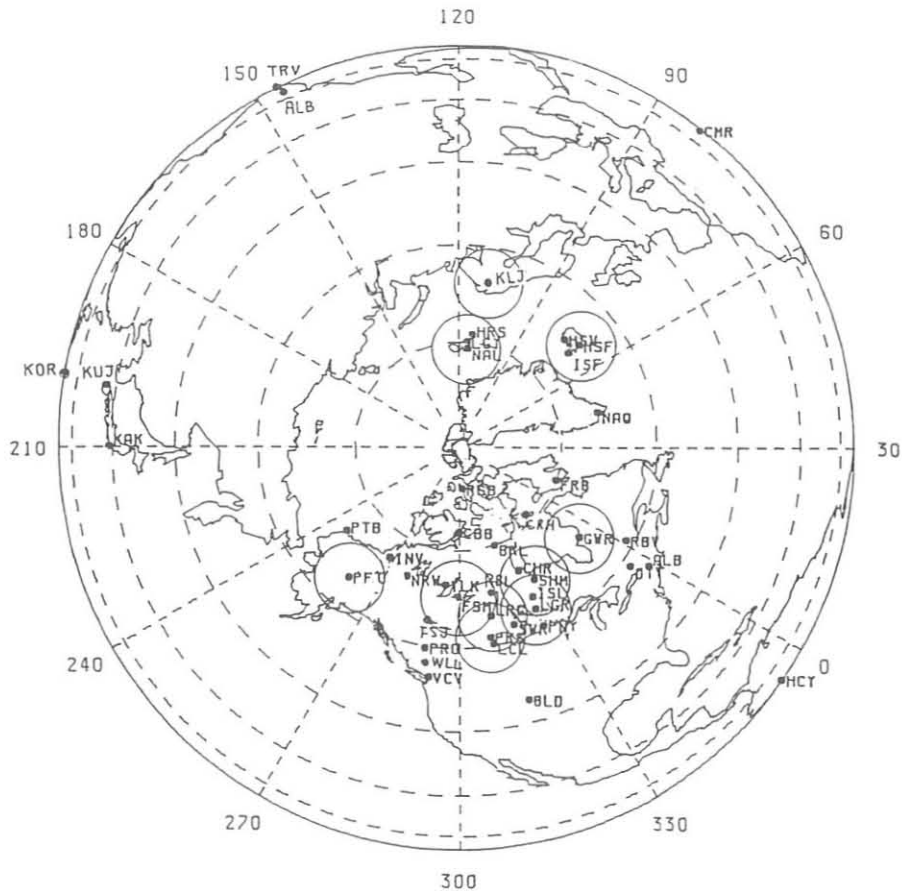

Fig. 1. Distribution of the campaign stations. The circled stations are the key stations. The circle approximately indicates the coverage of an all-sky TV camera from each station with elevation angle larger than 10°.

Research; Department of Physics and Astronomy, University of Victoria; Institute of Space and Atmospheric Studies, University of Saskatchewan; Department of Atmospheric Sciences, State University of New York, Albany; Geophysical Institute, University of Alaska; Department of Physics, University of Oslo; Norwegian Polar Research Institute; and Danish Meteorological Institute.

Nine of the 43 stations in the campaign network operated an all-sky TV camera, a VLF receiver, an induction magnetometer, and a fluxgate magnetometer. At 34 stations magnetic fields were measured with an induction and/or a fluxgate magnetometer(s). An introduction magnetometer was installed and continuously operated for 6 months at GMCC site at BRW where it could provide micropulsation information from the westernmost Arctic region in the global network. The campaign, specifications of instruments, data periods, and station descriptors are summarized by *Oguti et al.* [1988a]. The campaign period was originally planned to overlap with Swedish VIKING satellite program, but the VIKING launch was unfortunately delayed until February 22, 1986. Coordination with magnetic field observations onboard U.S. meteorological satellites in synchronous orbit, the GOES 4 and GOES 6, was successful at Great Whale River, Shamattawa, La Ronge, and Rabbit Lake, near the geomagnetic lines of force.

Analysis of data, 1000 video tapes and 600 cassette tapes, is still in progress. All initial results were published in a special issue, "Global Aurora Dynamics Campaign," in the *Journal of Geomagnetism and Geoelectricity, Vol. 40, No. 5*, 1988. The main results are related to the following: the first auroral evolution and related magnetic field changes [*Oguti et al.*, 1988b]; dynamic characteristics of IPDP magnetic pulsations [*Hayashi et al.*, 1988], auroral activities and long-period geomagnetic pulsations [*Yamamoto et al.*, 1988a, b], auroras and bursts of magnetic pulsations in the dayside cusp [*Kokubun et al.*, 1988].

2. THE 1988-1990 CAMPAIGN

In conjunction with a satellite program named EXOS D, which was launched in semipolar orbit on February 22, 1989, a new campaign of multistation observations is planned for December 1989 to January 1990. In the summer of 1988 an induction magnetometer was teprarily installed at BRW, and a test run was made. Problems with the recording system were discovered. The permanent installation and operation of a induction magnetometer at the BRW site was proposed for use in the campaign, and it was approved in 1988. The faulty recording system was replaced in August 1989.

REFERENCES

Hayashi, K., T. Yamamoto, S. Kokubun, T. Oguti, T. Ogawa, N. Iwagami, T. Araki, T. Kitamura, O. Saka, K. Makita, N. Sato, T. Watanabe, R.E. Horita, D. McEwen, J.S. Kim, and A. Egeland, Multi-station observation of IPDP micropulsations--Two-dimensional distribution and evolution of the source regions, *J. Geomagn. Geoelectr., 40*, 583-619, 1988.

Kokubun, S., T. Yamamoto, K. Hayashi, T. Oguti, and A. Egeland, Impulsive Pi bursts associated with poleward moving auroras near the polar cusp, *J. Geomagn. Geoelectr., 40*, 537-551, 1988.

Oguti, T., T. Kitamura, and T. Watanabe, Global Aurora Dynamics Campaign, 1985-1986, *J. Geomagn. Geoelectr., 40*, 458-504, 1988a.

Oguti, T., T. Yamamoto, K. Hayashi, S. Kokubun, T. Ogawa, N. Iwagami, T. Kitamura, O. Saka, T. Araki, K. Makita, N. Sato, T. Watanabe, R.E. Horita, and J.S. Kim, Fast auroral evolution and related magnetic fields changes on the ground and at conjugate satellites, *J. Geomagn. Geoelectr., 40*, 505-536, 1988b.

Yamamoto, T., K. Hayashi, S. Kokubun, T. Oguti, T. Ogawa, N. Iwagami, T. Kitamura, O. Saka, T. Araki, K. Makita, T. Watanabe, R.E. Horita, and J.S. Kim, Auroral activities and long period geomagnetic pulsations, 1, Pc5 pulsations and concurrent auroras in the dawn sector, *J. Geomagn. Geoelectr., 40*, 553-569, 1988a.

Yamamoto, T., K. Hayashi, S. Kokubun, T. Oguti, T. Ogawa, N. Iwagami, T. Kitamura, O. Saka, T. Araki, K. Makita, T. Watanabe, R.E. Horita, and J.S. Kim, Auroral activities and long period geomagnetic pulsations, 2, Ps5 pulsations following auroral breakup in the premidnight hours, *J. Geomagn. Geoelectr., 40*, 571-582, 1988b.

The Colorado State University Multiple Field of View Radiometer at the Mauna Loa Observatory
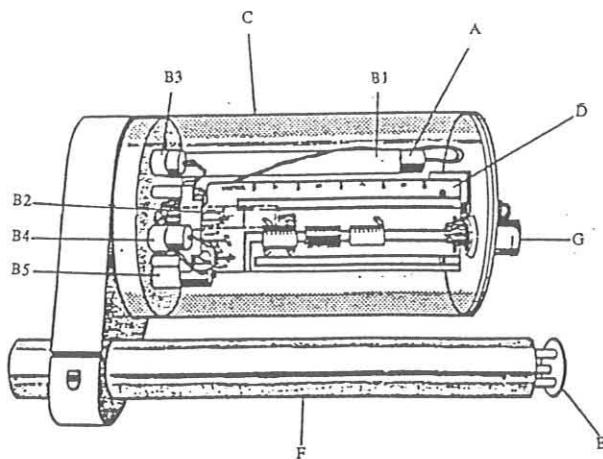
PAUL F. HEIN AND STEPHEN K. COX

Colorado State University, Department of Atmospheric Science, Ft. Collins, Colorado 80523

The MFOV was developed at Colorado State University to determine the bulk scattering properties of clouds by measuring the solar irradiance in different fields of view. The MFOV consists of five silicon photodiodes aligned along a common optical axis (Figure 1). Collimator tubes of different lengths give each of the photodiodes a different field of view (2°, 5°, 10°, 20°, and 28°). The photodiodes have a spectral range from 0.35 to 1.15 micrometers. The MFOV tracks the sun with a LICOR microprocessor-based solar tracker.

The MFOV data set for MLO extends from January 1985 to the present. The MFOV has been running nearly continuously, having an estimated 90% up time. The data collected for each photodiode consists of a 10-min average voltage, and a standard deviation, a minimum, and a maximum voltage for the period.

The MLO data set from May 1985 to June 1986 was analyzed by *Combs* [1988]. From the analysis of solar energy depletion at different fields of view, the mean daily irradiance and its standard deviation for the 10° field of view appear to

Fig. 2. Voltage versus time for thin clouds on March 30, 1986, using the 5° and 10° fields of view.
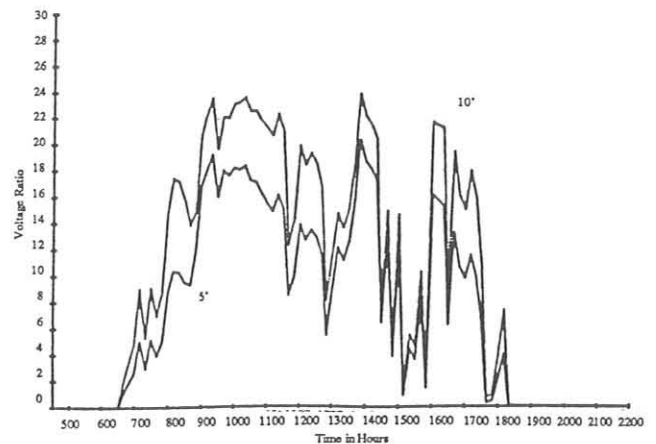
Fig. 3. Voltage versus time for broken cloud cover on March18, 1986, using the 5° and 10° fields of view.

Label	Description
A	Photodiode
B1	Collimator tube for 2°
B2	Collimator tube for 5°
B3	Collimator tube for 28°C
B4	Collimator tube for 20°C
B5	Collimator tube for 10°
C	Plexiglass weather-proof casing
D	Op amp pc board
E	Visual alignment disc
F	Mounting arm
G	Cable hookup

Fig. 1. The multiple field of view radiometer.

provide a useful way to categorize generic cloud cover information. Each type of cloud cover had a separate range of depleted energy. Figures 2 and 3 are examples of the MFOV output.

REFERENCES

Combs, C. L., Transmittance of solar radiation determined by the multiple field of view radiometer, M.S. Thesis, 76 pp., Colorado State University, Ft. Collins, 1988.

The Global ^{4}He Content of Near-Surface Atmospheric Air

P.W. HOLLAND AND D.E. EMERSON

U.S. Department of the Interior, Bureau of Mines, Helium Field Operations, Amarillo, Texas 79101

In a cooperative program with GMCC, the Bureau of Mines obtained near-surface atmospheric samples from five locations around the globe for subsequent ^{4}He analysis. The study was conducted to verify the constancy of the worldwide ^{4}He-in-air content and to provide a more accurate absolute value. The atmospheric samples were obtained from Hilo, Hawaii; Barrow, Alaska; Pago Pago, American Samoa; Mangilao, Guam; and Amundsen-Scott South Pole Station, Antarctica. Samples were collected from March 26, 1985, through February 5, 1988.

The study showed the ^{4}He content in the lower atmosphere to be constant at 5.2204 ± 0.0041 ppmv. This value is 0.0186 ppmv lower than the currently accepted global average of 5.239 ± 0.004 ppmv reported by *Glueckauf* [1946], but agrees with the values of 5.222 ± 0.107 ppmv and 5.2204 ± 0.0041 ppmv reported by *Oliver et al.* [1984] and *Holland and Emerson* [1987], respectively, for atmospheric samples collected within the continental United States.

The global ^{4}He content in the lower atmosphere was determined to an absolute accuracy of ± 0.0041 ppmv at the 68% confidence level. This accuracy was achievable using a specially modified ^{4}He mass spectrometer. The precision of this instrument for a 5-ppmv ^{4}He concentration is routinely ± 0.001 ppmv. The mass spectrometer was calibrated using gravimetrically prepared ^{4}He-in-nitrogen standards accurate to within ± 0.003 ppmv.

REFERENCES

Glueckauf, E., Micro-analysis of the helium and neon contents of air, *Proc. R. Soc. London, Ser. A, 185*, 98-119, 1946.

Holland, P.W., and D.E. Emerson, A determination of the helium-4 content of near-surface atmospheric air within the continental United States, *J. Geophys. Res., 92*, 12557-12566, 1987.

Oliver, B.M., J.G. Bradley, and H. Farrar IV, Helium concentration in the earth's lower atmosphere, *Geochim. Cosmochim. Acta, 48*, 1759-1767, 1984.

Nitric Acid and Aerosol Nitrate Variations at Mauna Loa

B. J. HUEBERT, G. L. LEE, AND W. M. WARREN

University of Rhode Island, Graduate School of Oceanography, Narragansett, Rhode Island 02882-1197

R. B. NORTON

NOAA, Aeronomy Laboratory, Boulder, Colorado 80303

1. INTRODUCTION

Much of the NO and NO_2 that is emitted into the atmosphere is converted to nitric acid vapor or aerosol nitrate before it is removed by dry or wet deposition. This conversion to nitrate is largely complete within a few days of the odd-nitrogen's emission; therefore, in remote areas such as MLO, the total nitrate concentration (vapor plus aerosol) represents a fair estimate of the total odd-nitrogen concentration [*Galasyn et al.,* 1987*a, b; Robinson and Harris,* 1987].

With support from NSF, we measured nitrate concentrations at MLO for several years, to help identify the important sources of odd-nitrogen compounds in remote parts of the globe. In 1988 we sampled intensively from the new walkup tower during the May-June MLOPEX experiment. We also changed from an intermittent to a nightly sampling strategy in the late summer. We are now measuring total nitrate every night, in collaboration with the MLO staff.

2. MATERIALS AND METHODS

We use a Teflon/nylon filter pack method for collecting atmospheric nitrate. Initially, the filter packs were exposed by our sequential sampler during 8-day visits to the site by researchers approximately every 2 months. Since August 1988, one filter is being exposed each night, from 2000 to 0800 LST. Filters are returned to our URI laboratory for extraction and analysis by ion chromatography. Our final data are sorted using three criteria (wind direction, humidity, and CN count) to eliminate those samples that were influenced by local sources on the island.

3. RESULTS AND DISCUSSION

3.1. MLOPEX EXPERIMENT

For about 6 weeks in May and June, we measured nitric acid and nitrate aerosol during five daily sampling periods, at three MLO locations. We found that samples taken from the deck atop the AEC building often had concentrations significantly different from those taken at the 23-m level of the tower, probably as a result of surface losses and turbulent flow over the irregular terrain. Gradients on the tower were unpredictable, sometimes showing the expected higher concentrations at higher altitude, but occasionally inverting to give slightly higher concentrations at 4 m than 23 m.

Two episodes are evident in Figure 1: the first (days 139-142) was characterized by visible haze, some very high CN counts (Figure 2), and high dewpoints; the second (days 143-146), by contrast, was very clean and dry, and had relatively high ozone. Although we suspect that upper-tropospheric air was present during the second event, we are still working on piecing together the history leading to both events. These events (and results from some 1989 CPACE flights in the vicinity using NCAR's Electra) suggest that the free troposphere is highly inhomogeneous even in the mid-Pacific, having a thin laminae of widely varying composition.

The existence of the high-concentration events at MLO suggests that our initial sampling strategy (8-10 days, once every 2 months) was incapable of defining the climatology of nitrate concentrations at MLO. In collaboration with the MLO staff, we initiated a nightly sampling program, and so our data are now more representative.
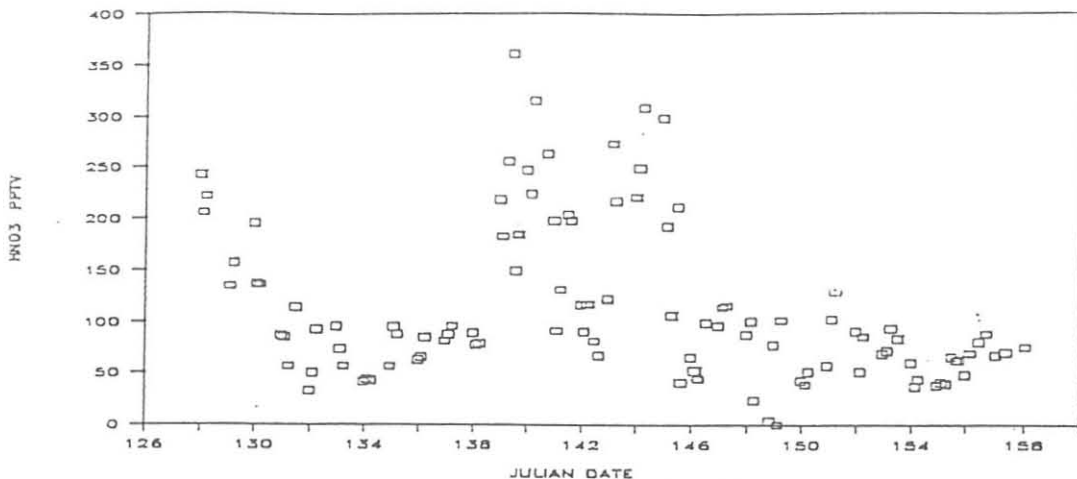

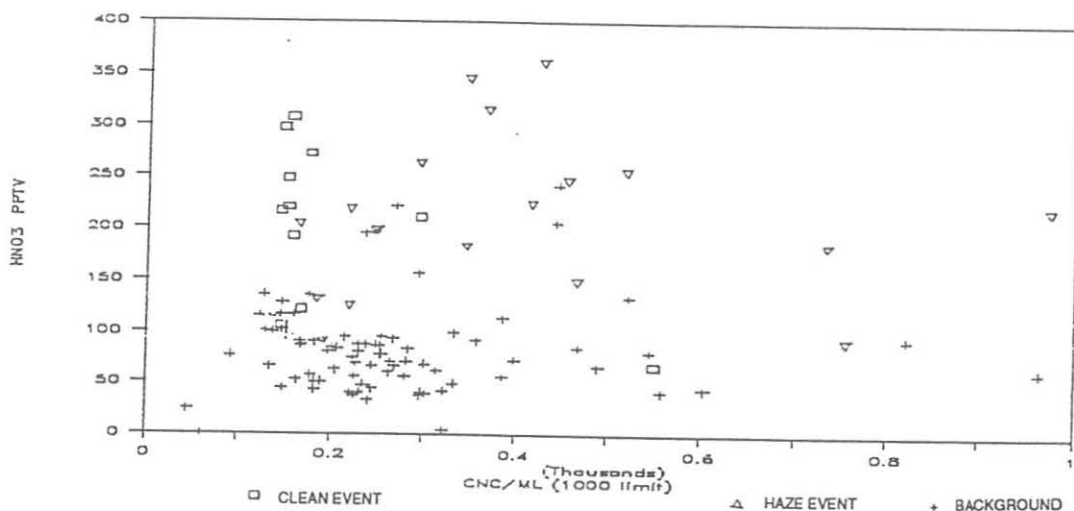Fig. 1. Nitric acid versus time during MLOPEX.

Fig. 2. Nitric acid versus CNC during MLOPEX.
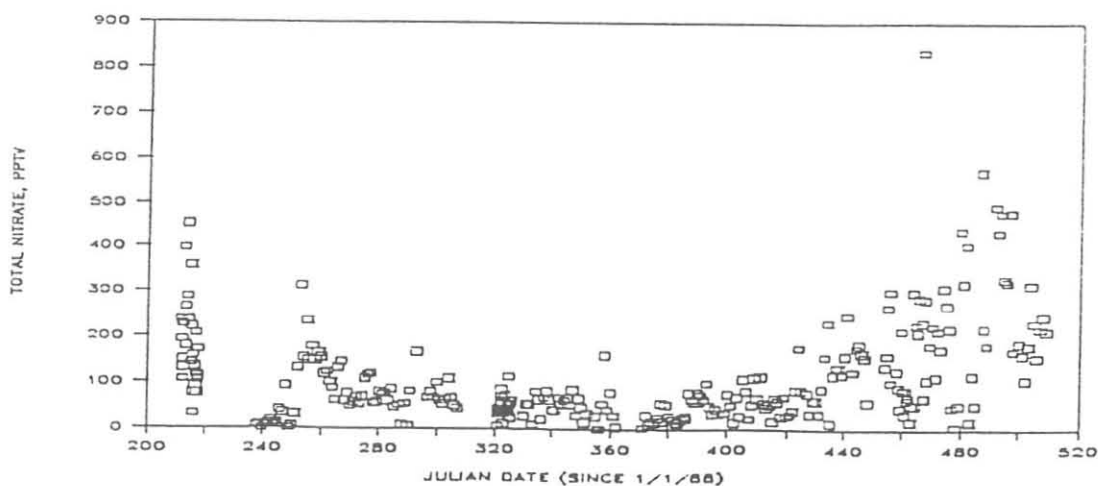
Fig. 3. Total nitrate versus time, August 1988-May 1989.

3.2. ANNUAL VARIATION

During all MLO sampling, we observed a sharp maximum in nitric acid and aerosol nitrate concentrations in the summer. The search for an explanation for this maximum continues to stimulate our science.

Although our nightly sampling has not yet completed a full year, it appears that the same trend is evident in these data. Figure 3 shows 2000 to 0800 LST concentrations of total nitrate, starting in August 1988 and ending in May 1989. The lowest sustained concentrations are still evident in the winter, and a mix of high-concentration events and clean periods occurs in the spring and late summer.

4. ONGOING RESEARCH

We are continuing our inclusive nightly sampling from the tower, with the help of the MLO staff. Although equipment failures and bad weather (which prevents filter changes on the tower) have occasionally caused brief lapses in the data, a very interesting record is emerging. We hope to identify both the frequency and source of high-nitric events during the next year or so.

REFERENCES

Galasyn, J.F., K.L Tschudy, and B.J. Huebert, Seasonal and diurnal variability of nitric acid vapor and ionic aerosol species in the remote free troposphere at Mauna Loa, Hawaii, *J. Geophys. Res.*, 92, 3105-3113, 1987a.

Galasyn, J.F., K.L. Tschudy, and B.J. Huebert, Authors' Reply to the Comment of Robinson and Harris, *J. Geophys. Res.*, 92, 14868, 1987b.

Robinson, E., and J. Harris, Comment on "Seasonal..." by Galasyn, Tschudy, & Huebert, *J. Geophys. Res.*, 92, 14,865-14,867, 1987.

Nitrogen Oxide Measurements at Barrow

DANIEL A. JAFFE AND RICHARD E. HONRATH

University of Alaska, Department of Chemistry and Geophysical Institute, Fairbanks, Alaska 99775-0800

1. INTRODUCTION

Nitrogen oxides are critical in the chemistry of the troposphere. At NO_x ($NO+NO_2$) concentrations greater than about 30 pptv, net O_3 production can occur [*Fishman et al.*, 1979; *Liu et al.*, 1987]. O_3 is a radiatively and chemically important gas, and its tropospheric concentration in the northern hemisphere is increasing at approximately 1% yr^{-1} [*Oltmans and Komhyr*, 1986; *Logan*, 1985]. At BRW, the surface O_3 increase is observed only during summer, when the rate is approximately 2% yr^{-1} [*Oltmans and Komhyr*, 1986].

The well-known occurrence of Arctic haze, the transport of middle-latitude pollution to the Arctic, is primarily a winter-spring phenomenon. During summer, measurements of inert continental tracers such as ^{210}Pb [*Larsen and Feely*, 1986], chlorinated hydrocarbons, and chlorofluorocarbons [*Khalil and Rasmussen*, 1984] indicate that long-range transport to the Arctic from the middle-latitudes is least efficient. This observation has prompted the suggestion that Arctic sources of NO_x may be responsible for the observed Barrow surface O_3 increase [*Jaffe and Honrath*, 1988].

2. EXPERIMENTAL DETAILS

Measurements of NO and NO_y (sum of all reactive nitrogen oxides, $NO+NO_2+HNO_3+PAN+...$) were conducted at the GMCC BRW site during July and August 1988, using a high-sensitivity chemiluminescent instrument built at the University of Alaska, similar in design to that previously reported [*Kley and McFarland*, 1980; *Ridley et al.*, 1987]. Measurements of NO_y were conducted by means of thermal conversion of the NO_y compounds to NO at 375°C on a commercially available molybdenum mesh converter. A flow diagram of the chemiluminescent instrument used for these measurements is shown in Figure 1.

This was the first field measurement campaign attempted with this instrument, and overall we were pleased with the result. However, several problems were encountered that limit the accuracy of the data. A variable instrument artifact was observed, which was not corrected by the zeroing process. This artifact was observed to be approximately ±50 pptv, limiting the absolute accuracy of the data to approximately this level. Additionally, uncertainties in conversion efficiency limit the NO_y accuracy to approximately 30%. Design changes in the chemiluminescent instrument were made that reduce these uncertainties considerably.

In addition to the data quality, a primary concern in the development of this instrument is that it be able to run with minimal supervision. To this end, data collection, calibration, and zeroing functions are all performed automatically by a PC-AT (286) microcomputer. During the approximately 6-week summer 1988 measurement campaign, University of Alaska personnel were on site for approximately 3 weeks. After this
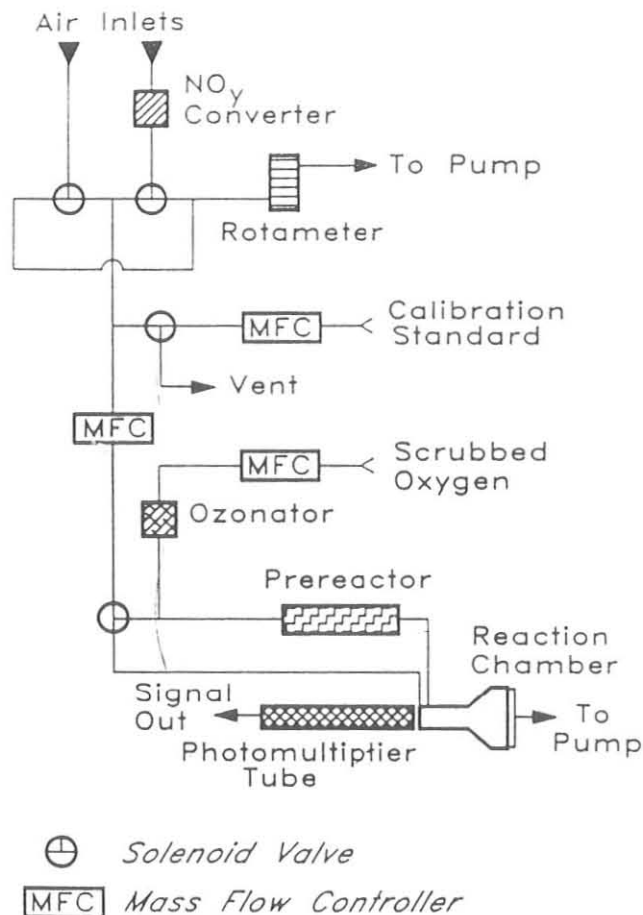
Fig. 1.   Schematic of the NO/NO_y chemiluminescent instrument.

initial period, GMCC personnel performed minor daily checks on the instrument.

3. RESULTS

During the summer of 1988, an unusual predominance of winds with a southwesterly component was observed, resulting in a number of observations with very high NO and NO_y concentrations, presumably due to local emissions from the town of Barrow. A time series of the hourly-averaged measured NO and NO_y concentrations is shown in Figure 2. Maximum concentrations of NO and NO_y of 6.5 ppbv and 13.7 ppbv were observed, corresponding to locally polluted air.

However, despite the unfavorable wind conditions, a large number of very low concentrations were observed. Because the chemiluminescent instrument makes numerous repetitive measurements during each 100-s cycle, we can screen the data
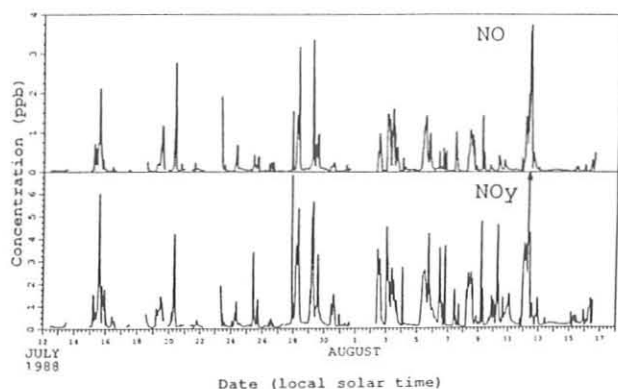
Fig. 2. Hourly averages of the unscreened NO and NO_y data.
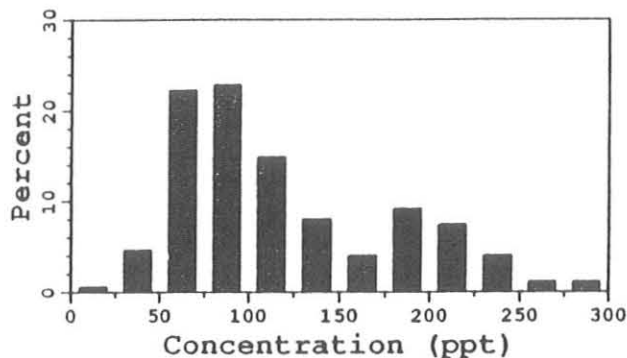
Fig. 3. Histogram of the screened (clean-sector) NO_y measurements.

on the basis of the observed variability (as compared with what we would expect due to photon-counting statistics alone). Those observations with high variability are very likely contaminated by local pollution [Bodhaine et al., 1981]. Screening the data for high variability reduces the incidence of high NO and NO_y concentrations considerably. Additionally, we can use only data from the local "clean air" sector between 45° and 130° [Bodhaine et al., 1981]. Figure 3 is a histogram of the data screened by variability and wind direction. The median, mean, and standard deviation of the NO_y concentrations from the clean-air sector are 100, 120, and 60 pptv. NO concentrations in the clean-air sector were generally below our detection limit (50 pptv), having a maximum of 100 pptv.

A small, but statistically significant diurnal trend was observed, greater NO_y concentrations being observed during the day. The mean daytime NO_y concentration is 140 pptv, approximately 40 pptv greater than at night.

4. DISCUSSION AND FUTURE WORK

NO_y concentrations observed at BRW in the clean-air sector during summer 1988 were generally very low, and comparable with those at other remote locations where similar measurements have been conducted. During this measurement period, no evidence for pollution sources outside of the BRW vicinity was observed. The diurnal cycle of NO_y concentrations at BRW may have several causes, including the following:

(1) Biogenic production of NO_y compounds.
(2) Diurnal changes in the mixed layer.
(3) A diurnal cycle in fog scrubbing of water soluble NO_y species (e.g., HNO_3).

Measurements of these important compounds at BRW will continue during 1989 and 1990 as an aid to elucidating atmospheric chemical pathways and processes.

REFERENCES

Bodhaine, B.A., J.M. Harris, and G.A. Herbert, Aerosol light scattering and condensation nuclei measurements at Barrow, Alaska, *Atmos. Environ., 15*, 1375-1389, 1981.

Fishman, J., S. Solomon, and P.J. Crutzen, Observational and theoretical evidence in support of a significant, in-situ photochemical source of tropospheric ozone, *Tellus, 31*, 432-446, 1979.

Jaffe, D.A., and R.E. Honrath, Ozone in the Arctic troposphere, American Geophysical Union, Fall Meeting, San Francisco, December 1988, *EOS, 69(44)*, 1078, 1988.

Khalil, M.H.K., and R.A. Rasmussen, Statistical analysis of trace gases in the Arctic, *Geophys. Res. Lett., 11*, 437-440, 1984.

Kley, D., and M. McFarland, Chemiluminescence detector for NO and NO_2, *Atmos. Technol., 12*, 63-69, 1980.

Larsen, R., and H. Feely, Seasonal variation of ^{210}Pb and ^7Be at Mauna Loa and Barrow, *Geophysical Monitoring for Climatic Change, No. 14: Summary Report 1985*, NOAA Air Resources Laboratory, Boulder, CO, 1986.

Liu, S.C., M. Trainer, F.C. Fehsenfeld, D.D. Parrish, E.J. Williams, D.W. Fahey, G. Hubler, and P.C. Murphy, Ozone production in the rural troposphere and the implications for regional and global ozone distributions, *J. Geophys. Res., 92*, 4191-4207, 1987.

Logan, J.A., Tropospheric ozone: Seasonal behavior, trends, and anthropogenic influences, *J. Geophys. Res., 90*, 10,463-10,482, 1985.

Oltmans, S., and W.D. Komhyr, Surface ozone distributions and variations from 1973-1984 measurements at the NOAA Geophysical Monitoring for Climatic Change baseline observatories, *J. Geophys. Res., 91*, 5229-5236, 1986.

Ridley, B.A., M.A. Carroll, and G. L. Gregory, Measurements of nitric oxide in the boundary layer and free troposphere over the Pacific Ocean. *J. Geophys. Res., 92*, 2025-2047, 1987.

Estimates of Uncertainty in Trajectory Ensembles

JONATHAN D. KAHL

NRC Research Associate, NOAA/GMCC, Boulder, Colorado 80303

1. INTRODUCTION

A modeled trajectory represents the estimated pathway of an individual air parcel. An ensemble of trajectories represents a time-history, or climatology, of air parcel transport. Although individual trajectories have known uncertainties resulting from spatial and temporal interpolation of meteorological data [*Kahl and Samson*, 1986], trajectory ensembles are thought to benefit from the partial cancellation of random interpolation errors. The purpose of this paper is to demonstrate a means for estimating the residual uncertainty in trajectory ensembles.

We followed a concept introduced by *Samson and Moody* [1981] that considers a trajectory to be the center of mass of a locus of possible paths. Figure 1 shows 1000 stochastic trajectory endpoints clustered about an analytical trajectory based on a simple, artificial wind field (a 5 m s^{-1} westerly wind over the entire domain, invariant with time). The stochastic trajectories were generated by randomly perturbing the wind field, using statistical properties of wind interpolation errors [*Kahl and Samson*, 1986]. Note that the cluster of trajectory endpoints diffuses as it is advected from the point of origin. The diffusing clusters depict the increasing error, with time, in modeled trajectories using interpolated data.

The alongwind and crosswind error diffusivities K_x and K_y, derived from the spread of the normally-distributed stochastic trajectory endpoints as a function of time, are 1.5×10^5 m^2 s^{-1} and 2.0×10^5 m^2 s^{-1}, respectively. The lateral trajectory error diffusivity K_y is 4 times greater than the large-scale eddy
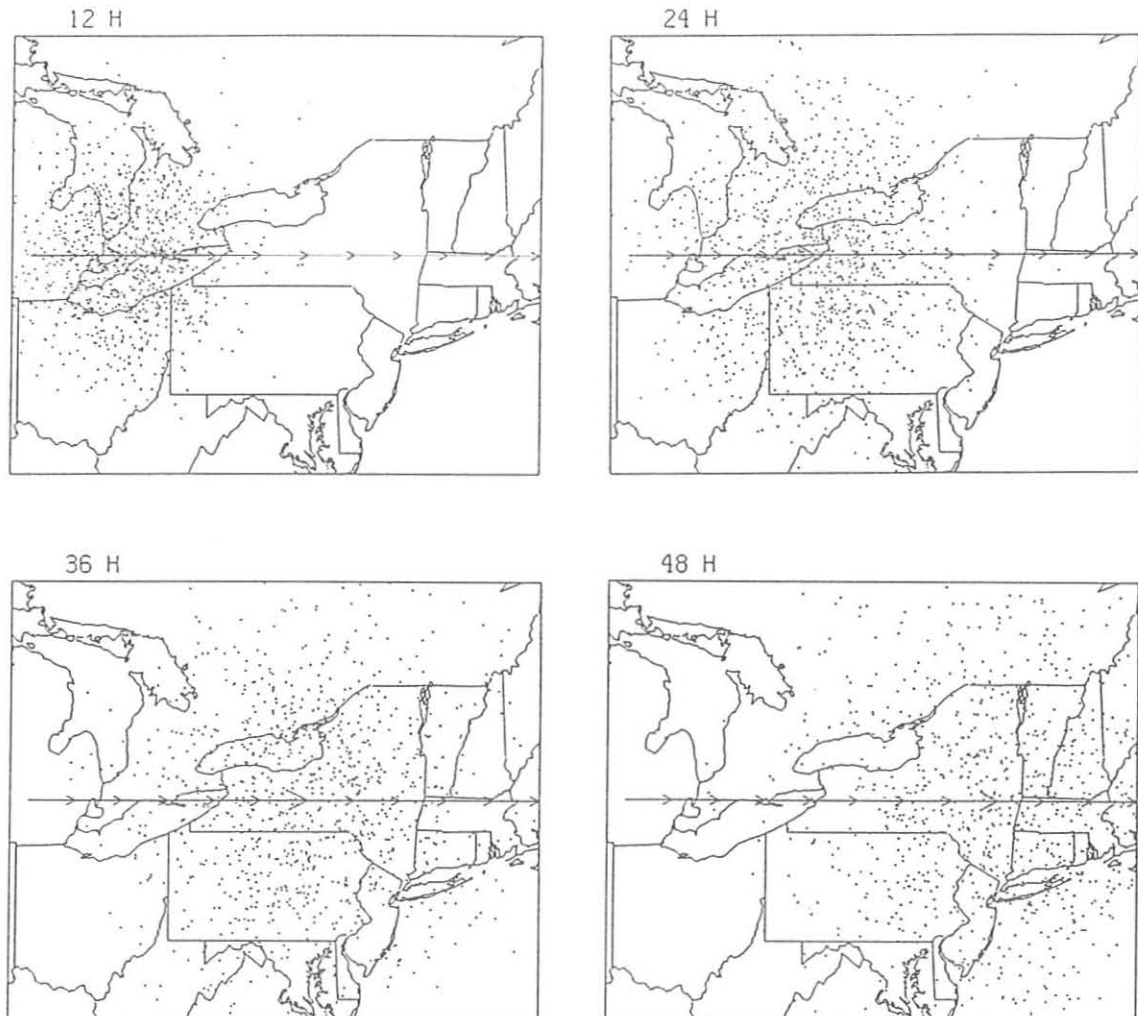

Fig. 1. Stochastic trajectory endpoints after 12, 24, 36, and 48 hours of simulated travel. The solid line is the analytical trajectory; arrows are drawn at 6 h intervals. The largest arrow on each trajectory indicates the "true" location.

diffusivity reported in *Gifford's* [1977] summary of tropospheric diffusion data. This implies that the downwind spread of estimated trajectory endpoints is twice as great as the dispersion of material about a trajectory. This result has important implications for the confidence that one may place in trajectory ensembles.

In describing atmospheric transport, trajectories represent the mean pathway of a cloud of windborne material. Turbulent diffusion causes the cloud dimensions to grow with time. Since the uncertainty in estimating the center of mass of a cloud of airborne material (i.e., the trajectory) is greater than the diffusive spread of material about that center of mass, there must be an upper limit to the accuracy of long-range atmospheric transport and diffusion calculations based on trajectory ensembles. In other words, even if it were possible to estimate diffusion with complete accuracy, a certain amount of error would still remain because of the uncertainty in estimating trajectories.

2. METHODOLOGY

A model was developed to define the uncertainty in trajectory ensembles as applied to the estimation of impact areas downwind of a passive, nondepositing atmospheric pollutant source. Full details and equations were given by *Kahl* [1989].

The model estimates the percent accuracy, or confidence, in the identification of impact areas downwind of a continuous pollution point source. We begin with the stochastic trajectory ensemble shown in Figure 1. Each stochastic trajectory has a probability of occurrence that decreases isotropically from the "true" trajectory. At discrete times downwind of the pollutant source, each endpoint is assumed to represent the center of a two-dimensional Gaussian probability field describing the possible location of the pollutant cloud. Beginning at gridded intervals within each probability field, the cloud is allowed to diffuse at rates dictated by long-range diffusion theory [*Gifford*, 1982]. The probability of material impact within each grid square is the product of each trajectory's probability of occurrence and the corresponding normalized pollutant concentration, integrated over the entire ensemble of trajectories. The result is an estimate of the spatial extent of material impact from the pollution source.

The confidence that may be placed in this estimate is determined by integrating the material impact probability field over the "true" impact area. The true area is determined by applying atmospheric diffusion about the analytical trajectory only, and is necessarily smaller than the estimated impact area.

3. RESULTS

The confidence model was applied with variations in grid spacing Δh and large-scale eddy diffusivity K. A reference experiment (run 1) was conducted with $\Delta h = 80$ km, a common value used in regional air quality models [*National Research Council*, 1983], and $K = 5 \times 10^4$ m^2 s^{-1}, an average value deduced from empirical tropospheric diffusion data [*Gifford*, 1977]. Subsequent experiments are

compared with the reference experiment to determine sensitivity to these model parameters.

Results of the simulations are presented in Table 1. The average confidence for the reference experiment, run 1, was 77%. This means that the estimate of downwind material impact will account for the fate of only 77% of the pollutant emitted at the source, and that 23% of the material will be incorrectly placed outside the actual impact area.

The model is inherently sensitive to grid spacing because the trajectory probability distributions and pollutant concentrations are assumed to be uniform within each grid square. As a result, runs 2-4 (Table 1) were designed to investigate the effects of variable grid spacing on the calculations. Two distinct effects related to grid spacing are apparent. The first is that for transport times of 1 day or less, larger grid spacing resulted in greater accuracy in estimated impact areas. It is easier to accurately locate the grid cell containing the center of a pollutant cloud if the grid squares are large relative to the horizontal cloud dimensions. The average confidence values for runs 2, 3, and 4 were 72%, 81%, and 89%, respectively. Increasing Δh therefore has the effect of decreasing the area incorrectly identified as being subject to impact from a particular pollution source. It must be recognized however that the increased confidence values for runs 3 and 4 do not necessarily indicate that increasing Δh will result in a better model. On the contrary, the larger grid spacing will reduce the model's ability to identify spatial gradients in pollutant concentration.

The second effect of variable grid spacing is that the range of accuracy increases as Δh is increased. This results from the fact that the impact probability is assessed at discrete locations in time and space. As the transport time increases, the modeled pollutant cloud diffuses and occupies a larger area. With grid spacing as large as 320 km (run 4), several time steps may be required before the cloud "jumps" into an adjacent grid cell.

The large-scale eddy diffusivity K governs the rate of horizontal diffusion. *Barr and Gifford* [1987] noted that in individual long-range diffusion events, K values may differ from the average value of 5×10^4 m^2 s^{-1} reported by *Gifford* [1977] by as much as a factor of 2. Model runs 5-9 were thus designed to

Table 1. Confidence Model Results for
Transport Times of 1-5 Days

Run	Δh* (km)	K† (m^2 s^{-1})	Confidence				
			1	2	3	4	5
1	80	5.0×10^4	73	79	77	77	78
2	40	5.0×10^4	68	70	74	75	71
3	160	5.0×10^4	94	74	82	72	81
4	320	5.0×10^4	100	90	75	93	88
5	80	2.0×10^4	54	53	56	46	52
6	80	3.0×10^4	52	69	69	58	62
7	80	4.0×10^4	74	67	67	68	71
8	80	1.0×10^5	84	91	87	90	89
9	80	1.5×10^5	90	93	93	94	93

*Horizontal grid spacing.
†Large-scale eddy diffusivity.

investigate the effects of varying the large-scale eddy diffusivity K. In runs 5, 6, and 7, the K value used in the reference experiment (run 1) was scaled by factors of 0.40, 0.60, and 0.80, respectively. In runs 8 and 9, K was scaled by factors of 2.0 and 3.0. The results in Table 1 show that as K approaches the values of the trajectory error diffusivities K_x and K_y (1.5×10^5 and 2.0×10^5 m^2 s^{-1}), the accuracy in estimated impact areas approaches 100% as an upper limit. In other words, the accuracy is limited as long as the spread of estimated trajectory endpoints is appreciably greater than the diffusive spread of material about the trajectories.

4. SUMMARY

Several recent studies have demonstrated that interpolation of routine meteorological data introduces errors into individual trajectory calculations. These errors are expected to decrease with the use of trajectory ensembles of increasing size. In this paper a model is described that allows quantitative calculation of the confidence that may be placed in estimates of impact areas downwind of a pollutant source. The upper limit to this confidence is 75%, although considerable sensitivity to horizontal grid spacing and large-scale diffusivity was observed.

Future work will focus on model verification using observed long-range diffusion data.

REFERENCES

Barr, S., and F.A. Gifford, The random force theory applied to regional scale tropospheric diffusion, *Atmos. Environ., 21*, 1737-1741, 1987.

Gifford, F., Tropospheric relative diffusion observations, *J. Appl. Meteorol., 16*, 311-313, 1977.

Gifford, F.A., Horizontal diffusion in the atmosphere: A Lagrangian-dynamical theory, *Atmos. Environ., 16*, 505-512, 1982.

Kahl, J.D., Confidence limits on source-receptor relationships determined by ensemble trajectory analysis, *Proceedings, 6th Joint Conference on Applications of Air Pollution Meteorology*, American Meteorological Society, Boston, 1989.

Kahl, J.D., and P.J. Samson, Uncertainty in trajectory calculations due to low resolution meteorological data, *J. Climate Appl. Meteorol., 25*, 1816-1831, 1986.

National Research Council, *Acid Deposition - Atmospheric Processes in Eastern North America: A Review of Current Scientific Understanding*, 375 pp., National Academy Press, Washington, DC, 1983.

Samson, P.J., and J.L. Moody, Trajectories as two-dimensional probability fields, in *Air Pollution Modeling and its Application, Vol. I*, edited by C.D. Wispelaere, pp. 43-54, Plenum Press, New York, 1981.

Determining Regional Emissions of Aerosol Black Carbon in the Arctic

JONATHAN D. KAHL

NRC Research Associate, NOAA/GMCC, Boulder, Colorado 80303

A.D.A. HANSEN

Lawrence Berkeley Laboratory, Berkeley, California 94720

1. INTRODUCTION

Black carbon (BC), a strong absorber of visible light, is an important component of the Arctic haze aerosol. When present in the atmosphere or deposited on the snow surface, it may lead to perturbations in the solar radiation balance. Estimates of the magnitude and geographical distribution of BC emissions are needed to model their effects on radiative transfer.

Aerosol BC is introduced into the atmosphere by the combustion of carbonaceous fuels; however its emission strength is strongly dependent on the level of sophistication of the fuel combustion technology employed. The percentage of fuel carbon emitted as BC typically ranges from 0.1% for sooty diesel engines to 0.0001% for modern natural gas installations [*Hansen et al.*, 1978]. Thus the distribution of BC emissions is not a simple function of the geographical fuel usage distribution. In fact, the least quantifiable sources may be the largest contributors to regionally averaged emissions.

We present a method for estimating regional BC emissions in the Arctic that is based on the synthesis of three independent pieces of information: correlated high-resolution measurements of BC and CO_2, long-range atmospheric trajectory analyses, and tabulations of regional fuel consumption. Further details were presented by *Kahl and Hansen* [1989].

2. METHOD AND RESULTS

During spring of 1986, hourly measurements of BC and CO_2 were made at BRW. Careful screening of the data to eliminate periods of local contamination resulted in identification of seven distinct events lasting between 13 and 37 hours during which BC and CO_2 increased relative to background concentrations. These events were interpreted as the passage over the station of air masses from distant regions impacted by strong fossil-fuel emissions [*Hansen et al.*, 1989].

Linear regression of BC and CO_2 measurement pairs revealed characteristic slopes for each event. The slopes, or BC/CO_2 ratios, represent the incremental mass ratios of BC relative to CO_2. If it were possible to measure BC and CO_2 in Lagrangian transit downwind of one of these point sources, with no losses or gains en route of one species relative to another, the BC/CO_2 ratio would be preserved from the source to the measurement point. Dilution due to turbulent diffusion would change the absolute concentrations, but the increments' ratio would remain unchanged and should be indicative of the source emission characteristics.

When considering a regional source, i.e., combustion emissions over an area of about 10^6 km^2 containing many source types, BC/CO_2 ratios will be indicative of the emission characteristics of the regional mixture of combustion effluent. If selective sources or sinks do not deplete one species relative to the other, the ratios measured at a distant location will be identical to those of the emitted quantities at the upwind source region. If the source region can be located, the ratio can be multiplied by tabulated values of regional fuel consumption [*Marland et al.*, 1985] to obtain emissions characteristics, since approximately 95% of carbonaceous fuel combustion effluent is CO_2.

To a first approximation, selective sources and sinks of BC and CO_2 may be neglected during winter and spring transport across the Arctic basin [*Hansen et al.*, 1989]. During that time of year natural combustion is unlikely, precipitation scavenging is minimal, biological production of CO_2 is largely dormant, and atmosphere-ocean exchange is inhibited by widespread ice cover. If the advected air mass is diluted during transport by polluted rather than pristine air, the ratios for each air mass will evolve toward a composite mean for the two air masses. Given a time sequence of measurements, it may still be possible to infer regional source emission ratios if the contributing regions can be located.

We inspected isobaric back-trajectories [*Harris*, 1982] corresponding to the seven events described by *Hansen et al.*, 1989, and selected three cases for the present analysis. The selection process was quite restrictive and required that an an upwind source region be unambiguously identified by the trajectories [*Kahl and Hansen*, 1989]. The dates and BC/CO_2 ratios for the three cases, and the correlation of BC and CO_2 measurements are listed in Table 1. In each case there is a sizable degree of correlation between the two species, suggesting that the sampled air mass probably retained its combustion emissions characteristics during transport across the Arctic. The other four events of *Hansen et al.* [989] showed similar correlations, but their trajectories did not offer a clear indication of their upwind source regions. Note that the analysis can be applied only to clearly defined transport events passing

TABLE 1. Salient Features of Cases 1-3

Case	Date* 1986	Time* (GMT)	Duration (hours)	BC/CO_2 ratio	r†
1	March 27	0000	23	0.0099	0.92
2	April 17	0400	37	0.0077	0.62
3	April 19	0000	19	0.0064	0.74

After *Hansen et al.* [1989].
*Refers to beginning of event.
†Correlation coefficient.

over the measurement station, and not to the general archive of background measurements.

The source regions for the three cases are shown in Figure 1. Also shown are lines indicating the average transport pathways for each case, and the corresponding travel times from the source regions to BRW. The trajectories for case 1 show that the air sampled at BRW originated in the Taymyr Peninsula/Novaya Zemlya regions of the U.S.S.R. some 4-8 days earlier. The BC/CO_2 ratio for this case was 0.0099%. Trajectories for case 2 initially tracked eastward from BRW before crossing the central polar basin toward the Soviet Arctic coast. After crossing the coast, the tracks turned westward and traversed a large sector of northern Siberia. Travel time from the indicated source area to BRW was 7-9 days. The BC/CO_2 ratio for this case was 0.0077%. Air sampled during case no. 3 represents background Arctic air. The trajectories track eastward across the Queen Elizabeth Islands before stalling in the central polar basin 8-10 days earlier. The BC/CO_2 ratio for this case was 0.0064%.

Cases 1-3 are ordered in terms of decreasing BC/CO_2 ratios. According to *Hansen et al.* 1989, [their Table I], these values are representative of a range of combustion types including automobiles, and natural gas and coal-fired power plants. The presence of these emission types in the Arctic is well known [*Halter et al.*, 1985], suggesting that the assumptions discussed earlier may be appropriate in these cases.

Cases 1-3 are also ordered in terms of increasing travel time from potential source regions. Case 1 involved transport over a period of 4-8 days. Because carbonaceous fuel combustion processes release at least 95% of the fuel carbon as CO_2, we can estimate the regional emission of aerosol black carbon by multiplying the BC/CO_2 ratio of 0.0099% by the estimates of total carbon consumption provided by *Marland et al.* [1985].

The results of this calculation imply annual BC emissions for the source region of about 10^8 g yr^{-1}. It should be noted that this represents a preliminary estimate subject to verification by similar analyses of an extended data base.

Transport events such as case 1, with fairly rapid, well-defined flow to a region with known combustion emissions, represent potentially useful cases for estimating upwind BC emissions. This example was linked to one geographic region by its particular trajectory; over a longer period, back-trajectories from any observation point within the Arctic can cover a large number of candidate source regions. Given a longer time series (>1 year) of correlated, high-resolution BC and CO_2 measurements, emissions for a number of upwind regions could be mapped. In addition, the variability in BC/CO_2 ratios and in transport times from a particular region could be used to evaluate the statistical confidence that may be placed in the emissions estimates.

The BC/CO_2 ratio for case 3, 0.0064%, was about two-thirds of the value for case 1. This type of transport event is useful for estimating the background levels of combustion-derived BC and CO_2 within the polluted Arctic air mass.

The BC/CO_2 ratio for case 2, 0.0077%, was midway between those for cases 1 and 3. Possible explanations include (1) that this ratio is characteristic of emissions from northern Siberia that differ from those of the Taymyr Peninsula region (case 1), (2) that the sampled air initially had emission ratios similar to case 1 but was diluted during transport with polluted air having different combustion emissions characteristics, and (3) that the assumption of no selective losses or gains may not be appropriate over this time scale (7-9 days), and that the decay of the BC numerator in the ratio may lead to a means for estimating the lifetime of BC aerosols in the winter and spring Arctic. When a longer time series of gas and aerosol measurements becomes available, episodes of this type may be compared with episodes similar to cases 1 and 3 to evaluate these hypotheses.

The preliminary results reported here suggest that this technique is a viable means for mapping regional black carbon emissions at Arctic latitudes. It is expected that the measurements needed to corroborate and expand these results will be available for at least one Arctic location within the next few years.

REFERENCES

Halter, B.C., J.M. Harris and K.A. Rahn, A study of winter variability in carbon dioxide and Arctic haze aerosols at Barrow, Alaska, *Atmos. Environ., 19*, 2033-2037, 1985.

Hansen, A.D.A., W.H. Benner, and T. Novakov, A carbon and lead emission inventory for the greater San Francisco Bay area, *Atmospheric Aerosol Research Annual Report LBL-8696, 1977-1978*, pp. 126-131, Lawrence Berkeley Laboratory, Berkeley, CA, 1978.

Hansen, A.D.A., T.J. Conway, L.P. Steele, B.A. Bodhaine, K.W. Thoning, P. Tans, and T. Novakov, Correlations among combustion effluent species at Barrow, Alaska: Aerosol black carbon, carbon dioxide, and methane, *J. Atmos. Chem.*, in press, 1989.

Harris, J.M., The GMCC atmospheric trajectory program, *NOAA Tech. Memo. ERL ARL-116*, 30 pp., NOAA, Air Resources Laboratory, Silver Spring, MD, 1982.

Kahl, J.D., and A.D.A. Hansen, Determination of regional sources of aerosol black carbon in the Arctic, *Geophys. Res. Lett., 16*, 327-330, 1989.

Marland, G., R.M. Rotty, and N.L. Treat, CO_2 from fossil fuel burning: Global distribution of emissions, *Tellus, 37B*, 243-258, 1985.
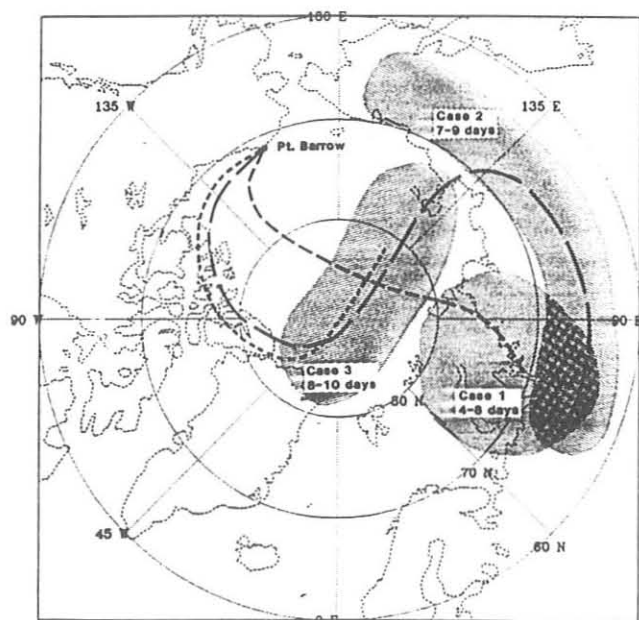
Fig. 1. Approximate upwind locations of air masses sampled at BRW, determined by examination of 850- and 700-mb isobaric back-trajectories, and corresponding travel times from the sources to BRW. Each plotted line represents an average trajectory for the ensemble: medium-dashed, case 1; long-dashed, case 2; short-dashed, case 3.

The Global Precipitation Chemistry Project

WILLIAM C. KEENE, KRYSTYNA GORZELSKA, AND JAMES N. GALLOWAY

University of Virginia, Charlottesville, Virginia 22903

GENE E. LIKENS

Institute of Ecosystem Studies, Cary Arboretum, Millbrook, New York 12545

JOHN M. MILLER

NOAA, Air Resources Laboratory, Silver Spring, Maryland 20910

1. INTRODUCTION

Anthropogenic emissions of SO_2 and NO_x have resulted in widespread acidification of precipitation and subsequent environmental damage in eastern North America and northern Europe. Of numerous research questions posed by this phenomenon, two are of special interest: (1) What was the composition of precipitation prior to the advent of fossil-fuel combustion? (2) To what degree does the long-distance transport of sulfur and nitrogen species influence the composition of the remote troposphere? The GPCP was initiated in 1979 to address these questions. Principal objectives are to measure the chemical composition of precipitation in remote areas of the world and to determine major processes controlling measured composition. Earlier reports of the GPCP compare the composition of precipitation in remote and impacted regions [*Galloway et al.*, 1982; 1984; 1987]; quantify the importance of, evaluate sources of, and intercompare measurement techniques for carboxylic acids in the atmosphere [*Keene et al.*, 1983; 1989a; *Keene and Galloway*, 1984a, b; 1985; 1986; 1988); assess factors controlling the chemical composition of precipitation at remote locations [*Jickells et al.*, 1982; *Church et al.*, 1982; *Galloway and Gaudry*, 1984; *Dayan et al.*, 1985; *Likens et al.*, 1987]; and present objective methods for differentiating seasalt and non-seasalt (nss) constituents in marine precipitation and aerosols [*Keene et al.*, 1986; *Hawley et al.*, 1988]. This report summarizes current research and reviews more recent contributions of the project.

2. MATERIALS AND METHODS

Samples of precipitation were collected by event in scrupulously washed polyethylene containers. Immediately after collection, pH was measured, samples were treated with $CHCl_3$ to prevent biological activity, and aliquots were subsequently sent to the University of Virginia for analyses for major organic and inorganic chemical constituents. To date, we have analyzed samples of precipitation collected at 14 land-based sites during 10 oceanic cruises. Reliable techniques to quantify primary amine compounds in precipitation and aerosols were developed to study the biogeochemical cycling of organic nitrogen through the troposphere. Wet-only samples of precipitation were collected by event and recovered within 2 hours after the episode ended. Samples were immediately filtered (0.2 μ Teflon) and frozen at −20°C [*Gorzelska and Galloway*, 1989a]. Atmospheric aerosols were collected on 47-mm Teflon (Zefluor) filters mounted in polycarbonate cassettes. Sampling periods averaged 24 hours. Immediately after collection, filters were wetted with 300 μL of methanol, extracted in three successive 5 mL aliquots of deionized water, and frozen at −20°C. Results indicate that these procedures are free of significant artifacts and stabilize organic nitrogen in samples for a period of 3 months.

3. RESULTS AND DISCUSSION

3.1. AMINE COMPOUNDS IN PRECIPITATION AND ATMOSPHERIC AEROSOLS

A 1-yr data record for precipitation from central Virginia reveals a range in total amine nitrogen from 5 to 7000 nM. The highest concentrations are during the spring, and there is a marked seasonal cycle [*Gorzelska and Galloway*, 1989b]. The maximum contribution of amine to total nitrogen for precipitation in central Virginia is about a few percent, but if the observed concentrations of amine nitrogen are representative of those for precipitation in remote regions, organic nitrogen compounds may represent a significant fraction of the total wet deposition of nitrogen originating with natural sources. During July through September 1988, concentrations of amine nitrogen in precipitation over the North Atlantic Ocean ranged from 30 to 800 nM and concentrations for the particulate-phase ranged from 0.003 to 1.614 nM^{-3} (at STP) [*Gorzelska and Galloway*, 1989c]. Spatial variability was evident, higher concentrations typically being observed near the North American continent and in the vicinity of the Arctic circle. Interpretation of the data in conjunction with atmospheric back trajectories and measurements of ^{222}Rn suggests that the long-distance transport of terrestrial material and direct injection from surface sea water are important processes controlling concentrations of amine nitrogen in the marine boundary layer of the North Atlantic Ocean.

3.2. PROCESSES CONTROLLING THE CHEMICAL COMPOSITION OF PRECIPITATION NEAR LIJIANG, CHINA

In cooperation with the Chinese Environmental Protection Agency and the Yunnan Province Environmental Monitoring Station, samples of precipitation were collected by event during the 1987 and 1988 wet seasons (May through October) at an

altitude of 3270 m on the east slope of Yulong Mountain (27°12'N, 100°9'E) near Lijiang, Yunnan Province, People's Republic of China [*Keene et al.*, 1989*b*]. Results indicate a volume-weighted average H^+ expressed as pH of 5.1. On the basis of ratios of anions to H^+, the maximum contributions of H_2SO_4, HCOOH, HCl, CH_3COOH, and NHO_3 to free acidity were 35%, 27%, 25%, 23%, and 14%, respectively. Consistent anion deficits indicate that a maximum of 14% of free acidity was contributed by unmeasured anions. Trajectory analyses revealed that events associated with air masses originating over eastern China were enriched in SO_4^{2-}, NO_3^-, HCOOH, H^+, and Ca^{2+} relative to those originating over India. Indirect evidence supports the hypothesis that these differences reflect differences in air mass history, and the strength and relative proximity of anthropogenic sources. However, the ionic strength of precipitation at the site is low compared with that at other remote continental locations, suggesting that anthropogenic influences, if present, are small and that natural sources for major chemical constituents are relatively weak.

4. Ongoing Research

Research efforts currently under way within the GPCP include the following:

- Evaluation of shipboard data to determine factors controlling the atmospheric chemistry of the equatorial Atlantic Ocean during August and September 1986.
- Analysis of a 15-yr data record for precipitation chemistry at MLO.
- Assessment of processes controlling the chemical composition of precipitation at Cape Point, South Africa.
- Measurement of the relative contribution of HCOOH emissions from formacine ants to total atmospheric concentrations.
- Evaluation of linkages between the cycling of S and N in the remote atmosphere.

References

Church, T. M., J. N. Galloway, T. D. Jickells, and A. H. Knap, The chemistry of western Atlantic precipitation at the mid-Atlantic coast and on Bermuda, *J. Geophys. Res.*, *87*, 11,013-11,018, 1982.

Dayan, U., J. M. Miller, W. C. Keene, and J. N. Galloway, A meteorological analysis of precipitation chemistry data from Alaska, *Atmos. Environ.*, *19*, 651-657, 1985.

Galloway, J. N., and A. Gaudry, The chemistry of precipitation on Amsterdam Island, Indian Ocean, *Atmos. Environ.*, *18*, 2649-2656, 1984.

Galloway, J. N., G. E. Likens, W. C. Keene, and J. M. Miller, The composition of precipitation in remote areas of the world, *J. Geophys. Res.*, *87*, 8771-8786, 1982.

Galloway, J. N., G. E. Likens, and M. E. Hawley, Acid precipitation: Natural versus anthropogenic compounds, *Science*, *226*, 829-830, 1984.

Galloway, J. N., D. Zhao, J. Xiong, and G. E. Likens, Acid rain: China, United States and a remote area, *Science*, *236*, 1559-1562, 1987.

Gorzelska, K., and J. N. Galloway, Amine species in precipitation: Collection-, storage-, and analytical-routine procedures, unpublished manuscript, University of Virginia, Charlottesville, 1989*a*.

Gorzelska, K., and J. N. Galloway, Contribution of organic nitrogen from primary amine compounds to the nitrogen budget of precipitation in central Virginia, unpublished manuscript, University of Virginia, Charlottesville, 1989*b*.

Gorzelska, K., and J. N. Galloway, Global Change Studies: Phase distribution, transport and deposition of amine compounds over the North Atlantic Ocean, unpublished manuscript, University of Virginia, Charlottesville, 1989*c*.

Hawley, M. E., J. N. Galloway, and W. C. Keene, Standard error calculations for non-sea-salt constituents in marine precipitation, *Water Air Soil Pollut.*, *42*, 87-102, 1988.

Jickells, T. C., A. H. Knap, T. M. Church, J. N. Galloway, and J. M. Miller, Acid precipitation on Bermuda, *Nature*, *297*, 55-56, 1982.

Keene, W. C., and J. N. Galloway, A note on acid rain in an Amazon rainforest, *Tellus*, *36B*, 137-138, 1984*a*.

Keene, W. C., and J. N. Galloway, Organic acidity in precipitation of North America, *Atmos. Environ.*, *18*, 2491-2497, 1984*b*.

Keene, W. C., and J. N. Galloway, Gran's titrations: Inherent errors in measuring the acidity of precipitation, *Atmos. Environ.*, *19*, 199-202, 1985.

Keene, W. C., and J. N. Galloway, Considerations regarding sources for formic and acetic acids in the troposphere, *J. Geophys. Res.*, *91*, 14,466-14,474, 1986.

Keene, W. C., and J. N. Galloway, The biogeochemical cycling of formic and acetic acids through the troposphere: An overview of current understanding, *Tellus*, *40B*, 322-334, 1988.

Keene, W. C., J. N. Galloway, and D. H. Holden, Jr., Measurement of weak organic acidity in precipitation from remote areas of the world, *J. Geophys. Res.*, *88*, 5122-5130, 1983.

Keene, W. C., A. A. P. Pszenny, J. N. Galloway, and M. E. Hawley, Sea-salt corrections and interpretation of constituent ratios in marine precipitation, *J. Geophys. Res.*, *91*, 6647-6658, 1986.

Keene, W. C., R. W. Talbot, M. O. Andreae, K. Beecher, H. Berresheim, M. Castro, J. C. Farmer, J. N. Galloway, M. R. Hoffmann, S.-M. Li, J. R. Maben, J. W. Munger, R. B. Norton, A. A. P. Pszenny, H. Puxbaum, H. Westberg, and W. Winiwarter, An intercomparison of measurement systems for vapor and particulate phase concentrations of formic and acetic acids, *J. Geophys. Res.*, *94*, 6457-6471, 1989*a*.

Keene, W. C., G. Wu, R. S. Artz, J. N. Galloway, J. Liu, J. M. Harris, and J. M. Miller, Processes controlling the chemical composition of precipitation at a remote temperate continental site in south-central China, in *Proceedings of the International Conferences on Global and Regional Environmental Atmospheric Chemistry*, edited by C. S. Kiang, Beijing, PRC, in press, 1989*b*.

Likens, G. E., W. C. Keene, J. M. Miller, and J. N. Galloway, The chemistry of precipitation from a remote, terrestrial site in Australia, *J. Geophys. Res.*, *92*, 13,299-13,314, 1987.

Stratospheric Trace Gas Measurements at South Pole Station, Antarctica

J.G. KEYS AND P.V. JOHNSTON

Department of Scientific and Industrial Research, Physics and Engineering Laboratory, Lauder, New Zealand

1. INTRODUCTION

Ground-based measurements of column NO_2 and O_3, using the DAS technique, have been made by GMCC staff at SPO since 1986. They complement similar measurements that are also part of the New Zealand DSIR program and that are being made at Arrival Heights (77.8°S, 166.7°E) and at the British Antarctic Survey base at Halley Bay (76°S, 27°W).

The DAS measurement technique uses scattered sunlight in the zenith sky [Brewer et al., 1973]. The first measurements of NO_2 and O_3 made in Antarctica in this way were at Arrival Heights [McKenzie and Johnston, 1984] and showed movement of NO_2 to and from storage reservoirs under changing photochemical conditions. Interesting dynamical influences were also identified [Keys and Johnston, 1986]. The ability to examine NO_2 column changes with the sun at nearly constant zenith angle (in the short term) prompted the installation of similar equipment at SPO.

2. DISCUSSION

Trends in stratospheric column NO_2 amounts obtained using the DAS technique are usually identified by making the measurements at constant solar zenith angle (SZA), commonly 90°. This is because the observed slant column amount increases rapidly with increasing SZA, giving an enhancement of ~20 times at SZA = 90°, because of changed path length and scattering conditions.

Therefore, meaningful long-term trend analysis for data acquired at SPO, because of the unique geometry in which the condition that the SZA = 90° is satisfied only at the equinoxes, requires that data be extrapolated to constant SZA, a process requiring prior knowledge of the enhancement function. It is this feature that qualified the usefulness of the data in the long term, although this qualification may not prove to be particularly restrictive.

The extrapolated data show the way in which the location modifies the NO_2 column through changed dynamical and photochemical effects [Keys and Johnston, 1988]. The springtime increase in NO_2 at SPO is quite free from the wave-driven transport modulation that is seen in the lower latitude Arrival Heights data (Figure 1).

A particularly interesting feature in the SPO data is a quasi-diurnal variation in NO_2 observed near the equinox (Figure 2). This unexpected variation is interpreted as being the signature of a horizontal gradient in NO_2, which is seen as the tangent point moves around the site [Keys and Johnston, 1988].
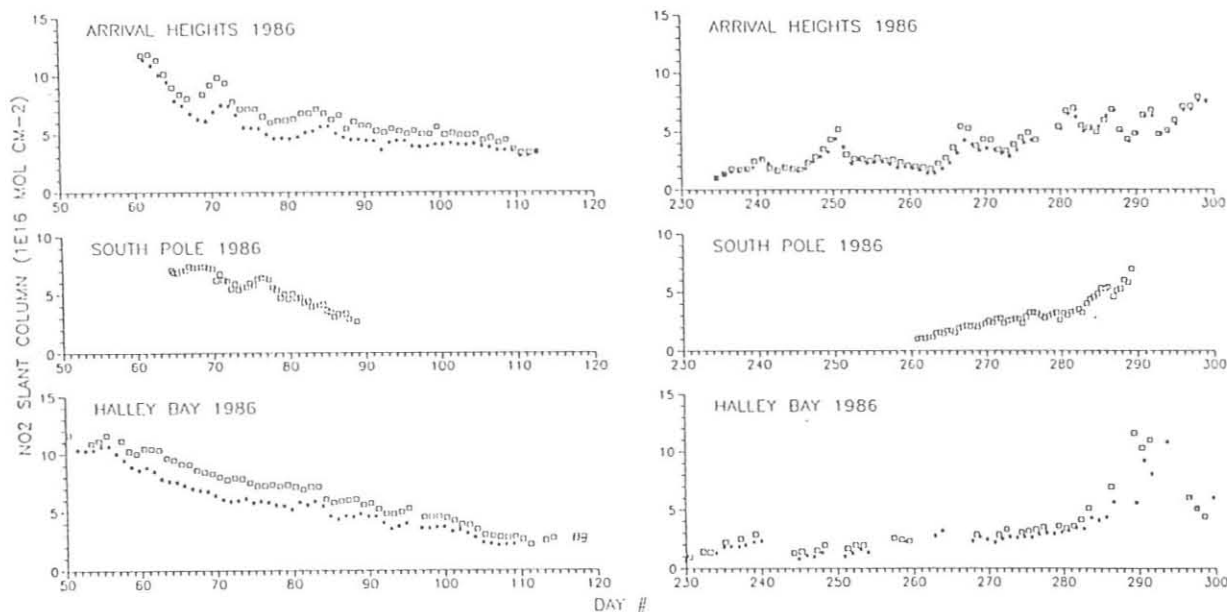
Fig 1. NO_2 slant column amounts (1×10^{16} mol cm^{-2}) for SZA = 90° (extrapolated for South Pole), 1986. Squares denote PM measurements, and asterisks denote AM measurements.
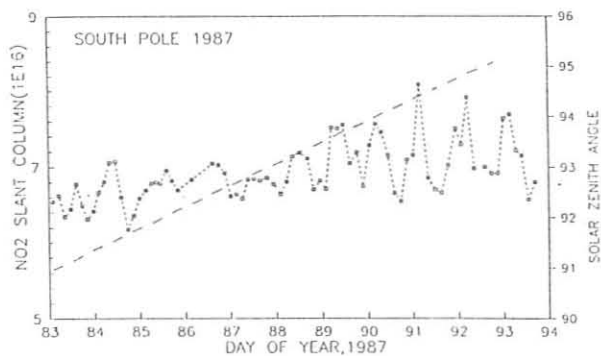
Fig 2. NO_2 slant column variations (1×10^{10} mol cm^{-2}) at SPO near the autumn equinox, 1987. The dashed line is the SZA and squares are the NO_2 slant column amounts.

REFERENCES

Brewer, A.W., C.T. McElroy, and J.B. Kerr, Nitrogen dioxide concentrations in the atmosphere, *Nature, 246*, 129-133, 1973.

McKenzie, R.L., and P.V. Johnston, Springtime stratospheric NO_2 in Antarctica, *Geophys. Res. Lett., 11*, 73-75, 1984.

Keys, J.G., and P.V. Johnston, Stratospheric NO_2 and O_3 in Antarctica: Dynamic and chemically controlled variations, *Geophys. Res. Lett., 13*, 1260-1263, 1986.

Keys, J.G., and P.V. Johnston, Stratospheric column NO_2 measurements from three Antarctic sites, *Proceedings, Polar Ozone Workshop*, Snowmass, CO, May 1988, edited by A. Atkin, pp. 115-117, *NASA CP 10014*, NASA, Washington, DC, 1988.

Distribution and Mass Balance of Molecular Hydrogen in the Earth's Atmosphere

M. A. K. KHALIL AND R. A. RASMUSSEN

Oregon Graduate Center, Institute of Atmospheric Sciences, Beaverton, Oregon 97006

1. INTRODUCTION

Molecular hydrogen (H_2) comes from the oceans, biomass and fossil fuel combustion, biological nitrogen fixation, volcanoes, and the oxidation of hydrocarbons including methane. It is removed from the atmosphere by reactions with OH in the troposphere, interactions with soils and by escaping from the atmosphere [see *Warneck*, 1988; *Schmidt*, 1974; *Crutzen et al.*, 1979; *Conrad and Seiler*, 1980].

For the last 10 years we have been taking weekly flask samples of air at seven sites spanning latitudes from the Arctic to the Antarctic (BRW; Cape Meares, Oregon; Cape Kumukahi and MLO; SMO; Cape Grim, Tasmania; and SPO). Samples are collected in 0.8-L stainless steel flasks and sent to our laboratory for analysis [*Rasmussen and Khalil*, 1980]. Measurements of H_2 have been made since 1985.

The behavior of H_2 is different from that of most trace gases observed at these sites. For instance, in the southern hemisphere the phase of the seasonal cycle of H_2 is opposite that of other gases such as CO [*Khalil and Rasmussen*, 1989]. Here we show that there is more H_2 in the southern hemisphere than in the northern hemisphere; for most trace gases, particularly gases such as H_2 that are affected by human activities, the gradient is opposite. The purpose of this paper is to document and explain the reversed gradient of H_2. We show that this behavior can be explained by the present estimates of the asymmetric latitudinal distribution of the sources and sinks in the two hemispheres.

2. LATITUDINAL DISTRIBUTION

The results reported here are based on measurements taken at the six sea-level sites (i.e., excluding MLO) between October 1985 and October 1987. We first removed the seasonal
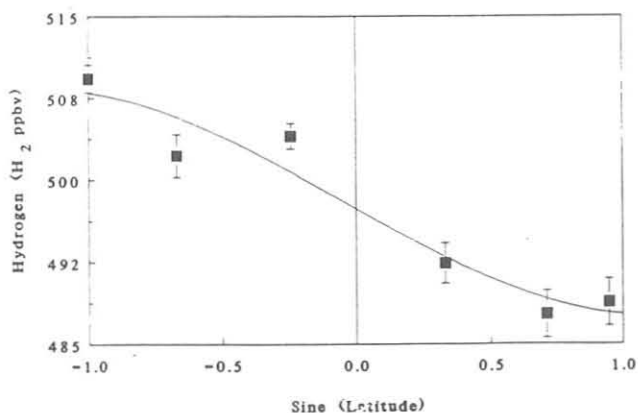

Fig. 1. The latitudinal distribution of H_2. From right to left the sites are BRW, Oregon, Hawaii, SMO, Tasmania, and SPO. Concentrations are average values of de-seasonalized time series spanning October 1985-October 1987. The vertical bars are 90% confidence limits.

variations from the monthly time series of concentrations. Then we calculated the average concentration (and 90% confidence limits) at each site over the 2-yr period. The resulting latitudinal distribution is shown in Figure 1. There is about 4% more H_2 in the Antarctic than in the Arctic.

3. SOURCES AND SINKS AND MASS BALANCE

3.1. PROCEDURES

To see whether this latitudinal distribution can be explained by the present understanding of the global H_2 budget as described by *Warneck* [1988], we constructed a mass balance model. The procedure for the calculations is as follows. We divided the atmosphere into four equal volume regions or boxes: 0°-30°N (nt, northern tropics and subtropics), 30°N-90°N (n, northern middle and polar latitudes), 0°-30°S (st), and 30°S - 90°S (s). Next, we divided the sinks proposed by *Warneck* [1988] over these four regions and estimated the sources required in each of the four regions to obtain the measured atmospheric concentrations, as in Figure 1. We then considered whether emissions from the individual sources can be made consistent with the total required source in each box. Finally, we used the latitudinal distribution of the emissions to estimate the contribution of each source to the observed concentration of H_2 in each box (source apportionment).

3.2. MODEL

The mass balance is written as

$$dC/dt = S + \Omega C \tag{1}$$

$$C_j = \sum_{k=1}^{6} C_{jk} \tag{2}$$

where C and S are (4 × 6) matrices of (calculated) concentrations C_{jk} and emissions S_{jk} in the j-th box ($j = 1, 2, 3, 4$ refer to n, nt, st, and s respectively) from the k-th source (one of the six listed in Table 1). The total concentration (which should match the observed concentration) is C_j the sum of the concentrations contributed by all the sources. H_2 is almost steady state, so we take $dC/dt \approx 0$; therefore

$$S \approx -\Omega C \tag{3}$$

$$C \approx -\Omega^{-1} S \tag{4}$$

where Ω is a (4 × 4) matrix consisting of (inverse) transport times and (inverse) atmospheric lifetimes in each of the boxes. The non-zero elements of Ω are

$$\Omega_{12} = \Omega_{21} = \Omega_{34} = \Omega_{43} = -(1/\tau_0) \tag{5a}$$

$$\Omega_{23} = \Omega_{32} = -(1/\tau_1) \tag{5b}$$

$$\Omega_{11} = (1/\Omega_0) + (1/\Omega_n) \qquad (5c)$$

$$\Omega_{22} = (1/\Omega_1) + (1/\Omega_{nt}) \qquad (5d)$$

$$\Omega_{33} = (1/\tau_0) + (1/\tau_{st}) \qquad (5e)$$

$$\Omega_{44} = (1/\Omega_0) + (1/\tau_s) \qquad (5f)$$

where τ is transport time, and in Ω_{ij}, i and $j = 1, 2, 3, 4$ refer to n, nt, st, s respectively.

3.3. RESULTS

We took τ_0 (transport time within a hemisphere) to be 1.5 months, τ_1 (transport time across nt and st, the tropical regions) to be 8 months, and the lifetimes to be as in Table 1 [see also *Khalil and Rasmussen*, 1983].

The soil sink, which is believed to be the main process for removing H_2 is taken to be proportional to the land area in each of the four regions excluding the polar ice caps. The resulting distribution of sinks is shown in Table 1.

The estimated emissions (Tg yr^{-1}) in the four boxes are $S_n = 35$, $S_{nt} = 23$, $S_{st} = 20$, $S_s = 12$ (also in Table 1). Each source is

TABLE 1. Sources, Sinks, and Concentrations of Molecular Hydrogen (H_2)

	n, 30°-90°N	nt, 0°-30°N	st, 0°-30°S	s, 30°-90°S	Total
Sources (Emissions in Tg yr^{-1})					
Anthropogenic	12	3	1	1	17
Biomass burning	5	5	4	1	15
Oceans	0	1	1	2	4
CH$_4$-oxidation	6	9	9	5	29
NMHC-oxidation	9	5	4	3	21
Other	2	1	1	0	4
Total sources	34	24	20	12	90
Calculated total sources*	35	23	20	12	90
Sinks (Lifetimes in years)					
Soil	1.2	2.5	3	6	2.4
OH	23	12	12	23	16
Other	47	47	47	47	47
Total sinks†	1.2	2	2.3	4.3	2
Global burdens (Tg)					
From measured concentrations‡	43.3	43.6	44.7	44.9	177

Global estimates taken from *Warneck* [1988], which includes results from *Schmidt* [1974], *Crutzen et al.* [1979], and *Conrad and Seiler* [1980].

*Calculated using measured concentrations.

†Total sinks: $\dfrac{1}{\tau_{total}} = \dfrac{1}{\tau_{soil}} + \dfrac{1}{\tau_{OH}} + \dfrac{1}{\tau_{other}}$

‡The conversion factor is: C (Tg in each region - 1/4 of the atmosphere) $= 0.0877 \times S$ (ppbv).

divided among the four boxes according to distributions of population, industrial activity, OH, and observed distributions of methane and nonmethane hydrocarbons. By this process the emissions from individual sources [*Warneck*, 1988] can be made consistent with the estimated total emissions in each box, as shown in Table 1.

Using Eq. (4), we estimated the contribution of each of the six sources to the total concentration of H_2 in each of the four boxes. The results are shown in Figure 2. Since the lifetimes of H_2 in the four regions are much greater than the transport times, every source contributes to concentrations in each box.

4. DISCUSSION AND CONCLUSIONS

We have shown that there is significantly more H_2 in the southern hemisphere than on the northern hemisphere. If we accept that the sink is mainly the Earth's land surface with small contributions from reactions with OH (as in Table 1), then the observed concentrations imply that the emissions must be 35 Tg yr^{-1} in the northern half of the northern hemisphere, 23 Tg yr^{-1} in the tropical and subtropical northern hemisphere, 20 Tg yr^{-1} in the southern tropics, and 12 Tg yr^{-1} in the far southern latitudes. These estimates are on fairly solid foundation, since we believe that the sinks are better known than the emissions from individual sources. We have also shown that the estimated emissions from each of six known sources of H_2 are consistent with this distribution of the total sources of H_2 among the four regions. There are, however, other combinations of emissions from the various sources and sinks that may also explain the observed latitudinal distribution.

Our calculations show that the main cause of the higher concentration of H_2 in the southern hemisphere compared with the northern hemisphere is the considerably more land surface area in the northern hemisphere over which H_2 is removed.
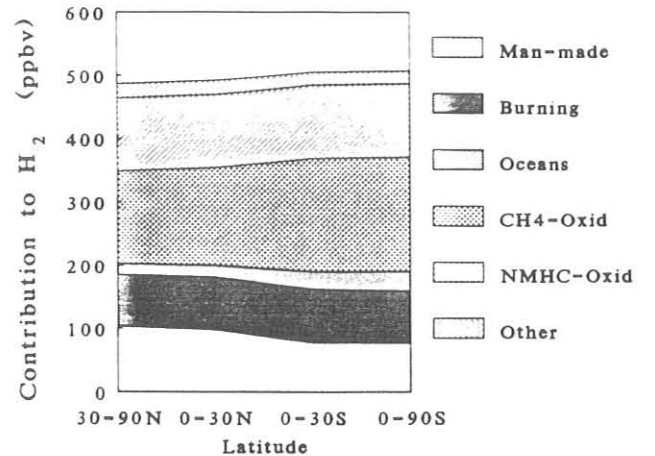
Fig. 2. Contributions of the various sources of H_2 to the atmospheric concentrations in four equal size regions of the atmosphere.

REFERENCES

Conrad, R., and W. Seiler, Contribution of hydrogen production by biological nitrogen fixation to the global hydrogen budget, *J. Geophys. Res., 85*, 5493-5498, 1980.

Crutzen, P.J., L.E. Heidt, J.P. Krasnec, W.H. Pollok, and W. Seiler, Biomass burning as a source of atmospheric trace gases, CO, H_2, N_2O, NO, $CHCl_3$, and COS, *Nature, 282*, 253-256, 1979.

Khalil, M.A.K., and R.A. Rasmussen, Sources, sinks and seasonal cycles of atmospheric methane, *J. Geophys. Res., 88*, 5131-5144, 1983.

Khalil, M.A.K., and R.A.Rasmussen, Seasonal cycles of hydrogen and carbon monoxide in the polar regions: Opposite phase relationships, *Ant. J. U. S., 23(5)*, 177-178, 1989.

Rasmussen, R.A., and M.A.K. Khalil, Atmospheric halocarbons: Measurements and analyses of selected trace gases, in *Proceedings of the NATO Advanced Study Institute on Atmospheric Ozone: Its Variations and Human Influences*, edited by A.C. Aikin, Dept. of Transportation, Washington, DC, 1980.

Schmidt, U., Molecular hydrogen in the atmosphere, *Tellus, 26*, 78-90, 1974 (Errata, *Tellus, 27*, 93-94, 1975).

Warneck, P., *The Chemistry of the Natural Atmosphere*, Academic Press, N.Y., 1988.

Radioactivity in the Surface Air at BRW, MLO, SMO, and SPO

RICHARD LARSEN AND COLIN SANDERSON

U.S. Department of Energy, Environmental Measurements Laboratory, New York, New York 10014-3621

1. INTRODUCTION

Air filter samples are routinely collected by GMCC personnel at BRW, MLO, SMO, and SPO for the SASP. The primary objective of this program is to study the temporal and spatial distribution of specific natural and manufactured radionuclides in the surface air. Two naturally occurring radioisotopes, ^{7}Be and ^{210}Pb, are continually detectable in the atmosphere. ^{7}Be (half-life 53.2 days) is produced by cosmic-ray interactions in the upper troposphere and the stratosphere. ^{210}Pb (half-life 21 years) is a decay product of ^{222}Rn, which is a natural radioisotope emitted from soils. Because of their distinctly different source regions, these nuclides serve as excellent tracers for upper and lower tropospheric sources and transport processes.

2. MATERIALS AND METHODS

High-volume air filter samples are continually collected on a weekly basis using Microdon filter material. The air samplers move ~1500 m³ of air per day through a 20-cm-diameter filter.

The weekly filter samples collected at BRW and MLO are analyzed by compressing a section of the filter into a 1-2 cm³ cylinder, which is analyzed by gamma-ray spectrometry using a high-purity germanium (HPGe) detector with a 1.5-cm-diameter well. For each site, sections of the weekly filter samples are added to form a monthly composite sample. These composite samples are compressed into a 45-cm³ plastic planchet, and are analyzed for gamma-ray-emitting nuclides using either HPGe n-type low-energy coaxial, or Ge(Li) or HPGe p-type coaxial

high resolution germanium detectors. Detailed information on SASP is periodically published [Feely et al., 1988].

3. RESULTS

Table 1 presents the long-term mean monthly surface air concentrations of ^{7}Be and ^{210}Pb at BRW, MLO, SMO, and SPO. Table 2 presents the surface air concentrations of ^{7}Be and ^{210}Pb in weekly filter samples collected at BRW and MLO during 1988. Table 3 presents the surface air concentrations of ^{7}Be and ^{210}Pb in monthly composite filter samples from SPO and ^{7}Be monthly concentrations from SMO, during 1988.

4. DISCUSSION

There were no announced atmospheric nuclear weapons tests or other significant releases of radioactive materials into the atmosphere during 1988, and the concentrations of fission products such as ^{95}Zr, ^{137}Cs, and ^{144}Ce were below the lower limits of detection by the techniques that we currently use to measure them.

The weekly concentrations of ^{7}Be and ^{210}Pb at BRW and MLO continue to show week-to-week variations superimposed on a seasonal cycle. Elevated ^{7}Be at MLO during the periods from ^{210}Pb source regions. The monthly concentrations of ^{7}Be measured at SPO and SMO during 1988 continue to follow the long-term trends, but the concentrations measured at SPO are significantly lower than those previously reported.

The long-term monthly mean concentrations of ^{7}Be continue to show a seasonal cycle at all GMCC sites, and ^{210}Pb has a seasonal cycle at BRW and MLO.

TABLE 1. Long-Term Monthly Mean Concentrations (fCi m^{-3}; ±1s) of ^{7}Be at BRW, MLO, SMO, and SPO, and ^{210}Pb at BRW, MLO, and SPO

| Month | ^{7}Be | | | | | | | | ^{210}Pb | | | | | |
	BRW		MLO		SMO		SPO		BRW		MLO		SPO	
	66 ± 19	(12)	228 ± 56	(18)	59 ± 24	(12)	164 ± 38	(18)	24 ± 7	(7)	8 ± 5	(11)	1 ± 1	(10)
Feb.	64 ± 20	(13)	196 ± 51	(19)	57 ± 14	(12)	144 ± 59	(12)	21 ± 9	(8)	9 ± 3	(12)	1 ± 1	(8)
March	72 ± 20	(12)	221 ± 44	(17)	54 ± 12	(12)	139 ± 61	(15)	21 ± 9	(7)	11 ± 3	(10)	1 ± 1	(8)
April	74 ± 19	(11)	205 ± 47	(16)	48 ± 11	(12)	101 ± 35	(14)	18 ± 6	(6)	14 ± 5	(10)	1 ± 1	(7)
May	55 ± 10	(13)	207 ± 40	(17)	65 ± 18	(13)	108 ± 72	(15)	9 ± 3	(7)	16 ± 7	(9)	1 ± 1	(8)
June	26 ± 7	(13)	222 ± 37	(17)	77 ± 25	(13)	77 ± 29	(17)	3 ± 1	(8)	13 ± 4	(10)	1 ± 1	(8)
July	24 ± 7	(12)	210 ± 38	(16)	89 ± 17	(13)	90 ± 37	(16)	3 ± 1	(8)	10 ± 3	(10)	1 ± 1	(7)
Aug.	19 ± 6	(11)	193 ± 48	(17)	86 ± 23	(12)	81 ± 28	(18)	2 ± 1	(7)	9 ± 2	(11)	1 ± 1	(8)
Sept.	27 ± 5	(14)	183 ± 50	(17)	89 ± 16	(12)	88 ± 27	(18)	4 ± 2	(8)	8 ± 3	(11)	1 ± 1	(9)
Oct.	41 ± 13	(14)	179 ± 33	(18)	78 ± 20	(12)	97 ± 21	(19)	9 ± 3	(9)	9 ± 4	(12)	1 ± 1	(9)
Nov.	56 ± 16	(13)	155 ± 52	(18)	78 ± 30	(13)	137 ± 38	(17)	15 ± 8	(8)	7 ± 3	(13)	2 ± 2	(9)
Dec.	52 ± 20	(12)	206 ± 55	(18)	58 ± 16	(12)	163 ± 49	(17)	22 ± 10	(7)	7 ± 3	(11)	2 ± 1	(9)
Mean	48 ± 23	(150)	200 ± 50	(208)	70 ± 24	(148)	115 ± 52	(196)	12 ± 10	(90)	10 ± 5	(130)	1 ± 1	(100)

The number of data points used to calculate each value is given in parentheses.

TABLE 2. Weekly Surface Air Concentrations (fCi m^{-3}) of ^{7}Be and ^{210}Pb at BRW and MLO During 1988

Sampling Interval, 1988	^{7}Be	^{210}Pb		Sampling Interval, 1988	^{7}Be	^{210}Pb
			BRW			
Dec. 29*–Jan. 4	43	6		June 8–June 13	65	5
Jan. 4–Jan. 13	38	4		June 13–June 28	9	1
Jan. 13–Jan. 20	70	24		June 28–July 14	36	3
Jan. 20–Jan. 25	49	28		July 14–July 19	17	3
Jan. 25–Feb. 1	62	27		July 19–Aug. 2	18	2
Feb. 1–Feb. 8	57	11		Aug. 2–Aug. 10	19	2
Feb. 8–Feb. 17	21	20		Aug. 10–Aug. 17	8	1
Feb. 17–Feb. 22	54	16		Aug. 17–Aug. 26	8	1
Feb. 22–March 4	40	10		Aug. 26–Aug. 30	18	2
March 4–March 8	55	12		Aug. 30–Sept. 6	31	3
March 8–March 15	59	17		Sept. 6–Sept. 13	16	2
March 15–March 21	69	23		Sept. 13–Sept. 21	8	1
March 21–March 29	68	24		Sept. 21–Sept. 29	15	2
March 29–March 31	73	28		Sept. 29–Oct. 6	24	4
March 31–April 5	46	21		Oct. 6–Oct. 12	17	4
April 5–April 11	70	22		Oct. 12–Oct. 20	26	6
April 11–April 18	68	7		Oct. 20–Nov. 1	31	5
April 18–April 26	80	13		Nov. 1–Nov. 9	40	14
April 26–May 3	59	7		Nov. 9–Nov. 22	32	13
May 3–May 10	41	13		Nov. 22–Nov. 30	71	24
May 10–May 19	59	6		Nov. 30–Dec. 6	38	25
May 19–May 24	44	3		Dec. 6–Dec. 26		
May 24–June 8	19	1				
			MLO			
Dec. 31*–Jan. 8	459	8		July 1–July 9	163	7
Jan. 8–Jan. 15	253	7		July 9–July 15	226	12
Jan. 15–Jan. 22	255	5		July 15–July 22	220	9
Jan. 22–Feb. 1	346	10		July 22–Aug. 1	188	7
Feb. 1– Dec. 8	483	12		Aug. 1–Aug. 8	111	4
Feb. 8–Feb. 16	241	8		Aug. 8–Aug. 15	111	3
Feb. 16–Feb. 22	250	13		Aug. 15–Aug. 22	207	4
Feb. 22–March 2	176	10		Aug. 22–Sept. 1	231	7
March 2–March 8	193	11		Sept. 1–Sept. 8	91	4
March 8–March 15	246	16		Sept. 8–Sept. 15	19	28
March 15–March 22	222	12		Sept. 15–Sept. 22	276	6
March 22–April 1	196	10		Sept. 22–Sept. 30	141	3
April 1–April 8	211	10		Sept. 30–Oct. 7	262	7
April 8–April 15	257	13		Oct. 7–Oct. 14	283	13
April 15–April 22	282	18		Oct. 14–Oct. 21	192	5
April 22–April 30	161	13		Oct. 21–Nov. 2	247	11
April 30–May 6	205	13		Nov. 2–Nov. 9	134	6
May 6–May 13	114	6		Nov. 9–Nov. 16	224	6
May 13–May 21	248	18		Nov. 16–Nov. 23	246	5
May 21–June 1	245	18		Nov. 23–Dec. 1	274	6
June 1–June 8	428	18		Dec. 1–Dec. 8	193	7
June 8–June 17	125	6		Dec. 8–Dec. 15	100	3
1,2,3 17–June 22	485	21		Dec. 15–Dec. 23	124	3
June 22–July 1	101	6		Dec. 23–Dec. 30	167	4

*1987.

TABLE 3. Monthly Surface Air Concentrations (fCi m^{-3})
of ^{7}Be at SMO and SPO, and ^{210}Pb at SPO During 1988

	^{7}Be		^{210}Pb		^{7}Be		^{210}Pb
Month	SMO	SPO	SPO	Month	SMO	SPO	SPO
Jan.	37	88	<1	July	80	31	1
Feb.	73	106	1	Aug.	65	35	<1
March	68	86	1	Sept.	70	39	<1
April	28	53	<1	Oct.	77	71	1
May	45	34	<1	Nov.	46	100	1
June	47	38	1	Dec.	48	92	1

REFERENCES

Feely, H.W., R.J. Larsen, and C.G. Sanderson, Annual report of the surface air sampling program, *EML-497*, 165 pp., U.S. DOE Environmental Measurements Laboratory, New York, 1988.

Tropospheric Radiocarbon at Amundsen-Scott South Pole Station, Antarctica, from 1972 to 1987

LESTER MACHTA

NOAA, Air Resources Laboratory, Silver Spring, Maryland 20910

GÖTE OSTLUND

University of Miami, Miami, Florida 33149

KIRBY HANSON

NOAA, Air Resources Laboratory, Miami, Florida 33149

It is generally assumed that for several thousand years prior to 1950, an approximate equilibrium existed between the production of ^{14}C by cosmic rays in the atmosphere and the natural decay associated with the ^{14}C half-life of 5730 years. Another recent source of production of ^{14}C is from fusion bomb tests in the atmosphere, especially those conducted during the 1950s and the more massive tests in 1961-1962, which perturbed the natural equilibrium. Most of the atmospheric ^{14}C exists mainly as, $^{14}CO_2$ [*Eisenbud*, 1987). Nuclear reactors also release some ^{14}C.

In collaboration with NSF, Division of Polar Programs, NOAA/GMCC collected whole air samples at the Amundsen-Scott SPO station since 1964 for the purpose of measuring atmospheric ^{14}C in CO_2. The samples taken between 1964 and 1968 were collected in cooperation with the NWS, analyzed by the Argonne National Laboratory, and reported in the DOE, Health and Safety Laboratory report, *HASL-243* [*Telegadas*, 1971]. Subsequent ^{14}C measurements for 1972-1987, analyzed in Miami, are reported here.

From 1972 to 1987, 6-day whole air samples were collected in stainless steel, 14.7-L spheres pressurized to 21 MPa in order to obtain CO_2 aliquots. Extraction of the CO_2 was made prior to the shipment to Miami. Nine liter-atms of CO_2 gas are required to fill the ^{14}C counting tubes for precision ^{14}C counting. Since most aliquots contained only about 1 L of CO_2, it was necessary to combine the discrete samples provided. Corrections for the measured ^{13}C isotopic composition of the sample were made, and the units of the reported values are the per mil ($\Delta^{14}C$) deviation from the NIST standard, which was age corrected to the year 1950. (Earlier SPO data, 1964-1968, were corrected in the same fashion.) Further details of the laboratory analyses are not within the scope of this report but can be obtained by writing the second author.

The ^{14}C measurements in per mil for SPO are shown in Figure 1, along with measurements for 1963-1980 from northern Norway [*Nydal and Lövseth*, 1983]; all values are on the scale ($\Delta^{14}C$). Also see *Levin et al.* [1985]. A few of the new SPO values that are obviously erroneous were omitted. The remaining 1972-1987 values depict a smooth, decreasing trend despite the 2.5-year break. Norway values are higher than those at SPO. One must note that the Soviet high-yield nuclear tests
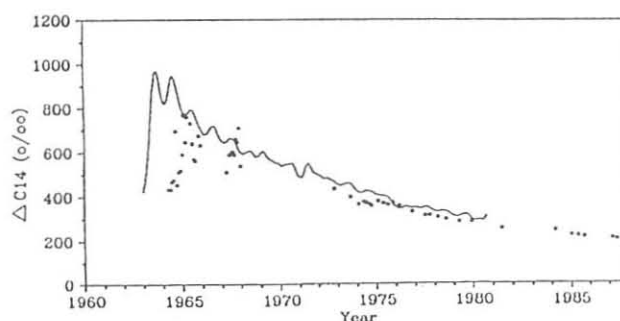

Fig. 1. $\Delta^{14}C$ concentrations. The solid line shows concentrations at Nordkapp, Norway (71°N, 24°E) [*Nydal and Lösveth*, 1983], and the circles show concentrations at SPO. The circles after 1972 are the newly presented values in this paper; those before 1968 were published previously.

at Novaya Zemlya were a major source of ^{14}C. However it is likely that most of the bomb test ^{14}C in both high northern and equatorial latitudes, as well as the cosmogenic ^{14}C, was initially injected into the stratosphere. Hence the small difference between the north polar and south polar ground-level concentrations might be expected at steady state.

The main sink for CO_2 is the oceans, although some of it later returns to the air. If in the future anthropogenic sources of ^{14}C remain small, it is expected that over the centuries, SPO ^{14}C readings will decrease toward the assumed pre-nuclear bomb era value of zero per mil, yet will remain somewhat higher.

REFERENCES

Eisenbud, M., *Environmental Radioactivity*, 3rd Ed., 475 pp., Academic Press, New York, 1987.

Levin, I., B. Kromer, H. Schoch-Fischer, M. Bruns, M. Munnich, D. Berdau, J. Vogel, and K. Munnich, 25 years of tropospheric ^{14}C observations in central Europe, *Radiocarbon, 27*, 1-19, 1985.

Nydal, R., and K. Lövseth, Tracing bomb ^{14}C in the atmosphere 1962-1980, *J. Geophys. Res., 88*, 3621-3642, 1983.

Telegadas, K., The seasonal atmospheric distribution and inventories of excess carbon-14 from March 1955 to July 1989, *HASL-243*, pp. I-2-I-86, DOE Health and Safety Laboratory, New York, 1971.

Seasonal and Latitudinal Trends in the $^{13}C/^{12}C$ Ratio of Methane

PAUL D. QUAY, STAGG L. KING, D. O. WILBUR, AND J. STUTZMAN

University of Washington, School of Oceanography WB-10, Seattle, Washington 98195

1. INTRODUCTION

Part of the recent research on atmospheric methane (CH_4) uses the isotopic composition of CH_4 to distinguish between various CH_4 sources [e.g. *Stevens and Engelkemeir*, 1988; *Quay et al.*, 1988]. A biogenically produced CH_4 from natural gas and biomass burning sources has a distinctly higher $^{13}C/^{12}C$ than does CH_4 biogenically produced primarily from rice paddies, wetlands, and ruminants. Our research has focused on measuring the seasonal and latitudinal trends in the $^{13}C/^{12}C$ ratio of CH_4 ($^{13}CH_4$). We intend to use the measured trends in $^{13}CH_4$ to constrain the spatial and temporal variations in abiogenic and biogenic CH_4 source strengths.

2. SAMPLING AND ANALYSIS

In 1986, we initiated an atmospheric sample collection program for $^{13}CH_4$ measurements at BRW and on the Washington coast. In 1987, we expanded our sample collection to include MLO. We send a pre-evacuated 35-L flask to the sampling site, where the flask is simply opened, allowed to fill to atmospheric pressure, and then returned to our laboratory. The CH_4 concentration at time of collection is provided by GMCC. Air samples are collected approximately biweekly. CH_4 in the air sample is extracted, purified, and combusted to CO_2 under high vacuum following the procedure developed by *Stevens and Rust* [1982]. The CO_2 is measured for its $^{13}C/^{12}C$ using a Finnigan MAT 251 mass spectrometer. This procedure yields a CO_2 sample volume of ~30 μl for mass spectrometric analysis.

$^{13}C/^{12}C$ of the atmospheric CH_4 is reported relative to $^{13}C/^{12}C$ of a standard (PDB) using the del notation (δ):

$$\delta^{13}C\ (^o/_{oo}) = \left(\frac{^{13}C}{^{12}C}\right)_{sam} \left[\left(\frac{^{13}C}{^{12}C}\right)_{std} - 1\right] * 1000$$

where sam is the sample and std is the standard. The precision of our $\delta^{13}C$ measurement is about ±0.04%, based on standards analyzed over the last year.

3. RESULTS

The results of $^{13}CH_4$ measurements at our three northern hemisphere sampling sites are presented in Figure 1. Three
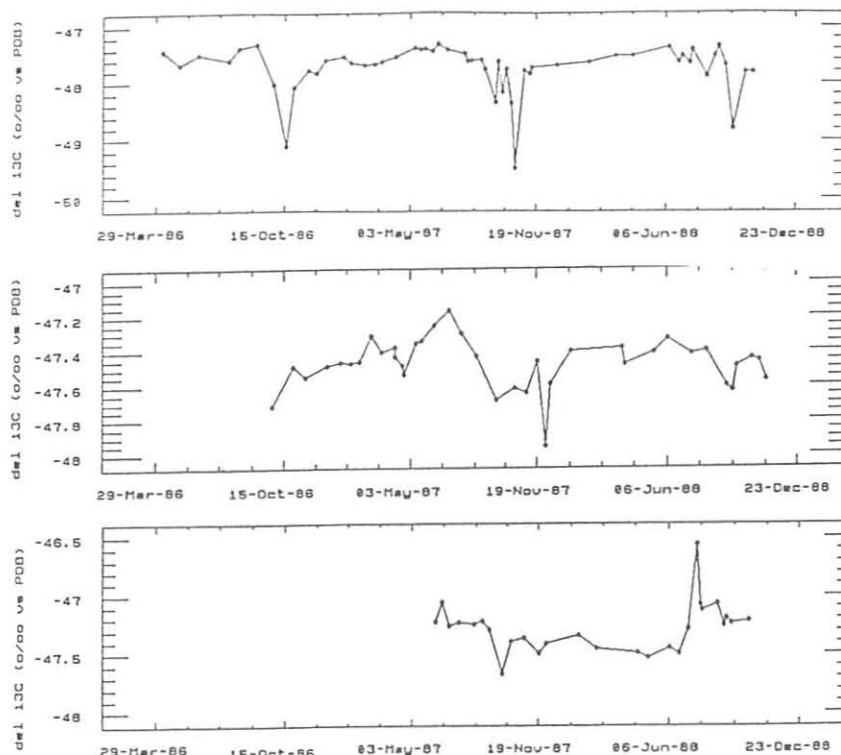

Fig. 1. Measured time series of $\delta^{13}C$ (‰ versus PDB) of atmospheric methane at (top to bottom) BRW (71°N, 157°W), Olympic Peninsula (48°N, 125°W), and MLO (19°N, 155°W).

118

trends appear in these data: (1) a poleward decrease in $^{13}CH_4$, (2) a fall minimum in $^{13}CH_4$ at 48°N and 71°N, and (3) a fall to summer increase in $^{13}CH_4$ at 48°N and 71°N.

$^{13}C/^{12}C$ of CH_4 depends on $^{13}C/^{12}C$ of the CH_4 sources and the isotopic fractionation during OH oxidation of CH_4 [*Davidson et al.*, 1987]. The poleward trend toward lower $^{13}CH_4$ values suggests that biogenic CH_4 sources are relatively more important than abiogenic sources at higher northern latitudes.

The importance of biogenic CH_4 input at high latitudes is also implied by the fall minimum in $^{13}CH_4$, which is strongest at BRW. The fall minimum in $^{13}CH_4$ is associated with peaks in CH_4 concentration (Figure 2). The $^{13}CH_4$ decrease associated with a CH_4 increase indicates that the fall CH_4 concentration maximum is derived from inputs of biogenically produced CH_4. We calculated a mean $\delta^{13}C$ of $-64‰$ for the CH_4 source producing the concentration maximum measured in the fall. We directly measured the $\delta^{13}C$ of CH_4 emitted from northern wetlands to be $-64 \pm 5‰$ [*Quay et al.*, 1988], in good agreement with the $\delta^{13}C$ of the CH_4 source producing these fall $^{13}CH_4$ minimum.

The gradual increase in $^{13}CH_4$ following the fall minimum is very likely the result of OH oxidation of CH_4. This $^{13}CH_4$ increase is associated with a CH_4 concentration decrease. The $^{13}CH_4$ increase occurs because $^{12}CH_4$ reacts with OH at a rate about 1% greater than $^{13}CH_4$ does [*Davidson et al.*, 1987].

4. SUMMARY

Measurements of the $^{13}C/^{12}C$ of atmospheric CH_4 provide important information on the strength of CH_4 sources. The seasonal and latitudinal trends in $^{13}CH_4$ depend on the relative strengths of biogenic versus abiogenic CH_4 input and CH_4 loss via OH oxidation. Biogenic CH_4 input, probably from wetlands, exerts significant controls on the seasonal CH_4 cycle at high northern latitudes. Continued $^{13}CH_4$ measurements at the GMCC sites should yield interannual trends in CH_4 source strengths.
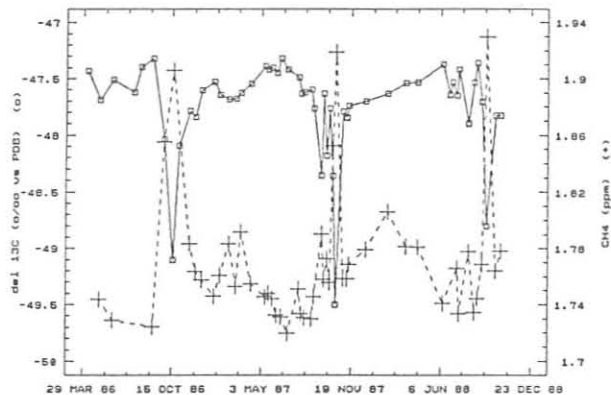

Fig 2. Time series of $\delta^{13}C$ (‰ versus PDB, solid line) and concentration of atmospheric CH_4 (dashed line) [*P. Steele*, personal communication] at BRW.

REFERENCES

Davidson, J.A., C.A. Cantrell, S.C. Tyler, R.E. Shetter, R.J. Cicerone, and J.G. Calvert, Carbon kinetic isotope effect in the reaction of CH_4 with OH, *J. Geophys. Res.*, 92, 2195-2199, 1987.

Quay, P.D., S.L. King, J.M. Lansdown, and D.O. Wilbur, Isotopic composition of methane released from wetlands: Implications for the increase in atmospheric methane, *Global Biogeochem. Cycles*, 2, 385-398, 1988.

Stevens, C.M., and A. Engelkemeir, Stable carbon isotopic composition of methane from some natural and anthropogenic sources, *J. Geophys. Res.*, 93, 725-733, 1988.

Stevens, C.M., and F.E. Rust, The carbon isotopic composition of atmospheric methane, *J. Geophys. Res.*, 87, 4879-4882, 1982.

Measurements of CFC-11, CCl_4, and CH_3CCl_3 in Flask Samples Collected at MLO and NWR

G.C. RHODERICK

National Institute of Standards and Technology (Formerly, National Bureau of Standards), Gaithersburg, Maryland 20899

1. INTRODUCTION

Since March 1988, the Gas Metrology Research Group of the Gas and Particulate Science Division of NIST has analyzed several gas samples submitted by the NOAH Group of GMCC. These were samples of ambient air that were collected in special stainless steel flasks at NWR and MLO and analyzed by NIST for specified halocarbons. A GC/ECD calibrated with primary standards prepared gravimetrically at NIST was used for the analyses.

2. SAMPLING AND ANALYSIS

The samples of ambient air that were collected in special stainless steel flasks at NWR and MLO were shipped directly to NIST. In most cases, the samples were analyzed within 10 days after being filled. To date, eight samples from NWR and nine samples from MLO have been analyzed.

A set of standards was previously prepared in treated aluminum cylinders with a balance gas of pure dry nitrogen. The nitrogen was analyzed for trace halocarbons prior to preparing the standards. Standards were prepared at NIST using a method developed several years ago involving a microgravimetric technique, along with dilution by gravimetry, to obtain gas standards at the part per trillion (ppt) level. The concentration range of the standards was from 50 to 500 ppt, several being around 100 ppt. The standards in the set were intercompared on an HP5880 GC with an ECD. Generally, a wide-bore capillary column was used for separation of the compounds. The regression plots, gravimetric concentration versus response, showed excellent correlation within the set of standards. Typically, one standard is used when analyzing a flask sample. However, periodically the complete set of standards are intercompared to assure stability of the halocarbons.

During April and May 1989, two gravimetric standards were prepared in a balance of pure air. One of the standards was prepared using blended air, and the other was prepared using air collected in 30-L aluminum cylinders by NOAA at NWR and scrubbed of water and halocarbons. Both of these sources of air were analyzed for trace halocarbons. The reason for preparing standards in air is discussed later, but since that time a standard in air and one in nitrogen have been used when analyzing the flask samples.

3. RESULTS AND DISCUSSION

The compounds that have been consistently determined at NIST in the flask samples have been CFC-11, CCl_4, and CH_3CCl_3. Table 1 shows the results for those flask samples collected in 1988 that have been analyzed. The data show a

TABLE 1. Flask Sample Measured Concentration

Data Collected	CFC-11 (ppt)	CCl_4 (ppt)	CH_3CCl_3 (ppt)
Niwot Ridge			
Feb. 23, 1988	235	118	219
March 29, 1988	256	118	174
Aug. 16, 1988	256	116	156
Oct. 4, 1988	262	116	169
Dec. 6, 1988	260	120	173
Mauna Loa			
July 11, 1988	255	113	149
Sept. 26, 1988	253		
Dec. 12, 1988	256	128	173
Jan. 30, 1989	235	116	157

TABLE 2. Measured Concentration of CCl_4 Using Air Matrix Versus Nitrogen Matrix Standards

	Measured Concentration of CCl_4			
Date Collected	Nitrogen Matrix (ppt)	Air Matrix (ppt)	% Difference (Air/Nitrogen)	Corrected for Difference* (ppt)
Niwot Ridge				
Feb. 23,1988	118			107
March 29, 1988	118			107
Aug. 8, 1988	116			104
Oct. 4, 1988	116			104
Dec. 6 1988	120			108
Feb. 28, 1989	119			107
April 18, 1989	119	108	91	
June 6, 1989	115	105	91	
Mauna Loa				
July 11, 1988	113			102
Dec. 12, 1988	128			115
Jan. 30, 1989	116			104
March 13, 1989	120			108
April 3, 1989	114	101	89	
May 2, 1989	115	104	90	
June 15, 1989	112	105	94	
July 3, 1989	116	98	84	
			Average = 90 %	

*Concentrations determined using nitrogen matrix standards are adjusted to the air matrix standards using the % difference factor determined between the nitrogen and air matrix standards.

steady increase in the concentration of CFC-11, which is consistent with NOAA's data. The CH_3CCl_3 data are misleading in that they show a decrease in concentration over time. However, this is probably due to contamination either in the sampling system or the flask themselves. Since the same flask is used per site for each sampling, then the original contamination, if any, may be purged by this time. The later data are more consistent. The data for the CCl_4 have been very consistent, having an average value over the period of sampling of about 118 ppt. These concentrations were determined using standards with a balance gas of nitrogen. The NOAH group of NOAA/GMCC has been determining CCl_4 at about 105 ppt, resulting in differences of about 12% between NOAA and NIST. To try to resolve this difference, NIST prepared standards in scrubbed air to more closely imitate the air in the flask samples. Analyses of the flask samples since have been done using a standard in air and one in nitrogen. Table 2 shows the results of those analyses. Samples collected in 1989 are shown in Table 2 in order to calculate a correction factor for all data. The concentration of CCl_4 as determined against the air standard is consistently around 105 ppt. If the percent mean difference in concentration of CCl_4, as determined using the air versus nitrogen standards (90%), is applied to the earlier data, then the average concentration of CCl_4 over the sampling period is 106 ppt for NWR and 103 ppt for MLO. This same effect is seen with the CH_3CCl_3; however the difference is only 8%. Currently I have no explanation for difference in the CCl_4 concentration using standards in an air matrix versus standards in a nitrogen matrix. However, the results obtained at NIST are consistent with NOAA for CCl_4 and the other compounds discussed.

REFERENCES

Bodhaine, B.A., and R.M. Rosson (Eds.), *Geophysical Monitoring for Climatic Change, No. 16: Summary Report 1987*, 110 pp., NOAA Air Resources Laboratory, Boulder, CO, 1988.

Rhoderick, G.C., and W. L. Zielinski, Jr., Preparation of accurate multicomponent gas standards of volatile toxic organic compounds in the low-parts-per-billion range, *Anal. Chem., 7*, 2454-2460, 1989.

The Mauna Loa Observatory Photochemistry Experiment

B. A. RIDLEY

National Center for Atmospheric Research, P.O. Box 3000, Boulder, Colorado 80307

MLOPEX was carried out at the GMCC site operated by NOAA on the island of Hawaii in April, May, and the first week of June 1988. The MLOPEX participants having experiments at the site, the major species measured, and the instrumentation are listed in Table 1. Measurements were made around the clock from May 1 to June 4, 1988.

The latter part of April was used to set up extra facilities at the GMCC site. This included installation of four 6-7.3 m trailers to house experiments, two 10-m sampling towers, and a PAM station provided by the Atmospheric Technology Division of NCAR. The director of the GMCC site also allowed us the use of a building next to the trailer site, one formerly used by the Atomic Energy Commission. Because of the size of the experiment and power requirements, local contractors installed additional power distribution from the transformer cage at MLO to the trailer site, and the Hawaii Electric Light Company installed a 70 KVA transformer for the duration of the experiment.

The emphasis of the experiment was to examine the abundances and partitioning of photochemically active species in the background troposphere through simultaneous measurements of a fairly large number of related trace species and over a period of time considerably longer than that available through aircraft studies. Furthermore, by contrasting the results with similar experiments in the continental United States, organized by NOAA/AL, we could examine the transformation of active species released mostly by anthropogenic activity to reservoir species. Thus, an emphasis was on the photochemical interactions of odd nitrogen and some odd hydrogen species. Specifically from these measurements, the photochemical production of ozone and estimates of hydroperoxy and organic peroxy radical concentrations can be estimated. Because the details of the photochemical transformations must be provided by modeling studies that require a knowledge of nonmethane hydrocarbon levels, a wide variety of these species were also measured.

The MLO site is a natural choice for examining background chemistry in the northern hemisphere. Daily 5-day isentropic back-trajectories calculated for the program showed no contact with continental areas. Only 10-day trajectories calculated by J. T. Merrill showed several short periods of origins from continental Asia or North America. The MLO site, of course, has been well characterized meteorologically and has a long history of measurements of some trace species and particulate matter. Furthermore, and of basic interest to our program, is the ability to make measurements in free tropospheric air during nighttime and early morning downslope conditions. Measurements during upslope conditions allowed for interesting observations of marine boundary layer air with local island influences.

Table 2 shows median levels of some of the trace species measured during the program. In the table, upslope data are defined as the data from 1100 to 1900 LST, and downslope data are defined as those from 2200 to 1000 LST with the wind

TABLE 1. Mauna Loa Observatory Photochemistry
Experiment (MLOPEX) May 1-June 4, 1988

Species	Instrumentation	Participants
CO_2, CH_4, CO, GC, N_2O, CFC's, meteorology	On-site NDIR, GC, meteorological instruments	E. Robinson, P. Tans, P. Steele, S. Oltmans, G. Herbert, J. Elkins--GMCC
Alkyl nitrates, halocarbons	Adsorption, chromatographic analysis	E. Atlas, S. Schauffler--Texas A & M University
HNO_3, NO_3, etc.	Filter samples, ion chromatography	B. Huebert, W. Warren--University of Rhode Island; R. Norton--NOAA/AL
Radon	Radon detector	J. Kay--Drexel University; J. Fox--NCAR
$J(NO_2)$	Actinometer, chemiluminescence, Eppley	R. Shetter, J. Calvert, A. McDaniel--NCAR
Peroxides, formaldehyde	Enzyme fluorescence	B. Heikes--NCAR
NMHCs, CO, CH_4, CO_2	On-site chromatograph, can samples analyzed at NCAR	P. Zimmerman, J. Greenberg, L. Heidt, B. Henry L. Mizoue, C. Gilliland, W. Pollock, R. Lueb--NCAR
NO, NO_2	NO/O_3 chemiluminescence + photolysis	M. A. Carroll--NOAA/AL; D. Montzka--CIRES; B. Ridley--NCAR
NO_y	Au/CO converter, NO/O_3 chemiluminescence	G. Hubler--NOAA/AL
PAN, PPN, methylnitrate, local meteorology, O_3	Gas chromatograph, cryogenic enrichment, TECO, PAM, Eppley	J. Walega. F. Grahek, J. Shetter, B. Ridley--NCAR
Air masses	Isentropic trajectory analysis for each day of the program	C. Hahn--CIRES, NOAA/AL; J. Merrill--NCAR

TABLE 2. MLOPEX Median Values

Species	All Data	Upslope	Downslope
NO_y, pptv	255	236	263
HNO_3, pptv	102	113	93
NO_3, pptv	26	37	15
NO_2, pptv	33	38	31
NO, pptv*	11	12	10
PAN, pptv	17	22	13
$\Sigma RONO_2$, pptv†	3.5	4.9	2.6
CH_3ONO_2, pptv	3.6	3.8	3.5
PPN, pptv	~0	0.2	~0
CO, ppbv	139	144	136
O_3, ppbv	40	34.5	43.7
H_2O_2, pptv	1009	927	1079
ROOH, pptv	144	145	145
H_2CO, pptv	124	183	102

*Daytime values.

†2-butyl-, 2-isopentyl-, 2-pentyl-, 3-pentyl-, isopropyl-, n-butyl-, n-pentyl-, n-propylnitrate.

speed being at least 1 m s^{-1}. The nitric oxide data included in the table represent only data from daytime hours.

At present, interpretation of the data is being furthered by modeling groups at NCAR and the NOAA/AL.

Nitrate and Non-Seasalt Sulfate in Aerosols at American Samoa

DENNIS L. SAVOIE AND JOSEPH M. PROSPERO

*University of Miami, Rosenstiel School of Marine and Atmospheric Science, Division of Marine and Atmospheric Chemistry,
Miami, Florida 33149-1098*

1. INTRODUCTION

A major goal of our involvement in the SEAREX sampling program was to define more clearly the the major sources and and atmospheric pathways and fluxes of nitrate and non-seasalt (nss) sulfate over the Pacific Ocean. This is largely accomplished through an evaluation of the temporal and spatial variations in their concentrations and an assessment of their relationships to other atmospheric constituents and atmospheric transport pathways. By providing an indication of the natural concentrations in marine air, the results from the sampling station at SMO (14°15'S, 170°35'W) have proved to be invaluable in this effort. Concentrations of mineral aerosol and trace metals at SMO are among the lowest ever recorded for the near-surface troposphere, and indicate that this region is minimally affected by transport of soil material and pollutants from the continents. The results from our analyses of the these data were presented in several recent manuscripts: *Prospero and Savoie* [1989]; *Savoie and Prospero* [1989]; and *Savoie et al.* [1989a, b].

Week-long bulk aerosol samples were collected from onshore winds using 20×25 cm Whatman 41 filters at a flow rate of 1.1 m^3 min^{-1}. Nitrate, sulfate, and methanesulfonate (MSA) in aqueous extracts of the filters were measured to within 5% by ion chromatography, and sodium to within 2% by flame atomic absorption. The measured nitrate is considered to be the sum of particulate nitrate and gaseous HNO_3, because in addition to aerosol, filters loaded with seasalt should collect vapor phase HNO_3 with essentially 100% efficiency.

2. RESULTS

For 1983 through most of 1987, the mean nitrate concentration at SMO was 0.116 ± 0.008. Similar mean concentrations were obtained at two other stations in the tropical South Pacific: 0.107 ± 0.011 µg m^{-3} at Funafuti, Tuvalu (8°30'S, 179°12'E), and 0.117 ± 0.010 at Rarotonga (21°15'S, 159°45'W). These concentrations are about a factor of 300% lower than those in the North Pacific and about 30% lower than those in the equatorial region (Figure 1). On the basis of the consistency of its ratio to MSA, nss sulfate at SMO has been attributed primarily to the oxidation of reduced sulfur gases emitted from the ocean [*Saltzman et al.*, 1985]; the geographical variation in the mean concentrations of these constituents is shown in Figure 1.

There is evidence of a significant seasonal cycle in the nitrate concentration. The lowest nitrate concentrations occur during March, April, and May when the average is 0.080 µg m^{-3} (Figure 2). During September, October, and November, the average is about 73% higher, 0.138 µg m^{-3}. The overall seasonal cycle of nitrate at SMO is very similar to that of nss sulfate. The lowest mean concentration of nss sulfate (0.28 µg m^3) at SMO occurs during April and May. During September and October, the concentrations are about 60% higher (0.45). Since nss sulfate at SMO is derived primarily from a marine biogenic source, the similar seasonal cycle in nitrate might suggest that it originates from a biogenic source as well. However, there is also a significant difference between the two seasonal cycles. During June through August, the nitrate
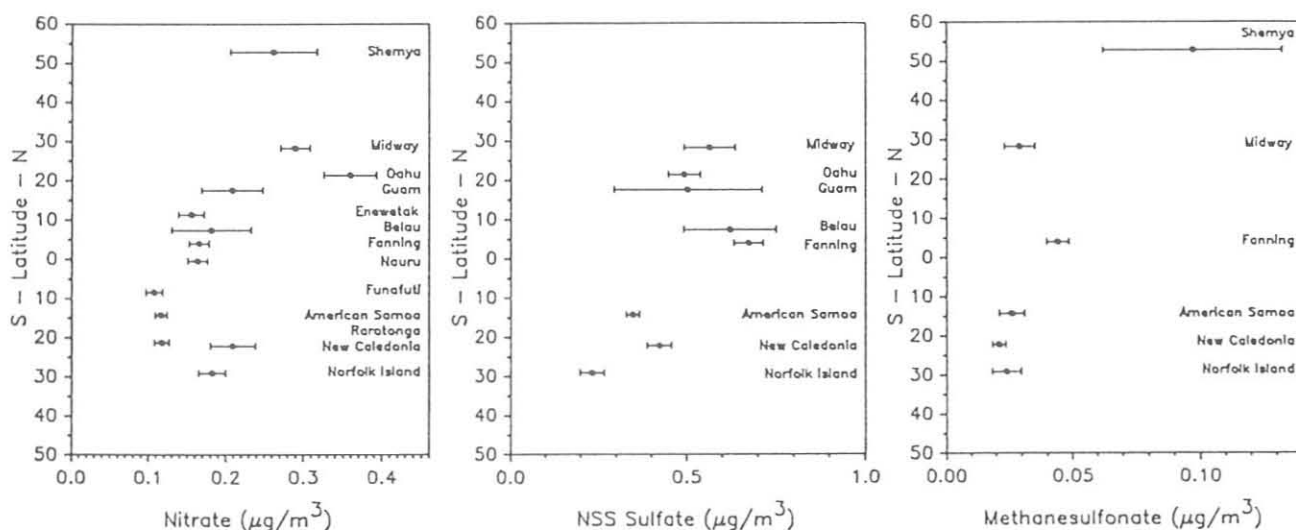

Fig. 1. Latitudinal variation in the mean concentrations of nitrate, nss sulfate, and MSA over the Pacific Ocean. The horizontal bars indicate the 95% confidence limits for the means.
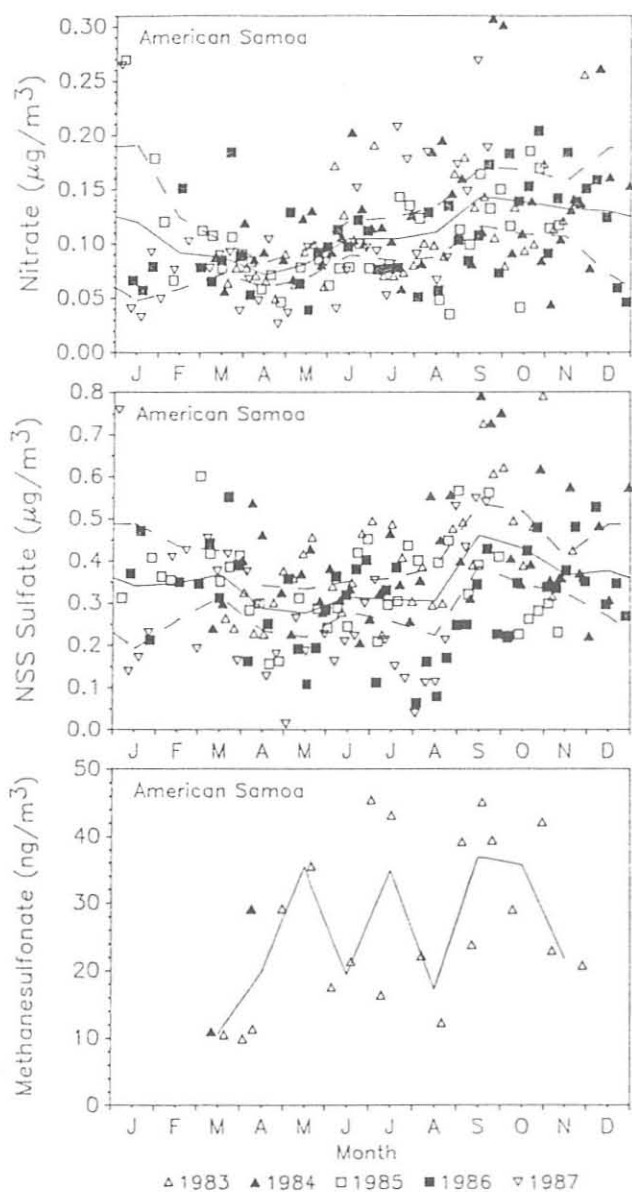
Fig. 2. Composited seasonal cycles of nitrate, nss sulfate, and MSA at SMO. The solid lines connect the monthly mean concentrations. For nitrate and nss sulfate, for which there are a large number of data points, the dashed lines indicate the upper and lower 95% confidence bounds of the monthly means.

dimethylsulfide, DMS) emitted from the ocean. The geographical distribution of the nitrate concentrations in remote areas is certainly compatible with that of primary productivity, and such a source could account for the consistency of the mean concentrations over a broad region of the ocean. The nitrate concentrations are most strongly correlated with those of ^{210}Pb [*Graustein and Turekian*, 1988], which is derived almost exclusively from the radioactive decay of ^{222}Rn emitted from soils. The production of NO_x by lightning, which occurs most frequently over the tropical regions of the continents, is a potential continental nitrate source that is not incompatible with the extremely low concentrations of trace metal pollutants at SMO. The active convection that is usually associated with lightning could be instrumental in rapidly transporting the ^{222}Rn and ^{210}Pb to higher altitudes where they as well as the NO_x could be effectively transported over long distances. On the basis of the model of *Crutzen and Gidel* [1983], lightning and stratospheric sources can readily account for the mean nitrate concentrations over the equatorial and southern tropical regions of the Pacific Ocean.

The seasonal cycle of ^7Be measured by M. Uematsu (Hokkaido Tokai University, Sapporo, Japan, personal communication) is consistent with its upper tropospheric and stratospheric source with relatively low concentrations from January through April and then significantly higher concentrations from June through September. The mean seasonal cycle reported by *Feely et al.* [1988] shows a similar trend except that the higher concentrations extend into October and November. A similar cycle occurs in the average monthly concentrations of ozone [*Oltmans*, 1981; *Oltmans and Komhyr*, 1986]. Ozone at SMO has been attributed to a stratospheric source, and its concentration and seasonal distribution are well modeled by considering the stratosphere to be the dominant source [*Levy et al.*, 1985]. Even recognizing that the variability in their concentrations yields considerable uncertainty in the monthly means for ^7Be and nitrate, the nitrate cycle differs considerably. There is virtually no correlation between nitrate and ^7Be ($r^2 = 0.08$, $N = 83$), nor between nitrate and ozone concentrations ($r^2 = 0.03$, $N = 115$) measured at SMO (S. Oltmans, NOAA/GMCC, Boulder, Colorado, personal communication). As expected, ozone does exhibit a significant correlation with ^7Be ($r^2 = 0.32$, $N = 76$). These results suggest that, contrary to the recent suggestion by *Levy and Moxim* [1989], the stratosphere is probably not the major source for the NO_x precursor of nitrate over the tropical South Pacific.

3. PLANS

In the near future we plan more detailed comparisons of our nitrate data and the ozone data gathered at SMO by GMCC as a further check on the sources of both constituents. In light of the strong interest in the relationship between sulfate aerosols and climate, we will also be analyzing more SMO samples for MSA and comparing those results and our nss sulfate data with the CCN data provided by GMCC to determine the role of marine biogenic sources in establishing the concentrations of both sulfate and CCN. A major program during fall 1989 will be run in support of the NASA GLOBE flight over the Pacific. The

concentrations are significantly higher than during April. In contrast, the nss sulfate concentrations remain low until the rather abrupt increase in September. The very weak correlation between nitrate and nss sulfate ($r^2 = 0.21$, $n = 194$) further indicates that the major sources of the two constituents may not be directly related. However, these results do not definitively preclude a biogenic source. Nitrate derived from the oxidation of marine-derived particulate organic nitrogen compounds would not necessarily be strongly correlated with nss sulfate produced by the oxidation of reduced sulfur gases (especially

125

primary objective of that mission is to establish the feasibilty of a space-based LAWS. Our results will place the aircraft data in a climatological context.

REFERENCES

Crutzen, P.J., and L.T. Gidel, A two-dimensional photochemical model of the atmosphere: 2, The tropospheric budgets of the anthropogenic chlorocarbons, CO, CH_4, CH_3Cl, and the effect of various NO_x sources on tropospheric ozone, *J. Geophys. Res., 88*, 6641-6661, 1983.

Feely, H.W., R.J. Larsen, and C.G. Sanderson, Annual report of the surface air sampling program, *EML-497*, 665 pp., Environmental Measurements Laboratory, Department of Energy, New York, July 1988.

Graustein, W.C., and K.K. Turekian, SEAREX ^{210}Pb in Pacific marine aerosols, *Tech. Rep. 1*, Atmospheric Geochemistry, Yale University, New London, CT, 1988.

Levy, H. II, and W.J. Moxim, Simulated global distribution and deposition of reactive nitrogen emitted by fossil fuel combustion, *Tellus*, in press, 1989.

Levy, H. II, J.D. Mahlman, W.J. Moxim, and S.C. Liu, Tropospheric ozone: The role of transport, *J. Geophys. Res., 90*, 3753-3772, 1985.

Oltmans, S. J., Surface ozone measurements in clean air, *J. Geophys. Res., 86*, 1174-1180, 1981.

Oltmans, S.J., and W.D. Komhyr, Surface ozone distributions and variations from 1973-1984 measurements at the NOAA Geophysical Monitoring for Climatic Change Baseline Observatories, *J. Geophys. Res., 91*, 5229-5236, 1986.

Prospero, J.M., and D.L. Savoie, Effect of continental sources on nitrate concentrations over the Pacific Ocean, *Nature, 339*, 687-689, 1989.

Saltzman, E.S., D.L. Savoie, J.M. Prospero, and R.G. Zika, Atmospheric methanesulfonic acid and non-seasalt sulfate at Fanning and American Samoa, *Geophys. Res. Lett., 12*, 437-440, 1985.

Savoie, D.L., and J.M. Prospero, Comparison of oceanic and continental sources of non-sea-salt sulphate over the Pacific Ocean, *Nature, 339*, 685-687, 1989.

Savoie, D.L., J.M. Prospero, and E. S. Saltzman, Nitrate, non-seasalt sulfate and methanesulfonate over the Pacific Ocean, in *Chemical Oceanography, vol. 10*, edited by J. P. Riley and R. Chester, Academic, San Diego, CA, in press, 1989a.

Savoie, D.L., J.M. Prospero, J.T. Merrill, and M. Uematsu, Nitrate in the atmospheric boundary layer of the tropical South Pacific: Implications regarding sources and transport, *J. Atmos. Chem.*, in press, 1989b.

Analytical Electron Microscope Studies of Size-Segregated Particles From the Springtime Arctic Aerosol

PATRICK J. SHERIDAN

National Research Council Associate, NOAA, GMCC, Boulder, Colorado 80303

1. INTRODUCTION

The marked reduction in springtime visibility over wide areas of the Arctic, a region once thought pristine, is now known to be due to the average tenfold increase in aerosol concentrations observed throughout the Arctic during Arctic spring. In spring 1986, aerosol samples were collected by cascade impactor over the Alaskan and Canadian Arctic during the six research flights of the AGASP-II field experiment. The particles in these samples were physically and chemically characterized on an individual particle basis using AEM [*Sheridan and Musselman*, 1985; *Sheridan*, 1989*a, b*]. Data presented here suggest that different types and concentrations of aerosols may be expected in the various layers of the stable springtime Arctic atmosphere.

2. EXPERIMENTAL DETAILS

The aircraft aerosol sampling system, thin-film collection substrates, and sampling strategies were described in detail by *Sheridan and Musselman* [1985] and *Sheridan* [1989*a, b*]. Particles were collected in the three-stage impactor directly onto 10-20-nm-thick Formvar films, which were supported by 200-mesh Cu TEM grids. Each grid was mounted in the center of the top surface of a collection plate, and during sampling was positioned directly beneath an impactor jet.

Aerosol collection was initiated when the aircraft reached the desired sampling altitude or air mass, and usually lasted 15-20 minutes. After sample collection, the exposed films were immediately returned to their field containers for shipment back to clean laboratory conditions and electron microscope analysis.

Individual particles were analyzed using a JEOL Model JEM-200CX research AEM. In addition to direct, high-resolution viewing of single particles, electron diffraction was employed to identify mineral phases. The AEM is equipped with two x-ray spectrometers (EDS), which are sensitive to x-rays given off by atoms heavier than Be and Ne in the particle under electron bombardment. Through the use of an extensive library of particle standards, quantitative and semiquantitative estimates of the elemental composition of individual particles were made [*Sheridan*, 1986, 1989*c*].

3. RESULTS AND DISCUSSION

The aerosol samples characterized by AEM were collected over a wide area of the North American Arctic. Figure 1 shows the collection location for each of the 16 (A through P) impactor samples. Three major aerosol sample types were collected: tropospheric haze layer, tropospheric background, and stratospheric background. In addition, one sample was a mixture of clean stratospheric and tropospheric air. In Table 1, the samples are listed by type and collection altitude. The

collection period for each sample (<20 min) was short enough to ensure that sampling was confined to a specific atmospheric zone. This was checked by concurrent in-situ gas and aerosol measurements made by other aircraft-based instruments. Characteristics of the major sample types and of discrete aerosol samples are discussed here.

For reasons discussed in *Sheridan* [1989*a*], absolute number concentrations of atmospheric particles are difficult or impossible to measure using conventional cascade impactors. Relative particle concentrations, however, as determined from point counts of equal areas on different grids, are easily calculated. Since the volumes for all samples were within 10% of each other, particle loadings on the films directly reflect ambient particle concentrations and may be used to determine whether a sample is more or less heavily loaded than another with particulate material.

All aerosol samples collected within the Arctic stratosphere were composed predominantly of small (0.1-0.5 μm diameter) liquid H_2SO_4 droplets. Point counts performed on the final (small-particle) stages of these impactor samples showed particle loadings to be in the moderate range when compared with the other types of samples. This means, for example, that more particles were counted in a finite area on these films than equal areas of most of the background tropospheric aerosol samples (mostly light loadings). These same counts revealed that >95% of the fine particles on final stage films were composed of H_2SO_4. The first two impactor stages in most of these samples collected larger liquid (i.e., acidic) sulfate droplets and some terrestrial dust in the 1-3 μm size range. With few rare exceptions, anthropogenic particles with sources at the Earth's surface were not observed in these samples. The numbers of these large particles averaged approximately 3 orders of magnitude less than those of the submicrometer H_2SO_4 droplets found on the final stages of each sample. Figure 2 shows several types of particles observed in the springtime Arctic aerosol; some of the larger liquid H_2SO_4 droplets from
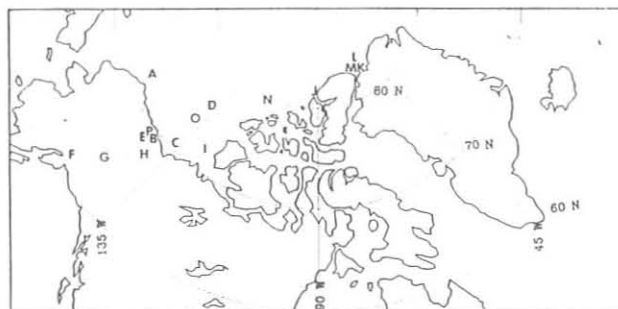

Fig. 1. Aerosol collection locations for the 16 cascade impactor samples (A-P).

TABLE 1. Aerosol Type and Collection Altitude for Cascade
Impactor Samples Collected During AGASP-II

Sample	Aerosol Type	Collection Altitude (m)
A	Tropospheric haze layer	1224-1866
B	Stratosphere	7533
C	Tropospheric haze layer	1720-2931
D	Tropospheric haze layer	1109-2210
E	Stratosphere	9271
F	Stratospheric/tropospheric background	2417-8140
G	Tropospheric background	7016-7036
H	Stratosphere	6970-7559
I	Tropospheric background	7484-7491
J	Stratosphere	8078
K	Tropospheric haze layer	391-1972
L	Tropospheric haze layer	2350
M	Tropospheric haze layer	5682-5859
N	Tropospheric background	8111-8406
O	Stratosphere	8366
P	Stratosphere	8365

the Arctic stratosphere are presented in Figure 2a. An x-ray spectrum from the particle shown by an arrow is presented in Figure 3a.

One of the stratospheric aerosol samples (sample F) was anomalous, in that very high loadings of terrestrial material were observed on all impactor stages, and relatively minor amounts of H_2SO_4 and other aerosol types. Figure 2b shows aerosol particles from the first stage of impactor sample F. This sample was collected during a descent through subsiding stratospheric air between Fairbanks and Anchorage, AK [Herbert et al., 1989]. The rough morphology, supermicrometer size of some of the particles, and elemental composition suggest a recent crustal input to this aerosol. Figure 3b shows an x-ray spectrum taken from particles within the indicated area in Figure 2b. Other evidence, including air trajectory calculations, aircraft observations, and elemental analyses of the bulk ash [Yount et al., 1987], suggests that the aerosol collected was ash from the recent (9-13 days previous) eruptions of Mt. Augustine volcano in the eastern Aleutian Islands.

Background tropospheric aerosol samples were quite similar to the "normal" stratospheric ones, with two major exceptions. First, particle loadings on these samples were lower by a factor of 2-4 than on stratospheric samples that were spatially and temporally closely collected. Since fine liquid H_2SO_4 droplets again constituted the bulk of the aerosol, and since most of these samples were collected in the middle to upper troposphere, the data suggest that higher springtime concentrations of H_2SO_4 aerosol may be expected in the Arctic stratosphere than in the background Arctic troposphere. Second, more particles of other types were observed in these tropospheric samples, including many with sources at the Earth's surface. These classes of particles included crustal dust, marine salt, fly ash, and carbon soot. Counted together, these particles accounted for approximately one-third of the supermicrometer particles collected in these samples, although the vast majority (90-95%) of submicrometer particles on the final stages (and, thus, of all particles in the aerosol) were H_2SO_4 droplets.

Aerosol samples collected in Arctic haze layers showed the most variability of any group of samples. Particle loadings were in the light to moderate range, with the heavier loadings being observed on the Alaskan Arctic samples A and C. These samples were collected just north of the coastline over the
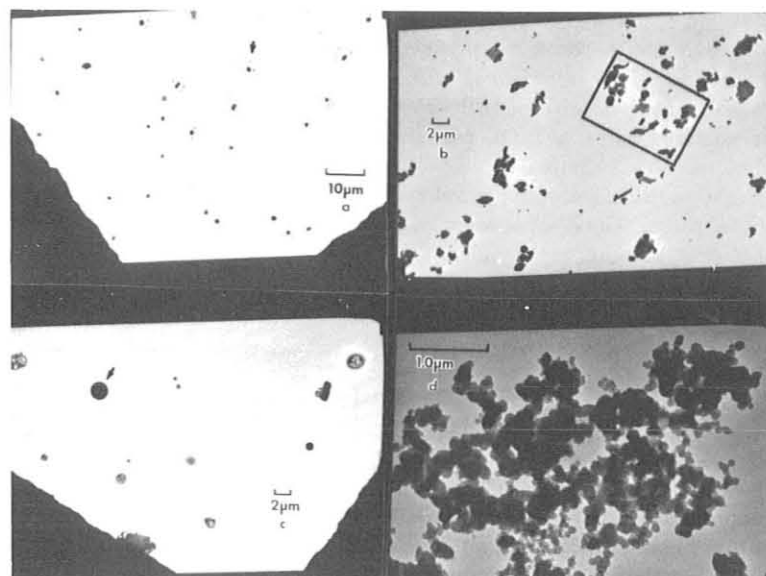

Fig. 2. Selected photomicrographs: (a) large H_2SO_4 droplets collected in the Arctic lower stratosphere, showing impaction satellite morphology; (b) solid, angular particles collected in stratospheric air over southern Alaska; (c) haze layer aerosol particles; (d) soot carbon chain aggregate. The arrows and rectangular area are referred to in Figure 3.
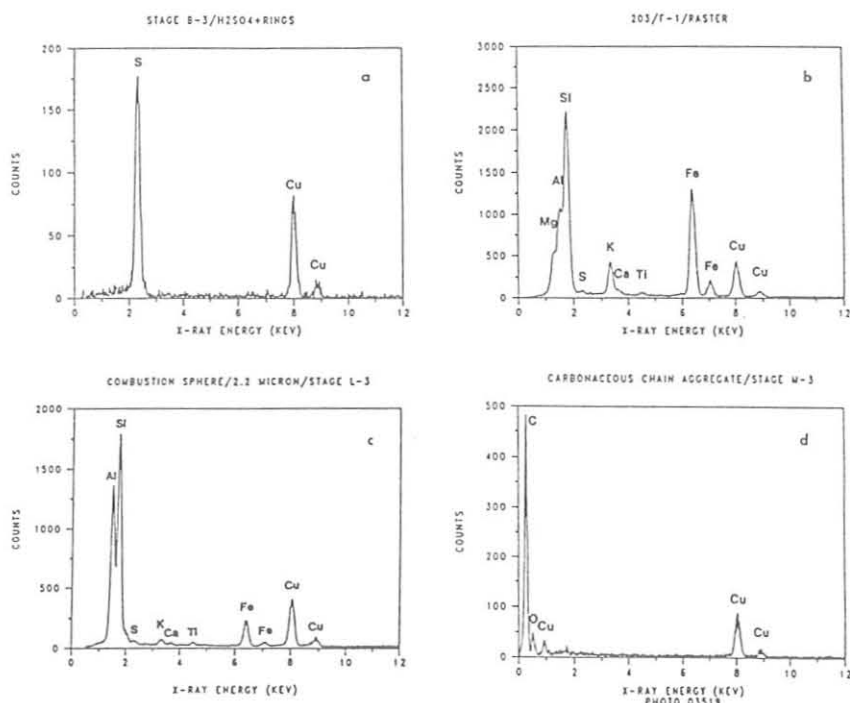
Figure 3. Conventional and ultra-thin window (UTW) x-ray spectra of particles in Figure 2. The Cu peaks in all spectra are artifacts caused by the grid. (a) Conventional spectrum of individual H_2SO_4 droplet indicated by the arrow; (b) Conventional spectrum of rectangular area in Figure 2b; (c) Conventional spectrum of the larger combustion sphere (indicated by the arrow); composition suggests coal-fired combustion; (d) UTW spectrum of carbonaceous chain aggregate, showing a major C peak.

Beaufort Sea, whereas the other haze samples were collected either well out over the ice (sample D) or off the coast near Alert, Northwest Territories (Samples K, L, and M). Aircraft CN and b_{sp} measurements agree well with the observed loadings on these samples, and show high particle concentrations and aerosol scattering during collection of samples A and C.

All haze samples showed a variety of particle types. On final-stage films, fine H_2SO_4 droplets were the most common class of particles, followed by solid $(NH_4)_2SO_4$ particles. Other particle types encountered included crustal dust and carbonaceous particles. First- and second-stage films showed many types of supermicrometer particles. Larger, liquid H_2SO_4 droplets were observed, many with smaller solid particles (usually crustal or carbonaceous) as cores. Anthropogenic particles were observed in all samples. These frequently included spherical coal fly ash and nonferrous smelter particles (rich in Cu, Zn, and Pb). Combustion soot (chain aggregate or spherical morphology) and noncombustion (probably organic) carbon particles were also observed in most samples. Figures 2c and 2d show two of these particles from major anthropogenic sources, and Figures 3c and 3d show corresponding x-ray spectra.

These results show that different types and concentrations of particles were present during spring 1986 in various Arctic atmospheric layers. Although liquid H_2SO_4 droplets were the dominant particle type observed in all Arctic aerosols, Arctic haze layers also contained significant concentrations of primary particles from anthropogenic and combustion processes (including soot carbon, coal fly ash and smelter-class particles), and solid $(NH_4)_2SO_4$ particles. Haze samples collected off Alert showed lower particle concentrations than similar samples taken at lower latitudes in the Alaskan Arctic, and these measurements were corroborated with concurrent in-situ aerosol measurements. Lower stratospheric aerosols showed higher particle (H_2SO_4) concentrations than did similar middle- to upper-troposphere background samples, but contained very few particles with surface sources. These data support the concept of a highly stable early-springtime Arctic atmosphere.

REFERENCES

Herbert, G.A., R.C. Schnell, H.A. Bridgman, B.A. Bodhaine, S.J. Oltmans, and G.E. Shaw, Meteorology and haze structure during AGASP-II: Part I, Alaskan Arctic flights, 2-10 April, 1986, J. Atmos. Chem., 9, in press, 1989.

Sheridan, P.J., The Use of Analytical Electron Microscopy for the Individual Particle Analysis of the Arctic Haze Aerosol, 281 pp., Ph.D. Dissertation, University of Maryland, College Park, 1986.

Sheridan, P.J., Analytical electron microscope studies of size segregated particles collected during AGASP-II, flights 201-203, J. Atmos. Chem., 9, in press, 1989a.

Sheridan, P.J., Characterization of size segregated particles collected over Alaska and the Canadian High Arctic, AGASP-II flights 204-206, Atmos. Environ., 23, in press, 1989b.

Sheridan, P.J., Determination of experimental and theoretical k-factors for a 200 kV analytical electron microscope, J. Electron Microsc. Tech., 11, 41-61, 1989c.

Sheridan, P.J., and I.H. Musselman, Characterization of aircraft-collected particles present in the Arctic aerosol: Alaskan Arctic, spring 1983, Atmos. Environ., 19, 2159-2166, 1985.

Yount, M.E., T.P. Miller, and B.M. Gamble, The 1986 eruptions of Augustine Volcano, Alaska: Hazards and effects, edited by T.D. Hamilton and J.P. Galloway, pp. 4-13, U.S. Geological Survey Circular 998, 1987.

Precipitation Chemistry at MLO: O-Ring Bias

G. J. STENSLAND

Illinois State Water Survey, Atmospheric Chemistry Section, Champaign, Illinois 61820

1. INTRODUCTION

The NADP/NTN and specifically the CAL at Illinois, have been doing numerous laboratory tests and data evaluations since about 1980 to assess the extent of the bias due to the O-ring in the lid of the collection/shipping container. No reasonable substitute for the O-ring has been found, because of increased cost per sample for possible replacements. The current lids and O-rings are used only one time before disposal. Washing methods for the lids have been improved considerably over time such that the O-ring bias has been minimized. Other users of this commonly used container could have considerably larger or smaller biases in their data because of washing procedures less rigorous than those at CAL and because of different sample handling procedures, respectively.

2. METHODS

With the cooperation of staff at MLO, extra samples have been collected to provide data for one more evaluation of the O-ring bias. The sampling procedure is as follows:

(1) The regular sample from the NADP/NTN wet/dry collector at MLO is shipped to CAL weekly, following standard procedures. Since the collection interval is weekly, the typical age of the rain sample when it reaches the laboratory in Hilo is about 4 days. As the sample is transported from the MLO collection site to the Hilo laboratory, about 32 km, the water splashes in the bucket and contacts the O-ring gasket in the lid. The sample is shipped in the bucket to CAL (about 6400 km) and is about 10 days old when the chemical measurements begin at CAL. During shipment, the sample can again be in contact with the O-ring because of splashing or the sample container being inverted during portions of the shipping process.

(2) At MLO an aliquot of about 100 mL is removed from the regular sample, placed in a plastic bottle, and shipped with the regular sample to CAL. The aliquot is thus identical to the regular sample except it is isolated from the O-ring during the 6400 km shipment to CAL.

(3) A third weekly sample is obtained from a separate wet/dry collector at MLO. This sample is isolated from the O-ring during the 32 km transport to Hilo and is then shipped in a 1-L plastic container to CAL along with the regular NADP/NTN sample and an aliquot of the same. This third sample is never in contact with the O-ring.

The pH is measured at the Hilo field laboratory and again in CAL. No preservatives are added to the samples, so organic acids will degrade during the typical 4 days before the pH is measured at Hilo and also during the shipment to CAL. We assume pH change due to particle dissolution is much smaller than pH change due to degradation of organic acids. All three samples are measured at CAL for inorganic cations and anions; these results will be presented in a later report.

3. RESULTS

The results from the pH measurements are shown in Table 1. Seven questions are listed and the mean and standard errors for either H^+ or H^+ differences are listed as answers to the questions. The results indicate that most of the O-ring effect occurs during shipment from Hilo to Illinois. This could thus be prevented by aliquoting the samples at the field laboratory in Hilo. The pH results in Table 1 indicate that the O-ring effect is much smaller than the natural pH change (due to degradation of organic acids). However, the O-ring concern is enhanced when changes in other ions (such as Na^+ or Mg^{++}) are considered. Results for all the other ions are being analyzed now that the data collection phase of this cooperative project has been completed.

TABLE 1. On the Loss of Hydrogen Ion for Rain Samples from the MLO Site

Question	Answer (µeq/bucket sample)
*For 1987, N = 21 Triplicates**	
Size of H^+ loss in current NADP/NTN procedure?	9.3 ± 2.6
Size of H^+ loss due to degradation of organic acids?	7.9 ± 2.4
Size of total H^+ loss due to O-ring	1.4 ± 0.6
Size of H^+ loss due to O-ring in first 20 miles?	0.1 ± 0.6
Size of H^+ loss due to O-ring in subsequent 4000 miles?	1.3 ± 0.3
Size of H^+ loss from time zero (i.e., time rain ended) to day 4 (i.e., day of Hilo pH measurement)	Unknown
For 1984-1986	
What are the median pH and H^+ at day 4 (i.e., Hilo value, for N = 58 samples)?	4.84; 14.5
What are the median pH and H^+ at day 10 (i.e. CAL value, N = 64)?	5.15; 7.1

*Mean ± standard error

Trends of the Carbon Isotopic Composition of Atmospheric Methane

C. M. STEVENS AND A. ENGELKEMEIR

Argonne National Laboratory, Chemistry and Chemical Technology Divisions, Argonne, Illinois 60439

A program of measuring the $^{13}C/^{12}C$ ratio of CH_4 in background air samples from both hemispheres has been carried out at Argonne National Laboratory since 1981. The objective of this program is to apply the results of the temporal isotopic trends in both hemispheres toward understanding the causes of the increasing global concentration of atmospheric CH_4, an important greenhouse gas [*Blake and Rowland*, 1988; *Khalil and Rasmussen*, 1983; *Steele et al.*, 1987]. The $^{13}C/^{12}C$ ratio of the atmospheric CH_4 from several important natural and anthropogenic sources varies over a wide range of 50 per mil, which constrains the relative distributions of the fluxes needed to satisfy the average isotopic composition in the atmosphere, corrected for the fractionation effect of the sink mechanisms. Likewise the relative distributions of the changing fluxes of different isotopic composition are constrained by the temporal trend in the isotopic composition in the atmosphere. Furthermore the very different distributions of the anthropogenic sources in the two hemispheres provide another constraint for

determining the causes of differences in the isotopic trends between hemispheres.

The CH_4 in 34 L (STP) of background air samples is separated and isotopically analyzed by procedures described by *Stevens and Rust* [1982] and *Stevens and Engelkemeir* [1988]. Prior to 1983 all southern hemisphere air samples and a majority of those from the northern hemisphere were provided from the air sample bank at the Oregon Graduate Center. These samples were collected at locations remote from urban centers: regions of the Pacific Ocean, Samoa, Tasmania, and Antarctica, in the southern hemisphere, and mainly Cape Meares, Oregon, in the northern hemisphere. Beginning in 1983 rural northern Illinois was used as a more convenient site for the northern hemisphere. NOAA's SMO provided most of the southern hemisphere samples after 1986.

Some of the early measurements were reported by *Stevens et al.* [1985], and a brief summary of the results up to 1988 was presented by *Stevens* [1989]. Figure 1 shows the measured
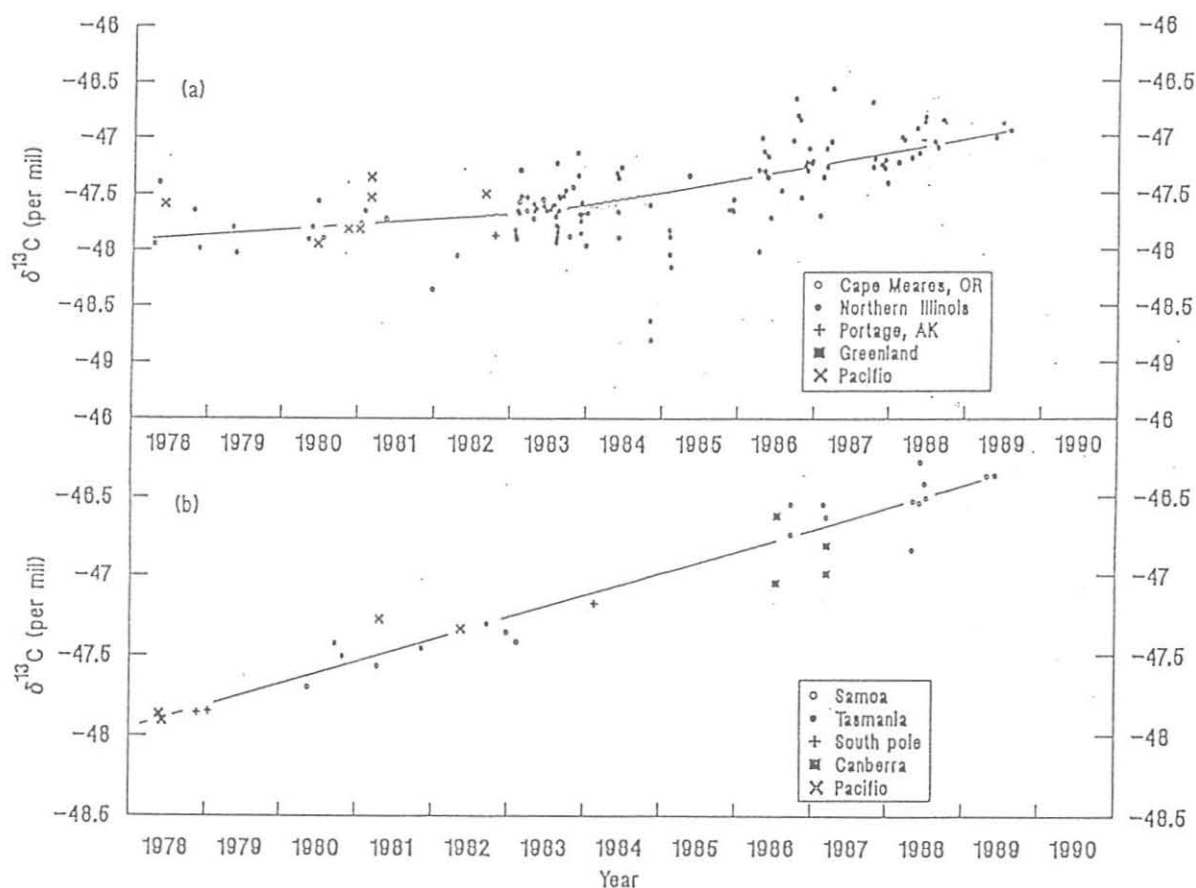

Figure 1. The stable carbon isotopic composition of atmospheric methane, in the del ^{13}C notation (per mil), for (a) the northern hemisphere and (b) the southern hemisphere, from 1978 to 1989.

131

isotopic composition, in the del ^{13}C notation, versus year from 1978 to 1989. These results show ^{13}CH$_4$ increasing in both hemispheres, but with a greater rate of increase in the southern hemisphere. The objective of these trend measurements is to determine as far as is possible the trends in the fluxes of the isotopically different sources, natural or anthropogenic, which could account for the increasing concentration. The trends of the average isotopic composition of atmospheric CH$_4$ in each hemisphere will reflect the trends of the average isotopic composition of the source fluxes in each hemisphere altered by interhemispheric exchange. The analysis of the atmospheric CH$_4$ isotopic trends shows that the ^{13}C of the source fluxes in the southern hemisphere have been increasing by an average of 0.5 per mil per year during the past decade; in the northern hemisphere the trend has been slightly decreasing by an average of 0.1 per mil per year. The increasing trend in the southern hemisphere is most plausibly attributed to increasing fluxes of H$_4$ from biomass burning, which is the principal anthropogenic source in this hemisphere. and is the most isotopically enriched in ^{13}C. The magnitude of the fluxes from the other isotopically heavy sources, losses from natural gas systems and coal mining, are negligible in this hemisphere. This conclusion confirms the reports of rapidly increasing destruction of the tropical rain forest in South America in recent years. The indicated decrease in ^{13}CH$_4$ in the northern hemisphere is more than can be accounted for by trends in the fluxes of the anthropogenic sources in this hemisphere. From this it is deduced that the fluxes from the abundant natural wetlands in the subarctic regions, which are the most isotopically light, have been increasing. A trend of increasing wetlands area and fluxes could be caused by amplified climate warming in the arctic, indicated

by the studies of *Lachenbruch and Marshall* [1988]. A detailed analysis of these isotopic results will be given in a forthcoming paper.

REFERENCES

Blake,D.R., and F.S. Rowland, Continuing worldwide increase in tropospheric methane, 1978 to 1987, *Science, 239*, 1129-1131, 1988.

Khalil, M.A.K., and R.A. Rasmussen, Sources, sinks, and seasonal cycles of atmospheric methane, *J. Geophys. Res., 88*, 5131-5144, 1983.

Lachenbruch, A.H., and B. V. Marshall, Changing climate: Geochemical evidence from permafrost in the Alaskan Arctic, *Science, 234*, 689-696, 1986.

Steele, L.P., G. Fraser, R.A. Rasmussen, M.A.K. Khalil, T.J. Conway, A.J. Crawford, R.H. Gammon, K.A. Masarie, and K.W. Thoning, The global distribution of methane in the troposphere, *J. Atmos. Chem., 5*, 125-171, 1987.

Stevens, C.M., Atmospheric methane, *Chem. Geol., 71*, 11-21, 1989.

Stevens, C.M., and A. Engelkemeir, The stable carbon isotopic composition of methane from some natural and anthropogenic sources, *J. Geophys. Res., 93*, 725-733, 1988.

Stevens, C.M., and F. Rust, The carbon isotopic composition of atmospheric methane, *J. Geophys. Res., 87*, 4879-4882, 1982.

Stevens, C.M., A. Engelkemeir, and R.A. Rasmussen, Causes of increasing methane fluxes based on carbon isotopic studies, WMO Technical Conference on Observations and measurement of Atmospheric Contaminants, *Spec. Environ. Rep. 16, WMO 647*, World Meterological Organization, Geneva, Switzerland, 1985.

Monitoring for Sulfur Dioxide and Total Suspended Particulate at Mauna Loa Observatory

HENRY YEE, WILFRED CHING, AND RICHARD SASAKI

Hawaii State Department of Health, Honolulu, Hawaii 96813

SO_2 and TSP monitoring were reinstituted for long-term study at MLO by the State of Hawaii at the request of EPA Region IX. The long-term trends in SO_2 and TSP (10-μm diameter and smaller) concentrations will be studied to determine the factors contributing to increases observed in the past. Also, the study will work toward determining the atmospheric lifetimes of the particular gases and particulates, and the chemical composition of the other particulates collected at the elevation of MLO.

Table 1 shows the integrated concentrations of 24-h TSP and SO_2 for samples collected at MLO in 1988.

TABLE 1. Twenty-Four Hour Concentrations of TSP (Hi-Vol, Gravimetric Method) and SO_2 (Pararosaniline Method) at MLO

1988	TSP (μg m^{-3})	SO_2 μg m^{-3})	1988	TSP (μg m^{-3})	SO_2 μg m^{-3})
Jan. 10	4.0	0.0	July 8	1.1	
Jan. 22	6.9	7.8	July 14		2.2
Feb. 3	8.8	0.0	July 20	18.5	1.6
Feb. 15	0.7	1.4	Aug. 1	6.6	1.6
Feb. 27	4.1	3.1	Aug. 13	5.2	0.8
March 10	6.2	2.4	Aug. 5	5.2	0.0
March 22	2.6	2.3	Sept. 6	10.0	0.0
April 3	6.2	6.0	Sept. 18	Void	0.8
April 15	13.5	0.0	Sept. 30	4.1	1.5
April 27	6.7	0.8	Oct. 12	3.6	2.0
May 9	8.3	0.0	Oct. 24	Void	Void
May 21	5.2	0.0	Nov. 15	0.0	2.2
June 2	Void	3.2	Nov. 17	3.6	0.8
June 14	4.3	6.3	Nov. 29	2.5	Void
June 26	0.4	0.8	Dec. 11	Void	0.0
			Dec. 29	3.1	1.5

Sampling of Aerosols and Particles at MLO

WILLIAM ZOLLER, DIANE HERMAN, CAI XING YING, DENISE CONNOR,
BRUCE UNDERWOOD, AND ALLAN WU

University of Washington, Seattle 98195

1. INTRODUCTION

The following is an update on the continuation of sampling at MLO. This report falls into two parts, covering data from two different time spans: 1979-1985 and 1988.

2. DATA FROM 1979 TO 1985: As, Al, Na

The filters used to collect the particles were 110-mm-diameter Nuclepore filters with 0.4-µg pore diameters. Filters were loaded into the filter holders in a Class-100 clean room at the University of Maryland. Filter packs were then placed in acid-washed polyethylene bags and mailed to MLO. Filters and filter holders were changed weekly by MLO personnel and shipped back to the University of Maryland for analysis. Sample filters were unpacked, removed from filter holders, cut into halves using a stainless-steel scalpel, and stored in acid-washed (HNO_3) polyethylene bags in a Class-100 clean room. One-half was analyzed for elemental concentrations by INAA, using a procedure similar to that of *Germani et al.* [1980]. The other half was stored for later analysis.

In 1979, particles were collected on a selective sampling system. In May 1980, the selective sampling system was replaced by a wind directional controller, which samples according to time of day, wind speed, and wind direction (i.e., upslope versus downslope). Three primary components make up the samples: crustal, marine, and enriched. Justification for using Al to represent crustal (Figure 1), As for enriched (Figure 2), and Na for marine (Figure 3) can be found in *Zoller et al.* [1979]. For results on the overall project (1979-1985) refer to *Parrington* [1983].

3. DATA FROM 1988: $SO_4^=$, NO_3^-

Packaging and shipping were similar to the process described in Section 2; however, all 1988 filters were analyzed at the University of Washington. Recently, blanks have been used to check the cleanliness of the shipping process. Results showed the shipping process caused little or no contamination to filter packs. Gaseous sulfur and nitrogen precursors were collected on LiOH-treated 110-mm diameter Whatman 541 filters. Filters were exposed for 7 days at MLO. Each filter was cut into four quarters and stored in Whirl-packs. One quarter was then analyzed for $SO_4^=$ and NO_3^- concentrations on a Dionex ion-chromatograph, Model Q1C-standard column. (Remaining quarters are stored in refrigeration for other analyses and archival purposes.)

The results shown in Figures 4 and 5 should not be taken as solid data. The results are being reported only to give the reader
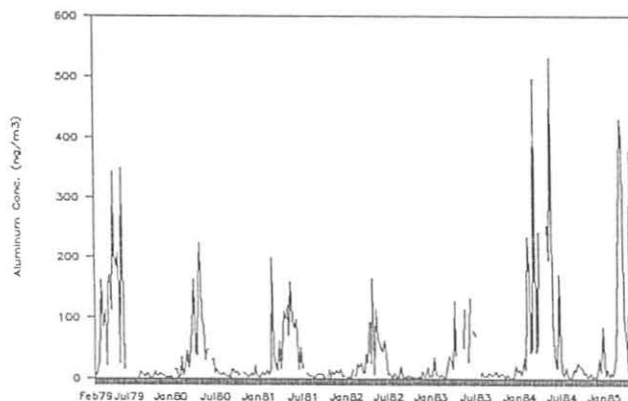

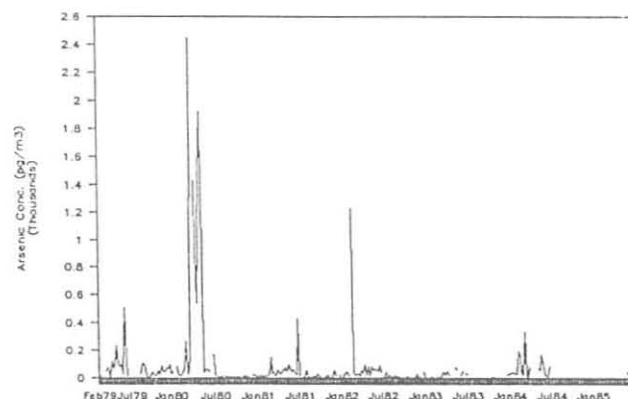Fig. 1. Aluminum concentrations at MLO, February 1979-May 1985.

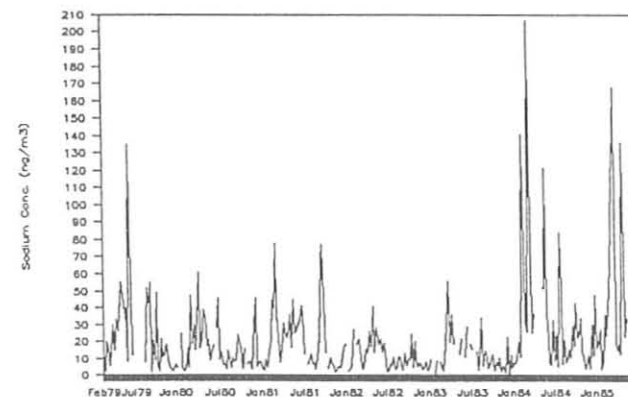Fig. 2. Arsenic concentrations at MLO, February 1979-May 1985.

Fig. 3. Sodium concentrations at MLO, February 1979-May 1985.

134
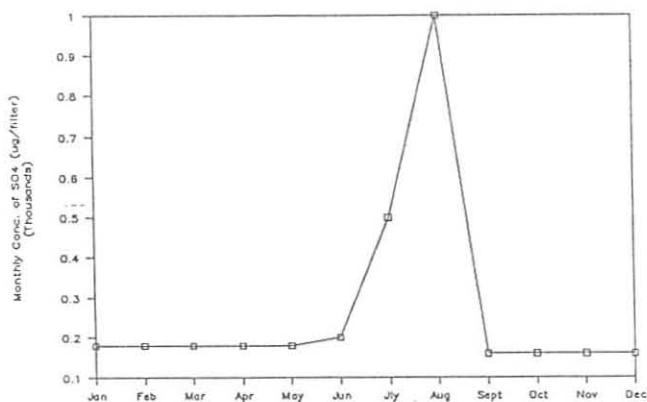
Fig. 4. Preliminary concentrations of $SO_4^=$ at MLO, 1988.
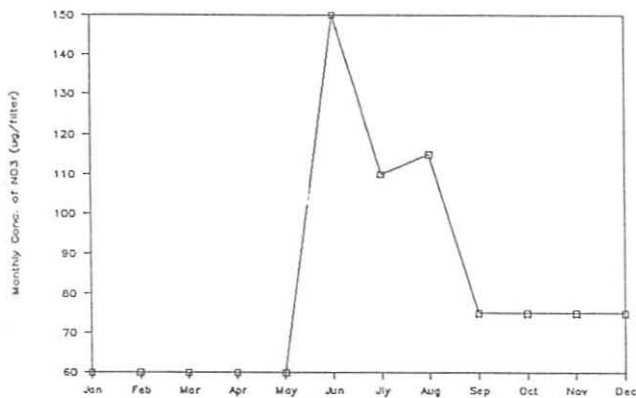
Fig. 5. Preliminary concentrations of NO_3^- at MLO, 1988.

a rough estimate of the MLO data. Actual volume of air sampled has not yet been determined because of a missing pump calibration curve. During the months of April and May, the system at MLO was inoperable. The figures are generated from rough data in 1988. Not all the filters for 1988 have been sampled yet. The baselines for $SO_4^=$ and NO_3^- were determined from previous studies. A more detailed and complete report on $SO_4^=$ and NO_3^- for 1988 at MLO will be published soon.

REFERENCES

Germani, M.S., Concentrations of elements in the National Bureau of Standards bituminous and subbituminous coal standard reference materials, *Anal. Chem., 52*(2), 240-244, 1980.

Parrington, J.R., The chemistry of background atmospheric particles collected at Mauna Loa Observatory, Hawaii, Ph.D. thesis, Univ. of Washington, Seattle, 1983.

Zoller, W.H., W.C. Cunningham, and N.K. Aras, Chemical composition of atmospheric aerosols, in *Geophysical Monitoring for Climatic Change, No. 8: Summary Report 1979*, edited by G.A. Herbert, pp. 88-93, NOAA Air Resources Laboratory, Boulder, CO, 1980.

11. International Activities, 1988

Dale Gillette attended planning sessions in the U.S.S.R. for the Working Group VIII experiment on desert dust to be conducted September 1989 in the Kurgan Tjube area of Tadzhikistan, U.S.S.R. The planning sessions took place in Dushanbe, Tadzhikistan, Moscow, and Leningrad. Among other Soviet institutions visited were the Soviet Academy of Sciences, the Hydrometeorological Service, the Leningrad Main Geophysical Observatory, and Leningrad State University.

J. Chin, a long-time member of the MLO staff with special responsibilities for the CO_2 instrumentation and flask sampling, was invited to visit the People's Republic of China in August. During this visit he served as a special consultant to PRC scientists in their program of CO_2 measurements and monitoring. He also presented several lectures describing MLO CO_2 and other monitoring programs.

During July 23-August 2, D. Wellman, L. Gunter, and J. Ray traveled to Bermuda to conduct research aircraft data flights as a part of the CASE-WATOX experiment.

H. Sievering toured the Bermuda Biological Station (BBS) and discussed the presentation and incorporation of dry deposition review into a BBS course entitled *Global Change*.

In August, M. Luria attended the *1988 Quadrennial International Ozone Symposium* at Göttingen, FRG to present a paper entitled "The relationship between O_3 and H_2O_2: Field observation and model evaluation."

During November 13-20, D. Wellman traveled to Garmisch-Partenkirchen, FRG, to attend the *ACID-MODES First Intensive Field Study Data Workshop and Planning Session*.

During October 3-7, Y. Kim traveled to Tokyo, Japan, to attend the *2nd International Conference on Atmospheric Sciences and Applications to Air Quality*.

In March, P. Tans participated in a conference in Washington, DC, sponsored by the National Geographic Society and the Egyptian Antiquities Organization. He presented the results of the GMCC measurements of air sampled from an ancient Egyptian tomb.

In August, L. Waterman visited Midway Island and Guam, two Flask Network sampling sites. The flask sampling locations were inspected, sampling techniques were observed, and suggestions for improvements were made.

J. Peterson and T. Conway attended the second *Scientific Application of Baseline Observations of Atmospheric Composition* conference, Aspendale, Australia, November 14-17. Two papers concerning GMCC CO_2 measurements were presented: "Short term variations of atmospheric carbon dioxide at the South Pole" and "Atmospheric CO_2 concentrations during and following the 1987 El Niño." Prior to the meeting a visit was made to the Australian Baseline Air Pollution Station at Cape Grim, Tasmania.

The GMCC cooperative flask sampling network continued flask sampling agreements with Australia (Cape Grim); Barbados (Ragged Point); Canada (Alert and Mould Bay); France (Amsterdam Island); Japan (Syowa Station, Antarctica); Norway (Station M); and the United Kingdom (Halley Bay, Antarctica and South Georgia Island).

In April, P. Steele visited the CSIRO Division of Atmospheric Research for discussions on collaborative programs. During June an international cooperative experiment was begun to collect large-volume air samples at Niwot Ridge and analyze them for many trace species, including isotopic ratios in CO_2 and CH_4. Participants in the experiment are from CIRES, GMCC, DSIR, and CSIRO, with overall coordination by P. Steele.

During July, P. Steele participated in the *Arctic Boundary Layer Expedition (ABLE-3A)* sponsored by NASA as part of its Global Tropospheric Experiment program and carried out in the Alaskan Arctic. This participation involved supplying calibration gases to other participants in the study, as well as collecting flask air samples on several flights made in the vicinity of Barrow.

In August, J. DeLuisi traveled to Leningrad with R. Cess, R. Schiffer (leader), and T. VanderHaar to establish a new section on Earth Radiation Budget (Section 13) under the U.S.-U.S.S.R. Bilateral Working Group VIII agreement. At this meeting data exchanges were proposed. An exchange of two GMCC radiation instruments with two similar instruments to be deployed for 1 year at Vostok and SPO was also proposed. Data for these two sites would also be exchanged.

At the *1988 Quadrennial International Ozone Symposium* held in Göttingen, F.R.G., J. DeLuisi was appointed to serve as a member of the International Ozone Commission. He will act as rapporteur for Umkehr measurements.

At the *XIV International Laser Radar Conference* held at San Candido, Italy, in June, J. DeLuisi held a small workshop to assess the progress of the World Lidar Network. He also gave a progress report at a discussion session that was held at the end of the conference. He had organized the network several years previously, following the eruption of El Chichon, to obtain stratospheric aerosol data for correcting Umkehr measurements. The Umkehr corrected measurements were used to assess the drift rate of the SBUV, which turned out to be very serious.

B. Bodhaine participated in the *Twelfth International Conference on Atmospheric Aerosols and Nucleation* in Vienna, Austria, and presented papers entitled "South Pole aerosol measurements during 1987," and "Aerosol formation and distribution in the Arctic during AGASP-II, March-April 1986."

As part of U.S.-U.S.S.R. Working Group XIII, B. Bodhaine traveled to Moscow and Dushanbe to assist in planning a desert dust experiment in southern U.S.S.R and to aid in planning a high-altitude continental background monitoring station near Dushanbe.

In August 1988, W. Komhyr, R. Evans, R. Grass, S. Oltmans, P. Franchois, and G. Koenig attended the *1988 Quadrennial International Ozone Symposium* held in Göttingen, West Germany.

S. Oltmans visited Tudor Hill, Bermuda, in October 1988, to begin a program for monitoring tropospheric ozone as part of the Atmosphere/Ocean Chemistry Experiment (AEROCE).

R. Grass, R. Evans, and K. Leonard participated in an intercomparison of Dobson ozone spectrophotometers in Perth,

Australia, in November. En route, Grass and Evans visited personnel of the Australian Weather Bureau in Melbourne to discuss Dobson instrument calibrations. Prior to returning to Boulder in December, Grass and Evans visited New Zealand to calibrate an automated Dobson spectrophotometer located in Lauder.

In addition to the Australian and New Zealand Dobson instrument calibrations, two instruments from the U.S.S.R. were calibrated in Boulder during 1988.

J. Elkins attended the SABOAC-II meeting in Aspendale, Australia, on November 11-19, 1988.

J. Butler attended the SAGA-II workshop to review the cruise data with American and Soviet scientists in Seattle, Washington, March 2-3, 1988.

J. Butler presented a paper entitled "Atmospheric distributions, deep-water profiles, and surface fluxes of N_2O from the Soviet-American Gas and Aerosol Experiment of 1987 (SAGA II)" at the Commonwealth Scientific and Industrial Research Organization (CSIRO), Aspendale, Australia, 1988.

12. Publications and Presentations by GMCC Staff, 1988

Artz, R.S., G.D. Rolph, and J.M. Harris, Meteorological summary of four WATOX 1985 research intensives, *Atmos. Environ.*, *22*, 2361-2369, 1988.

Barrie, L.A., J.W. Bottenheim, R.C. Schnell, P.J. Crutzen, and R.A. Rasmussen, Ozone destruction and photochemical reactions at polar sunrise in the lower Arctic atmosphere, *Nature, 334*, 138-141, 1988.

Barry, R.G., R.C. Cianflone, W.M. Miles, M.C. Serreze, and R.C. Schnell, Surface characteristics of Arctic sea ice from remote sensing data, *Preprints, IGS Symposium on Ice Dynamics*, Hobart, Tasmania, February 1988.

Boatman, J.F., M. Luria, C.C. Van Valin, and D.L. Wellman, Continuous atmospheric sulfur gas measurements aboard an aircraft: A comparison between the flame photometric and fluorescence methods, *Atmos. Environ., 22(9)*, 1949-1955, 1988.

Boatman, J.F., D.L. Wellman, R.C. Schnell, K.M. Busness, M. Luria, and C.C. Van Valin, In-flight intercomparisons of some aircraft meteorological and chemical measurement techniques, *Global Biogeochem. Cycles, 2(1)*, 1-11, 1988.

Bodhaine, B.A., and R.M. Rosson (Eds.), *Geophysical Monitoring for Climatic Change, No. 16: Summary Report 1987*, 110 pp., NOAA Air Resources Laboratory, Boulder, CO, 1988.

Bodhaine, B.A., E.G. Dutton, J.J. DeLuisi, J.M. Harris, G.E. Shaw, A.D.A. Hansen, and T. Novakov, South Pole aerosol measurements during 1987, *Preprints, 12th International Conference on Atmospheric Aerosols and Nucleation*, Vienna, Austria, August 22-27, 1988.

Bridgman, H.A., H. Sievering, and T. Watson, Large and giant aerosols in the marine boundary layer during WATOX, January 4-9, 1986, *Global Biogeochem. Cycles, 2(1)*, 13-21, 1988.

Bridgman, H.A., R.C. Schnell, B.A. Bodhaine, and S.J. Oltmans, Aerosol and ozone distributions over the western North Atlantic during WATOX-86, *Global Biogeochem. Cycles, 2*(1), 23-39, 1988.

Burkhardt, M.R., M.P. Buhr, J.D. Ray, and D.H. Stedman, A continuous monitor for nitric acid, *Atmos. Environ., 22*, 1575-1578, 1988.

Butler, J.H., Atmospheric distributions, deep-water profiles, and surface fluxes of N_2O from the Soviet-American Gas and Aerosol Experiment of 1987 (SAGA II), paper presented at the Commonwealth Scientific and Industrial Research Organization (CSIRO), Aspendale, Australia, 1988.

Butler, J.H., Trace gas measurements in the air and waters of the western Pacific and eastern Indian Oceans during SAGA II, paper presented at the College of Oceanography, Oregon State University, 1988.

Butler, J.H., J.E. Pequegnat, L.I. Gordon, and R.D. Jones, Cycling of methane, carbon monoxide, nitrous oxide, and hydroxylamine in a meromictic, coastal lagoon, *Estuar. Coast. Shelf Sci., 27*, 181-203, 1988.

Butler, J.H., J.W. Elkins, C.M. Brunson, K.B. Egan, T.M. Thompson, T.J. Conway, and B.D. Hall, Trace gases in and over the west Pacific and east Indian Oceans during the El Niño-Southern Oscillation event of 1987, *NOAA Data Report ERL ARL-16*, 104 pp., NOAA Air Resources Laboratory, Boulder, CO, 1988.

Conway, T.J., and K.W. Thoning, Short-term variations of atmospheric carbon dioxide at the South Pole, paper presented at the Second Scientific Application of Baseline Observations of Atmospheric Composition Conference, Aspendale, Australia, November 14-17, 1988.

Conway, T.J., P. Tans, L.S. Waterman, K.W. Thoning, K.A. Masarie, and R.H. Gammon, Atmospheric carbon dioxide measurements in the remote global troposphere, 1981-1984, *Tellus, 40B*, 81-115, 1988.

Elkins, J.W., T.M. Thompson, and J.H. Butler, Halocarbons CFC-12 and CFC-11, and nitrous oxide measurements from NOAA/GMCC baseline observatories since 1977, paper presented at the Second Scientific Application of Baseline Observations of Atmospheric Composition Conference, Aspendale, Australia, November 14-17, 1988.

Evans, R.D., G.L. Koenig, W.D. Komhyr, J. Easson, and P Marché, Umkehr observations at five automated Dobson spectrophotometer stations in 1986 and 1987, paper presented at the Quadrennial Ozone Symposium, Göttingen, FRG, August 8-13, 1988.

Franchois, P.R., G. Koenig, R.D. Evans, and W.D. Komhyr, Comparison of ECC ozonesonde and Umkehr profile at Boulder, Colorado, 1985-1987, and Mauna Loa, Hawaii, 1985-1987, paper presented at the Quadrennial Ozone Symposium, Göttingen, FRG, August 8-13, 1988.

Fried, A., R. Sams, W. Dorko, J.W. Elkins, and Z-t. Cai, Determination of nitrogen dioxide in air compressed gas mixtures by quantitative tunable diode laser absorption spectrometry and chemiluminescence detection, *Anal. Chem., 60*, 394-403, 1988.

Fryrear, D.W., J.E. Stout, and D.A. Gillette, Instrumentation for wind erosion, *Proceedings, 1988 Wind Erosion Conference*, Lubbock, TX, April 11-13, 1988, pp. 117-132, Texas Tech. Univ., 1988.

Galloway, J.N., R.S. Artz, U. Dayan, R.F. Pueschel, and J.F. Boatman, WATOX 85: An aircraft and ground sampling program to determine transport of trace gases and aerosols across the Western Atlantic Ocean, *Atmos. Environ., 22(11)*, 2345-2360, 1988.

Gillette, D.A., Estimation of dust production by wind erosion, for use by the National Acid Precipitation Assessment Program, *Proceedings, 1988 Wind Erosion Conference*, Lubbock, TX, April 11-13, 1988, pp. 188-197, Texas Tech. Univ., 1988.

Gillette, D.A., Threshold friction velocities for dust production for agricultural soils, *J. Geophys. Res., 93*, 12,645-12,662, 1988.

Gillette, D.A., and R. Passi, Modeling dust emission caused by wind erosion, *J. Geophys. Res., 93*, 14,233-14,242, 1988.

Grass, R.D., and W.D. Komhyr, Travelling standard lamp calibration checks of Dobson ozone spectrophotometers during 1985-1987, paper presented at the Quadrennial Ozone Symposium, Göttingen, FRG, August 8-13, 1988.

Halter, B.C., J.M. Harris, and T.J. Conway, Component signals in the record of atmospheric carbon dioxide concentration at American Samoa, *J. Geophys. Res., 93*, 15,914-15,918, 1988.

Hansen, A.D.A., B.A. Bodhaine, E.G. Dutton, and R.C. Schnell, Aerosol black carbon measurements at the South Pole: Initial results, 1986-1987, *Geophys. Res. Lett., 15*, 1193-1196, 1988.

Herbert, G.A., J.M. Harris, and B.A. Bodhaine, Atmospheric transport during AGASP-II: The Alaskan flights (2-10 April 1986), *Atmos. Environ., 23(11)*, 2521-2536, 1988.

Herbert, G.A., J.M. Harris, B.A. Bodhaine, and R.C. Schnell, A summary of atmospheric transport to Barrow, Alaska, during the Arctic Gas and Aerosol Sampling Program (March 1983 and April 1986), *Preprints, Second Conference on Polar Meteorology and Oceanography*, Madison, WI, March 29-31, 1988, pp. 116-118, American Meteorological Society, Boston, 1988.

Kahl, J.D., and P.J. Samson, Some limitations of rawinsondes in pollutant transport studies, *Proceedings, Symposium on Lower Tropospheric Profiling: Needs and Technologies*, Boulder, CO, May 31-June 3, 1988, pp. 67--68, American Meteorological Society, Boston, 1988.

Kahl, J.D., J.M. Harris, G.A. Herbert, and M.P. Olson, Intercomparison of three long-range trajectory models applied to Arctic haze, *Tellus, 41B*, 524-536, 1988.

Kim, Y.J., H.S. Sievering, and J.F. Boatman, Airborne measurements of atmospheric aerosol particles in the lower troposphere over the Central United States, *J. Geophys. Res., 93(D10)*, 12,631-12,644, 1988.

Komhyr, W.D., E.G. Dutton, and T.M. Thompson, A general gravimetric dilution technique for preparing trace calibration gases: N_2O calibration gas preparation, *Environ. Sci. Technol., 22*, 845-848, 1988.

Komhyr, W.D., R.D. Grass, and R.K. Leonard, Calibration of primary standard Dobson spectrophotometer no. 83 and total ozone trends at Mauna Loa Observatory, Hawaii, and American Samoa, South Pacific, paper presented at the Quadrennial Ozone Symposium,

Göttingen, FRG, August 8-13, 1988.

Komhyr, W.D., S.J. Oltmans, and R.D. Grass, Atmospheric ozone at South Pole, Antarctica, in 1986, *J. Geophys. Res., 93(5)*, 5167-5184, 1988.

Komhyr, W.D., P.R. Franchois, S.E. Kuester, P.J. Reitelbach, and M.L. Fanning, ECC ozonesonde observations at South Pole, Antarctica, during 1987, *NOAA Data Report ERL ARL-15*, 319 pp., NOAA Air Resources Laboratory, Boulder, CO, 1988.

Komhyr, W.D., R.D. Grass, R.D. Evans, and R.K. Leonard, Results of international Dobson spectrophotometer and Brewer spectrophotometer intercomparisons, Arosa, Switzerland, 1986, paper presented at the Quadrennial Ozone Symposium, Göttingen, FRG, August 8-13, 1988.

Komhyr, W.D., S.J. Oltmans, R.D. Grass, P.R. Franchois, and R.K. Leonard, Changes in total ozone and ozone vertical distributions at South Pole, Antarctica, 1962-1987, paper presented at the Quadrennial Ozone Symposium, Göttingen, FRG, August 8-13, 1988.

Komhyr, W.D., S.J. Oltmans, P.R. Franchois, W.F. Evans, and W.A. Matthews, The latitudinal distribution of ozone to 35 km altitude from ECC ozonesonde observations, paper presented at the Quadrennial Ozone Symposium, Göttingen, FRG, August 8-13, 1988.

Lepel, E.A., W.K. Hensley, J.F. Boatman, K.M. Busness, W.E. Davis, D.E. Robertson, and W.G.N. Slinn, Airborne radioactivity measurements from the Chernobyl plume, *J. Radioanal. Nucl. Chem., 123(1)*, 7-19, 1988.

Luria, M.L. and J.F. Meagher, Computer simulations of the boundary layer oxidation and removal of atmospheric pollutants over the Western Atlantic Ocean, *Atmos. Environ., 22*, 307-319, 1988.

Luria, M., C.C. Van Valin, W.C. Keene, D.L. Wellman, J.N. Galloway, and J.F. Boatman, Eastward sulfur flux from the Northeastern United States, *Atmos. Environ., 22*, 1847-1856, 1988.

Matthews, W.A., W.D. Komhyr, and P.R. Franchois, Vertical distribution and variation in atmospheric ozone over Lauder, New Zealand, paper presented at the Quadrennial Ozone Symposium, Göttingen, FRG, August 8-13, 1988.

McPeters, R.D., and W.D. Komhyr, Long-term changes in SBUV/TOMS relative to the world primary standard Dobson instrument, paper presented at the Quadrennial Ozone Symposium, Göttingen, FRG, August 8-13, 1988.

Oltmans, S.J., W.D. Komhyr, P.R. Franchois, and W.A. Matthews, Tropospheric ozone: Variations from surface and ECC ozonesonde observations, paper presented at the Quadrennial Ozone Symposium, Göttingen, FRG, August 8-13, 1988.

Oltmans, S.J., P.J. Sheridan, R.C. Schnell, and J.W. Winchester, Springtime surface ozone fluctuations at high Arctic latitude and the possible relationship to atmospheric bromine, *Preprints, Polar Ozone Workshop*, Aspen, CO, May 9-13, 1988.

Oltmans, S.J., P.J. Sheridan, R.C. Schnell, R.E. Peterson, J.W. Winchester, L.A. Barrie, J.D. Kahl, and W.D. Komhyr, Springtime ozone fluctuations at high Arctic latitudes and their possible relationship to atmospheric bromine, paper presented at the Quadrennial Ozone Symposium, Göttingen, FRG, August 8-13, 1988.

Pickering, K.E., R.R. Dickerson, G.J. Huffman, J.F. Boatman, and A. Schanot, Trace gas transport in the vicinity of frontal convective clouds, *J. Geophys. Res., 93(D1)*, 759-773, 1988.

Pueschel, R.F., J.F. Boatman, and R.S. Artz, Aerosols over the western Atlantic: Scale heights, concentrations and fluxes, *Atmos. Environ., 22(11)*, 2371-2380, 1988.

Rahn, K.A., D.H. Lowenthal, and J.M. Harris, Long-range transport of pollution aerosol from Asia and the Arctic to Okushiri Island, Japan, *Atmos. Environ., 23(11)*, 2597-2608, 1988.

Reinsel, G.R., G. C. Tiao, S.K. Ahn, M. Pugh, S. Basu, J.J. DeLuisi, C.L. Mateer, A.J. Miller, P.S. Connell, and D.J. Wuebbles, An analysis of the 7-year record of SBUV satellite ozone data: Global profile features and trends in total ozone, *J. Geophys. Res., 93*, 1689-1703, 1988.

Robinson, E., and L. Ashman, Book Review (*Acid Earth: The Global Threat of Acid Pollution*, Earthscan, 190 pp., Washington, DC, 1985), *Water Air Soil Pollut. 37*, 230-231, 1988.

Robinson, E., B.A. Bodhaine, W.D. Komhyr, S.J. Oltmans, L.P. Steele, P. Tans, and T.M. Thompson, Long-term air quality monitoring at the South Pole by the NOAA program Geophysical Monitoring for Climatic Change, *Rev. Geophys., 26*, 63-80, 1988.

Rosen, J.M., D.J. Hoffman, J.R. Carpenter, J.W. Harder, and S.J. Oltmans, Balloonborne Antarctic frost point measurements and their impact on polar stratospheric cloud theories, *Geophys. Res. Lett., 15*, 859-862, 1988.

Schnell R.C., Arctic air chemistry, *Arctic Res., 2*, 39-41, 1988.

Schnell, R.C., Arctic haze: Long-range pollution of the polar atmosphere, paper presented at the Global Effects of Atmospheric Contaminants Meeting, University of New Mexico, Albuquerque, NM, October 25, 1988.

Schnell, R.C., Bacteria produced atmospheric condensation and ice nuclei, *Preprints, AGU, Chapman Conference on the Gaia Hypothesis*, San Diego, CA, March 7-11, 1988.

Schnell, R.C., Long-residence time, high carbon content aerosol in the Arctic troposphere, abstract of paper presented at the DNA Global Effects Meeting, Santa Barbara, CA, April 19-21, 1988.

Schnell, R.C., J. D. Kahl, H.A. Bridgman, and G.A. Herbert, Aerosol formation and distribution in the Arctic during AGASP-II, in *Atmospheric Aerosols and Nucleation*, edited by P.E. Wagner and G. Vali, pp. 32-35, Springer-Verlag, New York, 1988.

Schnell, R.C., J.D. Kahl, H.A. Bridgman, and G.A. Herbert, A major Arctic haze event north of Point Barrow, Alaska, April 1986, *Preprints, Second Conference on Polar Meteorology and Oceanography*, Madison, WI, March 28-30, 1988, pp. 112-115, American Meteorology Society, Boston, 1988.

Schnell, R.C., P.J. Sheridan, R.E. Peterson, and S.J. Oltmans, Airborne measurements of tropospheric ozone destruction and particulate bromide formation in the Arctic, *Proceedings, Polar Ozone Workshop*, Aspen, CO, May 9-13, 1988, *NASA Conference Publication 1014*, pp. 204-205, National Aeronautics and Space Administration, Washington, DC, 1988.

Schnell, R.C., J.D. Kahl, H.A. Bridgman, G.A. Herbert, B.A. Bodhaine, and S.J. Oltmans, Aerosol formation and distribution in the Arctic during AGASP-II, March-April 1986, *Preprints, 12th International Conference on Atmospheric Aerosols and Nucleation*, Vienna, Austria, August, 22-27, 1988.

Tans, P.P., J.W. Elkins, D.R. Kitzis, Air sampling procedures and measurements of the air composition of the second boat pit of Khufu's pyramid, *NOAA Tech. Memo. ERL ARL-163*, 21 pp., NOAA Air Resources Laboratory, Boulder, CO, 1988.

Taylor, J.A., A stochastic global Lagrangian atmospheric transport model to determine global CO_2 sources and sinks--A preliminary discussion, *Tellus, 41B*, 272-285, 1989.

Thompson, T.M., Results from the SAGA-II expedition in 1987, paper presented at National Bureau of Standards, Gaithersburg, MD, 1988.

Thompson, T.M., J.W. Elkins, J.H. Butler, and K.B. Egan, Trichlorofluoromethane (CFC-11) and dichlorodifluoromethane (CFC-12) in the western Pacific and eastern Indian oceans' atmosphere and surface water, paper A31-07 paper presented at the AGU Spring Meeting, Baltimore, Maryland, May 16-20, *EOS, 69*, 313, 1988.

Thoning, K.W., T.J. Conway, P.P. Tans, and J.T. Peterson, Atmospheric CO_2 concentrations during and following the 1987 El Niño, paper presented at the Second Scientific Application of Baseline Observations of Atmospheric Composition Conference, Aspendale, Australia, November 14-17, 1988.

Van Valin, C.C., and M. Luria, O_3, CO, hydrocarbons, and dimethyl sulfide over the Western Atlantic Ocean, *Atmos. Environ., 22*, 2401-2409, 1988.

Whelpdale, D.M., W.C. Keene, A.D.A. Hansen, and J. Boatman, Aircraft measurements of sulfur, nitrogen, and carbon species during WATOX-86, *Global Biogeochem. Cycles, 1(4)*, 357-368, 1988.

Wilkison, S., and J.F. Boatman, The NOAA King Air airborne data acquisition system: Description and user's guide, *NOAA Tech. Memo. ERL ARL-164*, 19 pp., NOAA Air Resources Laboratory, Silver Spring, MD, 1988.

13. Acronyms and Abbreviations

ABLE	Atmospheric Boundary Layer Expedition
ACID-MODES	Acid Model Evaluation Studies
ACR	active cavity radiometer
AEC	Atomic Energy Commission
AEM	analytical electron microscope
AEROCE	Atmosphere/Ocean Chemistry Experiment
AES	Atmospheric Environment Service, Canada
AFOS	Automated Field Observing System
AGASP	Arctic Gas and Aerosol Sampling Program
AL	Aeronomy Laboratory, Boulder, Colorado (ERL)
ALE/GAGE	Atmospheric Lifetime Experiment/Global Atmospheric Gases Experiment
ALT	Alert Observatory, Canada
ANARE	Australian National Antarctic Research Expeditions
AOML	Atlantic Oceanographic and Meteorological Laboratory, Miami, Florida (ERL)
ARL	Air Resources Laboratory, Silver Spring, Maryland (ERL)
ARM	Aerosols and Radiation Monitoring Group, Boulder, Colorado (GMCC)
ASASP	Active Scattering Aerosol Spetromter Probe
ASCS	Alaska Soil Conservation Service
AQG	Air Quality Group, Boulder, Colorado (GMCC)
BAO	Boulder Atmospheric Observatory
BLM	Bureau of Land Management
BRW	Barrow Observatory, Barrow, Alaska (GMCC)
CAF	Clean Air Facility
CAL	Central Analytical Laboratory
CAMS	Control and Monitoring System
CASE	Coordinated Air-Sea Experiment
CFC	chlorofluorcarbon
CFC-11	trichlorofluoromethane
CFC-12	dichlorodifluoromethane
CGBAPS	Cape Grim Baseline Air Pollution Station, Australia
CIRES	Cooperative Institute for Research in Environmental Sciences, University of Colorado, Boulder, Colorado
CN	condensation nuclei
CNC	condensation nucleus counter
CPACE	Central Pacific Atmospheric Chemistry Experiment
CRREL	Cold Regions Research & Engineering Laboratory, U.S. Army, Hanover, New Hampshsire
CSI	Columbia Scientific, Inc.
CSIRO/DAR	Commonwealth Scientific and Industrial Research Organization/Division of Atmospheric Research, Australia
CSU	Colorado State University
CURTAIN	Central United States RADM Test and Assessment Intensives
DAS	differential absorption spectroscopy
DB	direct-beam [irradiance]
DEW	distant early warning
DOE	Department of Energy
DOI	Department of Interior
DOT	Department of Transportation
DSIR	Department of Scientific and Industrial Research, New Zealand
ECC	electrochemical concentration cell
ECD	electron capture detector
EC-GC	electron capture-gas chromatograph
ECP	Enhanced Chemistry Project
EDS	Energy Dispersive X-ray Spectrometry
EKTO	(a commercial name for a prefabricated building)
EML	Environmental Measurements Laboratory (DOE)
ENSO	El Niño/Southern Oscillation
EPA	Environmental Protection Agency

ERBE	Earth Radiation Budget Experiment
ERL	Environmental Research Laboratories, Boulder, Colorado (NOAA)
FAST	forward alpha scattering techniques
FID	flame ionization detector
FS	Forest Service
FTIR	Fourier transform infrared (spectroscopy)
GAGE	Global Atmospheric Gases Experiment
GC	gas chromatograph
GCE	Global Change Expedition
G.E.	General Electric
GLOBE	Global Backscatter Experiment
GMCC	Geophysical Monitoring for Climatic Change, Boulder, Colorado (ARL)
GMD	ground meteorological device
GOES	Global Orbiting Earth Satellite
GPCP	Global Precipitation Chemistry Project
HCFC	Hydrochloroflurocarbon
HFC	Hydrofluorocarbon
HP	Hewlett-Packard
IBM	International Business Machines
IMPROVE	Interagency Monitoring of Protected Visual Environments (NPS, EPA, FS, BLM, and DOI)
INAA	instrumental neutron activation analysis
IR	infrared
ISWS	Illinois State Water Survey
LANDSAT	Land Satellite
LAWS	Laser Atmospheric Wind Sounder
LEAPS	Low Electron Attachment Potential Species
LES	Lincoln Experimental Satellite [operated by Lincoln Laboratories, Lincoln, Massachusetts]
LIPM	Laser Integrating Plate Method
LOPC	laser optical particle counter
LST	local standard time
LW	longwave
LWD	longwave downward irradiance
LWRF	longwave radiative forcing
MABIE	Mauna Loa Aerosol Backscatter Intercomparison Experiment
MCCP	Mountain Cloud Chemistry Project
McIDAS	Man-computer Interactive Data Access System
MFOV	multiple field of view radiometer
MLO	Mauna Loa Observatory, Hawaii (GMCC)
MLOPEX	MLO Photochemical Experiment
MSFC	Marshall Space Flight Center, Huntsville, Alabama (NASA)
MSL	mean sea level
MUSIC	Multiple Species Intercomparison
NADP	National Atmospheric Deposition Program
NAPAP	National Acid Precipitation Assessment Program
NASA	National Aeronautics and Space Administration
NBS	National Bureau of Standards, Boulder, Colorado (now NIST)
NCAR	National Center for Atmospheric Research, Boulder, Colorado
NDIR	non-dispersive infrared analyzer
NERDDC	National Energy Research Development anf Demonstration Council, Australia
NESDIS	National Environmental Satellite, Data, and Information Service (NOAA)_
NIH	National Institutes of Health
NIP	normal incidence pyrheliometer
NIST	National Institute for Standards and Technology, Boulder, Colorado (formerly NBS)
NOAA	National Oceanic and Atmospheric Administration
NOAH	Nitrous Oxide And Halocarbons Group, Boulder, Colorado (GMCC)
NPS	National Park Service
NRBS	non-Rayleigh backscatter
NSF	National Science Foundation

NTN	National Trends Network
NWR	Niwot Ridge, Colorado
NWS	National Weather Service
NZARP	New Zealand Antarctic Research Program
OGC	Oregon Graduate Center, Beaverton, Oregon
PC	personal computer
PDB	Pee Dee Belemnite
PESA	proton elastic scattering analysis
P.I.	Principal Investigator
PIXE	Proton-Induced X-ray Emission
PMOD	Physikalisch-Meteorologisches Observatorium Davos (World Radiation Center)
PMT	photomultipier tube
PRC	People's Republic of China
PSCs	Polar stratospheric clouds
PVC	polyvinyl chloride
RADM	Regional Acid Deposition Model
RITS	Radiatively Important Trace Species
RSD	residual standard deviation
SABOAC	Scientific Application of Baseline Observations of Atmospheric Composition
SAGE	Stratospheric Aerosol and Gas Experiment
SASP	Surface Air Sampling Program
SBUV	solar backscattered ultraviolet (satellite ozone instrument)
SC	sky cover
SEAREX	Sea-Air Exchange Experiment
SIO	Scripps Institution of Oceanography, La Jolla, California
SMO	Samoa Observatory, American Samoa (GMCC)
SOI	Southern Oscillation Index
SOLRAD	Solar Radiation Facility (GMCC)
SPO	South Pole Observatory, Antarctica (GMCC)
SRM	standard reference material
STP	standard temperature and pressure (0°C and 1 atm)
SUNYA	State University of New York at Albany
TEM	transmission electron microscope
TOMS	Total Ozone Mapping Spectrometer
TSI	Thermo Systems Incorporated
TSP	total suspended particulate
ULF	ultra low frequency
UMT	Universal Mean Time
UPS	uninterruptable power supply
URAS	(a commercial CO_2 analyzer)
URI	University of Rhode Island, Kingston, Rhode Island
USDA	United States Department of Agriculture
USGS	United States Geological Survey
UV	ultraviolet
UVB	ultraviolet B band
VLF	very low frequency
WMO	World Meteorological Organization, Geneva, Switzerland
WPL	Wave Propagation Laboratory, Boulder, Colorado (ERL)